London South Bank University

School of Engineering

Effect of glass compositional variables on the structure and properties of phosphate glass/polyamide 11 hybrids

Luciana Serio

A thesis submitted in partial fulfilment of the requirements of London South Bank University for the degree of Doctor of Philosophy

January 2016

I would like to dedicate this thesis to my loving husband Giovanni and our angel Alessandro.

Declaration

I hereby declare that except where specific reference is made to the work of others, the contents of this dissertation are original and have not been submitted in whole or in part for consideration for any other degree or qualification in this, or any other University. This dissertation is the result of my own work and includes nothing which is the outcome of work done in collaboration, except where specifically indicated in the text.

Luciana Serio

Acknowledgements

This thesis would have been incomplete without the support of others.

I would like to express my sincere gratitude to Prof. David T. Gawne and Prof. Yuqing Bao for his valuable supervision and continuous support throughout the development of this research.

I would like to thank my colleagues and friends Pedro and Nora. These years of research would have not been the same without their friendship and support.

My thanks go to Jiming Gao for their devoted assistance throughout the experimental part of this study.

I would like to thank my husband and friend Giovanni and my family for their constant mental support no matter how far they are.

I gratefully acknowledge the funding source that made my PhD possible: the European Union Seventh Framework Programme (FP7-MC-ITN) under grant agreement No. 264710. I would like to thank the Directorate-General for Science, Research and Development of the European Commission for financial support of the research.

Abstract

The blending of polymers is a relatively inexpensive method of manipulating their properties and is common practice in the industry. Phosphate glass/polymer hybrids are an emerging class of nanomaterial with peculiar characteristics derived from nano-micro interactions of their components. Inorganic phosphate glasses are made up of chain-like molecules and are similar to polymer chains in their structure. These glasses are also unique in exhibiting similar processing temperatures to polymers, which opens up the possibility of co-processing and of greatly extending the range of obtainable properties. Both components being fluid during processing allow controlling and tailoring hybrid morphologies, and avoiding the problem of the intractable viscosity inherent from a high solid filler concentration. This work investigates the blending of an organic semi-crystalline polymer, polyamide 11 (PA 11), with different compositions of phosphate glasses. Experimental and theoretical studies of miscibility and phase behaviour of these unusual blends were analysed. In particular the research investigated the effect of glass composition on the rheological and thermo-chemical properties and nano/microstructure of these new materials, focusing on the tin fluoride (SnF_2) content in the glasses. The Flory Huggins equilibrium depression point model was employed to correlate and predict miscibility behaviour in these new systems. The experimental results showed that a high amount of SnF_2 could act as a proper compatibilizer for the novel Rilsan ® PA 11 matrix. Experiments showed that the halogen content lowered the glass transition temperature (Tg) and softening point (Ts) of the glasses, allowing both phases being fluid during melt-blending. However the water stability of the glasses was improved with increasing SnF_2 content in the network. The particle size of glass in the hybrids was inversely correlated with SnF_2 in the glass composition. This phenomenon resulted in lowering the equilibrium melting point (Tm^0) in the hybrids. The load force (F) generated during the extrusion process and the hybrid viscosities decreased, without compromising chemical and thermal stability of the materials. The Tg of PA 11, measured as shifts of the major peak in dissipation factor against temperature plot, was inversely correlated with SnF_2 content in the

glass composition, phenomenon often attributed to the partial miscibility of components in a system. The stiffness of the hybrid was improved by higher amount of SnF_2 in the glass compositions with polyamide reinforced by the glass having the lowest Tg (60 SnF_2 mol%). The longitudinal storage modulus was inversely correlated with temperature for PA 11 and all hybrids and increased with melting each phosphate glass with the polymer matrix. The storage modulus increased with SnF_2 content in the glass composition in the matrix at lower temperature and reached a constant value for all hybrids at higher temperature. The viscosity and shear modulus decreased and increased respectively with increasing angular frequency. Shear modulus of polyamide matrix was lowered by each phosphate glass. All samples showed a small upturn in the modulus versus angular frequency curve at the lowest viscosities, behaviour related to the presence of yield stress in the hybrids, more evident in the hybrids with the highest content of SnF_2 in the glass.

Table of Content

List of Figures

List of Tables

Nomenclature

a: indentation half-diagonal length

A: cross section area

as: asymmetric

ASTM: American Society for Testing and Materials

b: width

c: velocity of light

c (fracture toughness test): surface radial crack length

d: depth

D: screw diameter

d_1: indent diagonal 1

d_2: indent diagonal 2

DMA: Dynamic Mechanical Analysis

DSC: Differential Scanning Calorimetry

E_{fh}: static flexural modulus of hybrid

E_{th}: static tensile modulus of hybrid

E': elastic storage modulus

E": elastic loss modulus

E*: complex elastic dynamic modulus

F: force

Fe: equilibrium force

FTIR: Fourier Transform Infrared Spectroscopy

G': shear storage modulus

$G"$: shear loss modulus

G^*: dynamic shear complex modulus

G_c^*: complex modulus of the continuous phase

G_d^*: complex modulus of the dispersed phase

h: height

h_s: screw channel

H_v: Vickers hardness

H_2O: water

IR: infra-red

K_{IC}: fracture toughtness

L= d_1/d_2, the ratio between the two indent diagonals

LCP: liquid crystalline polymer

LDPE: low density polyethylene

L_s: support spam in three-point bending test

M_0: initial mass

M_f: mass after given immersion time

M_L: percentage mass loss

n: number of moles of molecules of a component

N: screw speed

NH_3: ammonia

$NH_4H_2PO_4$: ammonium phosphate monobasic

$N_{1,2}$: the number of segments in the chains of component 1 or 2

P: the indentation load

PA: polyamide

PA 6: polyamide 6

PA 11: polyamide 11

PA 12: polyamide 12

PEEK: poly(ether ether ketone)

PEI: polytherimide

Phosphate glass: PG

P_2O_5: Phosphate Oxide

PPS: polyphenilene sulphide

PS: polystyrene

PW: processing window

Q: heat

r: radius of the screw

r_c: capillary radius

R: universal gas constant

s: symmetric

S: slope of the initial straight-line portion of the load deflection curve

SA: surface area

SA_{ref}: reference surface area.

SnF_2: Tin Fluoride

SnO: Tin Oxide

$S_{1,2}(q)$: the form factors of either component

$S^{-1}(q)$: the structure factor of a binary blend

t: time

T: temperature expressed in K

Tr: torque

tan δ: loss tangent

T_c: crystallization temperature

TEM: transmission electron microscopy

TFP: tin-fluoride-phosphate

Tg: glass transition temperature

TGA: thermogravimetric analysis

Tm: melting point

Tm^0: equilibrium melting point

${T_{mb}}^0$: equilibrium melting point of blend

To: onset of crystallization temperature

Tp: crystallization peak

Ts: softening point

v: frequency

v_a: molar volume of the repeat unit of the amorphous component

v_c: molar volume of the repeat unit of the crystalline polymer

V: volume

w: width

W: wavenumber

W_a: weight in air

W_b: weight in the buoyant liquid

W_d: drop weight

X_c: percent of crystallinity

XRD: X-Ray diffraction

ZnO: zinc oxide

ΔG_m: Gibbs free energy of mixing

ΔS_m: entropy of mixing

ΔH_m: enthalpy of mixing

ΔH_f^0: heat of fusion of the crystalline component;

λ: wavelength

ϕ: molar fraction of a component

X: interaction parameter

σ: stress

σ_E: elongational stress

σ_{fh}: flexural strength of hybrid

σ_{th}: static tensile strength of hybrid

σ_{yh}: yield strength of hybrid

τ: shear stress

$\dot{\gamma}$: shear rate

γ: surface tension

μ_a: chemical potential of the amorphous phase

μ_c: chemical potential of the crystalline phase

ω: angular frequency

η: viscosity

η': dynamic viscosity

$\eta_{E:}$ elongational viscosity

ε: elongation

$\dot{\varepsilon_0}$: elongation rate

ρ: density

ρ_b: density of buoyant

θ: the indentation angle

Chapter 1 Introduction

1.1 Research background and objectives

The reinforcement of polymers with inorganic fillers, such as glass, is a well-established and highly successful industrial technique to enhance performance, reduce cost and tailor properties to meet specific end-user requirements [1]. However, the quantity of conventional fillers is limited to about 40 volume % in most polymers owing to the high viscosity resulting in poor processability (for example during extrusion and injection moulding) as well as limitations in ductility, toughness and surface appearance [1]. A possible way to overcome these drawbacks is to develop new inorganic-organic hybrids characterized by the reinforcing phase being in the liquid state during polymer melt processing.

One class of materials which has shown promise in this regard is that of the low-temperature processable glasses. The low glass transition temperatures Tg and softening point Ts of these materials is achieved by using P_2O_5 instead of SiO_2 as the primary glass former [2]. An important factor in the formation of low-temperature glasses is the number of cross-linkages per network-forming cation: structures with small numbers of bridging oxygens tend to decrease both Tg and Ts [2]. Phosphate glasses are built up from three bridging oxygens per phosphorus cation as compared with four bridging oxygens in the much higher melting silica glasses. In addition, alkali and alkaline earth oxides are used to aid the control of thermal properties and chemical durability [2, 3].

Phosphate glasses have low enough Tg and Ts to be fluid alongside the majority of the thermoplastic matrices during melt processing [4]. When both components of a glass/polymer hybrid are fluid during processing, mixing of the components on a molecular scale becomes possible. Because of the low Tg and Ts of the glass in question, these hybrids can be

processed conventionally with glass loadings of up to 60% by volume, managing to avoid the high viscosity problem inherent to high filler concentrations [4].

A number of composite materials in which this inorganic second phase has clearly melted during processing have been documented in the literature [4-6] and offer the possibility of forming homogeneous hybrids: radically new materials with different structures and improved properties compared to those achieved from classical polymer blends and composites.

The miscibility of polymers and glasses generally needs a negative change in the Gibbs free energy of mixing ΔG_m during the mixing process which, in turn, requires an increase in entropy (positive entropy change ΔS_m) and/or a decrease in enthalpy (negative enthalpy change ΔH_m). In reality, phosphate glasses and, in particular, polymers are composed of large network structures with low mobility, unfavourable possibilities of molecular mixing and limited change in the entropy of mixing. In view of this, the miscibility of polymers and glasses needs to rely more on reductions in the enthalpy of mixing by attractive interactions between the networks, chains and side groups of the two components. It is known that phosphate glass can be surface nitrided [7] and that amine groups can bond to the surface of phosphate glasses [7], condition that can improve the miscibility in the liquid state and the adhesion in the solid state of the phosphate glass component and the polyamide matrix.

Work has also been carried out [4-6] that documented that polyamide 6 (PA 6) and a specific tin fluoride (SnF_2) phosphate glasses were partially miscible during processing in an internal mixer and exhibited a depression of the melting point. However few studies are available in literature and, given the hydrophilic weak point of phosphate glasses in general, the effect of phosphate compositions on the thermal and chemical stability of these new hybrids has not been investigated yet.

This project was aimed at developing low Tg phosphate glass/PA 11 hybrids by controlling the network structure of the glasses. A series of low Tg SnF_2-SnO-P_2O_5 glasses was prepared on the laboratory-scale to produce feedstock powder for hybridization. The phosphate glass compositions were optimized and characterized. The glasses were blended with Rilsan ®, an innovative PA 11 produced by Arkema (France), in a micro-extruder. The performance during mixing of the low-Tg glasses with polyamide 11 was investigated. The performance

under mixing was related to processability in term of the steady-state torque reached during extrusion. The morphology of the extrudates was examined from the viewpoint of forming either homogenous miscible hybrids or heterogeneous two-phase glass-polyamide composites. The homogeneity of hybrid was studied by Fourier Transform Infrared Spectroscopy (FTIR), Dynamic Mechanical Analysis (DMA) and rheological analysis in conjunction with the Flory-Huggins analysis of melting point depression. This approach allowed to link theory to practical usefulness and to enable the extent of miscibility and two-phase morphology to be assessed. The research included optimizing the composition, temperature and blending for hybrids and evaluating their properties.

The objectives of the research were:

1. Developing phosphate glasses with low Tg values.
2. Characterising phosphate glasses
3. Understanding the evolution of the properties of phosphate glasses with the glass compositions.
4. Developing glass-polyamide materials with high processability in extrusion.
5. Understanding the relationships between glass composition and miscibility of hybrids.
6. Characterising and understanding the evolution of properties of hybrids as a function of process conditions and glass composition.

Special attention was given to the miscibility between the polyamide matrix and phosphate glasses, as miscibility played an important role on the properties of the final hybrids. Experimental evidence of miscibility was given by the analysis of the evolution of particle size of glasses in the PA 11 phases. While the requirement for a blend to be miscible/compatible was defined in terms of the strong interaction of the two phases, the compatibility in the systems were further investigated by Fourier Transform Infrared Spectrometry (FTIR) to verify changes in the interactions, such as hydrogen bonding and polar interaction, between the glass and polymer phases. The rheological behaviour of phosphate glass/PA 11 blends was analysed to identify any viscosity changes compared to pure PA 11. A miscible or compatible blend on a macroscopic scale can be identified by a

single Tg in hybrids, which were analysed via Dynamic Mechanical Analysis (DMA). The miscibility guide by Flory Huggins's equilibrium melting point Tm^0 depression technique [64-71] was used to interpret the miscibility behaviour of phosphate glass/PA 11 hybrids. Choices of the right temperature and composition ranges for blending were also important factors for obtaining miscible polymer blends because miscibility rarely extends to all compositions and temperatures for given polymer combinations.

1.2 Thesis structure

This thesis consists of 8 chapters, which include introduction, literature review, experimental details, experimental chapters, contribution to original knowledge and conclusions, as shown in Figure 1.1.

The main objective of this work is to develop enhanced properties phosphate glass/PA 11 hybrids via melt blending techniques with strong interactions between the components. In order to achieve that, several low Tg phosphate glasses were developed and the influence of glass composition was investigated.

The research is reported in three chapters. In Chapter 4, the optimization of different glass routes and glass compositions is presented in order to prepare good quality glasses for hybridization with polyamide. The influence of glass composition on glass transitions and softening point was studied. A good hybridization requires the organic phase (PA 11) and inorganic phase (phosphate glass) to have a similar glass transition temperature Tg and Ts to favourite the miscibility between the two phases. Phosphate glass quality depends, among others factors, on the hydrophilic nature of the material. Because the capacity of moisture-water absorption of these glasses could compromise the final hybrid properties, dissolution tests and thermal gravimetric analysis were performed in order to measure the chemical stability of the different types of glass produced. The influence of glass composition on glass structure was also investigated via FTIR. Mechanical characterisation of the different glasses (hardness, fracture toughness) is also presented in this chapter.

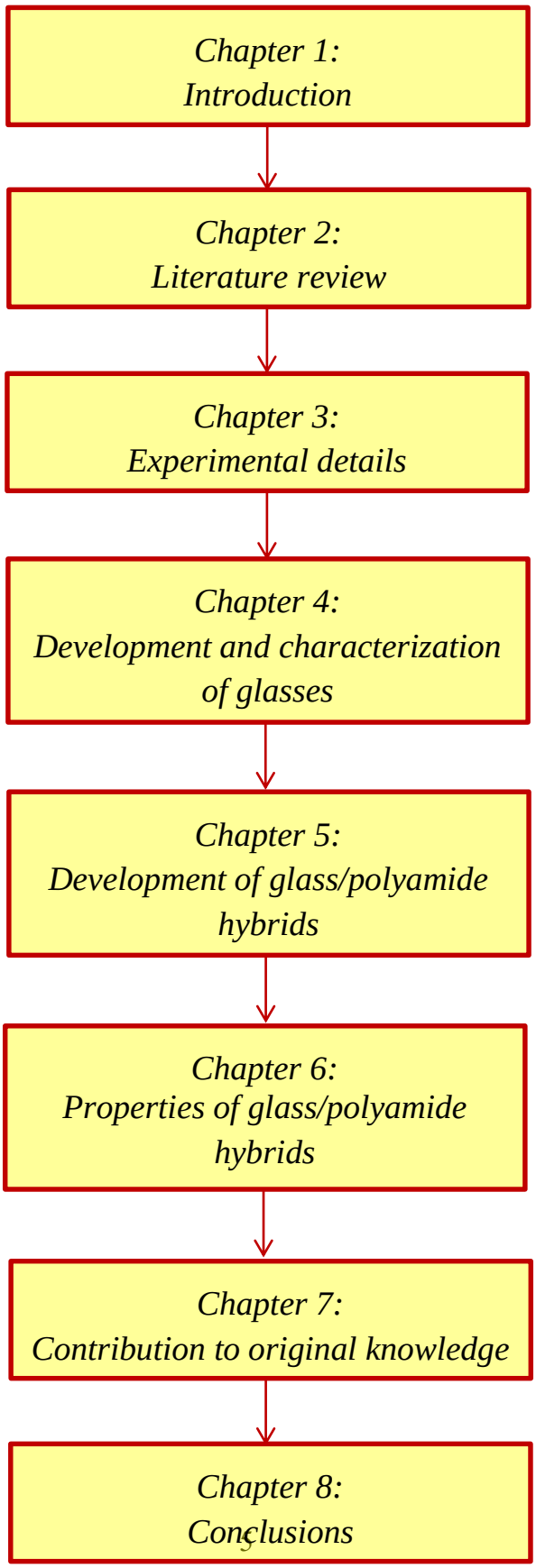

Figure 1.1: Schematic presentation of the thesis structure.

Chapters 5 focuses on processability of hybrids. The importance of glass composition on melt blending of hybrids is studied and its importance proved. The influence of working conditions (blending temperature, screw speed, residence time) and glass content and composition on reproducibility and quality of hybrids is also evaluated. The load force (F)/time trends recorded during extrusion are discussed in order to support the processability of hybrids.

In Chapter 6, the influence of glass composition on miscibility of hybrids is analyzed. In order to evaluate the effect of glass composition on the phase behaviour and interaction of glass and polyamide phases, morphology and structure of hybrids are analysed. The thermodynamic of miscibility is investigated using the melting point depression and Flory-Huggins approaches. The rheology, glass transitions, mechanical and thermal properties is discussed in order to support the miscibility findings in hybrids.

Chapter 2 Literature Review

2.1 Inorganic-organic hybrids: brief overview

The last couple of decades have seen a constant and rapid growth of the polymer blend industry, fuelled by the demand for improved materials. The synergetic effects of the blend of two or more polymers can be used to design materials with predicable properties and even tailored to specific applications, like reduced viscosity or improved mechanical properties, without requiring the expensive synthesis of an entirely new material.

Another group of materials, the inorganic/organic hybrids consisting of separate inorganic/organic regions, are increasingly being selected for wide range of applications whose needs cannot be met by more classical polymer blends and composites; these hybrids exhibit properties that do not change linearly with changes in ratio of the inorganic and organic content. The main advantage of these novel materials is the fine control over both composition and structure which results in highly improved properties compared to those of the organic and inorganic components in isolation [8]. These hybrid systems are traditionally classified in two main classes: homogeneous hybrids and heterogeneous hybrids [8].

Hybrids systems of the homogeneous class are produced from monomers or miscible inorganic/organic components. The *sol–gel process* is a well-known procedure to derive homogenous hybrid systems and consists in a series of hydrolysis and condensation reactions, leading to the formation of the hybrid network [9, 10]. During a typical sol-gel process the hydrolysis products of the metal alkoxide react with incorporated monomers or oligomers, and, depending on the specific design of the functional groups, result in a final material displaying a range of unique properties such as thermo-chemical stability, transparency and specific mechanical properties [9, 10].

Generally, due to the physical interactions or chemical bonds with the organic phase, the inorganic component is dispersed on nanometer level [11]. Nowadays the commercial applications of the sol-gel homogenous hybrids are limited as they have a few shortcomings: for instance they are expensive and difficult to fabricate; they are also toxic due to the high volatile organic nature of the precursor chemicals; additionally, pores and cracks in the final product are reported in literature due to the evaporation of the solvents in the gels [12].

The heterogeneous class of inorganic/organic hybrids consists in phase-separated inorganic/organic systems including conventional glass/ceramic polymer composites and polymer/clay nanocomposites.

Glass/ceramic polymer composites, whose main advantage is the low cost of the improvements, are conventionally prepared by blending rigid inorganic component with the organic polymer. The ability of flowing under stress at elevated temperatures, typical of thermoplastics, allows these materials to be melt processed, which is popular in the plastic industry. Furthermore these systems display domains with relatively small sizes ranging from angstroms to micrometers [8]. Usually the combination of the components in these material systems may lead to synergistic effects which achieve a balance between the properties of each composite component.

The properties of polymer blends are affected by a high number of parameters, such as the concentration, geometrical shape and the aspect ratio of filler and the degree of interfacial adhesion between the filler and the matrix [4, 11-13], all of which may influence the ability to transfer stresses across the matrix-filler interface causing a variation in the properties of the whole system.

Due to the presence of glass as a solid phase and its limited chemical interaction with the other components, despite their popularity these materials have major drawbacks: the intractable viscosity, the poor surface finish, the difficulty in orientating glass fibres, the presence of micro-defects at the glass-polymer interface, the high brittleness of the resulting hybrid [8].

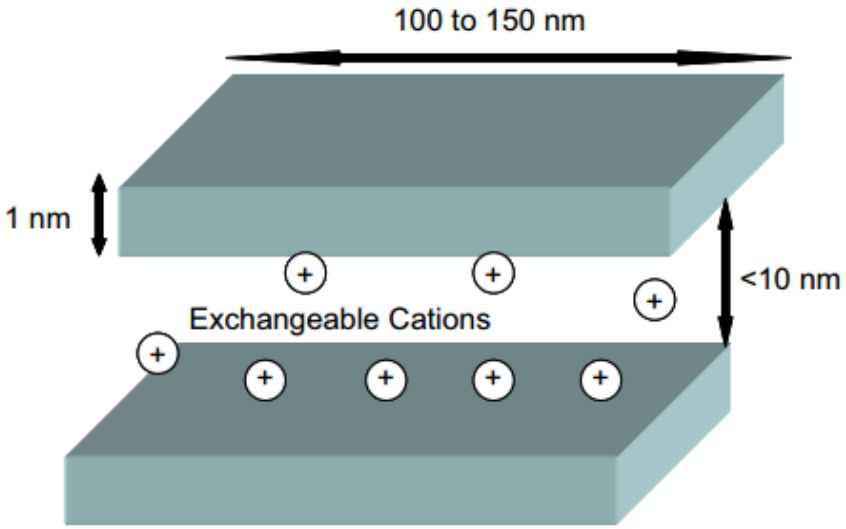

Figure 2.1: Schematic of the size scales and exchangeable cations in layered silicate clay [4].

Polymer/clay nanocomposites are formed by a polymer matrix with layers of dispersed silicate clays (see Figure 2.1) The layers are divided by a gap of about 10 nm [14] and assembled by platelets 1 nm thick and 100-150 nm in length [14, 15]. This separation between layers helps improve the properties of the resulting hybrid and, together with the adhesion to the polymer matrix, can be facilitated by filling the gap with cations [16]. Properties such as tensile modulus and strength, thermal stability, flame resistance and barrier properties are enormously improved even at low clay loading (5%) and without renouncing to high final impact strength [14]. As the full separation between layers is not easy to achieve, intercalated polymer/clay nanocomposites can be developed where the polymer chain inserts itself between the clay platelets [16]. The properties of these heterogeneous hybrids are similar to those of ceramics. Even though polymer/clay nanocomposites offer many advantages, the morphology of the inorganic phase is fixed preventing any customizations of the final properties of the hybrid required to satisfy any client specification.

The phosphate glass/polymer hybrids, exhibiting advantages of the conventional inorganic/organic hybrids, lie between the homogeneous and heterogeneous classes discussed above. As these novel materials are generally prepared by melt blending the two components,

the expensive and toxic preparation typical of sol-gel hybrids is not necessary. Unlike the conventional glass/polymer composites, the incorporation of up to 60 vol% inorganic component, while avoiding the incontrollable viscosity, is achievable because of the low glass transition temperature of the phosphate glass. Furthermore the morphology of the inorganic phase can be easy tailored during fabrication, allowing tuning the hybrid properties to meet the requirements for the final applications. The possibility of affecting the morphology and the composition of these systems has led to the development of novel materials characterized by improved and more controllable properties compared to those of the pure inorganic or organic components [8].

2.2 Glass formation

Glass is defined by Shelby [17] as "an amorphous solid completely lacking in long range, periodic atomic structure, and exhibiting a region of glass transformation behaviour" instead of a defined melting point. Furthermore, the American Society for Testing and Materials (ASTM) has defined a glass as any material that has been "cooled from the melt without crystallising" [18].

The principle of glass formation is illustrated in Figure 2.2 [19]. This picture represents a heated melt of fixed volume cooled to room temperature at a controlled rate. The path A-B-C corresponds to the cooling trajectory slightly below the melting point Tm. Point A represents a sufficiently high temperature for the material to be in liquid state. Point B represents the point where the liquid and solid forms have equal free enthalpies (Gibbs energies). As the temperature drops below Tm, the crystalline state is at the equilibrium state (trajectory B-D) and the thermodynamic system tends to reach its lowest enthalpy (trajectory D-E). Typically the crystalline state displays long range periodic atomic arrangement.

The formation of glassy materials is dependent upon achieving cooling rates high enough for kinetic factors to dominate the thermodynamic system and prevent crystallisation: if the crystallization rate and nucleation rate are slower than the cooling rates, the crystallization can be inhibited and the enthalpy of the system deviates from the equilibrium state. In this

case the material is present on the path B-C-F [19], a metastable state of a super-cooled liquid. This trajectory has a gradual slope defined as *the range of glass transition*.

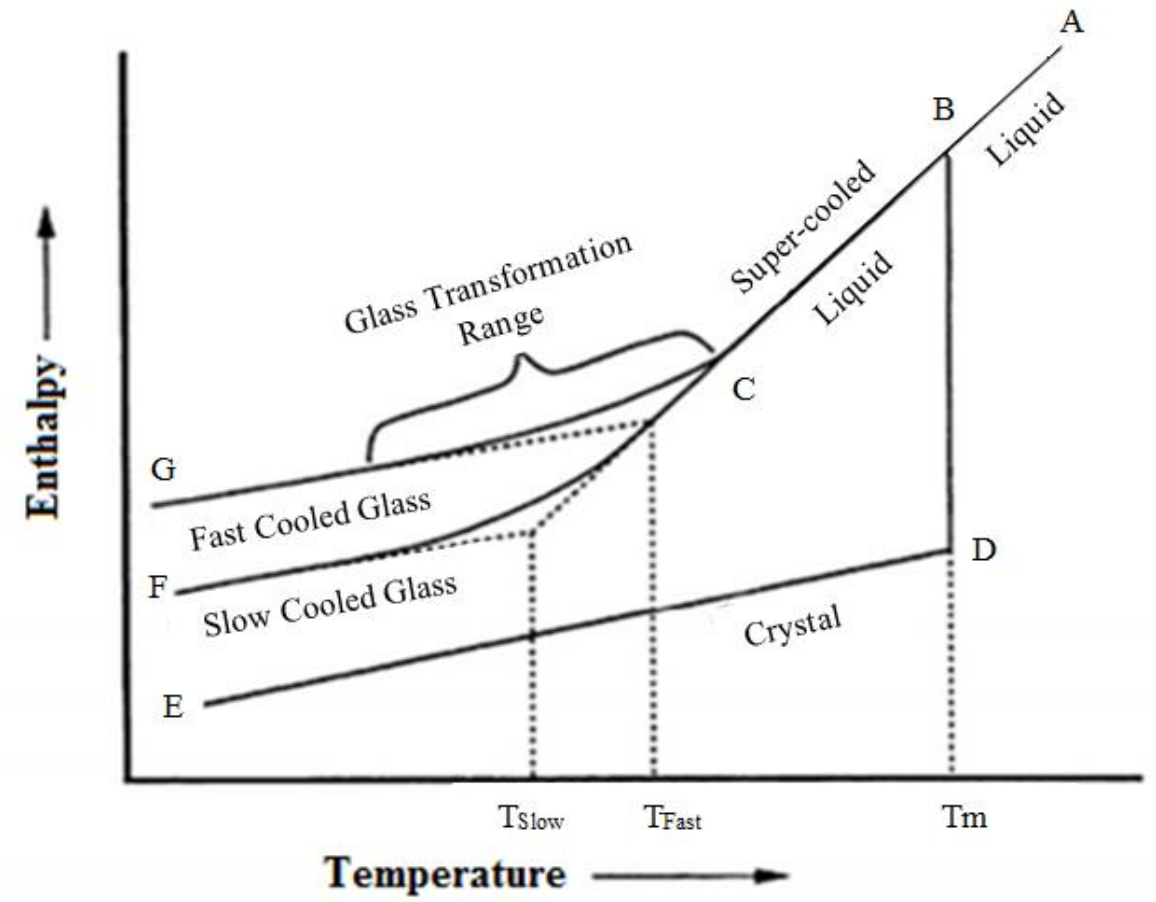

Figure 2.2: Enthalpy-temperature diagram showing formation of crystalline and glassy materials; the effect of cooling rate on glass formation is elucidated [19].

At the glass transition zone, the increasing viscosity of the liquid (values close to 1012-1013 Poise [19]) associated with the progressive cooling process leads to a structure becoming fixed without any atomic rearrangement. The so-called *frozen liquid* can now be considered as a glassy material. Additionally since deviation from the equilibrium state is dictated by the cooling rate, this kinetic factor controls the temperature at which the sample enters the glass transition region. For example, if a material is cooled at a reduced rate the B-D-E trajectory is observed. A shift of the glass transition temperature occurs to lower values (T_{Slow}) with the

atomic arrangement of the resulting glass reflective of its arrangement prior to its deviation from the equilibrium state [17, 18]. For example, inorganic silicate glasses are formed by cooling the melt at relatively slow cooling rates of about 20 ˚C min^{-1}. Instead, for faster cooling the B-C-G trajectory is followed and the glass transition temperature is shifted to higher values (T_{Fast}). An example is the generation of metallic glasses, materials that require rapid cooling rates of ≈ 2° sec^{-1} [17, 18].

2.3 Structure of phosphate glasses

2.3.1 Phosphorus tetrahedron and bridging oxygens

Phosphate glasses are composed by cross-linked and chain-like structures very similar to a network of polymer chains [20]. Thus, these materials are generally considered to be polymeric in nature [20-22]. However, these chains are much shorter than those of organic polymers. Furthermore, often an alkali metal cation aids in the network formation.

A fundamental work by Zachariasen (1932) introduced the theory of phosphate glass structure [23]. This study describes the phosphate glasses as composed by a three-dimensional structural network produced by reaction of glass forming phosphorus pentoxide (P_2O_5) compounds. Further influential studies by Hägg and Van Wazer questioned Zachaniasen theory, demonstrating that even a large one dimensional molecular group alone could constitute the phosphate glass structure [24, 25]. Following these researches, different glass structure models were developed and represented in terms of the short range bonds and long range length scales throughout the materials overall structure [21, 22].

The orthophosphate P-tetrahedron (PO_4^{3-}) is the basic structural unit (Figure 2.3) of phosphate glasses. The electronic configuration of phosphorus is $3s^2$, $3p^3$ with five valence electrons. In oxide systems, the favoured coordination is tetrahedral, which can be considered as sp^3 hybridization of the phosphorous valence shell atomic orbitals, with the third p electron promoted to an empty 3d orbital, where a strong π bonding molecular orbital is formed with 2p orbitals on the oxygen atoms [21].In the absence of cations, the molecule's three oxygen atoms are free and the tetrahedral phosphate anion is able to form covalent bonds via these

bridging oxygens (BOs) with any surrounding P-tetrahedrons (P-O-P bonds). Thus, the combination of orthophosphates allows the formation of various polyphosphate anions which may be branched or linear or a combination of the two.

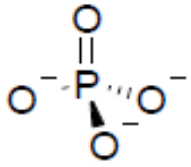

Figure 2.3: The tetrahedral phosphate anion; charges are balanced by either polymerisation or cations [21].

Figure 2.4 represents a three dimensional random network of covalently bonded P-tetrahedrons for a simple vitreous P_2O_5 glass (v-P_2O_5) as described by Zachariasen in [23].

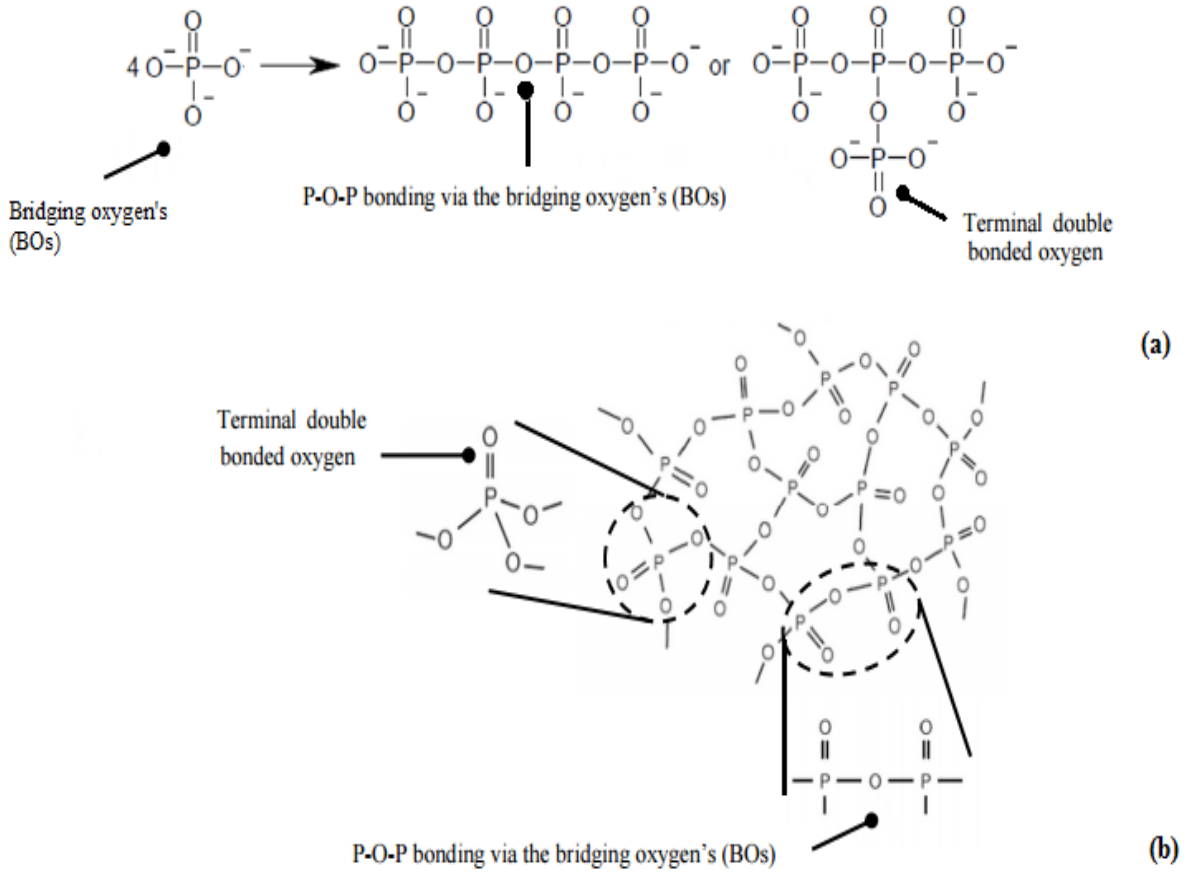

Figure 2.4: Polymerisation of the phosphate anion gives rise to various polyphosphate anions linked via oxygen bridges which may be linear or branched (a), or a combination of the two (b) [21].

The corresponding structure of a phosphate glass network is typically classified under the Q^i terminology where *i* represents the number of bridging oxygens BOs per tetrahedron (Figure 2.5). This terminology was originally devised for silicon glasses, e.g. but has been applied to phosphates [21].

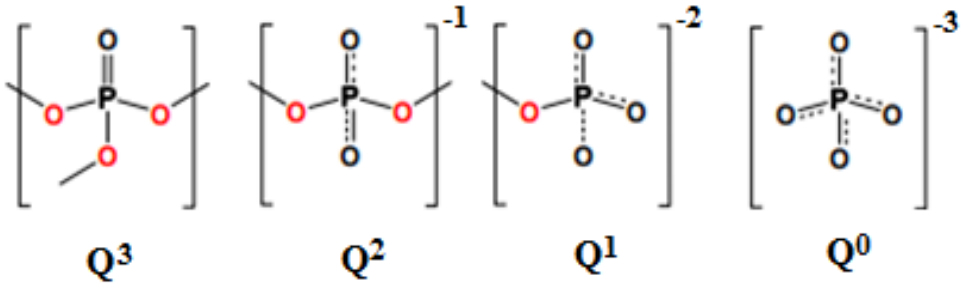

Figure 2.5: Schematic representation of phosphate tetrahedral units: the four types of Q^i represent the species found in phosphate glasses, where *i* is the number of bridging oxygens present within a particular phosphate tetrahedron [21].

2.3.2 Network-modifier oxides

Alkani and alkaline earth metal ions are commonly used to modify the Q^i unit content, i.e. phosphate glass structure, and to tailor the associated glass properties. These compounds are typically named as network-modifier oxides (MOs) [22]. If a charge on an oxygen atom is balanced by a cation, then it will not be possible for an oxygen bridge to form [20], as shown in Figure 2.6. Common MOs are calcium oxide (CaO), magnesium oxide (MgO), or titanium dioxide (TiO_2).

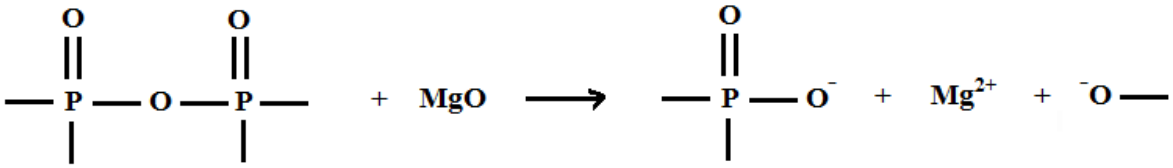

Figure 2.6: A Bridging oxygen atom is balanced by an Mg^{2+} cation and a P-O-P oxygen bridge cleaves [14].

Phosphate glasses can be classified based on the glass former content (P_2O_5 mol%), Q^i content and corresponding network structure, as shown in Table 2.1.

Table 2.1: Different phosphate glass structures are classified based on P_2O_5 content, Q^i terminology and network structure.

Classification [22]	P_2O_5 [mol%]	Q^i [22]	Structure [22]
Vitreous P_2O_5	100	Q^3	Cross-linked random network of Q^3 tetrahedra
Ultraphosphate	>50	Q^3/Q^2	50-75 mol%: randomly linked Q^3/Q^2 75-80 mol%: resembles v-P_2O_5
Metaphosphate	50	Q^2	Q^2 phosphate polymeric chains of infinite length and ring type structures
Polyphosphate	<50	Q^2/Q^1	Q^2 chains of various lengths terminated by Q^1 P-tetrahedra
Pyrophosphate	<33	Q^1/Q^0	Phosphate dimers (P_2O^{4-}) with isolated phosphate tetrahedral (PO_4^{3-})
Orthophosphate	N/A	Q^0	(PO_4^{3-}) phosphate tetrahedral

Phosphate glass structures are expressed diagrammatically in Figure 2.7, where the different types of networks formed by the Q^i unites are identified using the ratio R = M_2O/P_2O_5. For example, meta-phosphate glasses have a ratio of exactly 1, while pyro-ortho phosphate glasses have a ratio that ranges from 2 to 3.

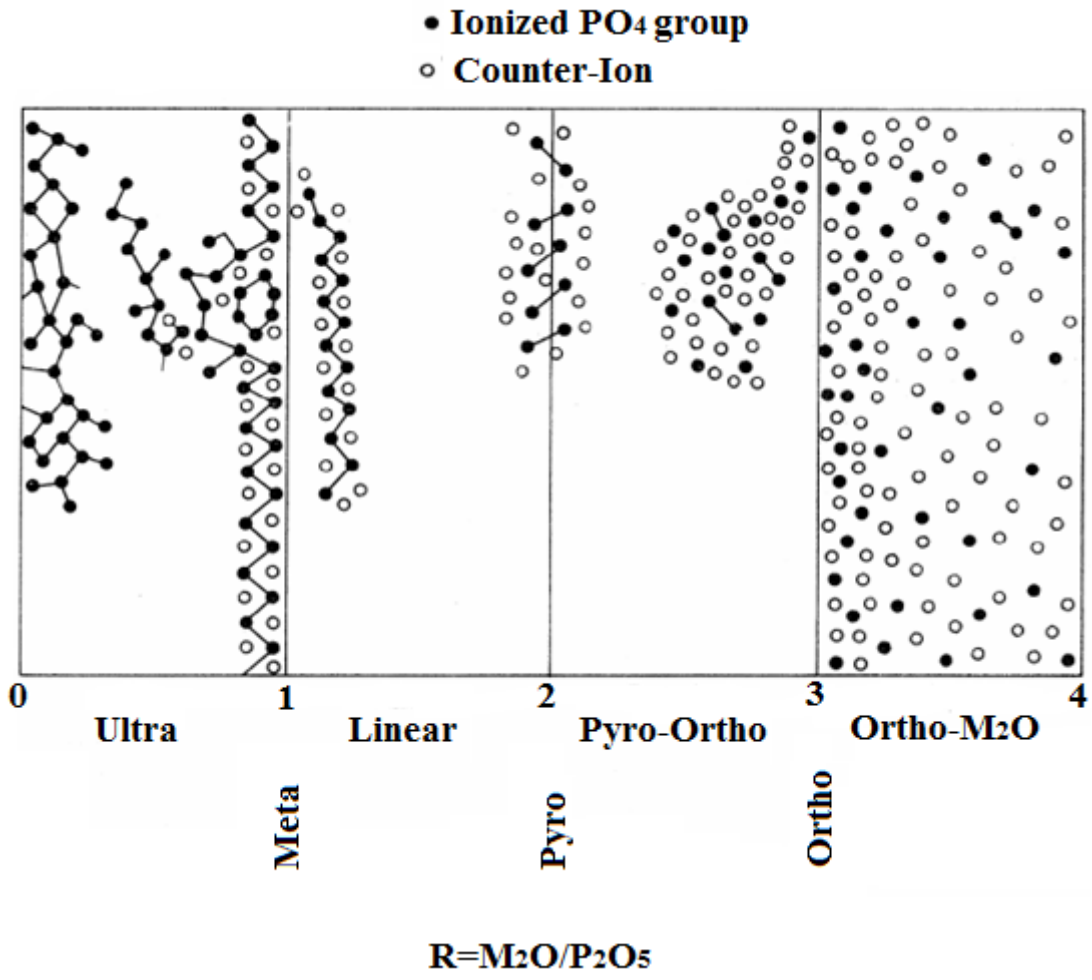

Figure 2.7: Schematic phosphate structures as a function of composition, note that linear phosphates are also known as polyphosphates [21, 22].

Different concentrations of metallic cations create a distribution of Q^i species, creating a chelate-like structure (Figure 2.8). This structure is formed with random ionically bonded crosslinks between the non-bridging oxygens (NBOs) of different phosphate groups/chains. A too high content of metal cations results in the phosphate glass network disruption, as the number of bridging oxygens available per phosphate anion decrease. As the concentration of

MOs is increased, the random three dimensional crosslinked P-tetrahedra network (Q^3) in a vP_2O_5 glass become linear polymer-like phosphate chains of decreasing length (Q^2/Q^1).

In ultra-phosphate glasses ([P_2O_5]>50 mol%), the structural types of unit are the tetrahedra Q^3 (units having three bridging oxygens (BOs) and one non-bridging oxygen (NBO) bonded to the phosphorous atom by a double bond) and Q^2 (unit having two bridging and two non-bridging oxygens, i.e. meta-phosphate structure). The Q^3 units form three-dimensional network, while Q^2 units assist the chain formation.

With a decrease in P_2O_5 content up to [P_2O_5] = 50%, the structure of phosphate network approaches to meta-phosphates, and the network is based mainly on Q^2 units. Hence, the chains formed by –(P-O-P)n- bridges and rings formed by Q^2 units, have formed the overall meta-phosphate network. Only free chain-ends are formed by Q^1 units (units having one bridging and three non-bridging oxygens, i.e. poly-phosphate structure). The part of Q^2 units has two non-bridging oxygens, which are usually assumed to be distinct since the first terminal oxygen is bonded by double bond (P=O) while the other terminal oxygen forms P-O- bond.

Further decrease in the P_2O_5 content, i.e. [P_2O_5] < 50 mol% leads to formation of poly-phosphate glasses. Their network is in fact a depolymerised meta-phosphate network formed by shorter chain of Q^2 units which are terminated by Q^1 units.

For the content of $P_2O_5 \approx$ 33mol% the structure of phosphate network is formed mainly by dimmers of Q^1 units, and for [P_2O_5] < 33% mainly isolated Q^0 units, having four non-bridging oxygens (ortho-phosphate), exist.

The transition from one type of Q^0 units to the other type of units depends on the actual chemical composition of the melt, i.e. on the formal content of P_2O_5, and on the content and properties of the other participating oxides (network former and/or network modifier).

At the end a glass composed of isolated orthophosphate groups (Q^0) can be formed. This phenomenon is named as network depolymerisation [21] (Figure 2.8).

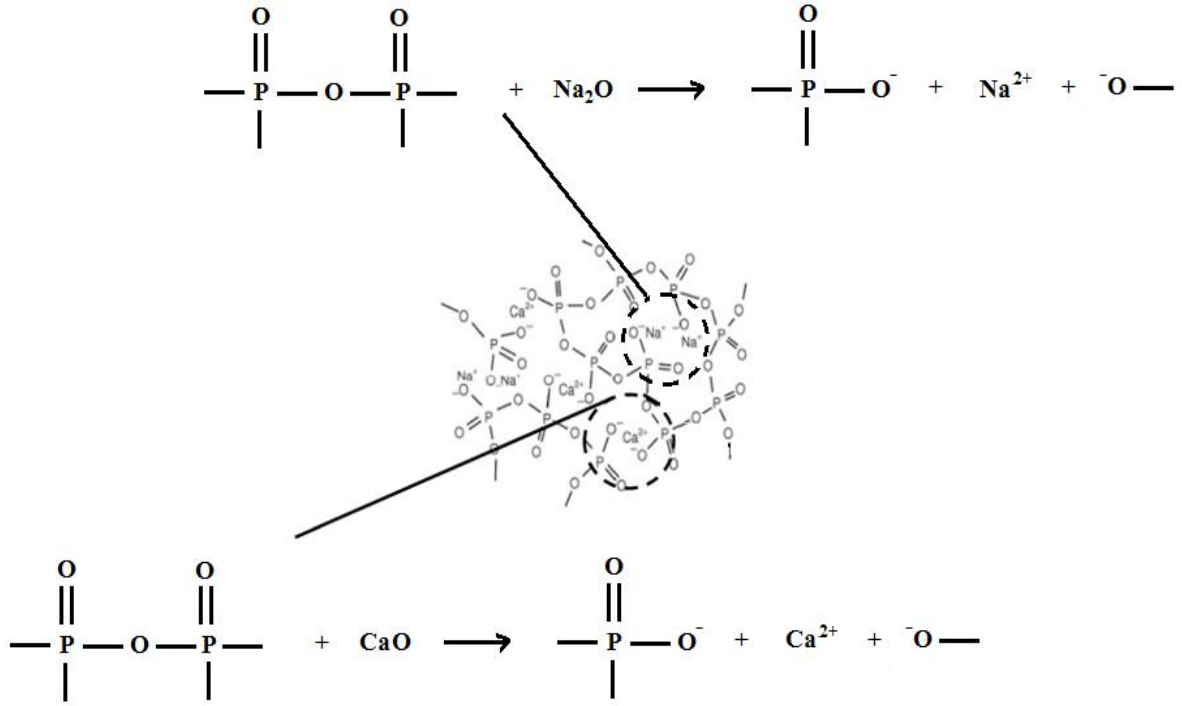

Figure 2.8: Introduction of CaO and Na_2O into a phosphate glass network and consequent formation of ionic bonds between the phosphate groups leading to the network depolymerisation [21].

2.3.3 Dissolution mechanism

One of the main issues of phosphate glasses is their relatively poor chemical stability, especially in water [22, 26, 27]. Water behaves like an alkali oxide as it reduces the polymerisation by the formation of hydroxyl groups in phosphate glasses [22].

Phosphate glass dissolution is a two stage process:

1. The initial diffusion of water into the glass surface leads to the immediate exchange of the sodium with hydrogen ions in water (Figure 2.9). This causes the formation of a smooth hydrated surface layer across the glass surface. This phenomenon depends on the diffusion rate of water molecules into the bulk glass, which is strongly governed by the phosphate glass composition.

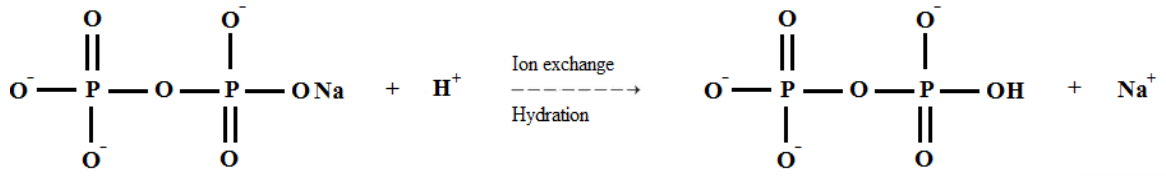

Figure 2.9: An ion exchange reaction between the Na^+ ions in the glass and the water H^+ ions at the phosphate chain ends during hydration [22, 26, 27].

2. P-O-P chains are attacked by H_2O water molecules, leading to their disentanglement and release into the aqueous media (Figure 2.10). The hydration of these phosphate chains is accompanied by the release of network-modifier oxides which changes the ionic concentration in the aqueous environment [26, 27].

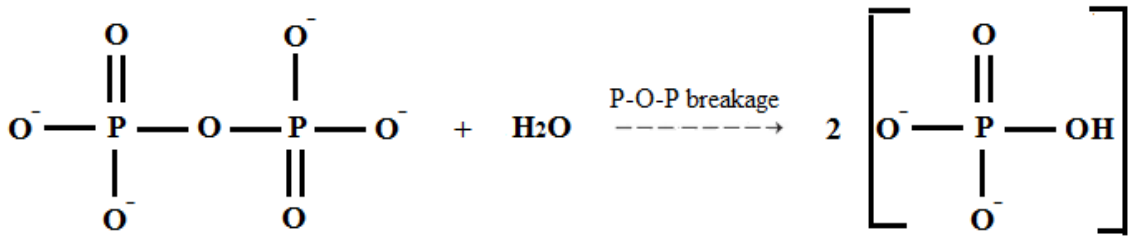

Figure 2.10: P-O-P bonds react with H_2O water molecule and break [27].

Multiple efforts have been undertaken to increase the chemical durability of phosphate glasses, but improvements are normally accompanied by an increased glass transition temperature [18, 26, 28].

For example a phosphate glass network can be modified by introducing an intermediate oxide, often referred as M, like those based on magnesium, iron, aluminium and zinc [18]. These additional oxides, behaving as either a network-modifier oxide or a network-former, permit the formation of covalent bonds (i.e. P-O-M-O-P) inside the glass's backbone which are resistant to hydration.

2.3.4 Effects of network-modifier oxides

The addition of specific network-modifier oxides at different concentrations in the phosphate glass network allows tailoring a vast range of phosphate glass properties, like thermal stability, mechanical properties, and dissolution rate. The magnitude of change of phosphate glass properties is determined on both the atomic radius and the valence of the selected modifier oxide cations [18].

According to the research conducted by *Appen* [29], the water resistance of a phosphate glass network is proportional to the difference of the ionic radii of the atoms. It has been shown that the effect is significant in the range of total concentration of the metal oxides 10 – 17% [29].

Boron oxide can be used to increase the chemical stability of ultra-phosphates. It has been shown that when B_2O_3 is introduced into ultra-phosphates in the amount 5% (molar content) the water resistance of the polymer increases; this can be explained by the depolymerization of phosphate chains and the appearance of – B – O – P – [29]. The appearance of bridge bonds – B – O – P – is most fully manifested for the ratios $Na_2O/B_2O_3 > 1.3$ [29]. Several studies [26, 27], have shown that water resistance of boro-phosphate glasses is preserved while their Tg decreases.

The introduction of alkali-earth metals MgO, BaO, CaO, into polyphosphate glasses caused the formation of low-melting ultra-phosphates with high water resistance and chemical stability [17, 26, 27]. The same effect was seen when adding ZnO in large concentrations [28]. In fact the introduction of bivalent metals into a phosphate network of cations not only cross-links the polymer chains but also decreases the fraction of the acceptor-bonds of the protons as a result of the redistribution of the multiple bonds in the PO_4 tetrahehdron [28].

Phosphate glasses with very low Tg were obtained by varying the ratio of P_2O_5 and Me_2O, where *Me* is a univalent alkali metal (Li, K, Na) [30]. Furthermore a decrease of the glass transition temperature Tg was accompanied paradoxically by an increase in the number of cross-links [30]. This is explained by the fact that the force of interaction of the fragments $O=P\text{-}OMe^+$ is larger than the rotation barrier of O=P-O (Figure 2.11). In addition, it was

shown that Tg depends on the nature of the alkali metal and decreases with increasing ionic radius of the metal ion. Thus, using potassium instead of sodium decreases the glass transition temperature of the polymer by 60°C [30].

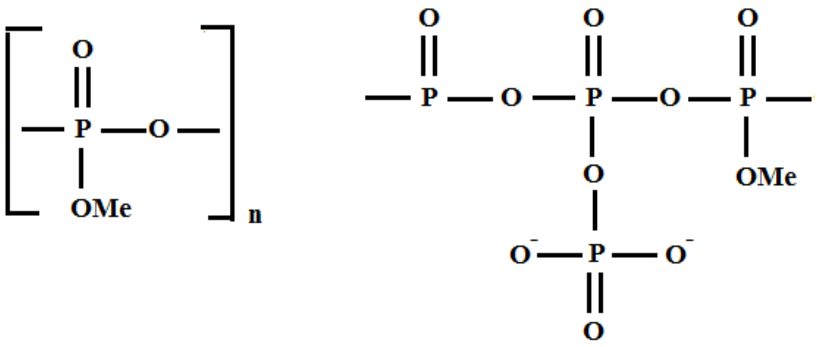

Figure 2.11: Schematic phosphate structures linked to alkali metal [30].

In a study by Urman [31], the addition of SnO in the phosphate glass network was reported to improve the chemical stability and mechanical properties of the phosphate glass and polymer/glass composite. However many problems regarding the mechanism of its influence still remain unsolved. Furthermore one obstacle in producing tin-phosphate glasses is oxidation or disproportionation of SnO at high temperature that cause a decrease in the glass stability [31]. Tin-oxide glasses are often used as reinforcement for thermoplastics, in particular for polyamides: the amine groups of the polyamide have been found to interact strongly with a tin-based phosphate glass, leading to an improvement of the composite [31].

Alumina Al_2O_3 has been reported to improve durability, but also to raise Tg because of its ionic crosslinking effect on the glass network [30]. In the same work [30] alumina was added together with B_2O_3. B_2O_3 plays a similar role as Al_2O_3 in enhancing chemical durability without excessively raising the Tg. Furthermore a relatively durable phosphate glass having lower transition temperature was developed in the same study [30]; the glass former (P_2O_5) percentage was kept as low as possible.

2.3.5 Ultra-low melting point phosphate glasses

Research reported by a number of workers [4, 5, 6, 18, 20-22, 28-31] shows some phosphate glass compositions have low enough Tg to be fluid alongside the majority of the thermoplastic matrices during melt processing. The condition in which both components of a glass/polymer hybrid are fluid during processing allows for the mixing of the components on a molecular scale. Because of the low Tg of these glasses, these hybrids can be processed conventionally with glass loadings of up to 60% by volume, managing to avoid the high viscosity issue inherent with a too high filler concentration [1].

Some ultra-low Tg phosphate glass compositions are reported in Table 2.2: the halogens fluoride and chloride are responsible for a significant reduction of the Tg of glasses. In particular, Tgs value compatible with common thermoplastics can be achieved with a really low content of fluoride.

2.3.6 Fluoride-oxy-phosphate glasses

The phosphate glasses of principal interest for glass/polyamide hybrids are the tin-fluoride-oxy-phosphates (TFOP) glasses, which are characterized by an ultra-low Tg. Their main properties are a low and ultra-low melting temperature, a lower softening point than other glasses found in literature, good water durability and chemical resistance; because of these desirable properties, there are a great number of studies of the structure, characteristics and factors that affect the production of these glasses [4-32].

The addition of fluoride to phosphate glasses leads to a network depolymerisation as the P-P bonds are broken to form mono- or di-fluoro-phosphate ($P0_3F–Q^1$ units or $PO_2F_2–Q^0$ units) [32]. Owing to this depolymerisation process, the average phosphate chain length is successively decreased, as increasing amounts of fluoride species are incorporated into the meta-phosphate glass structure, leading to pyro-phosphate dimers.

One of the first studies on tin-fluoride-oxy- phosphates glasses was conducted by Tick and Sanford in 1982 [33]. The reported stannous fluoro-phosphates glasses exhibit extraordinarily low glass transformation temperatures, good chemical durability, good water resistance and

optimal optical properties. Furthermore, and unlike the other phosphate glasses, these materials display excellent water resistance [35]. Tick continued his research and found a new application for these tin-fluoride-oxy-phosphates glasses as a supporting matrix for light-responsive polycyclic aromatic hydrocarbons [36]. The properties of tin-fluoride-phosphate glasses and their possible network repeat unit were elucidated in a work by Tick (1984) [2]. Xu and Day supported Tick's study in further researches [37, 38].

Table 2.2: Examples of low Tg glasses compositions present in literature [34].

System	Components	SnO (mol%)	Tg (°C)	Range of melting (°C)
Sn-Si-O	$SnO-SiO_2$	17-72	651-428	950
Sn-B-O	$SnO-B_2O_3$	58	350	900-1100
Sn-B-O	$SnO-B_2O_3$	75-77	Max 384	850-1200
Sn-P-O	$SnO-P_2O_5$	50-85		500-1200
Sn-P-O	$SnO-P_2O_5$	40	1500-300	500-1200
Pb-Sn-P-O-Cl	$SnCl_2$-$PbCl_2$-P_2O_5	50-75	189-225	500
Sn-P-O-Cl	$SnO-SnCl_2$ - P_2O_5	80	75-160	450
Sn-P-O-Cl	$SnO-SnCl_2$ - P_2O_5	60	170-220	500
Sn-P-O-Cl	$SnO-SnCl_2$ - P_2O_5	70	350	500
Sn-P-O-F	SnF_2 -P_2O_5	20-75	70-260	450

A basic structural unit for these glasses is an ortho-phosphate unit, similar to A_lPO_4 or BPO_4, and is composed of Sn-O-P-O bonds (Figure 2.12). In this case, the divalent acts as network former, in tetrahedral coordination bonding with phosphorus via oxygen (Sn-O-P).

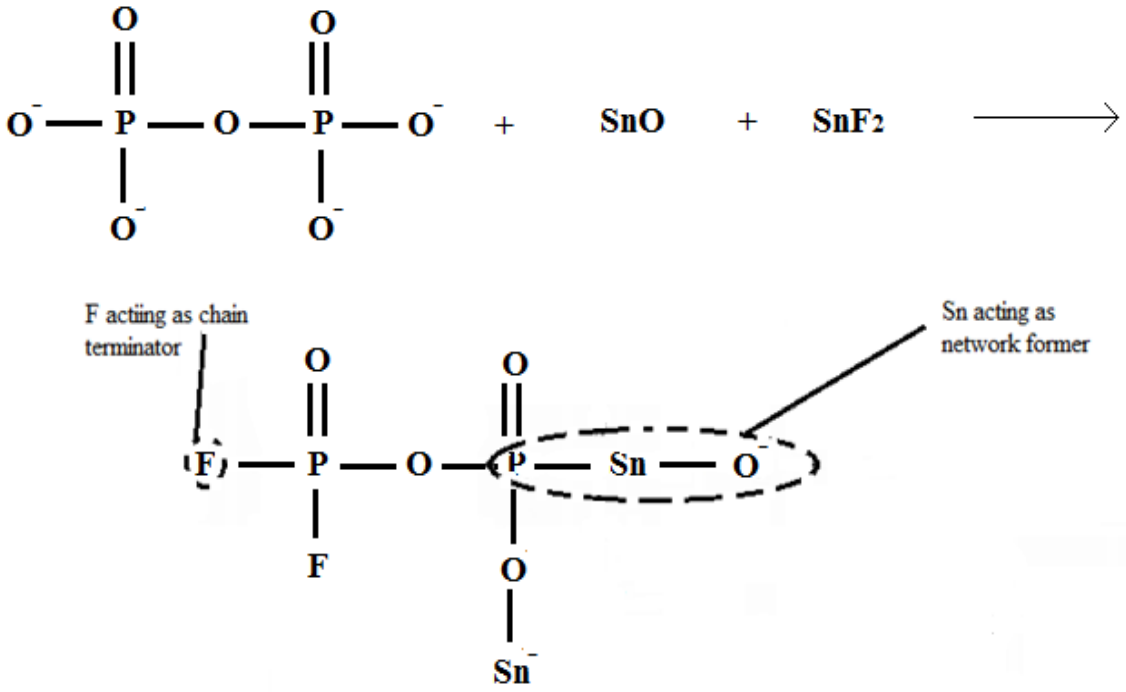

Figure 2.12: Sn-O-P-O bonds are formed when Sn is added to a phosphate glass network Sn behaves a network former while F behaves as a chain terminator [36-38].

Tick has also proposed that the linkage of the glass network increases as the P-O-P and Sn-O-P bridges increase [36]. Weak points in the network are provided by the low water resistance of both Sn-F-Sn and P-O-P and, since P-O-P bridges are incorporated in the basic structural unit, it follows that durability would be inversely proportional to the number of P-O-P bridges. Sn-F-Sn bridges are of lesser importance [36, 37].

Excess of tin and fluorine result in the structures shown in Figure 2.13.

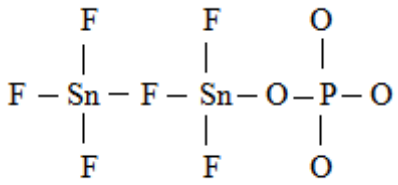

Figure 2.13: Structure of phosphate glasses resulting by an excess of tin and fluoride [36].

The formation of these units decreases the linkage of the network, resulting in a decrease in viscosity, glass transformation temperature, and chemical durability as the tin and fluorine content increases [36, 37].

The experimental evidence suggests structural changes in the glass network occur at or near to 40 mol% of P_2O_5 [36-38]. A decrease in the P_2O_5 content leads to an increase in the Sn-O-P-O bridges, a decrease in the number of weak sites (P-O-P bonds) and an increase in the linkage of the glass network [36-38]. A significant increase in density was measured at approximately 40 mol% P_2O_5, which is also the composition exhibiting the best resistance to attack by water. At this composition the P:Sn ratio might be optimal as the number of Sn-O-P-P bonds is at a maximum; any further decreases in the P_2O_5 content eventually results in the formation of Sn-F-Sn, which are also easily attacked by water and which, again, lead to a decrease in chemical durability [36-38].

Both melting history and glass composition influence the amount of mass loss due to volatilisation during melting. In particular, Tick's patent [36] shows that fluorine as HF represents the major loss. Other works [35, 39-41] have observed a decrease in mass loss as SnF_2 was added to the glass composition. This behaviour is due to the structural changes which occur in the melt as the Sn^{2+} content increases, i.e. as more Sn-O-P-O bonds replace P-O-P bonds.

The glass transition temperatures of these glasses range from 75 to 150 ˚C, and in the best cases, weathering behaviour comparable to commercial soda-lime-silica glasses has been observed [35, 39-41].

2.3.7 Glass composition 50% SnF_2 + 20% SnO + 30% P_2O_5 mol%

A specific molar glass composition, 50% SnF_2+ 20% SnO + 30% P_2O_5, whose structure is shown in Figure 2.14, has been the subject of recent research efforts.

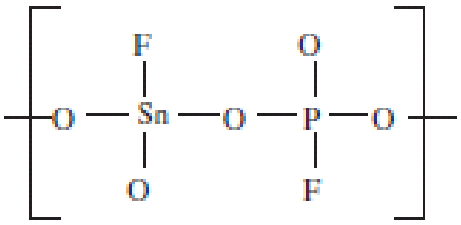

Figure 2.14: Structure of 50% SnF_2+ 20% SnO + 30% P_2O_5 as described by Tick [2, 36].

This composition results in a phosphate glass with a Tg of approximately 125 ˚C and a density of 3750 Kg/m^3 [2, 36]; due to their low Tg, these type of glasses are liquid over a range of temperatures overlapping the melt processing temperature of many polymers; this opens up the possibility of blending these inorganic glasses with inorganic polymers by conventional processing techniques and developing new inorganic/organic hybrid materials containing phosphate glass loadings of up to 60% by volume [2, 31, 36, 42-44].

The rheological behaviour of tin-fluoride-phosphate glasses has been analysed by Urman and Otaigbe in several studies [31, 42-44]. In a study conducted on phosphate glass/LDPE hybrids [45], a small rise in complex viscosity of phosphate glass at the very low frequencies was observed. This phenomenon, independent of annealing process, was found to be due to some structural rearrangement of the phosphate glass network structure [45]. In the same research [45] it was shown that the liquid phosphate glass behaved essentially like a Newtonian fluid over the 190-250 ˚C range of temperatures analyzed and over the 0.1–100 rad/s experimental range of frequencies, and its viscosity was strongly temperature dependent. The same behaviour was reported by others for zinc alkali phosphate glass in the liquid state [42]. The shear-induced crystallization of the phosphate glass was evidenced by a small increase in the viscosity and an increase in storage modulus at high frequency for these types of glasses [45].

In a research conducted by Urman et Al. on phosphate glass/PA 12 hybrids [31, 44] the phosphate glass behaved like a Newtonian fluid over the whole range of temperatures analyzed (from 190 to 250 ˚C).

2.4 Characterization of phosphate glass structure

One of the most common spectroscopy techniques used to identify the structure of phosphate glasses is the Fourier transform infrared spectroscopy (FTIR). FTIR allows identifying the structure of a material sample through the absorption of mid-IR radiation corresponding to the sample's natural molecular vibrations due to its specific molecular structure (see Appendix C). These results are typically expressed as plots of IR absorbance against wavenumber where the incident radiations wavenumber W is defined as the inverse of the signal wavelength λ as shown in Equation 2.1 [46].

$$W = \frac{1}{\lambda} = \frac{v}{c} \tag{2.1}$$

Where: W is the wavenumber; λ is the wavelength; c is the velocity of light; v is the frequency.

The absorbance/wavelength plots, in conjunction with the use of a reference spectrum database, allow the identification of the functional groups of the material sample (4000-1000 cm^{-1}) and fingerprint regions (≈ 1000-400 $cm\text{-}^{1}$) of the FTIR spectra of phosphate glasses [46].

The IR spectroscopy of phosphate glasses has been studied in many researches [47-51]. The infrared response of a phosphate network can roughly be divided into the three spectral regions related to the activity of: (a) non-bridging oxygen modes, $\nu\sim$ 940-1380 cm^{-1}; (b) bridging oxygen modes $\nu\sim$ 700-900 cm^{-1}; (c) deformation modes, $\nu\sim$ 500 cm^{-1}. Commonly, the vibrational spectra of meta-, pyro-, and ortho-phosphate and phosphate glasses show, in addition to a few P=O and $P\text{-}O^{-}$ groups, the (PO_2^{-}), (PO_3^{2-}), and (PO_4^{3-}) groups. These units, represented by Ducel et al. in [50], are shown in Figure 2.15.

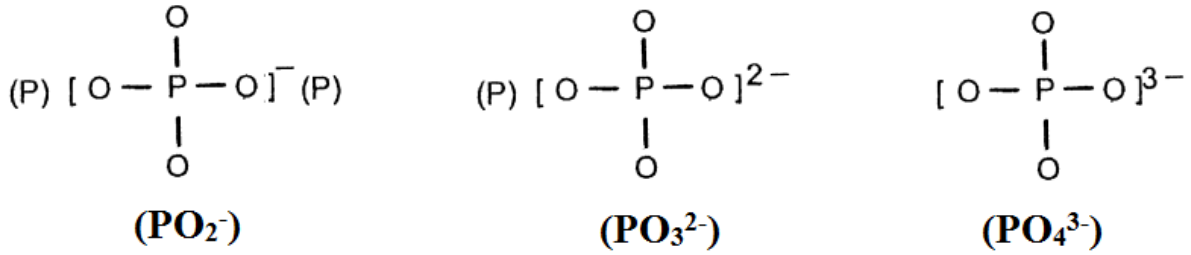

Figure 2.15: Representation of the (PO_2^-), (PO_3^{2-}) and (PO_4^{3-}) groups [50].

The (PO_2^-), the meta-phosphate unit, is linked to two phosphorous atoms; the (PO_3^{2-}) unis is linked to one phosphorous atom; the (PO_4^{3-}) unit is a monomer unit not linked with any phosphorous atoms.

The bands of P=O, P-O^-, (PO_2^-), (PO_3^{2-}) and (PO_4^{3-}) structural groups and their intensities have been found to change according to the composition ranges of the phosphate glasses. The frequency ranges found in literature [51], related to the corresponding asymmetric and symmetric vibrations of the structural groups in various phosphate glasses, are listed in Table 2.3.

Generally, the characteristic bands appearing in the vibrational spectrum of pyro-phosphate anions comprises the P=O=P bridges and the stretching vibrations of (PO_3^{2-}) terminal group [47-51]. The characteristic bands of meta-phosphate chains are the P=O=P bridge and the stretching vibrations of the (PO_2^-) terminal groups [47-51]. Therefore, any anions with intermediate chain length between those of pyro-phosphate and meta-phosphate anions show IR characteristic bands related to the P=O=P bridge and the stretching vibrations of (PO_2^-) and (PO_3^{2-}) terminal groups, [47-51]. The isolated (PO_4^{3-}) anion is the only characteristic band of ortho-phosphate anions [47-51].

X-ray diffraction (XRD) investigates the atomic/molecular structure of a material via the scattering, interference and diffraction of a monochromatic incident X-ray radiation source with the samples internal atomic arrangement (see Appendix C). Specific diffraction peaks at specific incident angles are identified by the *Bragg's Law* [52, 53]:

$$n\lambda = 2d \sin\theta \qquad (2.2)$$

Where: n is an integer; λ is the wavelength of incident X-ray; θ is the angle of incident X-ray; d is the spacing between planes in the atomic lattice.

The results are commonly expressed as plots of 2θ against intensity. The detected diffraction peaks and measured intensities, in conjunction with materials reference databases, allow the characterization of the crystalline state of the material sample.

Phosphate glasses, differently from common glasses which are amorphous, tends to crystallize. The XRD trace of a typical phosphate glass have been reported to display a clear absence of any defined crystallisation peaks over the 2θ = 5-85° range with a broad spectrum peak centred at 2θ ≈ 23°-30 [52, 53] which changes according to the glass composition. The broad peak corresponds with the dominant crystalline phase formed from phosphate glass composition [52].

Table 2.3: Frequencies of the IR related to the asymmetric and symmetric stretching vibrations of various phosphate structural groups [51].

Group	Frequency of asymmetric stretches (cm^{-1})	Frequency of symmetric stretches (cm^{-1})
P-O-P bridge	840-1050	690-800
(PO_4^{3-}) anion	980-1020	940-950
(PO_3^{2-}) terminal group	1080-1120	900-1050
(PO_2^{-}) terminal group	1080-1330	1020-1200

2.5 Processing of phosphate glasses

Conventionally phosphate glass are manufactured via melt-quenching, a simple and low cost technique where raw materials are mixed and heated inside a ceramic or platinum crucible till a homogenous melt is formed [54]. The temperature of melting typically range between 700-1500˚C depending on the proportion of each reagents for given the specific glass composition

(mol%). The melt is then quenched in water or rapidly cooled into a metal or graphite preheated mould with the production of bulk monoliths. The samples are then subjected to annealing, a process involving the slowly cooling of the sample from a set value to room temperature at a controlled rate. This step allows reducing any residual internal stresses derived from the initial cast of the glass [54]. Typically the bulk glass sample is ground into powder and sieved using ISO standard sieves to get the required particle size [54].

Phosphate glass can also be manufactured via relatively modern sol-gel processes where the sample is produced from a polymer-type reaction of a compositionally specific solution. The advantageous low processing temperature allows the incorporation of growth factors and drugs inside the sol-gel glasses and the development of polymer-glass hybrid materials [55]. Typically, these glasses exhibit higher porosity and surface area compared to the melt-derived glasses [54, 55]. Ease of control of the textural properties is documented [55]. However sol-gel phosphate glasses are reported to be especially fragile [55].

2.6 Phosphate glass/polymer blending

2.6.1 Industrial scale extrusion

A polymer blend is a macroscopically homogeneous mixture of two or more different polymers, which can be binary, ternary, or quaternary depending on the number of constituents in the blend [56]. Polymer blending is the method used to mix polymers together to create a new material with different physical properties [56]. Due to their cross-linked structures similar to polymer chain networks, inorganic phosphate glasses are generally considered to be polymeric in nature [20-22, 25-51].

The most common blending method is the hot melt extrusion [57, 58]. During this process a material, known as the *extrudate,* is pushed and/or drawn though a die via a screw by a machine, known as *extruder*, to create a shaped rod, rail or pipe. The purpose of extrusion is to deliver at a constant output rate to the forming die an extrudate uniform in temperature and molecular weight and free of contamination or faults such as bubbles or un-melted polymer.

One or more polymers and additives can be extruded at the same time to increase the quality of the final product.

An example of extruder is shown in Figure 2.16 (a); as shown, the material enters through the hopper and comes into contact with the screw. A generic screw is shown in Figure 2.16 (b); generally, a screw is composed of three sections:

- Feed sections: this zone feeds the resin into the extruder; the channel depth is constant throughout the section.
- Melting section (transition or compression zone): in this section most of the polymer is melted; the channel depth becomes progressively smaller.
- Metering sections: the last particles are melted and mixed to a uniform temperature and composition; in this section the channel depth is constant.

The plastic beads are then forced by the rotating screw forward into the barrel, heated to the desired melt temperature of the molten plastic.

Heaters are present throughout the barrel and a heating temperature profile is created to allow a gradual melting of the plastic beads as they are pushed through the barrel: generally, the temperature of the barrel is lower at the rear (where the plastic enters) than at the front because this heating profile leads to lower risk of overheating and lower degradation in the polymer. The high pressure of the process and the friction taking place inside the barrel contribute to the generation of heat. In general the energy required for melting is obtained both from the heater and the shearing effect produced by the rotating screw.

At the front of the barrel, the molten plastic leaves the screw and travels through a breaker plate. This contributes to create back pressure in the barrel. Back pressure is required for uniform melting and proper mixing of the polymer. After passing through the breaker plate the molten plastic enters the die that gives the final product profile.

The product must then be cooled in a water bath. Once the product has cooled, it can be spooled, or cut into lengths for later use. Extrudates can also be processed by downstream

methods after extrusion, such as cutting into pellets, or being milled into powder after cooling. It is recommended to premix raw materials before the hot melt extrusion process itself. Since the moisture or water can function as a plasticizer and affect the process as well as the long term stability of the final products, all components in the desired formulation should be dried to avoid any moisture absorption.

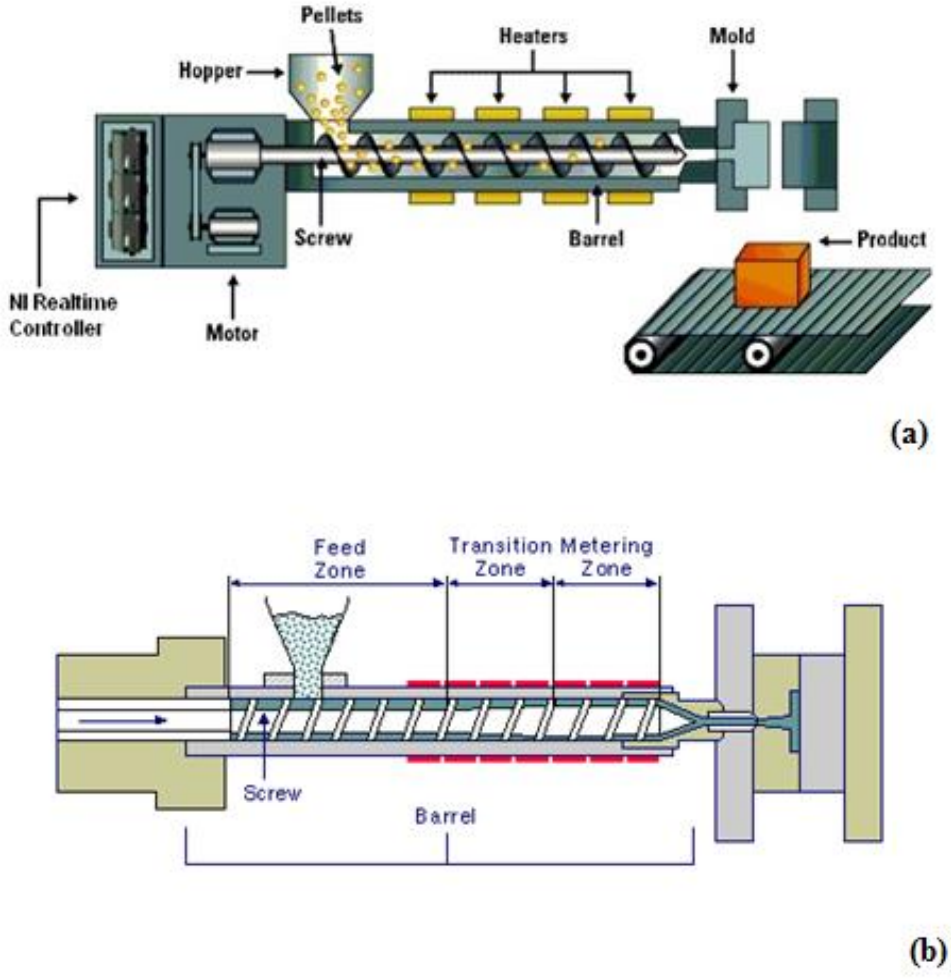

Figure 2.16: (a) Example of a single screw extruder [58]; (b) feed zone, transition zone and metering zone in a single screw extruder [59].

2.6.2 Flow mechanisms of glass/polymer blends in a twin screw extruder

The main types of screw configuration used in hot melt extrusion are single screw and twin screw extrusions. Even though the single screw extruder is efficiently used for profiling applications, it has limited use in more rigorous compounding applications [58] as it may not provide sufficient mixing of different materials if the screw is not long enough [57]. Twin-screw extruders utilize two screws usually arranged side by side which rotate in the same or opposite directions (co-rotation and counter-rotation, respectively).

The barrel with the screws is the key part of the extruder, not only for imposing high temperature and pressure on the materials to ensure a uniform mix, but also to convey the mixtures as a continuous transportation. The co-rotating twin screw extruders have become the most important commercial machine for continuous compounding of thermoplastic [58].

Understanding the flow mechanisms around a twin screw extruder is challenging but can help to optimize the mixing process between the polymer and the phosphate glass phase.

The geometry of a twin-screws extruder is highly complex, especially in the vicinity of the inter-screw regions. Furthermore, the melt undergoes large deformations because of the strong shear flow field produced by intermeshing screws [58, 60].

The flow fields of a twin screws extruder can be divided into two regions: the intermeshing region, in which the screws intermesh and the convey region, where the flow is considered to be similar to the one of a single-screw extruder. The advantages of a twin-screw extruder over a single-screw extruder are often attributed to this intermeshing region [60]. However, due to the high shear stress produced by the two screws, droplet interactions (rupturing, coalescence, and suspension) can take place affecting the microstructure of melt [60].

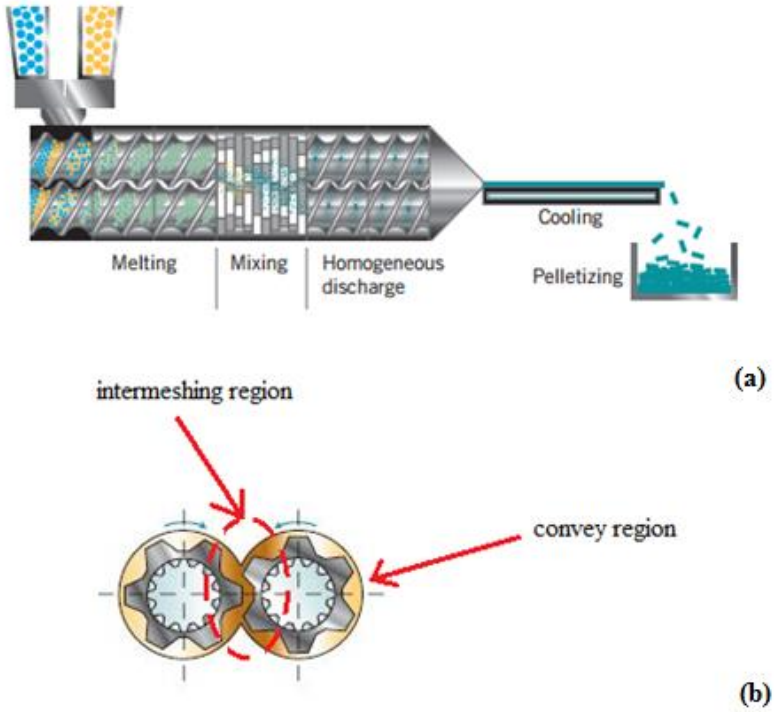

Figure 2.17: (a) Example of a twin-screws extruder; (b) Inter-meshing region and convey region in a twin-screw extruder [60].

Figure 2.18 shows the flow configurations along the twin screws axis. The flow dynamic of conventional glass/polymer blends can be summarized in four steps, even though the details can vary depending to the specific rheological behaviour of the melt [60]:

1. Formation of glass drops in the polymer matrix liquid phase: the shear stresses induced by the action of the mechanical devices favours the formation from the two liquid phases of large drops of glass, the minority phase.

2. Rupture and coalescence of glass drops: the glass drops are broken up into small droplets by the twin-screw at high speeds.

3. Collision of glass droplet and polymer particle: the turbulent flow, mainly activated by mixing, causes the glass droplets to be broken up into finer droplets by collision with polymer solid particles.

4. Dispersion and suspension stability: the glass droplets are dispersed by turbulence and suspended in the polymer matrix phase by the increased viscosity of the polymer matrix phase in semi-solid state.

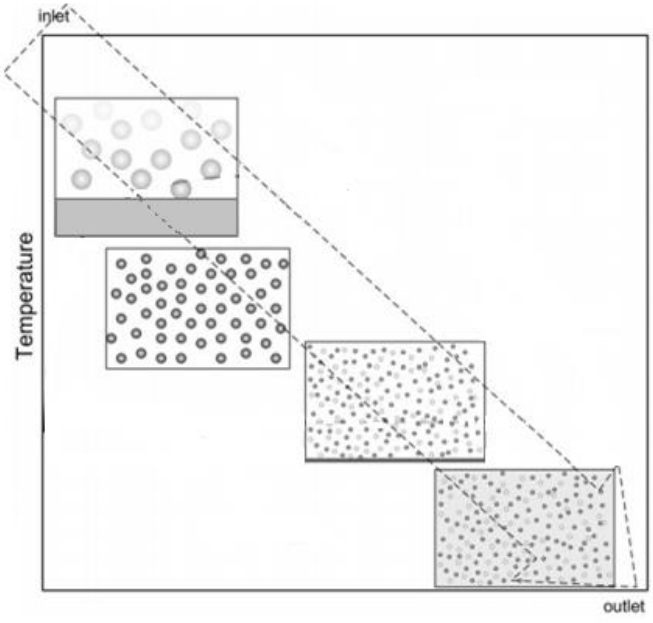

Figure 2.18: Morphology change of glass droplets along the twin screw extruder [60].

2.6.3 Flow mechanisms of polymer/polymer blends in a twin screw extruder

The majority of polymeric blends are immiscible because of the small gain in entropy and unfavourable interactions among the polymeric components [61]. The morphology development of immiscible polymer blends subjected to shear flows has been recently well understood [61]. The majority of immiscible polymer blends have a morphology consisting of droplets dispersed in matrix phase. The inclusions of a biphasic liquid/liquid system subjected to flow and shear stress undergo many mechanisms of microstructural change such as droplet deformation and orientation, droplet break-up and coalescence [61]. The microstructural changes depend on the viscosity ratio and the interfacial forces between the blend components. The ratio between the hydrodynamic and the interfacial stresses is expressed as:

$$Ca = \eta_m \dot{\gamma} R/\alpha \tag{2.3}$$

Where: Ca is the capillary number; η_m is the viscosity of the matrix phase; $\dot{\gamma}$ is the shear rate; R is the radius of the droplet; α is the interfacial tension.

During flow, droplet break-up may occur above a critical value of the capillary number Ca_{crit} by different mechanisms [61] as summarized in Figure 2.19; here, the X-axis is the ratio of the viscosities of the dispersed phase η_d and the matrix η_m.

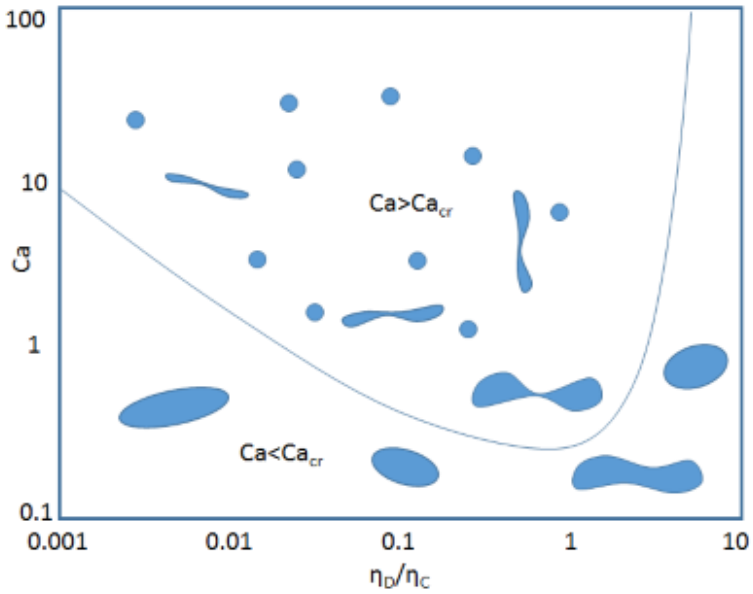

Figure 2.19: Representation of the different modes of deformation and break-up in a biphasic liquid/liquid polymeric blend in shear flow [61].

Whenever $Ca \gg Ca_{crit}$ the droplet will extend and very long threads will be formed. These threads finally break up in multiple droplets. When a relatively fast flow is applied to a biphasic polymeric system, the droplet break-up is delayed [61].

2.6.4 Laboratory scale extrusion

Laboratory scale extrusion can be used to conduct a variety of mixing tests on different types of materials and to avoid the wastage of expensive raw materials for experimental formulations [4-6, 8, 12, 31, 35, 44, 45].

One of the most common melting equipment used in literature to compound inorganic/organic phosphate glass/polymer hybrids is the C.W. Brabender® Plastograph® internal mixer [4-6, 8, 12, 31, 35, 44, 45], a torque rheometer capable of measuring the resistance of the sample material to the rotating blades. This equipment consists of an electrically heated mixer/measuring head that is a miniature internal mixer on a laboratory scale volume. The material blend is homogenised by two non-intermeshing, counter-rotating mixing blades.

The torque generated by the mixing process moves a dynamometer out of its zero position. A typical *plastogram* (torque and stock temperature vs. time) is recorded for each sample material. This diagram shows the relationship between torque and temperature/time in consideration of structural changes of the material. To ensure the complete mixing of materials and composites, the melted materials is recirculated back into the constant-temperature heating zone. The melted materials can be recirculated through the mixing zone several times before being discharged from the extruder.

Thanks to the Brabender three separate, independent heating zones a precise and constant heating/cooling profile can be achieved with operating temperatures of up to 500°C [61]. However, as the geometry of the mixer and blades differs from a common extruder and extrusion screws, the behaviour of a melt during the extrusion process is not reproduced accurately by the Brabender [100].

The Brabender was used in a few studies [4-6, 8, 12, 31, 35, 44, 45] to develop experimental phosphate glass/polymer hybrids. In the research by Urman et al. [45], LDPE hybrids containing the desired amount of phosphate glass were mixed at 200˚C [66], while the polyamide 6 and the polyamide 12 were mixed at 250˚C [5, 6] and 220˚C [31, 44], respectively. Prior to processing, the materials were dried in a vacuum oven to avoid moisture adsorption [4-6, 8, 12, 31, 35, 44, 45]. The Brabender was calibrated to the appropriate mixing speed. In order to reach the thermal equilibrium, the equipment was preheated to the desired mixing temperature for at least 20 min before mixing [4-6, 8, 12, 31, 35, 44, 45]. The polymer was added to the mixing bowl. After producing a homogeneous melt the required amount of phosphate glass was added to the mixer and blended for the necessary period of time. The addition of the hybrid component materials to the Brabender was monitored in a

graph of torque versus time. The melted hybrid materials were collected in *chunks* and dried in a vacuum oven. The samples were then formed into a variety of shapes for testing using both compression moulding and injection moulding. The mould was kept similar to that one used during melt-mixing [4-6, 8, 12, 31, 35, 44, 45].

2.7 Miscibility of phosphate glass/polymer hybrids

As one of the objectives of this thesis is the identification of a potentially useful low Tg glass/polymer blend combination, it is important to distinguish between the definition of a miscible polymer blend, where the criteria for true thermodynamic miscibility must be satisfied, and experimental detection of apparent miscibility.

In this section a general overview of polymer blends is presented. After discussing the basis of thermodynamics of polymer blends, the concept of miscibility and some related terms will be defined. The method used in this work to prove the miscibility between the blend components in the hybrids will be described. Furthermore a literature of rheology and miscibility of phosphate glasses/polymers will be presented.

2.7.1 Definition of miscibility

According to the International Union of Pure and Applied Chemistry (IUPAC) "Miscibility is defined as the capability of a mixture to form a single phase over certain ranges of temperature, pressure, and composition" [56].

Whether or not a single phase exists depends on the chemical structure, molar mass distribution, and molecular architecture of the components present.

In the case of polymers that are physically and chemically similar, the occurrence of miscibility is comprehendible. For dissimilar polymers, the major driving force for miscibility must be the enthalpic contributions to the free energy [62]. There are two non-mutually exclusive ways of explaining favourable enthalpic contributions [62, 63]: positive interactions between the two polymers, and unfavourable interactions between groups on the same polymer, causing an overall favourable interaction with another polymer.

Examples of favourable interactions between the polymer chains include specific intermolecular interactions, such as Lewis acid–base interactions involving hydrogen bonds. In these cases, phase separation that occurs on heating may be due to dissociation of the hydrogen bond matrix. If the groups within the same polymer chain have a large enough unfavourable interaction, they will prefer to mix with another polymer group, in order to minimize the number of unfavourable–unfavourable contacts [62].

According to the thermodynamics of blends, the IUPAC definitions for miscible, compatible, and immiscible polymer blend are as follows [56]:

1. A *miscible polymer blend* or homogeneous polymer blend is a polymer blend that exhibits miscibility. One must be aware of the following points, though:
    - For a polymer blend to be miscible, it must satisfy the criteria of miscibility.
    - Miscibility is sometimes erroneously assigned on the basis that a blend exhibits a single Tg or optical clarity.
    - A miscible system can be thermodynamically stable or metastable.
    - For components of chain structures that would be expected to be miscible, miscibility may not occur if molecular architecture is changed, e.g., by crosslinking.
2. A *immiscible polymer blend* or heterogeneous polymer blend is a polymer blend that exhibits immiscibility.
3. A *compatible polymer blend* is an immiscible polymer blend or partially miscible polymer blend in which part of one blend component is dissolved in the other. Generally a compatible polymer blend exhibits macroscopically uniform physical properties throughout its whole volume caused by sufficiently strong interactions between the components.

The terms immiscibility, miscibility, and compatibility are sometimes misused and given different meanings. Many research papers classify as immiscible those polymer blends or heterogeneous polymer blends that show distinct glass transition temperature (Tg) for each

polymer components, while classifying as miscible polymer blends or homogeneous polymer blends those that show a single Tg from a single phase structure.

2.7.2 Thermodynamics of miscibility

As phosphate glasses can considered to be polymeric in nature [20-22, 25-51], the thermodynamic principles that govern the miscibility of polymer blend can be applied to the thermodynamics of mixing of phosphate glass/polymer hybrids.

The fundamental relationship used to describe the behaviour of polymers and/or polymer-like materials in solution is given by [56, 58]:

$$\Delta G_m = \Delta H_m - T\Delta S_m \quad (2.4)$$

Where: ΔG_m is the Gibbs free energy of mixing; ΔH_m is the enthalpy of mixing; ΔS_m is the entropy of mixing.

The change in the free energy of mixing (ΔG_m) should be negative for a homogenous polymer solution to be formed [56]. Thus, assuming a system composed by component A and component B, the sum of the individual free energy of each component of the mixture (G_A + G_B) should be higher than the free energy of the solution (G_{AB}):

$$\Delta G_m = G_{AB} - (G_A + G_B) < 0 \quad (2.5)$$

This criteria is necessary (but not sufficient) for the miscibility of polymers in a solution [56].

For high molecular weight polymer blends, the gain in entropy is negligible [56]. Hence, the free energy of mixing can only be negative if the heat of mixing is negative [56]. Thus, according to the first criterion of miscibility, the free enthalpy of mixing must be negative, so:

$$\Delta H_m - T\Delta S_m < 0 \quad (2.6)$$

This means that the mixing must be exothermic, which usually requires specific interactions between the blend components [56]. These interactions may range from strongly ionic to weak and non-bonding, including hydrogen bonding, ion-dipole, dipole-dipole, and donor-

acceptor interactions [56]. Here, ΔH_M denotes the enthalpy of mixing and $T\Delta S_M$ denotes the entropy of mixing.

The enthalpic and entropic contributions can be expressed as functions of component volume fractions according to the lattice theory [62]:

$$\Delta H_m = RTn_1\Phi_2\chi_{12} \tag{2.7}$$

$$\Delta S_m = -R(n_1 \ln(\phi_1) + n_2 \ln(\phi_2)) \tag{2.8}$$

Where: $\Phi_{1/2}$ is the molar fraction of component 1/component 2 in the mix; R is the Boltzmann gas constant (1.3806×10^{-23} J/K); T is the temperature in Kelvin degrees; $n_{1/2}$ is the number of moles of molecules of component 1/component 2; χ_{12} is the Flory-Huggins interaction parameter, a dimensionless quantity which characterizes the interaction energy.

Assuming that the combinatorial entropy represents the total entropy change (ΔS_m), Equation 2.7 and Equation 2.8 can be combined in order to give the expression for the free energy of mixing in polymer solutions, i.e. $\Delta G_m = \Delta \mathrm{H}_m - T\Delta S_m$, as:

$$\Delta G_m = RT(n_1 \ln(\phi_1) + n_2 \ln(\phi_2) + n_1\Phi_2\chi_{12}) \tag{2.9}$$

This is the classical Flory-Huggins expression for the free energy change on mixing polymer and solvent components [56] and is a major foundation stone in polymer solution thermodynamics.

Considering that:

$$n_1 = \phi_1/v_1 \tag{2.10}$$

and

$$n_2 = \phi_2/v_2 \tag{2.11}$$

Where v_1, v_2 are the molar volumes of the component 1 and component 2 respectively.

Combining Equation 2.9, Equation 2.10 and Equation 2.11 results in Equation 2.12, the Flory-Huggins expression for the free energy of mixing of a binary polymer blend [64]:

$$\frac{\Delta G_m}{RT} = \frac{\phi_1}{v_1} ln\, \phi_1 + \frac{\phi_2}{v_2} ln\, \phi_2 + \phi_1 \phi_2 \frac{\chi_{12}}{v_1} \tag{2.12}$$

By examining the temperature and composition dependence of the free energy change on mixing polymer components, as previously derived by the Flory-Huggins lattice theory, predictions can be made regarding the phase equilibria and miscibility within these systems.

2.7.3 Miscibility and Melting Point Depression

The *melting point depression* is a thermodynamic approach derived from the original Flory-Huggins lattice theory used to characterised miscibility in blends. This technique shows good agreement with other predictors of blend miscibility and with experimental observations via microscopy [62-66].

At the equilibrium melting point (T_m^0) of a semi-crystalline polymer, the amorphous and crystalline phases are in equilibrium i.e. the chemical potential (μ) of both phases are equal ($\mu_a = \mu_c$). If a low molecular weight diluent is added to the amorphous phase, the chemical potential μ_a of this phase is reduced. To re-establish the equilibrium position ($\mu_a = \mu_c$) the crystalline phase melts at a lower temperature [62-66], i.e. the "diluent effect" can be said to depress the melting point of the crystalline phase. The thermodynamic considerations of mixing in polymer-diluent systems [64] have been successfully extended to crystalline polymer-amorphous polymer systems by Nishi and Wang [67]. Amorphous polymers which are miscible with the amorphous phase of semi-crystalline polymers can act as diluents, depressing the melting point of the crystalline phase, as discussed above.

A quantitative analysis of the melting point depression in binary polymer blends, based upon studies by Scott [68] and developed by Nishi and Wang [67], is shown below:

$$\frac{1}{{T_{mb}}^0} - \frac{1}{{T_m}^0} = -\frac{RV_2}{\Delta H_2 V_1}\left[\chi {\phi_1}^2\right] \tag{2.13}$$

Which is the well-known Nish-Wang expression [70], relating the equilibrium melting point depression to the thermodynamic mixing i.e. miscibility, of crystalline and amorphous polymers. This equation clearly shows the decisive role of the interaction parameter, χ on the melting behaviour of the crystalline polymer/amorphous polymer blends and hybrids. The χ values are estimated by conventionally plotting $\frac{1}{{T_{mb}}^0} - \frac{1}{{T_m}^0}$ against ${\phi_1}^2$ and deriving χ from the slope. In this case, a depression in melting point can only be achieved if χ is negative, which agrees with Scott's condition for miscibility to occur between the two polymers [68].

The use of melting point values of various blend compositions to determine χ values is based on the view that the depression in the melting point of a semi-crystalline polymer is primarily the result of thermodynamic interactions between the crystalline phase and a miscible amorphous phase (consisting of a mixture of the two polymers) with which it is in equilibrium. The determined melting points should therefore strictly be equilibrium values (${T_m}^0$) i.e. the "true" melting temperature of the crystalline phase at infinite lamellar thickness without morphological changes such as imperfections and thickness variations within the crystalline regions which can also be responsible for melting point variations [71].

The ${T_m}^0$ value of a completely crystalline polymer is never actually achieved and is usually determined by DSC using the indirect method of plotting melting temperature (T_m) against crystallization temperature (T_c) and extrapolating to $T_m = T_c$ to give the ${T_m}^0$value.

2.7.4 Melting point depression in phosphate glass/polymer hybrids

Urman et al. analysed in [5] the miscibility between the two components of a phosphate glass/polymer hybrid using the melting point depression technique. The drop in melting point was attributed to thermodynamically favourable interactions between the polymers, and the melting point depression was used to successfully calculate the miscibility parameter χ between two components of a blend in many different systems using the mathematical model of the Flory-Huggins solution theory [69]. The calculated χ value (–0.067) satisfies the condition for polymer miscibility and represents the first reported evidence of miscibility of inorganic glass and organic polymer [5].

A few recent researches by Urman et al. [5, 6, 31, 44, 45] found that phosphate glass act as plasticizer for a polyamide matrix. Plasticizers are materials that are blended into polymer to improve its processability and reduce the risk of thermal degradation during processing. Plasticizers, generally, affect the matrix properties by lowering its melt viscosity and glass temperature resulting in greater adhesion, reduced phase separation and ultimately, a decrease in the tensile modulus of polymer matrix and an increase in both the elongation at break and impact strength [5, 6, 31, 44, 45]. The ideal plasticizer is expected to be a polymer-like material composed by segments having good soluble (or miscible) affinity for segments of polymer chain, and showing a glass transition temperature (Tg) similar to the one of polymer chains.

Phosphate glass/polyamide 6 was examined by Urman and Otaigbe in several studies [5, 6] which found that the sites for potential interaction between the polyamide 6 and phosphate glass were doubled compared to the use of polyamide 12 as polymer matrix [31], leading to a stronger interaction between the two components and an higher degree of miscibility.

2.7.5 Miscibility and glass transition temperature

One of the most fundamental measurements made on polymeric materials is the measurement of the glass transition temperature Tg. In general, transitions in materials are associated with distinct localized and medium-to long-range cooperative motions of molecular segments. The glass transition is associated with cooperative motion among a large number of chain segments, including those from neighbouring polymer chains.

A common experimental method of classifying a miscible blend on a macroscopic scale is the identification of a single Tg value lying between the Tg values of the pure blend components. In this case miscibility would be an indication of blend homogeneity on a size scale similar to that responsible for the Tg values of the polymer components. However, the claim of miscibility is hard to support when macroscopic and microscopic experimental evidence conflicts; for example in some polymer blends, heterogeneous (immiscible) structure has been observed at high levels of magnification even though macroscopic properties, e.g. a single Tg, imply single phase behaviour [64, 65].

Other studies have often claimed miscibility on the basis optical clarity and a single Tg of the experimental samples. However these results may be observed just because the samples are kinetically frozen in a state of apparent miscibility, which is not permanently miscible. So, while it is perfectly legitimate to make an experimentally based comment about the sample at that time when clarity and single Tg are observed, it is not enough evidence to assume that the thermodynamic conditions for miscibility have been precisely met [64, 65].

Although there are several thermal techniques available to make Tg measurements, by far the most sensitive technique is dynamic mechanical analysis, DMA, which works by applying a sinusoidal deformation to a sample of known geometry. The sample is subjected to a controlled stress or a controlled strain. For a known stress, the sample will then deform a certain amount. Under tension/compression deformations, the measured elastic component is referred to as the *storage modulus* (E'), while the measured viscous component is referred to as the *loss modulus* (E″) [72]. The ratio of the loss modulus to the storage modulus is referred to as the *loss tangent* (E″/E′), or *tan δ* [72]. In addition, a *complex dynamic modulus*, denoted by E*, is calculated as the magnitude of a complex number which is defined by a real elastic part (E′) and a imaginary viscous component (E″): E* = E' + iE". The DMA gives information on the change in stiffness and energy dissipation of the sample. In particular, the loss factor tan δ (dissipation factor) corresponds to the dissipation of energy during solicitations, in particular during glass transitions. Often, the glass transition Tg of the sample is identified as the temperature that maximizes tan δ, a value that usually agrees with the inflection point of the complex dynamic modulus when plotted as a function of temperature.

Differential scanning calorimetry (DSC) is another technique utilized to determine glass transition of materials. It involves the simultaneous application of a heat flow to the sample and a reference while measuring the differential heat flow between the sample and a reference. DSC is typically used to detect and measure the melting temperatures of polymers and biomaterials through measurement of enthalpic changes undergone by these materials during phase transitions produced by changes in temperature. The heat (enthalpy) needed for melting (J/g), as well as, the onset, final, and conclusion melting temperatures are typically measured with a DSC instrument. In a conventional DSC, the temperature is increased linearly as a function of time. Usually different molecular segmental motions accompany the glass transition

temperature and thus result in small relaxation endotherms [72]. In some cases, the glass transition is hard to detect using the conventional DSC methodology.

Even though both DMA and DSC methods reveal similar information, the two instruments vary greatly not only in their analyses and sample preparation, but also in their sensitivity. Temperature transitions are more detectable by DMA than by DSC as mechanical changes are more dramatic than changes in the heat capacity and DMA is able to detect short range motion before the glass transition range is attained and thus identify the onset of main chain motion [72]. DSC has been shown to also be of limited use in measuring the Tg of certain hybrid-materials [72]. This has been explained by the amorphous (where a Tg range is observed) and crystalline (where melting is observed) zones of the hybrid granule which make the Tg thermal events difficult to detect especially when they occur close to the melting point.

2.7.6 Transition temperatures behaviour in phosphate glass/polyamide 6 hybrids

The effect of phosphate glass on the glass transition temperature of a phosphate glass/polyamide 6 (PA 6) hybrid system was examined by Urman et al. in [5, 6] where the Tg was detected by dynamic mechanical analysis (DMA). All measured hybrids indicated a single glass transition temperature, whose value was dependent on the phosphate glass concentration. Also, the presence of glass caused the decrease of the Tg of the hybrid, which has been attributed to partial miscibility of the components in the polymer blend [5, 6, 64, 65, 73, 74]. The dynamic mechanic analysis results in [5, 6] suggested a plasticizing effect of the phosphate glass on the tensile mechanical properties of the hybrids as well as a high degree of interaction, demonstrated by a 10 K drop in Tg when the glass amount was increased. The Young's Modulus and the energy at break decreased with increasing phosphate glass content in the hybrid, matching the effects of the addition of a plasticizer to a pure polymer, as reported in [5, 6, 64, 65, 73, 74]. This behaviour is the opposite of that of conventional solid glass filler composites, where an increase in Young's modulus and a decrease in the strain at break are observed as reported in [17, 58].

[5, 6] also investigated the temperature dependence of dielectric loss of the pure hybrid components and phosphate glass/PA 6 hybrid with 10 vol% of phosphate glass. The results suggested a partial miscibility of phosphate glass and PA 6 in the solid state.

A single relaxation occurred in the pure phosphate glass, most likely due to separated ion pairs. This characteristic was not evident in the isochronal graph of the hybrid due to the high conductivity of the pure phosphate glass at high temperatures [5, 6].

Three relaxations were identified for the hybrid and the pure PA 6: a γ-relaxation at low temperature, β-relaxation, and an α- relaxation at higher temperature [5, 6]. The γ-relaxation was related to the motion of very short $–CH_2$ segments and an amide group. This characteristic remained similar in the hybrid and the pure PA 6 due to the inability of phosphate glass to significantly impact very short (i.e., approximately two $–CH_2$ units) motions. The β-relaxation, appearing at lower temperature in the hybrid than in pure PA 6, was attributed to $-NH_2$ and -OH chain. The effect of water-polymer complex on β-relaxation was considered to be negligible due to the drying procedure performed on the hybrids prior to testing. The highest temperature relaxation, α- relaxation, was related to large-scale motions of the chains segment in proximity of Tg. This single relaxation was observed in the hybrid at a lower temperature than either of the pure components, implying that the addition of phosphate glass to the PA 6 accelerated the α-relaxation of the polymer chains. This behaviour was associated to a possible physiochemical interaction between the hybrid phases.

In the same studies, the hybrids showed a lower apparent activation energy than pure PA 6 and phosphate glass which, together to the reduction of the hybrid's Tg was attributed to a partial miscibility of the pure components of the hybrid in the solid state [5, 6].

Urman et al. conjectured in [5, 6] that the addition of phosphate glass to the hybrid modified the relaxation in a similar way similar to polymers reinforced with nano-sized fillers. The phosphate glass was assumed to be distributed on the molecular level in the PA 6 matrix, to decrease the intermolecular hydrogen bonding of the polyamide 6 chains, and to disrupt the network of hydrogen bonded long chains. This could result in an autonomous chain movement and the accelerated long range segmental motions related to it, as discussed before.

The transmission electron microscopy (TEM) analysis of phosphate glass/polyamide 6 in [5, 6] showed a two-phase microstructure with the phosphate glass being distributed as droplets in the polymer matrix, which conflicts with the presence of a single Tg in the hybrid system, as mention above, which, as discussed earlier, makes the claim of miscibility harder to support.

2.8 Rheology of tin-fluoride-oxy-phosphate glass/polymer blending

As understanding the rheological behaviour is crucial in determining the final morphology of the material, a large number of studies has been focused on characterizing the hybrid viscoelastic proprieties. These works reported on phosphate glass mixed with LDPE, polypropylene, polystyrene (PS), polyphenilene sulphide (PPS), polytherimide (PEI), polyrysulfone, poly(ether ether ketone) (PEEK), and a liquid crystalline polymer (LCP) [74-77].

2.8.1 Shear rheology

The shear viscosity is defined as the resistance of a material against the flow and is defined as the ratio between the applied shear stress τ and the shear rate $\dot{\gamma}$ [72]. Oscillatory shear measurements are usually obtained by subjecting a specimen to an oscillatory stress σ and determining the elastic and viscous response and damping characteristics using a cone and plate viscometer.

The cone is forced into oscillatory shear (angular frequency ω) or rotation. The sample is placed between the plate and the cone. The sample, generally exposed to a sinusoidal strain $\gamma = \gamma_0 \sin \omega t$ at an angular frequency of ω, will respond with a gradual approach to a steady sinusoidal stress $\sigma = \gamma_0\left(G'(\omega) \sin \omega t + G^{"}(\omega) \cos \omega t\right)$, where G' is the storage modulus, $G^{"}$ is the loss modulus and the dynamic viscosity η' can be determined as $G^{"}/\omega$. The loss tangent $\tan \delta = G^{"}/G'$ is the measure of damping of the sample.

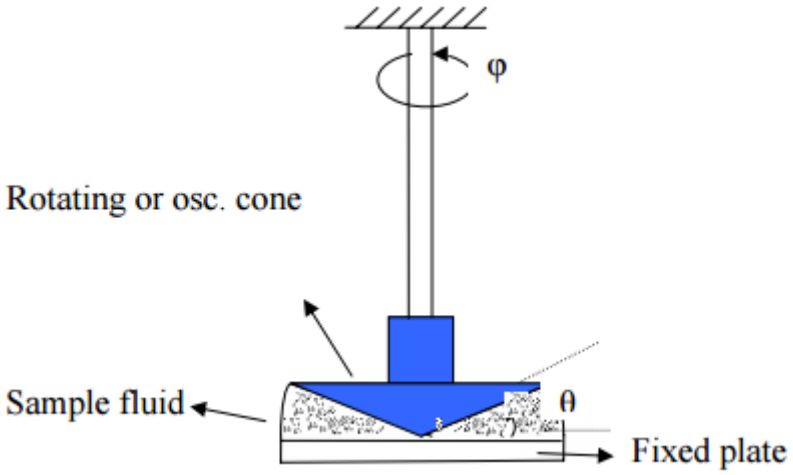

Figure 2.20: Cone and plate viscometer [78].

2.8.2 Elongational rheology

Phosphate glass/polymer hybrids are generally prepared by extrusion, which is essentially dominated by extensional flow. The final product properties are strongly affected by phenomena related to extensional flows, considerably orienting molecules, asymmetric particles or the dispersed phase in blends. It is thus fundamental to study the elongational rheology behaviour of the hybrid materials. Furthermore the elongational viscosity at large strains is more sensitive to variations in long chain branching than the linear viscoelastic shear properties.

The elongational viscosity η_E is defined as the stress, i.e. the force divided by the surface area normal to the direction of deformation, divided by the elongation rate [72]. For an incompressible material, the volume is conserved and the surface area must decrease exponentially as $A(t)=A_0 \exp((d\varepsilon H/dt)t)$ with the sample length increasing (Figure 2.21) while the experiment proceeds.

The elongational viscosity is generally determined by a rotary clamps rheometer. The sample is elongated within a confined space and expelled with rotary clamps put in motion by an actuator. One clamp is rotating; the clamp measuring the force is fixed and can be directly coupled with the torque transducer. During the experiment the reactive force at the transducer is measured as a function of time or deformation. After a short period, the measured force

goes through a maximum and continuously decreases from then on more or less exponentially. The reason for the force decrease is the exponentially decreasing cross section of the sample with increasing total deformation. The corresponding viscosity is calculated as the ratio of the force F(t) and sample cross section A(t) divided by the elongation rate $\dot{\varepsilon}_0$.

$$L_o w_o h_o = L_o A_o = const. \quad \text{(incompressible)}$$
$$\Rightarrow A(t) = A_o e^{-\dot{\varepsilon}_o t} \text{ and } h(t) = h_o e^{-\frac{1}{2}\dot{\varepsilon}_o t}$$
$$\Rightarrow \sigma_E(t) = \frac{F(t)}{A(t)} = \frac{F(t)}{A_o} e^{\dot{\varepsilon}_o t} \text{ and } \eta_E(t) = \frac{\sigma_E(t)}{\dot{\varepsilon}_o}$$

Figure 2.21: Elongational stress and viscosity in a uniaxial elongation experiment.

2.8.3 Rheology studies on tin-fluoride-oxy-phosphate glass/polymer blends

The rheology of the hybrids of zinc alkani phosphate glasses (Tgs > 272˚C) and thermoplastic with high melt flow temperature have been analysed in [74-77] which characterize these materials by a variety of morphologies, such as droplets and fibrils. It was shown that processing history was an essential factor in determining the final morphology and properties of zinc alkali phosphate glass/LCP and zinc alkali/poly(ether ether ketone) hybrids. The polymer matrix of these systems was found in [74] to affect the thermo-rheological stability of hybrids.

Young et al. analysed in [77] the processing behaviour of phosphate glass/PEI systems. In this work the rheology of PEI matrix was modified by phosphate glass and the processability of PEI was found to be improved.

No changes in viscosity at high shear rate were reported in [75, 76] for Xydars/LCP [poly(p-hydroxybenzoic acid-cobisphenol terephthalate)] hybrids compared to the pure LCP system. In opposition an increase of hybrid viscosity was found at low shear rates.

Tin fluoride phosphate glass (TFP)/LDPE hybrids and their rheology have been analysed in [73, 78-82]. As the reported Tg of the TFP glass was 125˚C, this glass is in the liquid state at the processing temperature of the LDPE matrix, allowing the two phases to be mixed easily.

In [78], Adalja et al. induced a reduced creep in the solid state and an evident shear thinning behaviour by melting phosphate glass to LDPE. Also the time-temperature superposition principle was found to be applicable to the system.

Hybrid systems of TFP glasses and PS/PP/LDPE matrixes were characterized in [81] in the liquid state by a torque rheometer in shear oscillatory mode. The interfacial tension between the two phases was measured for these systems in [81]. The results were compared to the Palierne theoretical emulsion models [82], which resulted to be inadequate for phosphate glass/LDPE hybrids containing more than 30 vol% of the inorganic phase [81].

Moderate phosphate glass concentration (< 30 vol%) was found in [83] to modify strongly the shear rheology on the liquid state of phosphate glass/PS/LDPE hybrid. This system was characterized by a flow behaviour which was similar to that of liquid crystal polymers.

The crystallization kinetics of TFP glass/PP and TFP glass/LDPE hybrids were reported in [35, 84, 85] and were found to be dependent on both phosphate glass content and the polymer matrix. In [35] the crystalline structure of LDPE was found not to be affected by TFP glass that undergoes significant structural changes upon hybrid formation. In addition, increased content of phosphate glass in the hybrids caused a strong decrease of the overall crystallinity of the each matrix in [85].

The interfacial tension behaviour of these unique hybrid materials was studied in [86]. A modified drop shape method was used to measure the interfacial free energy in phosphate glass/polyethersulfone hybrids. Increasing content of zinc oxide ZnO in the phosphate glasses resulted to reduced interfacial tension between the components.

The mechanical behaviour of different hybrid systems was researched in [75]. Phosphate glass hybrids exhibited higher Young's modulus and flexural strength than equivalently filled conventional composites [35, 75-77, 87]. The flexural properties of hybrids of phosphate glass and poly(ether ether ketone) and polyether sulfone matrixes were analyzed in [75, 76] and the

flexural modulus was found to increase dramatically by increasing the phosphate glass content in the systems.

Phosphate glass/LDPE hybrids where shown in [80] to have interesting properties due to their particular morphologies of the two non-interacting phases.

The shear rheological behaviour of phosphate glass/LDPE and the elongational flow behaviour of this hybrid were studied by Urman et al. [45] to a better understanding of the morphology development of the hybrid in the liquid state under melt-blending processes. The hybrids with < 30 vol% phosphate glass content showed a Newtonian plate and a shear-thinning behaviour at low frequency and high frequencies, respectively. A strong shear thinning behaviour was present in hybrids with > 30 vol% phosphate glass content over the whole range of frequencies investigated. Furthermore the viscosity increased with increasing phosphate glass content. The Newtonian region was not evident in the phosphate glass/LDPE hybrids with high glass. [45] A strong dependence of viscosity on morphology was also revealed due to the shear rheological behaviour of phosphate glass/LDPE hybrids. The yield stress behaviour, used as a criterion for rheological compatibility between the two components of the hybrids, was evident in hybrids with phosphate glass concentrations > 30 vol%. In opposition, at phosphate glass < 30 vol%, the hybrids approached a Newtonian behaviour at low frequencies with no evidence a yield stress. This phase inversion point was consistent with a morphology change from deformable droplet to a formation of an interpenetrating network structure in the hybrid system. Furthermore the complex viscosity behaviour of hybrids over the range of frequencies analyzed showed the potential of phosphate glass/LDPE to be processed, while easily controlling its morphologies, via conventional processing methods such as extrusion and injection moulding. The hybrids at phosphate glass concentrations > 10 vol% showed a dramatic decreasing of elongational viscosity. A decrease in the crystallinity of the matrix with increasing amount of phosphate glass content in the phosphate glass/LDPE hybrid system was showed in the same study [45].

Phosphate glass/polyamide 12 systems were the first example of hybrid materials showing high and beneficial interaction between the components and in which the phases exhibited a possible partial miscibility at higher temperature [31].

The rheological behaviour of phosphate glass/polyamide 12 hybrids was discussed in [4] where the pure phosphate glass showed a Newtonian behaviour; a long Newtonian region was displayed in pure polyamide 12 and all hybrids. Furthermore all the materials showed some slight shear-thinning behaviour at high frequency.

The addition of glass influenced strongly the viscosity of the polyamide matrix: at 190 ˚C a dramatic decrease in viscosity was evident in hybrids with phosphate glass content > 2 vol%, despite the high viscosity of the pure phosphate glass at the same temperature analysed. This behaviour suggested a plausible disentanglement of the polymer chains due to the phosphate glass presence. At this temperature the phosphate glass/polyamide 12 hybrids exhibited a Newtonian behaviour at low frequencies with no evident of yield stress behaviour. As the temperature was further increased an increase of the complex viscosity as reported in the hybrids with a content of phosphate glass > 5 vol%. This behaviour was related to yield stress behaviour and interfacial effects: at this temperature phosphate glass was liquid but the dispersed glass particles could still interact with themselves to cause a morphological change of the phase and a derived enhancement of the interactions between polyamide 12 and the inorganic component [4].

The pure polyamide 12 and the hybrids containing 1 vol% showed a microstructure unaffected by temperature, temperature independence behaviour, typical behaviour reported for immiscible blends in [88-90]. As the vol% of phosphate glass was increased in the hybrid the temperature dependence broke down and the deviation from temperature independence increased with increasing phosphate glass content.

An increasing temperature was conjectured in [4] to cause an increasing miscibility of the polyamide 12 and phosphate glass phases, leading to a morphological evolution of the hybrids and to a partially miscible material in the liquid state. In fact, at lower temperatures the phosphate glass/polyamide 12 showed a similar morphology, independent from the volume percent of phosphate glass in the hybrid. This composition independence behaviour disappeared almost completely as the temperature was increased [4].

The interfacial tension calculated at 250˚C for the hybrid with 10 vol% of phosphate glass was extraordinarily small, 1.69 nN m, indicating a favourable interaction taking place between the two phases at high temperatures [4].

Chapter 3 Experimental Details

3.1 Materials

3.1.1 Polymer matrix

The thermoplastic matrix selected for the hybridization process was the polyamide 11 (PA 11) Rilsan ® supplied by ARKEMA, in the BMNO powder grade with an average particle size of 105 µm and inherent viscosity of 0.97-1.16 dL/g. Before any testing and characterization the polymer was dried at 50˚C, a temperature close to the glass transition temperature Tg of the polymer under vacuum for two hours to avoid moisture absorption.

Selected properties of the PA 11 used are summarized in Table 3.1. A detailed description of Rilsan ® PA 11 is presented in Appendix A.

3.1.2 Raw materials for glasses

The glasses chosen for hybridization with PA 11 were Tin-Fluoro-Oxy-Phosphate glasses as good miscibility in the glass/thermoplastic melt and good glass-polyamide adhesion in the solid state were previously reported [4-6, 31, 44].

The raw materials used for the synthesis of glasses were: Ammonium phosphate monobasic $NH_4H_2PO_4$ reagent-grade oxide powder, Tin (II) oxide SnO and Tin (II) fluoride SnF_2. The chemicals were supplied by Sigma Aldrich Ltd Company. Some selected properties of these reagents are summarized in Table 3.2.

Table 3.1: Properties of BMNO Rilsan ® PA 11.

Physical Properties	Test method	Unit	Typical Value
Density	ISO 1183	kg/m^3	1030
Thermo/Mechanical Properties	Test Method	Unit	Typical Value
Melting Point	ISO 11357	˚C	189
Glass Transition Temperature	ISO 11357–2	˚C	45
Vicat Softening Point (loading 1 N)	ISO 306	˚C	180
Vicat Softening Point (loading 5 N)	ISO 306	˚C	160
Young's Modulus (at 23 ˚C, dry state)	ISO 527	MPa	1450
Stress at Yield	ISO 527	MPa	40
Elongation at Yield	ISO 527	%	6
Tensile Strength at Break	ISO 527	MPa	53
Elongation at Break	ISO 527	%	300
Flexural Modulus	ISO 178	MPa	1200

Table 3.2: Properties of the raw materials used for the synthesis of glasses.

Property	$NH_4H_2PO_4$	SnO	SnF_2
Molar Mass [Kg mol^{-1} * 10^3]	115	135	157
Density [kg/m^3]	1800	6450	4570
Melting Point [°C]	190	1080	215
Solubility in water[kg/L* 10^3]	404	Insoluble	350 (20 °C)

The ammonium phosphate monobasic was used for producing the glass former phosphorus pentoxide (P_2O_5), according to the following reaction:

$$2NH_4H_2PO_4 \rightleftharpoons P_2O_5+2NH_3+3H_2O \quad (3.1)$$

The Tin-base reagents were selected to interact strongly with the amine groups of PA. SnF_2 was essential for lowering the Tg of the phosphate glasses. The chemical SnO was used to impart good chemical stability and mechanical properties to the glass, without changing considerably the Tg of the glass network.

3.2 Preparation of glasses

3.2.1 Synthesis routes

The raw materials needed for each composition were weighted and prepared in small batches (10-20 gr). Three different synthesizing routes were investigated.

1 $NH_4H_2PO_4$ and SnO were mixed manually and charged into a 100 ml porcelain crucible according to the chosen composition at room temperature. The mixture was melted in a laboratory convection oven under atmospheric conditions at 900°C for 15-30 minutes. The furnace was cooled down to 300°C and SnF_2 was added. It was not necessary to stir as the melt was solid. The furnace was maintained at 300˚C for 15-30 minutes. The glass was cast in stainless steel moulds and cooled to room temperature.

2 The first stage of this procedure was similar to Route 1. After melting the $NH_4H_2PO_4$ and SnO at 900˚C for 15-30 minutes, the furnace temperature was decreased to 700˚C. The melt was removed from the furnace and cooled down in a steel plate. The obtained tin phosphate glass was ground manually using a mortar. SnF_2 was added to the powder in the crucible at room temperature. The crucible was put in the furnace at 500˚C. The temperature was kept constant for 15-30 minutes. The melt was cast in a stainless steel mould and cooled to room temperature.

3 $NH_4H_2PO_4$, SnO and SnF_2 were thoroughly mixed and ground for 30-40 min in a mortar pestle and then the mixture (25g) was melted in an alumina crucible using muffle furnace

for 1-2 hrs at temperature ranging from 500 to 600 ºC depending on composition. When the melt was thoroughly homogenized and had attained the desirable viscosity it was poured either onto a metal plate or into a graphite crucible. The prepared glass was then annealed at the appropriate temperatures (between 120 and 200 °C) for 2 hrs and stored in a desiccator prior to evaluation.

Some phases of the glass synthesis are shown in Figure 3.1. A glass sample produced is displayed in Figure 3.2.

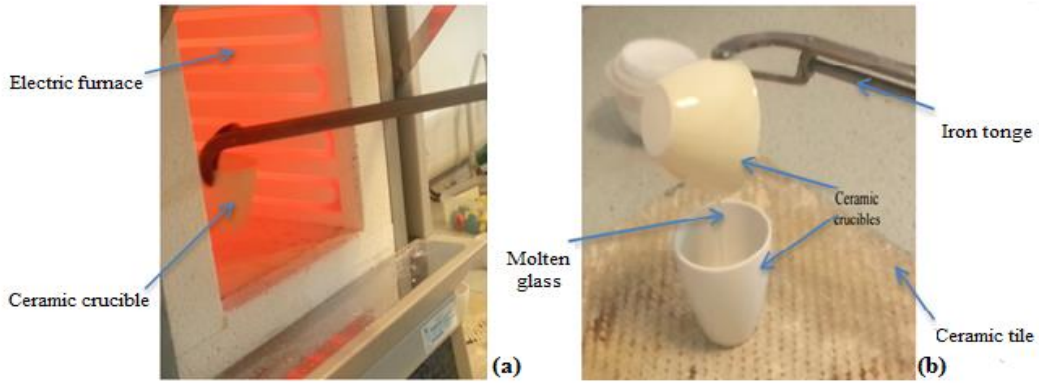

Figure 3.1: Two phases for producing a phosphate glass of a given composition in the chemical laboratory at London South Bank University: a) raw materials melted inside an electric; b) melted glass poured into a ceramic crucible for cooling.

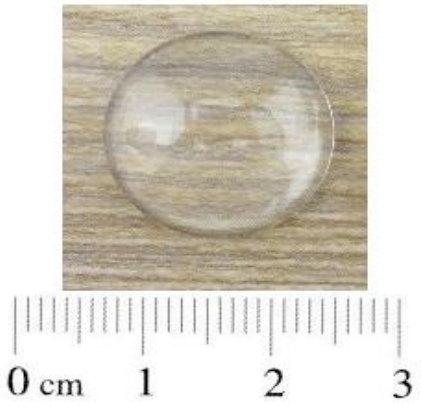

Figure 3.2: 50 SnF_2 +20 SnO + 30 P_2O_5 composition (Glass 0) produced with Route 3.

3.2.2 Glass powder preparation

After drying in a laboratory furnace at 100˚C for 24 hours, each glass sample was ground manually. After drying the powder at 100 ˚C, the glass was sieved at < 100µm using a sieve shaker Endecotts EFL 2000 for 15 minutes. The powders were weighted according to the hybrid composition to be produced and stored in plastic bags in a desiccator to avoid moisture absorption. Some powder samples were subjected to thermal, structural and chemical stability analysis.

3.3 Processing of glass-polymer hybrids

3.3.1 Extrusion

The mixed powder glass-polyamide 11 compositions were extruded using the twin screw 15 cm^3 Xplore ® Micro-DSM compounder (Figure 3.3) equipped with a DSM research laboratory injection moulding machine. The list of technical specification of the micro-extruder is presented in Appendix B.1. The equipment contains three different heating zones to reproduce the heating profile of a melt during extrusion processing. The core of the compounders is a vertically positioned barrel with two detachable conical mixing screws. A description of the screw design is presented in Appendix B.2.

The glass powder and polymer were prepared according to the chosen hybrid composition and mixed together using a laboratory roller. Before the compounding procedure, each hybrid powder sample was dried for 24 hour and stored in a sealed plastic bag in a desiccator. The Micro-DSM was switched on. When the set temperature and torque reached the nominal set values the selected hybrid powder was introduced into the extruder.

The extrusion processing variables are describes as follows:

- Screw speed:

  A high screw speed can be used for improving the particle dispersion and homogenising the melt. However, extruding at high screw speed may cause

degradation as the melt is subjected to high shear stress. To determine the effect of this parameter on the extruder process and on the final extrudate, experiments have been performed over a wide range of screw speed values (50-200 rpm) for selected hybrid compositions.

- Residence time:

  The experiments were performed at 300 min and 400 min to evaluate the optimum value. A minimum residence time value is needed to disperse the glass phase and stabilize the blend morphology. However a too high residence time can lead to degradation phenomena of the melt.

- Profile temperature:

  The micro-DSM extruder has three temperature control zones along the barrel length. These were individually set to precise temperatures to optimize the extrusion process. The final two downstream barrel zones were set at different temperatures (230, 250 ˚C and 270 ˚C), values reasonably close to the melting temperature of PA 11 Rilsan, in order to allow melting of the polymer matrix and avoiding degradation. The rear zone temperature was set at 210˚C, slightly below the barrel zone temperature to avoid melting the material in the feeding zone.

Each hybrid composition was compounded three times. All process parameters were acquired, displayed graphically during each experiment and stored in Excel file formats.

The force/time data generating by the extruder were extrapolated for each experiment. Monitoring the melt compounding process of glass/PA 11 hybrids can give information on the rheological behaviour of the melt as, for a constant volume of the compounded material and the same processing speed, the magnitude of the extrusion force (F) generated during mixing is directly proportional to the torque experienced by the micro-extruder and to the viscosity of the material.

The force/time data generated during extrusion and the smoothness of each extrudate were analysed and used as quality control parameters for the hybrid samples. The high quality

samples were injection moulded and subjected to micro-structural characterization. The rheological, chemical-thermal and mechanical properties of each sample were evaluated.

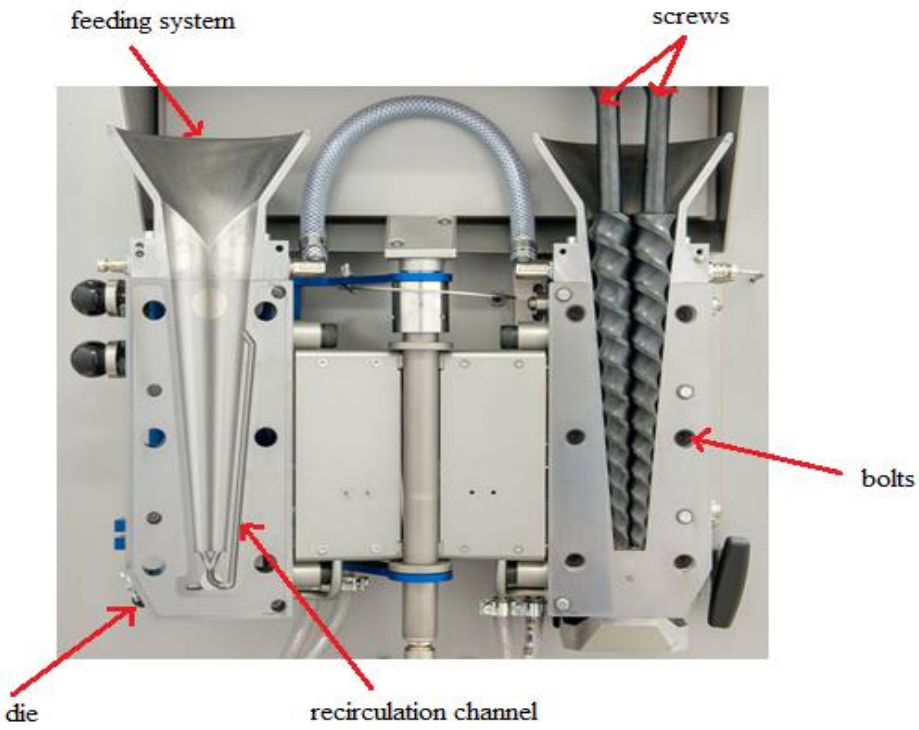

Figure 3.3: Open MC 15 Xplore Micro DSM two screw extruder.

3.3.2 Injection moulding

The selected hybrid compositions were subjected to a extrusion-injection moulding cycle. The micro-DSM extruder was connected to the Xplore micro injection moulder IM 12DSM machine with a shot volume of 12 ml (Figure 3.4). The injection unit was quickly filled by compounded material directly from the micro-compounder.

The core of the Xplore micro-injection moulder IM 12DSM consists of a temperature controlled mould housing for a conically shaped mould, in combination with a heated, removable injection nozzle unit.

Compounded material was injected into the temperature controlled mould with a plunger powered by compressed air. Holding pressure and time were controllable to avoid shrinkage of the moulded test sample.

The micro-injection processing parameters were:

- Mould temperature:

  A uniform mould temperature in the range required for the material being processed helps to ensure even heat transfer from both mould surfaces. This leaved the part in a balanced condition, providing a uniform wall thickness and the amount of residual stress to be minimized. The mould temperature was set at 40 ˚C, a value slightly below the Tg of PA 11, which was ≅ 64 ˚C measured via DMA.

- Injection temperature:

  This parameter was set at 250 ˚C, close to the barrel temperature of micro-DSM extruder during compounding.

- Injection cycle:

  One injection cycle was performed for each batch of the Xplore micro-compounder. The cycle begins when the mould closes, followed by the injection of the polymer into the mould cavity (fill phase). A filling pressure of 4 bar was applied for 60 s, which completed mould filling and compensated for thermal shrinkage. A packing pressure of 6 bar was applied for 300 s until the gate (cavity entrance) solidified. Once the gate solidified, no more material could enter the cavity and was completely filled. Thus, a holding pressure of 6 bar was maintained for 180 s to compensate for material shrinkage (holding phase). Once the material within the mould was sufficiently cool and dimensionally stable, the mould was removed from the machine and opened by hand.

The specific parameters for PA 11 used in the injection moulding process are summarized in Table 3.3.

The maximum injection pressure of 6 bar was high enough to feed the material to the sprue at a rate that eliminated voids but did not over -pack the sprue.

Injected dog bones samples of 1-mm-thick and 5-mm-wide were produced as shown in Figure 3.5, according to the ISO 527 standard. The dog bone samples were dried at 80 °C for 24 hours in a vacuum oven prior to testing and subjected to rheological, mechanical and thermodynamic analysis.

Figure 3.4: Xplore micro injection moulder IM 12DSM.

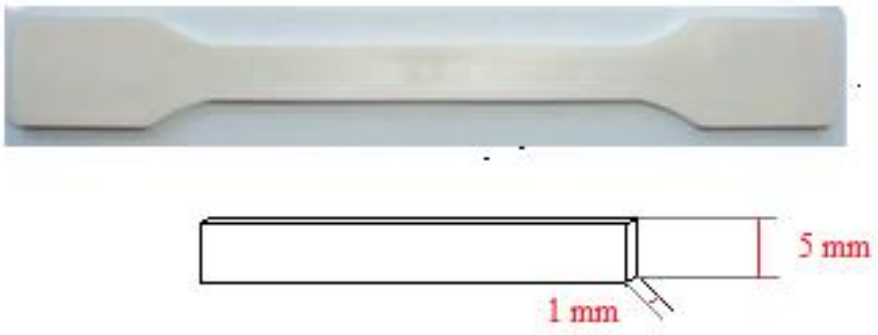

Figure 3.5: Dog bones injected samples produced according to the standard ISO. 527. The samples are 1-mm-thick and 5-mm-wide in the rectangular cross-section area.

Table 3.3: Steps of injection cycle for glass/polymer hybrid production.

Step of injection cycle	Pressure (bar)	Time (s)
Filling	4	60
Packaging	6	300
Holding	6	180

3.4 Microstructural characterization

3.4.1 Microscopy techniques

Each glass sample was polished (METASERV 2000, Grinder/Polisher, BUEHLER, Düsseldorf, Germany) using silicon carbide papers (BUEHLER-MET, Metallographic grinding paper 8 in., grades P240, P600, P800, P1200 and P2500). In order to evaluate the degree of miscibility of glass components and investigate the macroscopic morphological characteristics of the glasses, the bulk polished glass samples were analyzed under an optical microscope, the Olympus BX63 Microscope, using 100 X and 200 X magnifications.

To establish the degree of dispersion of glass within the PA 11 matrix and the nature of unidentified elements, selected hybrid samples were examined by Scanning Electron Microscopy (SEM HITACHI S-4300, USA). The samples were immersed in liquid nitrogen for 30 minutes and subjected to cryogenic fracture. The cross-section area of the specimen was gold-coated using a BIO RAD Polaron Division SEM Coating System to make the sample conductive.

3.4.2 Spectroscopy techniques

Powders and specimens of glasses, PA 11 and hybrids were analyzed with a Fourier transform infrared (FTIR) spectrometer (Perkin-Elmer 16PC) to investigate the influence of glass composition on the structure of glasses and hybrids. Reflectance spectra were obtained in the region of 4000–500 cm^{-1} with a resolution of 4 cm^{-1}. 16 scans were averaged in order to obtain clear spectra of each sample. The IR spectral data of glasses and hybrids were

interpreted in terms of the vibrations of a structural repeat unit. The changes of structure and interactions in glasses and hybrids were assessed by any modification from the characteristic IR absorption bands of Glass 0 and polyamide 11 reference samples, respectively.

X-Ray diffraction (XRD) was used in conjunction with FTIR to detect the effect of the preparation routes and glass compositions on the quality and structure of the glasses. X-ray diffraction (XRD) is an analytical tool used to investigate a crystalline material's atomic or molecular structure (Section 2.4). A D2 Phaser Desktop X-Ray Diffractometer was used to obtain the X-ray spectra of base glass sample composition. The glass powder was dried and positioned on an aluminium sample holder where the sample was exposed to the radiation.

3.5 Density

Density was measured for all glass samples and selected hybrid at room temperature using water or xylene as the immersion liquid, following the standards ISO 1183-1:2004.

According the Archimedes principle, the buoyancy equals the weight of the displaced fluid. Archimedes Principle using xylene as the buoyant medium evaluated the density of the glass samples. The density was obtained by employing the following relation:

$$\rho = W_a \ \rho_b / (W_a - W_b) \tag{3.2}$$

Where: W_a is the weight of glass sample in air; W_b is the weight of glass sample in buoyant liquid; $(W_a - W_b)$ is the buoyancy; ρ_b is the density of buoyant.

All the measurements were made using a digital balance (Contech and SARTORIUS IAC 210P). The inert liquid xylene was selected as the immersion medium for those samples that could react with water.

3.6 Thermal properties

3.6.1 Transition temperatures

Thermal analysis of phosphate glasses was evaluated by differential scanning calorimetry (DSC) using a Mettler DSC 25 and a Perkin-Elmer DSC-7 equipments on glass fragments. The weight of the samples was typically 8-10 mg and the samples were encapsulated in hermetically sealed aluminium pans. The DSC was performed by heating samples from 25 to 600 °C at 20 °C min^{-1} in inert nitrogen atmosphere before cooling at 30 °C min^{-1} with air as the purge gas.

The resulting plot of the derivative $d\Delta Q/dt$ (where t is time) as a function of temperature T allowed the detection of endothermic and exothermic processes: the change in the slope of the graph may indicate glass transition, an exothermic process may indicate crystallization or an exothermic reaction, an endothermic process may indicate melting, vaporization, etc. Phase transformation temperatures were then analyzed by the instrument's Proteus® software (Netzsch, Germany). The glass transition temperature and crystallization temperature were determined from the point of intersection of the tangents below and above the slope change, as shown in Figure 3.6.

Glass is an amorphous material, however under certain conditions glass crystallizes easily. In general, the more disrupted the phosphate structure is, the more the phosphate glass tends to crystallize. In order to quantify the tendency of the glasses to undergo crystallization, their processing window (PW) were determined. The processing window is the temperature range between glass transition temperature (Tg) and the onset of crystallization (To) and was determined from DSC curves where possible using Equation 3.3:

$$PW = To - Tg \tag{3.3}$$

Where: PW is the processing window (°C); To is the crystallisation onset temperature (°C); Tg is the glass transition temperature (°C).

The Tgs of the hybrids were determined using a DMA 242 Netzsch dynamic mechanical analyser. The test was conducted on selected hybrid dog bone samples at a frequency rate of

1 Hz under 1% strain and a ramp temperature of 2°C/min over a wide range of temperature from -50°C to 200°C. The glass transition was measured as the maximum in the storage modulus when viewed on a log scale against a linear temperature scale. A concurrent peak in the tan δ was also detected. The values of the dissipation factor of the hybrids were compared with the corresponding neat polymer values. A typical dissipation factor/temperature trend for a selected hybrid is shown in Figure 3.7.

In order to measure the melting point of the hybrids, samples of about 2 mg were heated from 25˚C to 250˚C, a temperature above the melting point (Tm_1), at a rate of 20˚C·min^{-1}. The samples were held at 250˚C for 3 min, then rapidly cooled (cooling rate ~ 40˚C·min^{-1}) to the desired crystallization temperature (Tc) and maintained at this temperature for 2 min. After that, the samples were heated to 200˚C, at a rate of 20˚C·min^{-1}, for the measurement of the melting point (Tm_2). This procedure was repeated for different crystallization temperatures in the range of 150-180 ˚C.

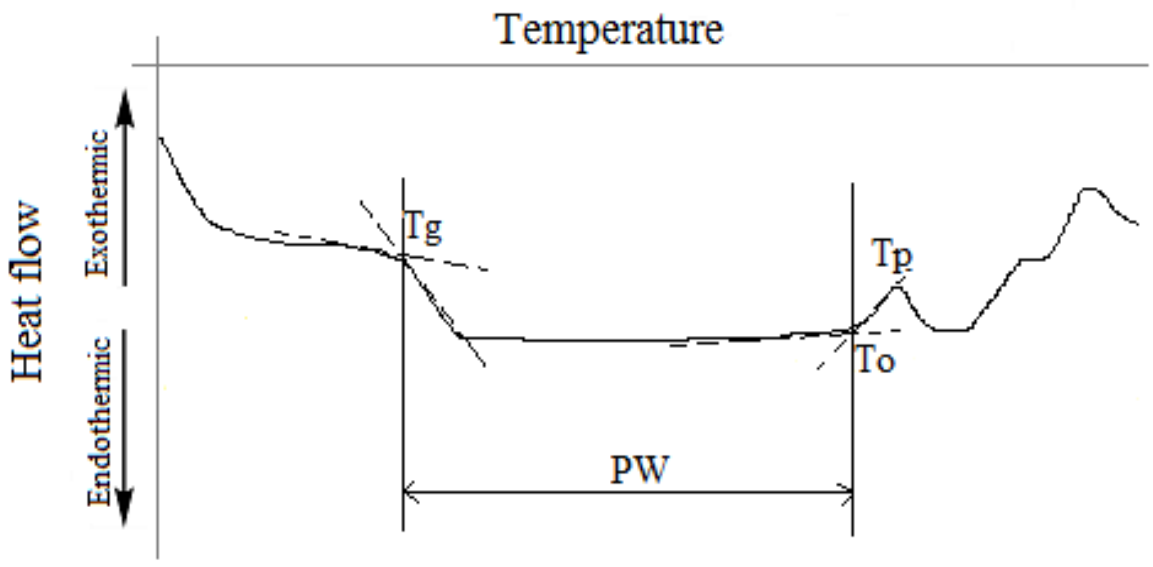

Figure 3.6: Determination of glass transitions of a selected sample.

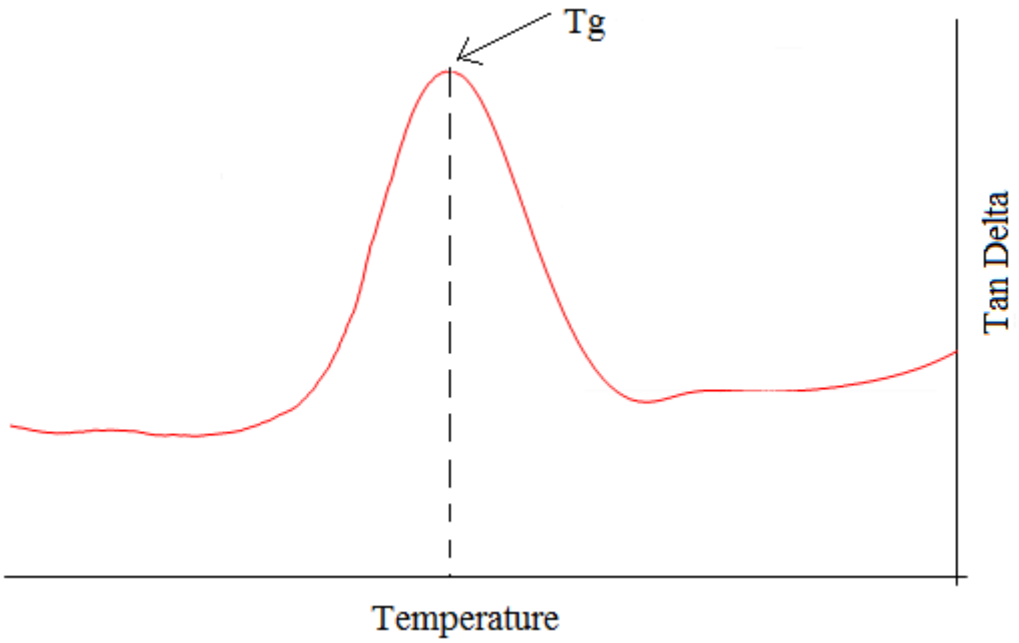

Figure 3.7: Tg of a selected hybrid measured by dynamic mechanical analysis.

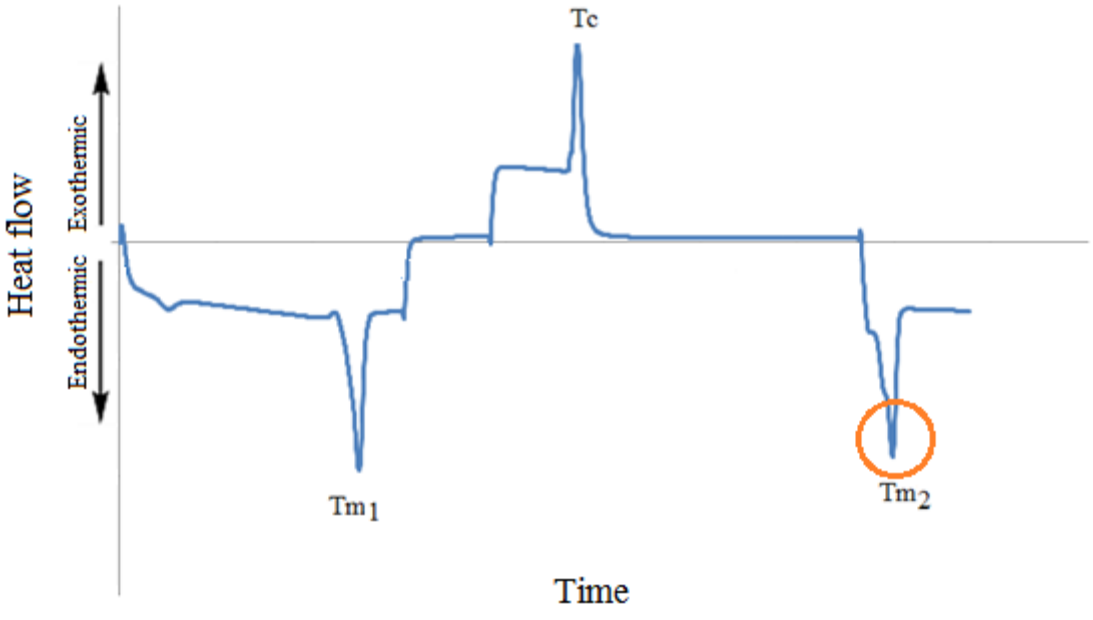

Figure 3.8: Melting point Tm of a selected hybrid measured by differential scanning calorimetry.

3.6.2 Softening point

The softening point of a glass is the most widely used production control parameter and may be an indicator of chemistry changes in the material. In this experiment the *Littleton softening point*, i.e. the temperature at which the glass deforms visibly under its own weight, was determined. Cylindrical glass samples (8 mm diameter and 13 mm height) were produced by pressing the dry glass powder in a cylinder mould by a hydraulic jack under a 5 N/mm^2 pressure. Samples of each composition were heated in a furnace from room temperature to 600°C. The Littleton softening point of each glass was judged when the top surface started to melt (British Standard 1344-18:1981). For each glass composition, the experiment was repeated four times.

3.7 Chemical and thermal stability

3.7.1 Stability in water

The dissolution rate method was employed to quantify the stability in water of the glasses and hybrids. The dissolution rate of a substance is a measure of how quickly that substance will dissolve in water, and is consequently a good indicator of chemical durability of the glass. Generally, high dissolution rates are accompanied by a significant decrease in the structural stability of the glass and hybrids. So the dissolution rates were used as screening test to select the phosphate glass compositions to be used for hybridization. Each glass sample was polished (METASERV 2000, Grinder/Polisher, BUEHLER, Düsseldorf, Germany) using silicon carbide papers (BUEHLER-MET, metallographic grinding paper 8 in., grades P240, P600, P800, P1200 and P2500). After recording its mass and the surface area, the glass sample was immersed in a laboratory bath filled with distilled water at 30 ˚C. After 96 hours the sample was taken out of the water bath, dried at 100 °C for 24 hours, weighted and finally taken back to the bath. The procedure was repeated 4 times for an overall duration of 14 days. Each composition was tested three times. The weight loss was normalized by each sample's surface area to take into account slight differences in sample sizes. The dissolution rate of the samples was calculated using Equation 3.4:

$$M_L = \frac{M_f - M_0}{M_0} \times \frac{SA}{SA_{ref}} \times 100 \quad (3.4)$$

Where: M_L is the percentage mass loss (%); M_0 is the initial mass (g); M_f is the mass after given immersion time (g); SA is the tested sample's surface area (mm^2); SA_{ref} is the reference sample's surface area.

3.7.2 Thermal stability

The thermal stability of the glasses was examined by thermogravimetric analysis (TGA) to ensure glasses would not degrade over the range of temperatures employed during extrusion processing. A Perkin Elmer TGA 7 was used for glass characterization. The effect of hybrid composition on weight loss at the set temperature range was monitored by a TG209 F1 Netzsch TGA. The glass and hybrid samples were heated by a furnace in air atmosphere while the loss or gain of sample weight was monitored by a sensitive balance. Experiments were carried out within the range of the TGA (100-800 °C) at scan rates of 10 °C/min.

3.8 Rheological properties

The shear rheology of PA 11 and hybrids was investigated with a rotational rheometer. The measurements were performed on dog bone sample at 250 °C, the temperature of extrusion of the samples, and over an angular frequencies range of 0.1-1000 rad/s.

The elongational viscosity of PA 11 and hybrids was measured by the rotary clamp technique. Each dog-bone sample was subjected to homogeneous elongation at a constant strain rate of 1.0 s^{-1} at 250 ˚C. A reliable stress measurement was calculated by using the force applied on the clamps. The sample was supported by a cushion of nitrogen.

3.9 Mechanical properties

3.9.1 Indentation techniques

The hardness measurements were performed on small glass samples. The specimens were introduced in a plastic cylinder mould, embedded in a 2-part resin (EpoxiCure 2, resin + hardener, volume ratio 5:1). After curing for 48 hours, the samples were ground and polished. To ensure adequate surface quality prior to testing, the polished sample surfaces were visually inspected by an Eclipse MF600 optical microscope (Nikon, Japan).

Micro-hardness testing of glasses was performed using a Struers Duramin-5 Vickers Hardness tester to determine the resistance of glass samples to localized plastic deformation from a standardized stress source (Figure 3.9).

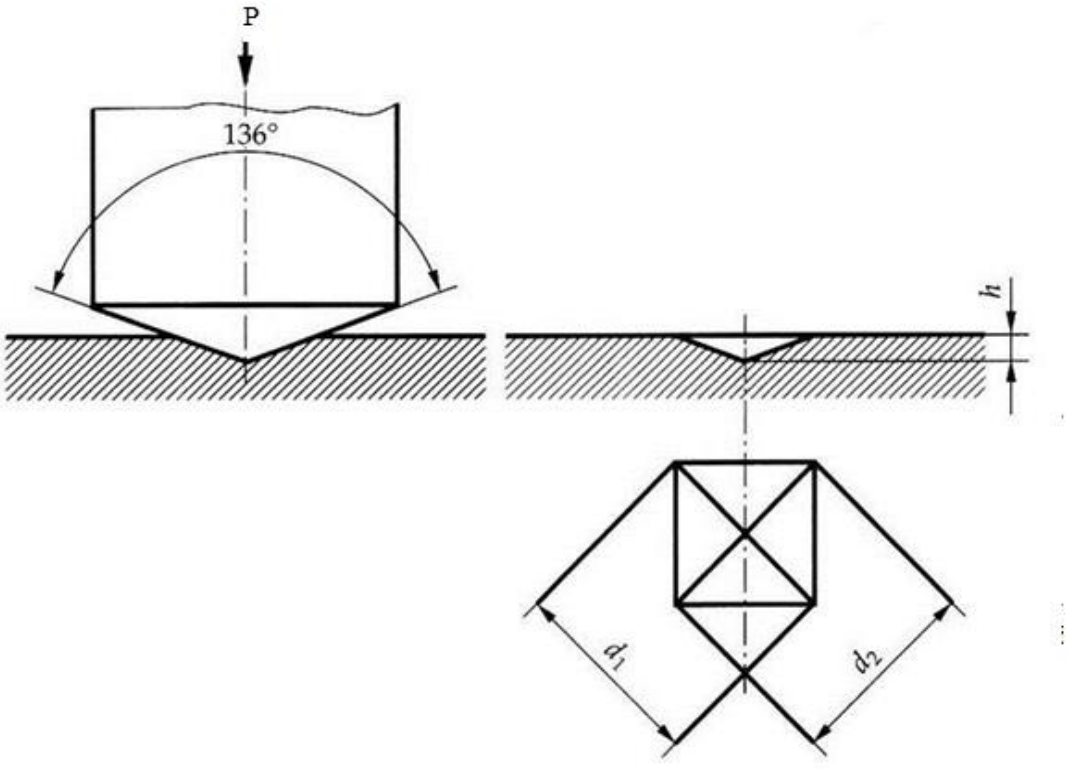

Figure 3.9: Geometry and indentation with a Vickers indenter [91].

Micro-hardness testing on polishing disks was conducted with indentation loads of 2.94 N and 4.91 N at an indentation loading time of 10 seconds. The indentation loads were selected based on previous Vickers hardness testing.

The test was performed under atmospheric conditions at ambient temperature with four micro-hardness tests performed on each glass composition at each indentation load. The resulting indent diagonals, d_1 and d_2, were then measured using the optical microscopy equipment attached to the testing unit. The Vickers hardness value was calculated from the equation below:

$$H_v = \frac{2P \sin\left(\frac{\theta}{2}\right)}{L^2} \tag{3.5}$$

Where: H_v is the Vickers hardness; P is the indentation load (Kg); L is the ratio between the two indent diagonals defined as d_1/d_2; θ is the indentation angle, 136˚ wide.

The fracture toughness of each glass was determined using the radial crack lengths produced by the indent depressions from the micro-hardness testing and using the Evans and Wilshaw equation [92]:

$$K_{IC} = 0.079 \left(\frac{P}{a^{\frac{3}{2}}}\right) \log\left(\frac{4.5a}{c}\right) \tag{3.6}$$

Where: K_{IC} is the fracture toughness ($MPa.m^{0.5}$); P is the indentation load (mN); a is the indentation half-diagonal length (μm); c is the surface radial crack length (μm).

This equation is reliable if $0.6 \leq c/a \leq 4.5$. The indentation half-diagonal length (a) corresponds to the distance between the centre of the indentation mark and its tip. The surface radial crack length corresponds to the distance between the centre of the indentation mark and the end of the crack as shown in Figure 3.10.

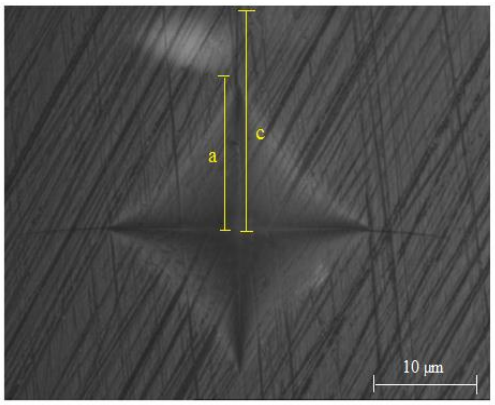

Figure 3.10: Crack formation during hardness measurements in phosphate glass sample with base composition (30 P_2O_5-50SnF_2-20 SnO).

3.9.2 Tensile properties

Tensile testing on injection moulded hybrid samples was performed using a Zwick Material Testing Machine Z1455, equipped with an optical extensometer and a 200 [N] load-cell at a cross-head speed of 5 mm/min at room temperature. The tensile properties were measured on at least four samples of each composition according to the standard ISO 527-1BA.

The tensile modulus of each hybrid (E_{th}) was calculated from the slope of the linear part of the stress-strain curve. The tensile strengths were extrapolated and calculated from the maximum of the curve and according to Equation 3.7:

$$\sigma_{th} = \frac{F}{bd} \tag{3.7}$$

Where: σ_{th} is the tensile strengths of hybrid; b is the width of the rectangular cross section of the hybrid sample; d is the depth of the rectangular cross section of the hybrid sample.

The yield strength of each hybrid (σ_{yh}), defined as the stress at which a material begins to deform plastically, was calculated at 0.2% plastic strain. Other tensile parameters, i.e. yield deformation, fracture strength, deformation at fracture, were calculated from the stress-strain curve.

3.9.3 Flexural properties

The setup for the three-point flexural test was mounted on an Olsen universal mechanical testing machine equipped with a 9 kN load cell. The flexural samples were simply supported over a span of 50 mm. The tests were performed at a cross-head displacement rate of 5 mm/min. At least four specimens for each composition were tested at room temperature.

The flexural strength was calculated from the maximum on the load-deflection curve. The flexural modulus was calculated from linear part of the curve. The following linear elastic equations were used:

$$\sigma_{fh} = \frac{3FL}{2bd^2} \tag{3.8}$$

$$E_{fh} = \frac{L_s{}^3 S}{4bd^3} \tag{3.9}$$

Where: σ_{fh} is the flexural strength of hybrid; E_{fh} is the flexural modulus of hybrid; F is the applied load; L_s is support spam; b is the width of the sample; d is the depth of the sample; S is the slope of the initial straight-line portion of the load deflection curve (N/mm).

Chapter 4 Development and Characterization of Glasses

4.1 Glass requirements

The hybridization of glass with PA 11 requires a sufficiently low glass transition temperatures and softening point to allow the glass to be fluid in the same range of temperatures of the matrix, without significantly compromising the mechanical and chemical properties of the hybrids. The glass properties required for hybridization of glass-polyamide are the following:

1. Good microstructure with no phase separations.
2. Low glass transition temperature Tg in the range of 70-170 °C;
3. Softening point Ts in the range of 200-350 °C;
4. Low water absorption.

4.2 Design of the Glass compositions

The 50 SnF_2 +20 SnO + 30 P_2O_5 base composition (Glass 0) was used as the starting point for the design of experimentation. The molar ratios of components in the base composition are: SnF_2/P_2O_5 = 1.67, P_2O_5/SnO = 1.5, SnF_2/SnO = 2.5. This glass is known to have a Tg of approximately 125 ˚C, a density of 3750 Kg/m^3, and an excellent water resistance [4-6, 31, 42, 44, 45]; the glass transition of Glass 0 was low enough to provide a good hybridization with selected thermoplastics, especially PAs.

These properties have been re-measured as part of this work and the measured results closely match the values reported in literature; the details of the measurements will be reported in Section 4.3.

As stated in Section 4.1, the effect of the compositions on the microstructure, glass transitions, chemical stability in glass were the main concern at this point. In [26, 27] P_2O_5 was found to decrease the Tg of the glasses at the expense of water absorption; on other hand, in [2, 4, 18, 20-23, 33, 37-39, 42] fluoride was shown to be responsible for decreasing Tg and leading to glass network depolymerisation in water. Finally [2, 4, 18, 20-23, 33, 37-39, 42] reported that tin is responsible for increasing the durability of the glass in water increasing the glass transition temperature.

Sixteen glass compositions ($xSnO\text{-}ySnF_2\text{-}zP_2O_5$) were designed by slightly modifying the composition of the base glass in order to evaluate the effect of each component on microstructure, glass transitions and water adsorption of glass, as these properties may affect remarkably the hybridization with PA 11.

The following limits were used as design guidelines:

- P_2O_5 mol% >20 to guarantee the necessary quantity of glass former in the composition.
- P_2O_5 mol% < 60 to avoid high water absorption in phosphate glasses;
- SnF_2 mol% < 65 to avoid depolymerisation phenomena due to the high amount of fluoride in the glass composition.
- SnO mol% < 50 to allow the Tg and Ts to be low enough to meet the requirement 1 and 2 in Section 4.1.

The different compositions are shown in Table 4.1 and in the ternary phase diagram in Figure 4.1. Three classes of glasses were designed by keeping a constant molar ratio between two of the components of the base composition at a time:

- Class 1: glasses with SnF_2/P_2O_5 molar ratio equal to 1.67 and SnO in the range of 0-30 mol%;

- Class 2: glasses with P_2O_5/SnO molar ratio equal to 1.5 and SnF_2 in the range of 30-60 mol%;
- Class 3: glasses with SnF_2/SnO molar ratio equal to 2.5 and P_2O_5 in the range of 20-40 mol%.

Table 4.1: Glass compositions prepared as candidates for hybridization.

	Quantity of component [mol%]		
	SnF_2	P_2O_5	SnO
Base glass			
0	50.0	30.0	20.0
Class 1 SnF_2/P_2O_5 =1.67			
1	62.1	37.9	0.0
2	59.4	35.6	5.0
3	56.3	33.7	10.0
4	53.1	31.9	15.0
5	46.9	28.1	25.0
6	43.8	26.2	30.0
Class 2 (P_2O_5/SnO molar ratio = 1.5)			
7	30.0	42.0	28.0
8	35.0	39.0	26.0
9	40.0	36.0	24.0
10	45.0	33.0	22.0
11	55.0	27.0	18.0
12	60.0	24.0	16.0
Class 3 (SnF_2/SnO molar = 2.5)			
13	57.1	20.0	22.9
14	56.2	25.0	18.8
15	46.4	35.0	18.6
16	42.9	40.0	17.1

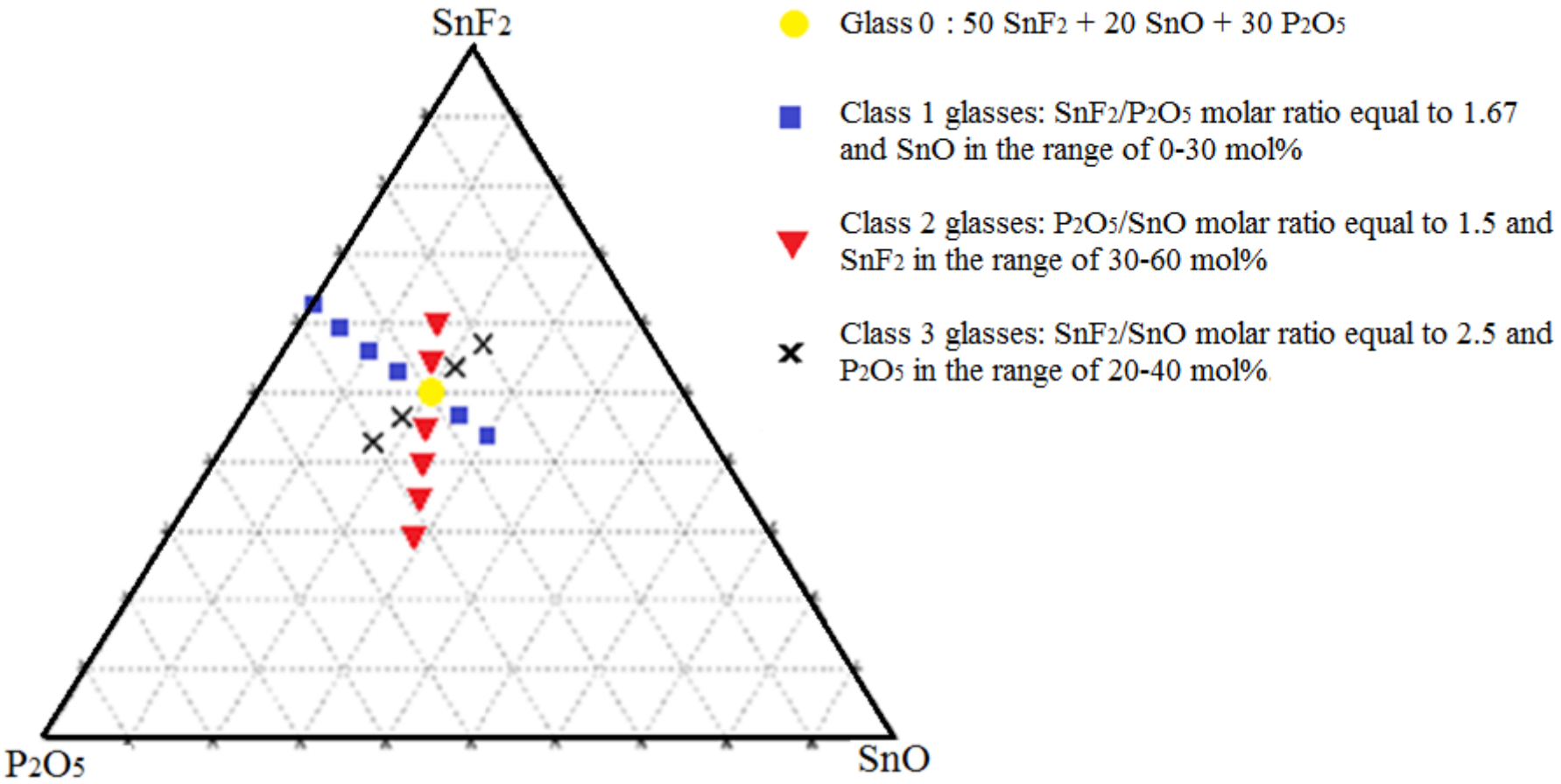

Figure 4.1: Phase diagram summarizing the glass compositions prepared as candidates for hybridization with PA 11.

4.3 Processing of glasses

In order to optimize the manufacturing procedure and maintain the composition accurate, the base glass (Glass 0) was at first produced in batches of 20-30 grams in the laboratory using three different routes. The raw materials used and the descriptions of the processing routes used to synthesize the glasses are summarized in Section 3.2.

The densities of the glass samples were determined using Archimedes principle as described in Section 3.5. The results are given in Figure 4.2. The density of the glasses prepared by Route 1 was measured as 3970 kg/m^3, slightly higher than the 3755 kg/m^3 found in [2, 4, 18, 20-23, 26, 27, 33, 37-39, 42]. The density of the Route 2 samples was 4050 kg/m^3, a value higher than the value reported in [2, 4, 18, 20-23, 26, 27, 33, 37-39, 42] for the same composition. Furthermore the standard deviation of the results was high in both Route 1 and Route 2, possible due to issues with process reproducibility and homogeneity of the glass samples. The calculated density for Route 3 glass was 3720 kg/m^3 in agreement with the value reported in [2, 4, 18, 20-23, 26, 27, 33, 37-39, 42] for the same compositions. The low standard deviation is evidence of good reproducibility of the Route 3.

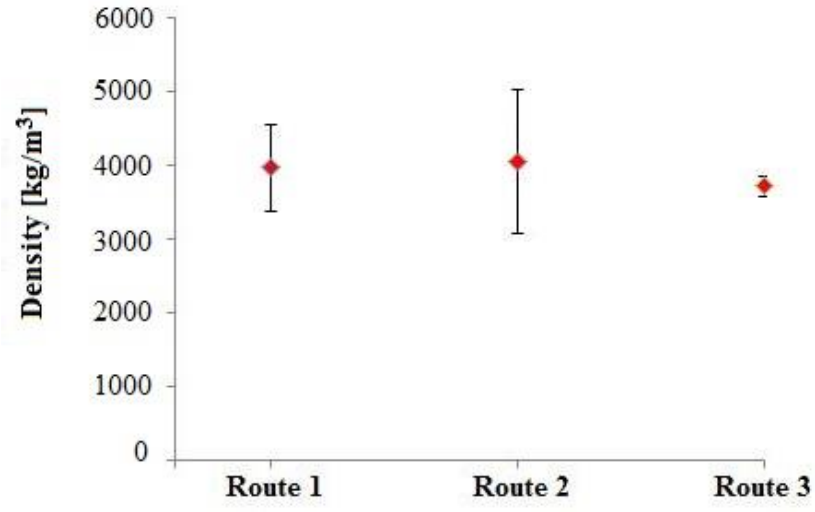

Figure 4.2: Density of base glass (composition of 50 SnF_2 +20 SnO + 30 P_2O_5 mol%) prepared using Route 1, Route 2 and Route 3.

The cross section area of the glass samples were polished using the procedure described in Section 3.4.1 and examined by optical microscopy. The results are given in Figure 4.3.

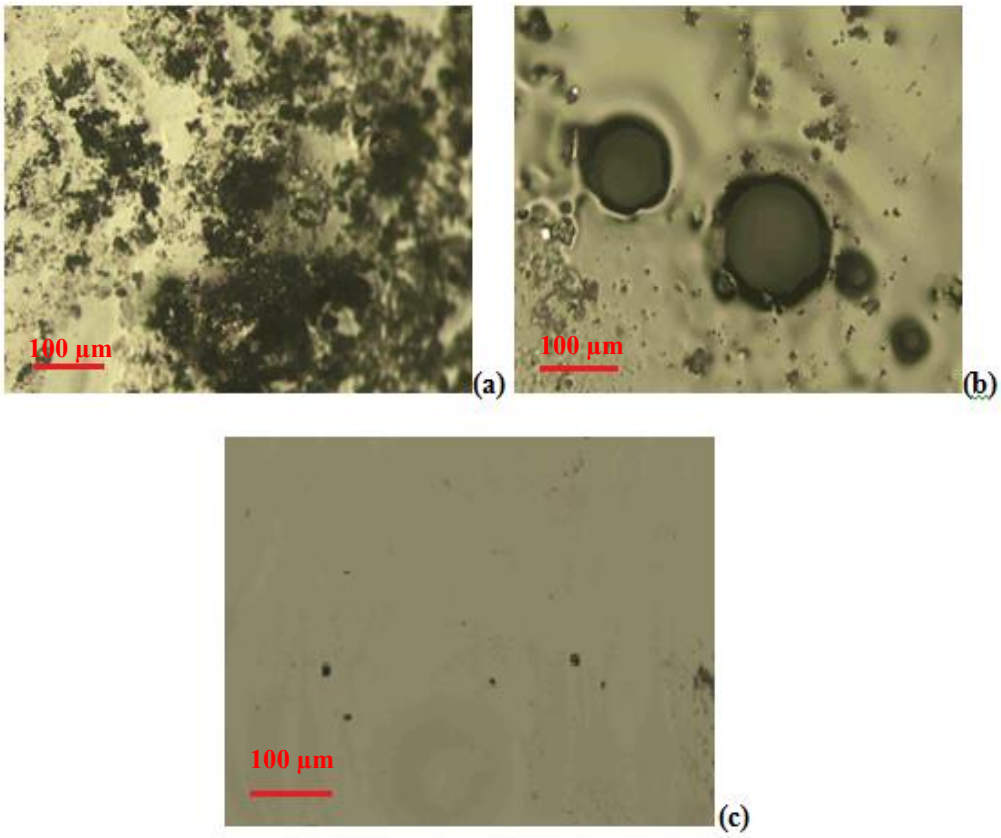

Figure 4.3: Optical micrograph of cross section of base glass (composition of 50 SnF_2 +20 SnO + 30 P_2O_5 mol%) prepared using (a) Route 1, (b) Route 2, (c) Route 3.

The glass prepared by Route 1 showed black spots along the whole cross section area, while the cross section area of the glass sample manufactured by Route 2 was characterized by big black spots and bubbles.

EDX analysis, shown in Figure 4.4, revealed that the black spots were composed of a high content of carbon, oxygen and fluorine suggesting a failure to completely convert the $NH_4H_2P_2O_4$ reactant into the P_2O_5, NH_3 and H_2O products.

Ideally, during the melting, the ammonium phosphate oxide reagent would completely decompose and form phosphate oxide, releasing NH_3 and water (Equation 3.1); in practice a lower reaction yield[1] is possible because of the hydroscopic nature of P_2O_5 can lead to the incomplete release of water from the $NH_4H_2P_2O_4$ reactant. Furthermore when SnO and $NH_4H_2P_2O_4$ were melted together two or more reactions might occur simultaneously; as a result some undesired by-products could be released. These products, together with SnO and P_2O_5 might react with the SnF_2 added on the second stage of Route 1 and Route 2, causing the formation of new compounds, possibly incorporating environmental carbon, based on tin-fluoride-oxygen. In Route 3 the reactants $NH_4H_2PO_4$, SnO and SnF_2 were mixed and melted together for 1-2 hrs at temperature ranging from 400-500 ºC. The cross section area of glass prepared by Route 3 showed good homogeneity (Figure 4.3 (c)).

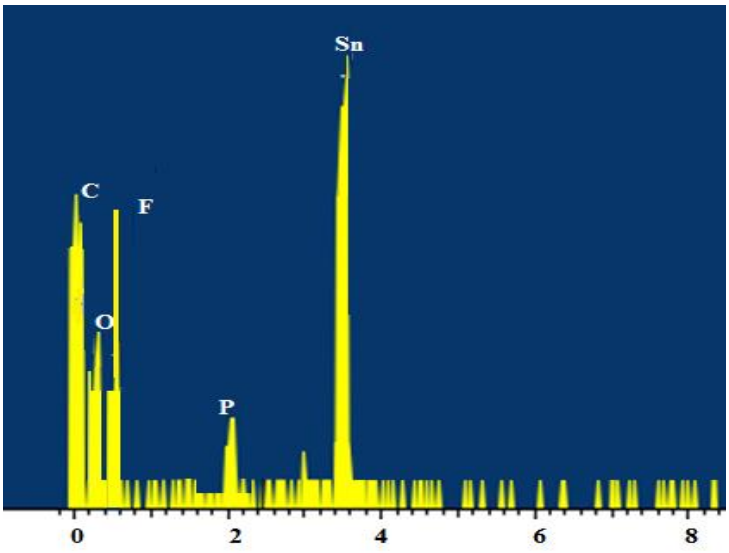

Figure 4.4: EDX of an area of cross section of base glass (composition of 50 SnF_2 +20 SnO + 30 P_2O_5 mol%) prepared according Route 1.

[1] The reaction yield is the amount of product obtained in a chemical reaction [93]; the theoretical yield is the amount of product predicted by a stoichiometric calculation based on the number of moles of all reactants present, assuming that only one reaction occurs and the reactant reacts completely; however in practice the actual yield is always lower than the theoretical yield because of inefficiencies in the reaction itself.

In order to validate the homogeneity of the samples, thermo-calorimetric analysis was conducted on the glasses manufactured using the three routes. The resulting DSC thermographs are shown in Figure 4.5.

The glass transition (Tg) was determined by the intersection of tangents overlaid across the endothermic events.

The sample prepared by Route 1 displayed two Tgs, respectively at 113˚C and 305˚C. A similar behaviour was evident in the glass prepared by Route 2 where the two Tgs detected were 165 ˚C and 229 ˚C respectively. This time the two Tgs were closer in value.

The presence of two Tgs suggests that there might be phase separations that result in in-homogeneity in samples prepared by Route 1 and Route 2. The two peaks were related to the presence of tin-fluoride-phosphate compounds produced during the glass manufacturing, phenomenon already confirmed by the micrographs. The reduced difference of the Tgs in the samples prepared by Route 2 compared to the Tgs of sample prepared by Route 1 were linked to the decreased phase separations in glass prepared by Route 2.

The glass sample prepared by Route 3 displayed only one Tg. The Tg was in the range of 116-125°C, similar to the results found in literature [2, 4, 18, 20-23, 26, 27, 33, 37-39, 42]. The identification of a single Tg value indicates good homogeneity of the glass prepared by Route 3 on a microscopic scale, as shown in the micrograph in Figure 4.3 (c).

XRD analysis of the base composition prepared by Route 3 confirmed the amorphous structure of the glass. The XRD trace, matching a typical phosphate glass, displays a broad peak centred at $2\theta \approx 27°$ as shown in Figure 4.6.

The broad peak corresponds with the dominant crystalline phase of phosphate the tetrahedron PO_4^{3-} formed from the processing [52, 53]. The clear absence of further defined crystallization peaks over the 2θ = 5-85° range was considered as an indication of good degree of compactness in a glass's network [53].

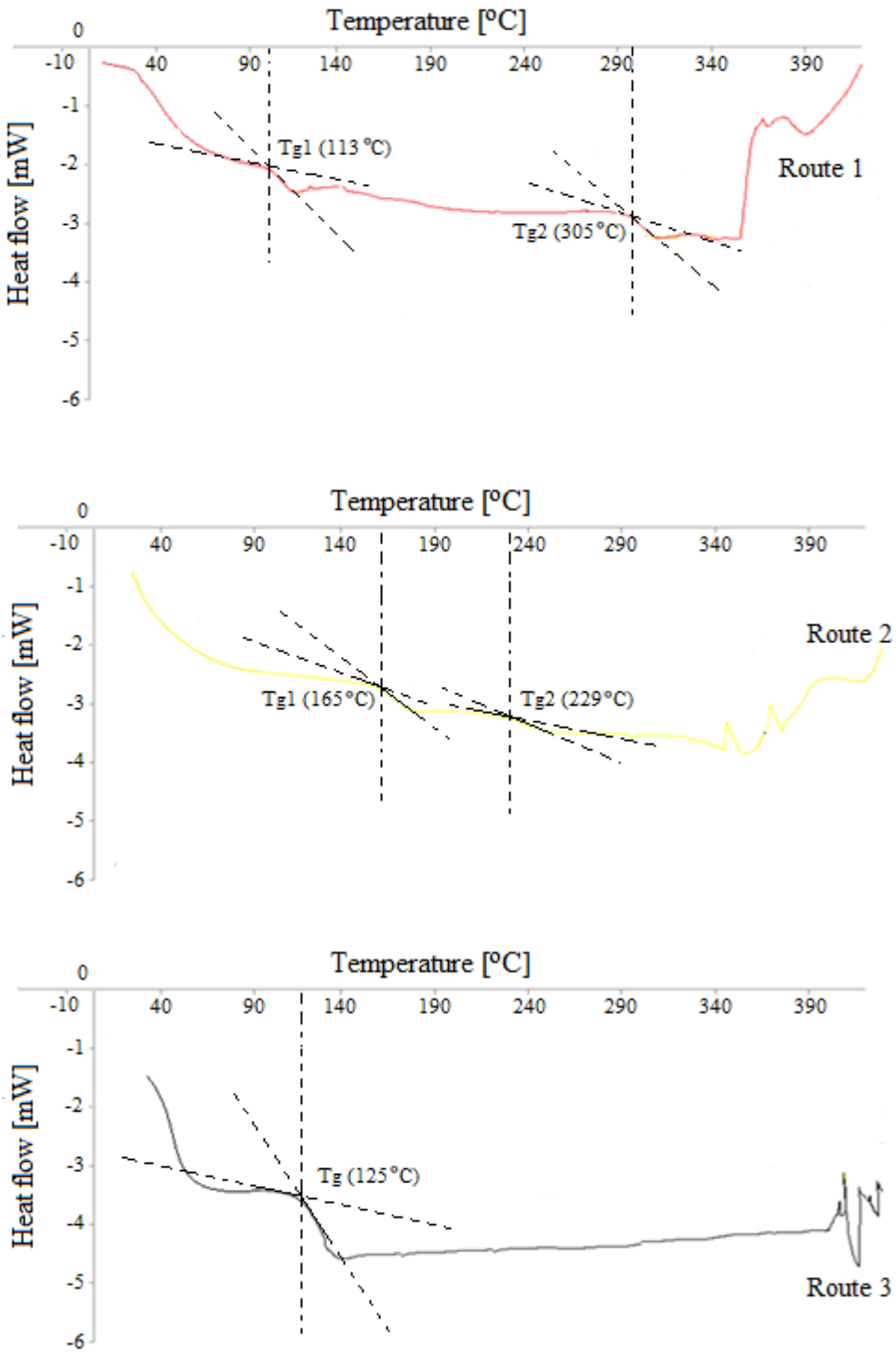

Figure 4.5: DSC trace of the phosphate glass (base composition) prepared by Route 1, Route 2 and Route 3 over the pre-programmed heating cycle indicative of endothermic and exothermic events.

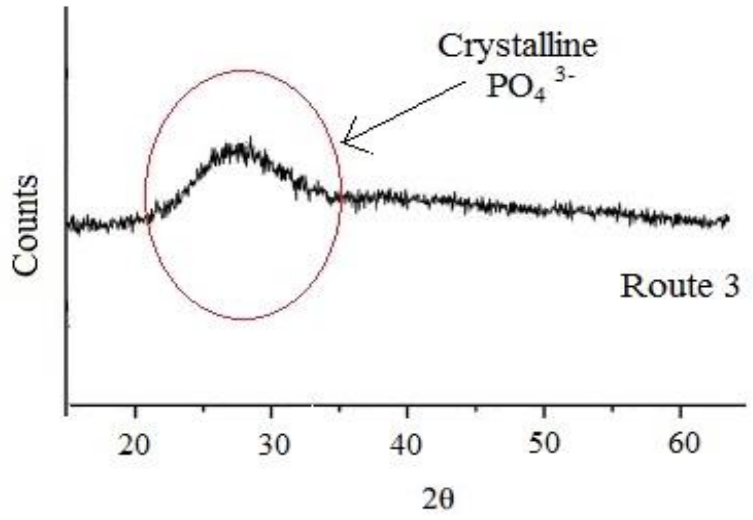

Figure 4.6: XRD traces of base composition of glasses prepared by Route 3 over 15-65° 2θ.

The features identified in the FTIR spectrum of the Glass 0 and the other glass compositions are summarized in Table 4.2. As the FTIR peaks associated with the phosphate network appears in the range 1200-500 cm^{-1}, a magnification of the FTIR trace (2000-400 cm^{-1}) of Glass 0 prepared with Route 3 is shown in Figure 4.7.

The low intensity absorption peak centred at ~ 1442 cm^{-1} has been assigned to C=O, which was hypothesized to originate from the atmospheric CO_2, as variously reported in [47-51]. The broad shoulder centred at 1180 cm^{-1} identified the asymmetric stretching of P=O associated with with Q^3 tetrahedra superposed with Q^2 $(PO_2)^-$ [ν_{as}] units [49]. The peak at ~ 1112 cm^{-1} has been assigned to the symmetric stretching of the Q^2 $(PO_2)^-$ units [49, 50]. The band at ~ 1014 cm^{-1} has been assigned to the asymmetric stretching of (PO_4^{3-}) end groups Q^0. The absorption band at ~ 910 cm^{-1} has been assigned to the symmetric stretching modes of chain-terminating Q^0 units $\nu_s(PO_4^{3-})$ and Q^1 units $\nu_s(PO_3^{2-})$. The absorption bands ν_{as}(P–O–P) and ν_s(P–O–P) occurring at ~ 845 and 750 cm^{-1} have been assigned, respectively, to the asymmetric and symmetric stretching of the bridging oxygen atoms bonded to a phosphorus atom in a Q^2 phosphate tetrahedron. The peak at 520 cm^{-1} was associated to the bending vibrations of bridging phosphorus δ(O-P-O) and/or δ(P=O).

The positions and intensities of the peaks/shoulders are reflective of the poly-pyro phosphate glass structure of Glass 0 (see Table 2.1 and Table 2.3), in agreement with the theory of Moustafa & Egili in [49].

Route 3 was the procedure used to process the glass compositions listed in Table 4.1 based on the homogeneity of the glass sample, the presence of a single low Tg, and a well-defined glass structure.

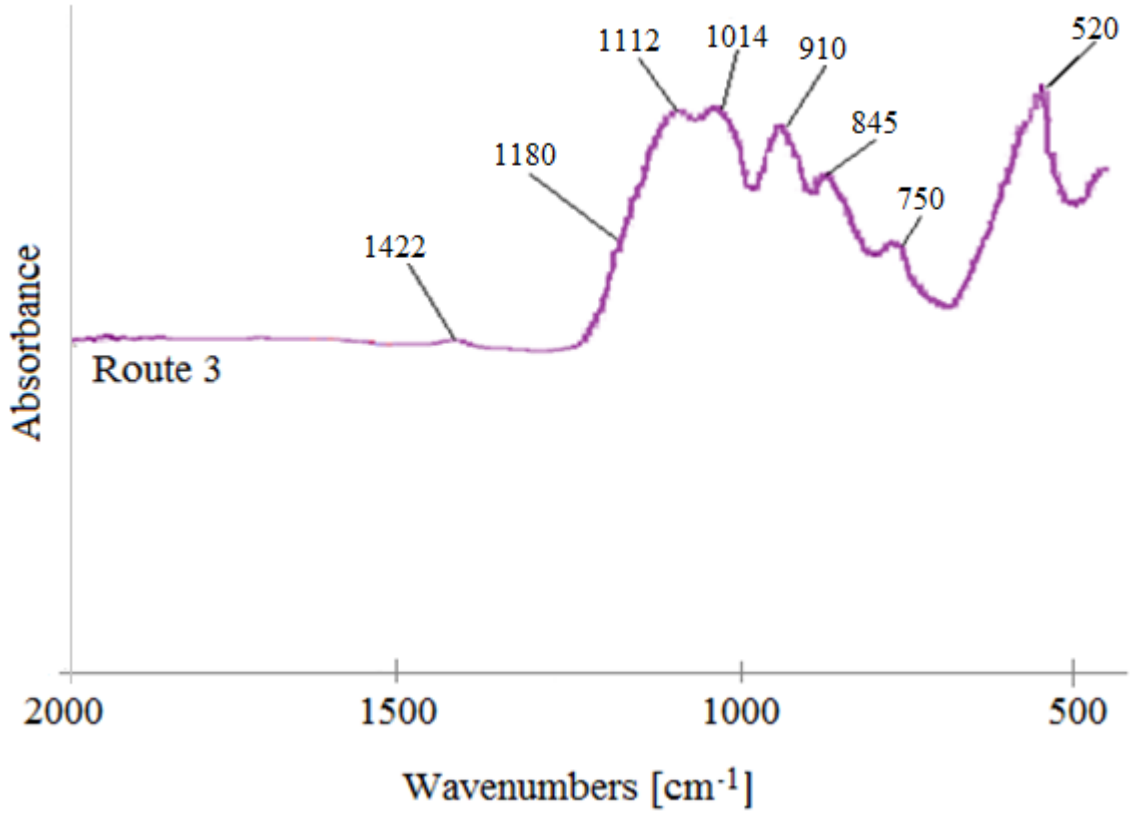

Figure 4.7: FTIR spectrum of Glass 0 prepared using Route 3 over the IR range 2000-400 cm^{-1}, showing absorption peaks and shoulders corresponding to the glass's structure with the wavenumbers of identified spectral features labelled.

4.4 Effect of composition on micro-structure of glasses

The structures of the glasses were assessed by FTIR. The characteristic absorption bands of the glasses are reported in Table 4.2. The assignment of wavenumber peaks/shoulders to

specific phosphate groups (i.e. Q^3, Q^2, Q^1, Q^0 units) was helped by the studies on phosphate glass structure present in [47-51], (see Table 2.3).

The structural modification of the glass compositions was assessed by comparing any deviation from the characteristic FTIR trace of Glass 0 (see Figure 4.7 and Table 4.2).

It was considered that shifts in absorbance peaks between each glass composition and the base composition (Glass 0) might occur because of changes in the bond strengths within the glass network induced by the different types and quantities of modifier oxides.

Table 4.2: FTIR spectral features identified for the Glass 0 over the 4000-400cm^{-1} wavenumber range.

	Feature	Wavenumber [cm^{-1}]	Assignment
A	Broad shoulder	1180	$(P=O)_{as}$ associated with Q^3 tetrahedra superposed with Q^2 $(PO_2)^-$ [ν_{as}] units
B	Peak/shoulder	1112	$(P\text{-}O^-)$ vibration in Q^2 units
C	Peak	1014	(PO_4^{3-})as in Q^0 units
D	Peak	910	(PO_3^{2-})s in Q^1 units
E	Peak	845	(P-O-P)as vibration in Q^2 units
F	Peak	750	(P-O-P)s vibration in Q^2 units
G	Peak	520	δ(O-P-O) and/or δ(P=O)

Effect of SnO content

Figure 4.8 shows the FTIR traces (2000-400cm^{-1}) of Class 1 glasses (SnF_2/P_2O_5 molar ratio equal to 1.67 and SnO in the range of 0-30 mol%).

The content of SnO greater than 20 mol% led to a shift of the broad shoulder centred at 1180 cm^{-1} (peak A) toward higher frequencies, indicating the formation of a few Q^3 phosphate units at the expense of Q^2 units. The feature at ~ 1112 cm^{-1} (peak B), assigned to the symmetric stretching of the Q^2 $(PO_2)^-$ units [49, 50], also shifted toward higher frequencies. The feature at ~1014 cm^{-1} (peak C), which corresponds to the asymmetric stretching of (PO_4^{3-}) end groups Q^0, decreased in intensity and again shifted toward higher frequencies.

This has been attributed to the decrease of Q^0 units in the glass network. The peaks at ~ 910 cm^{-1} (peak D), which corresponds to the symmetric stretching of (PO_3^{2-}) end groups Q^1, remained unaltered. The absorption band $(P–O–P)_{as}$ at ~ 845 cm^{-1} (peak E) moved toward higher frequency, while the band $(P–O–P)_s$ at 750 cm^{-1} (peak F) remained unaltered. The peak at 520 cm^{-1} (peak G), associated with the bending vibrations of bridging phosphorus δ(O-P-O) and/or δ(P=O), was unchanged by the increasing SnO above 20 mol%. The transition of the Class 1 glasses from an intermediate pyro-poly phosphate glass structure to a poly-phosphate structure is evident from the shifts and changes in intensities of the peaks in the FTIR spectra. Glass 5 (25 SnO mol%) and Glass 6 (30 SnO mol%) were thus classified as poly-phosphate glasses.

Decreasing the content of SnO from 20 mol% (Glass 0) to 15 mol% (Glass 4) led to a shift of the ~1014 and 910 cm^{-1} bands toward lower frequencies, which has been attributed to an increase of Q^0 units in the glass network. Glass 4 (15 SnO mol%) was classified as pyro-phosphate glass (Table 2.1).

FTIR could not generate a clear trace for a further decrease of SnO content below 15 mol%, possibly because of depolymerisation phenomena. These phenomena are triggered by the high quantity of F in the glass network which leads to the breakage of the P-P bonds and the formation of $P0_3F$- Q_1 units or PO_2F_2 –Q_0 units as explained in details in Section 2.3. For this composition any Sn quantity comes solely from SnF_2. as SnO is absent; it was hypothesized that the quantity of Sn was not sufficient to act as network former. On the other hand the high quantity of F acted as chain terminator causing the disruption of the Sn-O-P-O basic structural units (Figure 2.12). It was hypothesized that the high molar content of P_2O_5 in these glasses (> 38 mol%) led to the formation of both Sn-F-Sn and P-O-P, which are weak points in the network inducing a low chemical stability in the glass network. Glass 1, Glass 2 and Glass 3 were classified as ortho-phosphate glasses, which are formed mainly by Q^0 units

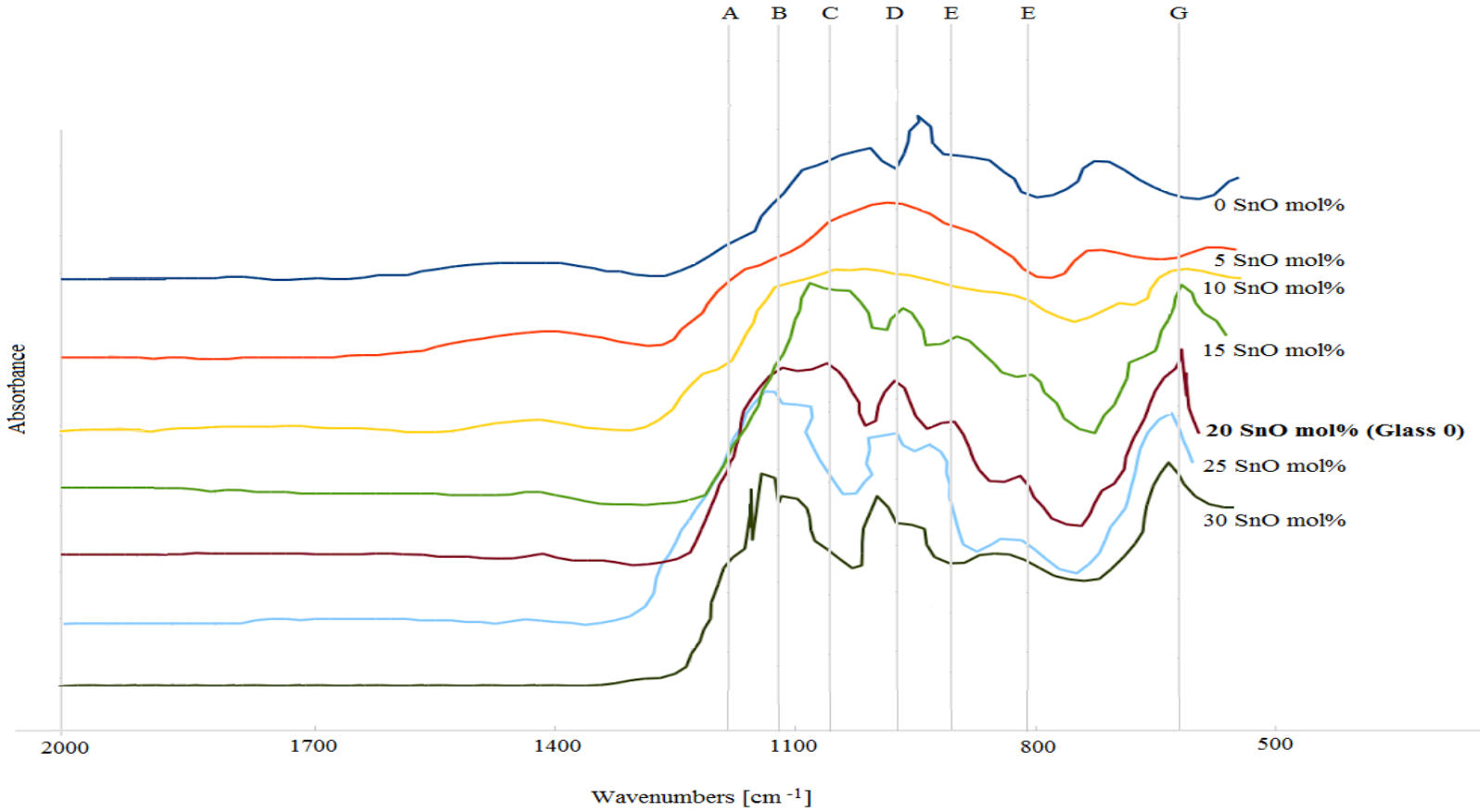

Figure 4.8: Magnification of FTIR vibrational spectra of the Class 1 phosphate glasses (SnF_2/P_2O_5 molar ratio equal to 1.67 and SnO in the range of 0-30 mol%) prepared using Route 3, showing absorption peaks and shoulders corresponding to the glass's structure with the wavenumber of identified spectral features of Glass 0 labelled.

Effect of SnF_2 content

Figure 4.9 shows the FTIR traces of Class 2 glasses (P_2O_5/SnO molar ratio equal to 1.5 and SnF_2 in the range of 30-60 mol%).

A shift of the broad shoulder centred at 1180 cm^{-1} (peak A) toward higher frequencies was observed at content of SnF_2 lower than the 50 mol% of Glass 0. Recall that the shoulder was attributed to overlap of the asymmetric $(P=O)_{as}$ stretching vibration of Q^3 units and $(PO_2)^-_{as}$ stretching vibration of Q^2 units. The peak at ~ 1112 cm^{-1} (peak B), assigned to the symmetric stretching of the Q^2 $(PO_2)^-$ units [49, 50], also shifted toward higher frequencies. This shift of these features is probably due to the polymerisation of phosphate network and the formation of longer of Q^2 chain and Q^3 as the SnF_2 decreases in the glass composition. The peak at ~1014 cm^{-1} (peak C), assigned to the asymmetric stretching of (PO_4^{3-}) end groups Q^0, decreased in intensity and again shifted toward higher frequencies, which has been attributed to the decrease of Q^0 units in the glass network. The peak at ~ 910 cm^{-1} (peak D), assigned to the symmetric stretching of (PO_3^{2-}) end groups Q^1 increased in intensity, which has been attributed to the decrease of Q^0 units and the increase of Q^1 units in the glass network. The absorption band ν_{as}(P–O–P) at ~845 cm^{-1} (peak E) remained unaltered, while the band ν_s(P–O–P) at 750 cm^{-1} (peak F) moved toward lower frequencies. The peak at 520 cm^{-1} (peak G), associated with the bending vibrations of bridging phosphorus δ(O-P-O) and/or δ(P=O) shifted toward lower frequencies. The transition of the Class 2 glasses from an intermediate pyro-poly phosphate glass structure to a poly-phosphate structure with decreasing SnF_2 content below the 50 mol% of Glass 0 is evident from the shifts and changes in intensities of the peaks in the FTIR spectra. Glass 10 (45 SnF_2 mol%) was classified as pyro-poly phosphate glass. Glass 7 (30 SnF_2 mol%) to Glass 9 (40 SnF_2 mol%) were classified as poly-phosphate glasses.

Increasing the content of SnF_2 from 50 mol% of Glass 0, led to a shift of the feature at 1180 cm^{-1} toward lower frequencies, indicating the decrease of non-bridging P=O bonds and asymmetric stretch mode of Q^3 units. The peak at ~ 1112 cm^{-1}, assigned to the symmetric stretching of the Q^2 $(PO_2)^-$ units, decreased in intensity, until completely disappeared at 60 SnF_2 mol%.

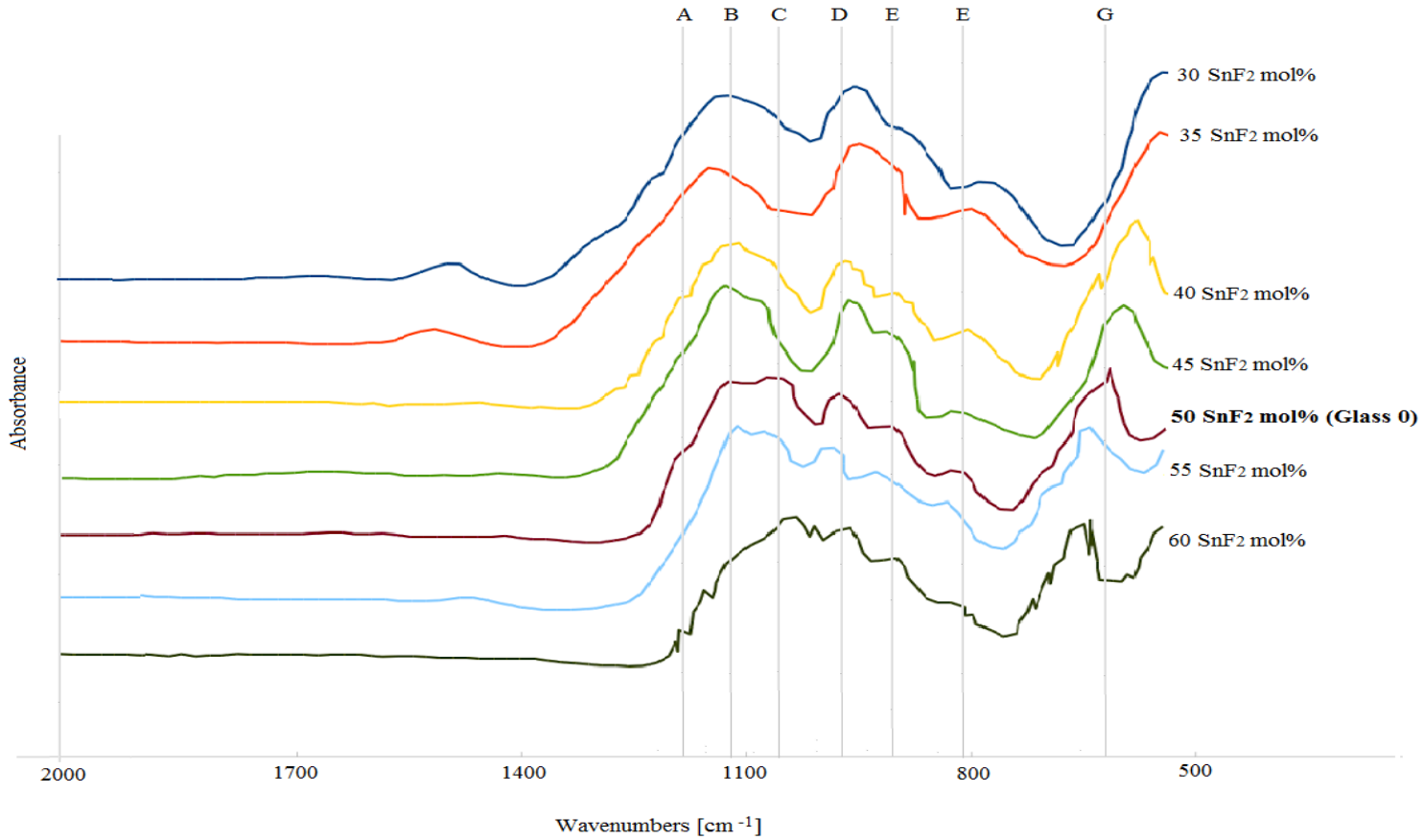

Figure 4.9: Magnification of FTIR vibrational spectra of the Class 2 phosphate glasses (P_2O_5/SnO molar ratio equal to 1.5 and SnF_2 in the range of 30-60 mol%) prepared using Route 3, showing absorption peaks and shoulders corresponding to the glass's structure with the wavenumbers of identified spectral features of Glass 0 labelled.

The peak at ~1014 cm^{-1}, which correspond to the asymmetric stretching of (PO_4^{3-}) end groups Q^0, increased in intensity and shifted toward lower frequencies. A new peak appeared at ~992 cm^{-1}, which has been assigned to the symmetric stretching of (PO_4^{3-}) end groups Q^0. This shifting behaviour has been attributed to the increase of Q^0 units in the glass network. The peak at ~ 910 cm^{-1}, which corresponds to the symmetric stretching of (PO_3^{2-}) end groups Q^1 decreased in intensity. The absorption band ν_{as}(P–O–P) at ~845 cm^{-1} moved toward lower frequencies, while the band ν_s(P–O–P) at 750 cm^{-1} remained unaltered. The peak at 520 cm^{-1}, associated with the bending vibrations of bridging phosphorus δ(O-P-O) and/or δ(P=O), shifted toward higher frequencies. The transition of the Class 2 glasses from an intermediate pyro-poly phosphate glass structure to a pyro-phosphate structure is evident from the shifts and changes in intensities of the peaks in the FTIR spectra. Glass 11 (55 SnF_2 mol%) and Glass 12 (60 SnF_2 mol%) were thus classified as poly-phosphate and pyro-phosphate glasses, respectively.

Effect of P_2O_5

Figure 4.10 shows the FTIR traces of Class 3 glasses (SnF_2/SnO molar ratio equal to 2.5 and P_2O_5 in the range of 20-40 mol%).

Reducing the content of P_2O_5 from 30 mol% (Glass 0) to 25 mol% (Glass 14) did not lead to any relevant changes and shifts in the FTIR traces. The absorption bands associated with the Q^3, Q^2, Q^1 and Q^0 units were still present and similar to those of Glass 0. Glass 14 was classified thus as a pyro-poly phosphate glass.

FTIR could not generate a clear trace for a further decrease of P_2O_5 content below 25 mol%, possibly because of depolymerisation phenomena. The amount of P_2O_5 was not sufficient to form the glassy structure. On the other hand the high amount of F in the glass network (57 SnF_2 mol%) acted as chain terminator causing the disruption of the Sn-O-P-O basic structural units, the breakage of the P-P bonds and the formation of PO_2F_2 –Q_0 units, as explained in details in Section 2.3. Glass 13 was thus classified as ortho-phosphate glass.

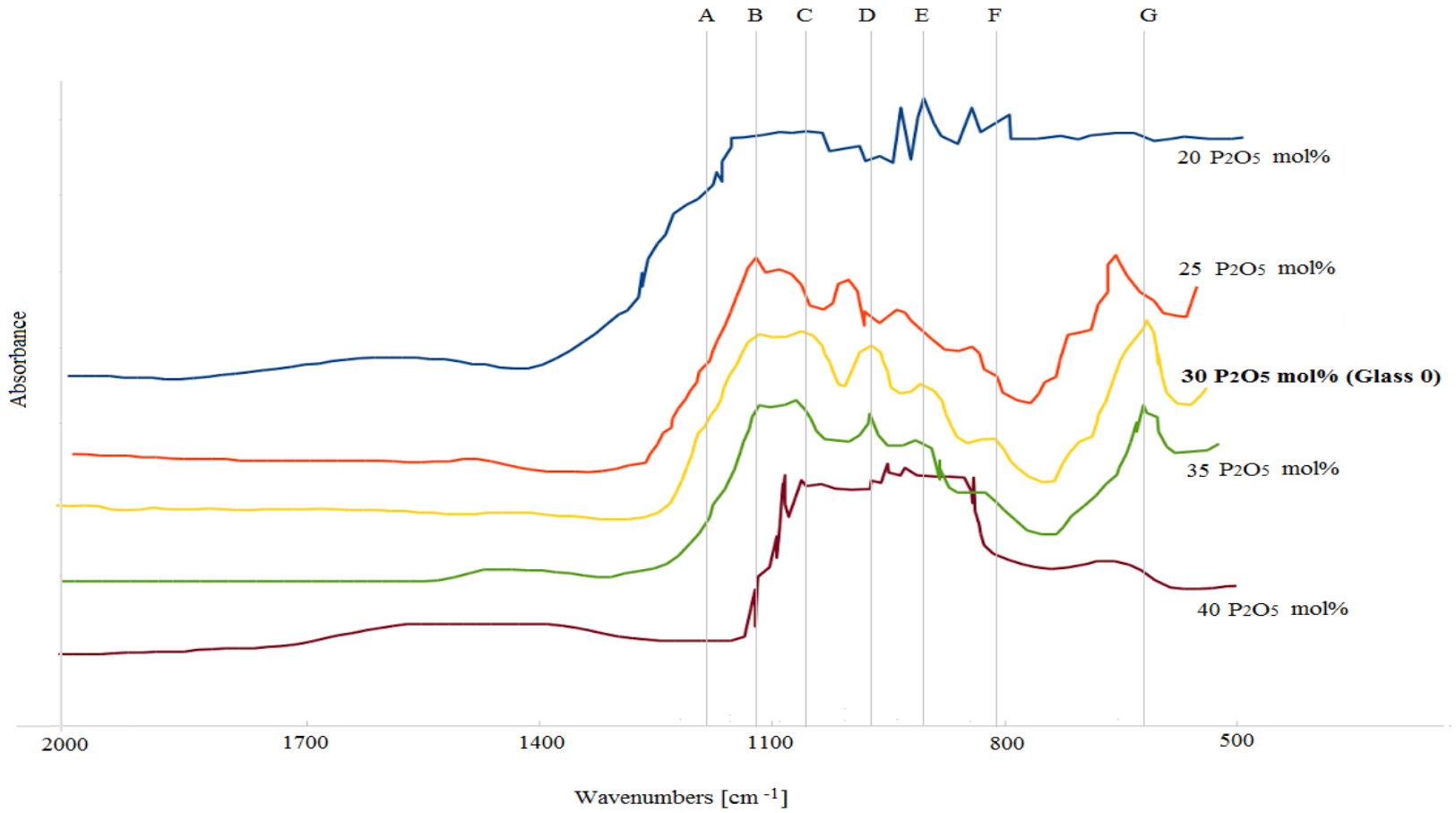

Figure 4.10: Magnification of FTIR vibrational spectra of the Class 3 phosphate glasses (SnF_2/SnO molar ratio equal to 2.5 and P_2O_5 in the range of 20-40 mol%) prepared using Route 3, showing absorption peaks and shoulders corresponding to the glass's structure with the wavenumbers of identified spectral features of Glass 0 labelled.

Increasing the content of P_2O_5 from 30 mol% (Glass 0) to 35 mol% (Glass 15) did not lead to any relevant changes and shifts in the FTIR traces. The absorption bands associated with the Q^3, Q^2, Q^1 and Q^0 units were still present and remained similar to those of Glass 0. Glass 15 was thus classified as a pyro-poly phosphate glass.

A clear FTIR trace was not produced for a further increase of P_2O_5 content, which was attributed to the high amount of P_2O_5 (~ 40 mol%) and its hydrophilic nature. On the other hand the decreased content of SnO (~ 17 mol%) and increased content of fluoride (SnF_2 ~ 43 mol%) did not allow the formation of sufficient crosslinks along the glass chains. Glass 16 was thus classified as ortho-phosphate glass.

4.5 Effect of composition on density of glasses

In general both the packing of the glass network and the molecular weight of each contributed oxide affect the density of the glass system. The density of the glasses was measured at 21 ˚C using the Archimedes' method described in Section 3.5; the results of these measurements are shown in Table 4.3 and Figure 4.11. The measured density of the base composition (50 SnF_2 – 30 P_2O_5 – 20 Sn0) was 3570 kg/m^3; which agrees well with the value reported by [2, 4, 18, 20-23, 26, 27, 33, 37-39, 42]. The measured densities of Class 1 glasses (SnF_2/P_2O_5 = 1.67) increased from ~ 3190 to ~ 3820 kg/m^3 as the amount of SnO increased from 0 to 30 mol%. In Class 2 glasses (P_2O_5/SnO = 1.5) the measured densities increased from ~ 3450 to ~ 3920 kg/m^3 as the amount of SnF_2 increased from 30 to 60 mol%. The measured densities of Class 3 glasses (SnF_2/SnO = 2.5) increased from ~ 3350 to ~ 3760 kg/m^3 as the amount of P_2O_5 increased from 20 to 40 mol%. It is generally accepted that the density increases when the concentration of the third component is increased while the ratio of the other concentrations remain constant, in agreement with the results reported in this section [2, 4, 18, 20-23, 26, 27, 33, 37-39, 42].

On the other hand the increase of density in Class 2 glasses might be as the result of the formation of a denser glass structure associated with close packing of atoms by the strong P–O–Sn bonds [49].

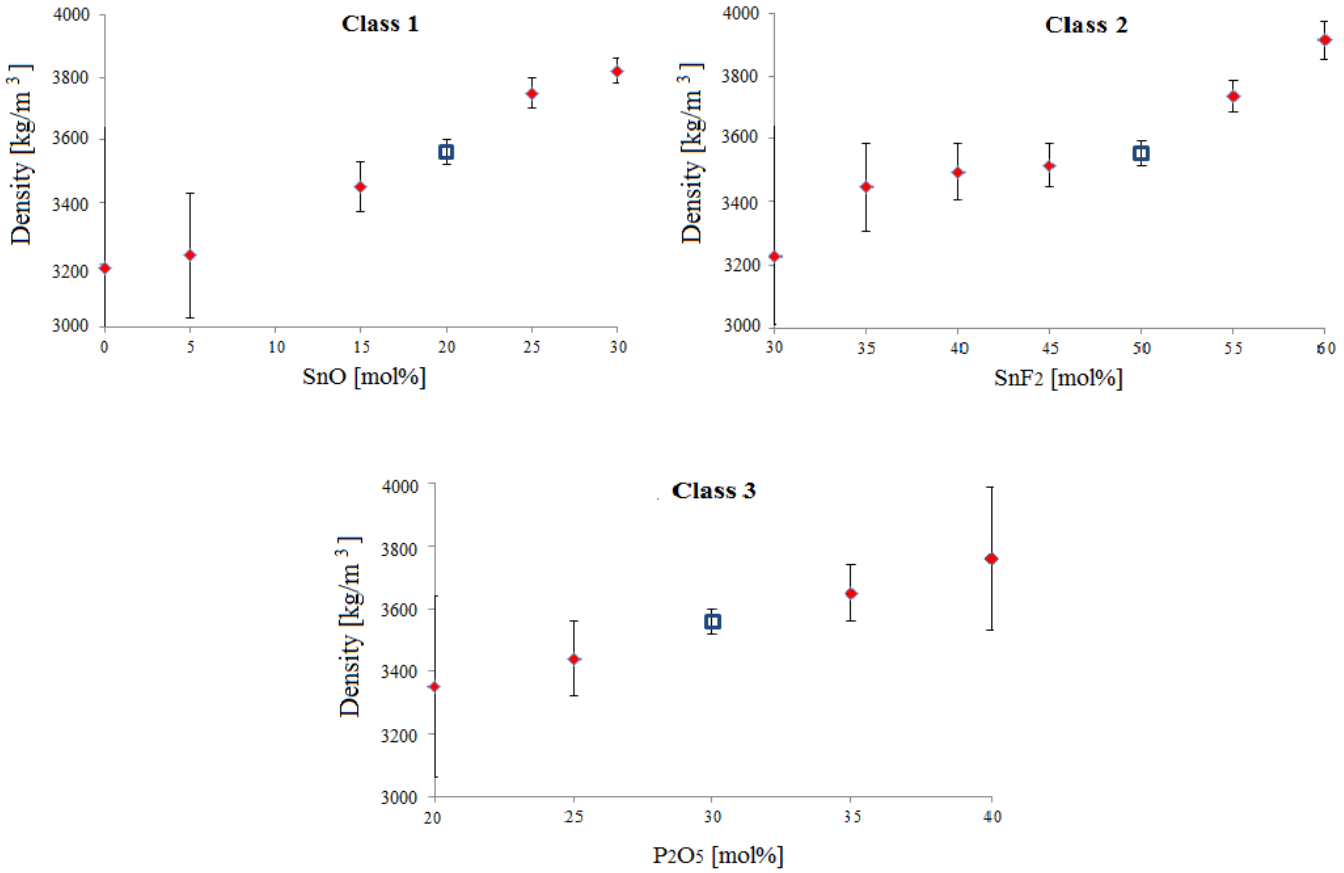

Figure 4.11: Effect of glass composition on the measured density of Class 1 (SnF_2/P_2O_5 molar ratio equal to 1.67 and SnO in the range of 0-30 mol%), Class 2 (P_2O_5/SnO molar ratio equal to 1.5 and SnF_2 in the range of 30-60 mol%) and Class 3 (SnF_2/SnO molar ratio equal to 2.5 and P_2O_5 in the range of 20-40 mol%) glasses.

Table 4.3: Density of phosphate glasses measured at 21 ˚C using the Archimedes' method.

Glass	SnF_2 [mol%]	P_2O_5 [mol%]	SnO [mol%]	Density ρ [kg/m^3]
Base glass				
0	50.0	30.0	20.0	3560 ± 400
Class 1 (SnF_2/P_2O_5 = 1.67)				
1	62.1	37.9	0.0	3190 ± 450
2	59.4	35.6	5.0	3230 ± 200
3	56.3	33.7	10.0	3300 ± 250
4	53.1	31.9	15.0	3450 ± 80
5	46.9	28.1	25.0	3750 ± 50
6	43.7	26.3	30.0	3820 ± 40
Class 2 (P_2O_5/SnO = 1.5)				
7	30.0	42.0	28.0	3230 ± 220
8	35.0	39.0	26.0	3450 ± 140
9	40.0	36.0	24.0	3500 ± 90
10	45.0	33.0	22.0	3520 ± 70
11	55.0	27.0	18.0	3740 ± 50
12	60.0	24.0	16.0	3920 ± 60
Class 3 (SnF_2/SnO = 2.5)				
13	57.1	20.0	22.9	3350 ± 290
14	56.2	25.0	18.8	3440 ± 120
15	46.4	35.0	18.6	3650 ± 90
16	42.9	40.0	17.1	3760 ± 230

4.6 Effect of composition on glass transitions of glasses

As stated in Section 4.1, a low Tg in the range of 70-170˚C and a low softening point in the range of 180-300˚C, close in value to the extrusion working temperature, was required from the glasses to achieve a good glass-polymer hybridization. Transition temperatures of glasses were determined by DSC and calculated as reported in Section 3.6.1. The glass transition Tg and crystallization onset To values of glass compositions are summarized in Table 4.4.

Effect of SnO

DSC traces of Class 1 glasses (SnF_2/P_2O_5 molar ratio equal to 1.67 and SnO in the range of 0-30 mol%) are compared in Figure 4.12. One Tg has been revealed from the heat flow/temperature trends for each composition.

The Tgs of Class 1 glasses vary in the range of 110-146 ˚C, meeting the glass transition temperature requirement stated in Section 4.1. Tg increases with SnO content in the glass composition, which has been related to the formation of cross links in the phosphate glass chains consequently to the introduction of the SnO into the glass network. Tg does not increase linearly with SnO, which has been linked to the quantity of the acceptor oxygen available inside the network. It was hypothesized that an increasing quantity of SnO led to a decrease in the fraction of the acceptor-bonds of the protons until further crosslinks could no longer form, and to a further increase of the Tg. For SnO ≤ 15 mol%, the Tg values were not accurate given the high standard deviation of the results. This was believed to have arisen from the low quantity of Sn, which was not sufficient to act as network former. It was considered that the high quantity of SnF_2 allowed the fluoride F to act as chain terminator causing the breakage of the P-P bonds and the formation of $P0_3F$- Q_1 units or PO_2F_2 –Q_0 units as explained in details in Section 2.3.

As phosphate glasses tend to crystallize, crystallization peak may be observed in the DSC traces. The tendency of glass to undergo crystallization was quantified using the processing window (PW) parameter. The processing window, defined as the temperature difference

between Tg and To, was determined from the DSC trace using the procedure reported in Section 3.6.1.

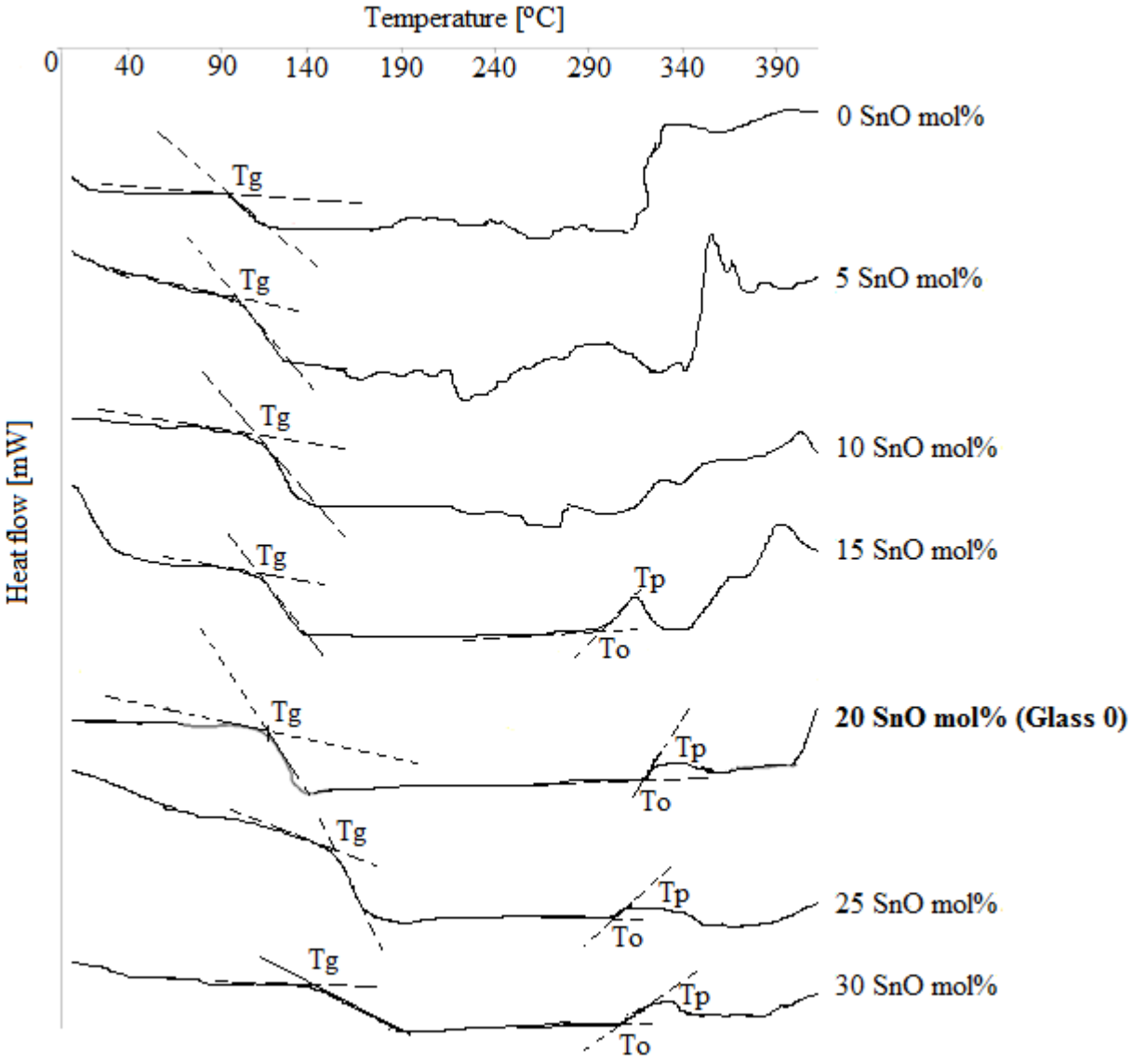

Figure 4.12: DSC traces of Class 1 phosphate (SnF_2/P_2O_5 molar ratio equal to 1.67 and SnO in the range of 0-30 mol%). The glass transition temperature (Tg), crystallization onset (To) and crystallization peak temperature (Tp) are labelled in each trace.

A defined crystallization peak Tp was not seen in the thermograph for glasses having SnO content of less than 15 mol% (Figure 4.12). For the remaining Class 1 glasses the crystallization onset temperatures Tos were in the range of 300-330 ˚C, with a processing window (PW) in the range of 179-188˚C.

These results suggest that the SnO content affects the tendency of glass toward crystallization: as the width of the processing window (PW) increased with SnO in the glass, Class 1 glasses with high amount of SnO have a lower tendency to crystallize. It is considered that the introduction of SnO into the phosphate glass network increased the density of cross links among the phosphate chains, leading to an increased entanglement of the glass network; this prevents the network components to arrange in an ordered crystalline structure.

Effect of SnF_2

DSC traces of Class 2 glasses (P_2O_5/SnO molar ratio equal to 1.5 and SnF_2 in the range of 30-60 mol%) are compared in Figure 4.13. Each Class 2 composition revealed a single Tg.

The Tgs of Class 2 glasses are in the range of 106-162 ˚C, meeting the glass transition temperature requirement stated in Section 4.1. Tg decreases with increasing SnF_2 mol% in the compositions as reported in Table 4.4 and shown in Figure 4.13. The increase of SnF_2 content to the glass network led to the breaking of P-P bonds to form $P0_3F$- Q_1 units or PO_2F_2 –Q_0 units, as explained in details in Section 2.3. This decreased the average chain length and, thus, the Tg of glasses. It was hypothesized that the formation of these units can lead to some network rearrangements, which explains why Tg does not decrease proportionally with SnF_2 content.

A weak crystallization peak can be seen in all the thermographs. The crystallization onset temperature To of Class 2 glasses are in the range of 327˚C-334 ˚C, with a trend independent from SnF_2 content in the composition. The introduction of fluoride into a phosphate network was reported in [36-38] to reduce the entanglement of glass network, which results in short

phosphate units with low viscosity of the melt. This structure should have a high tendency to crystallize [52].

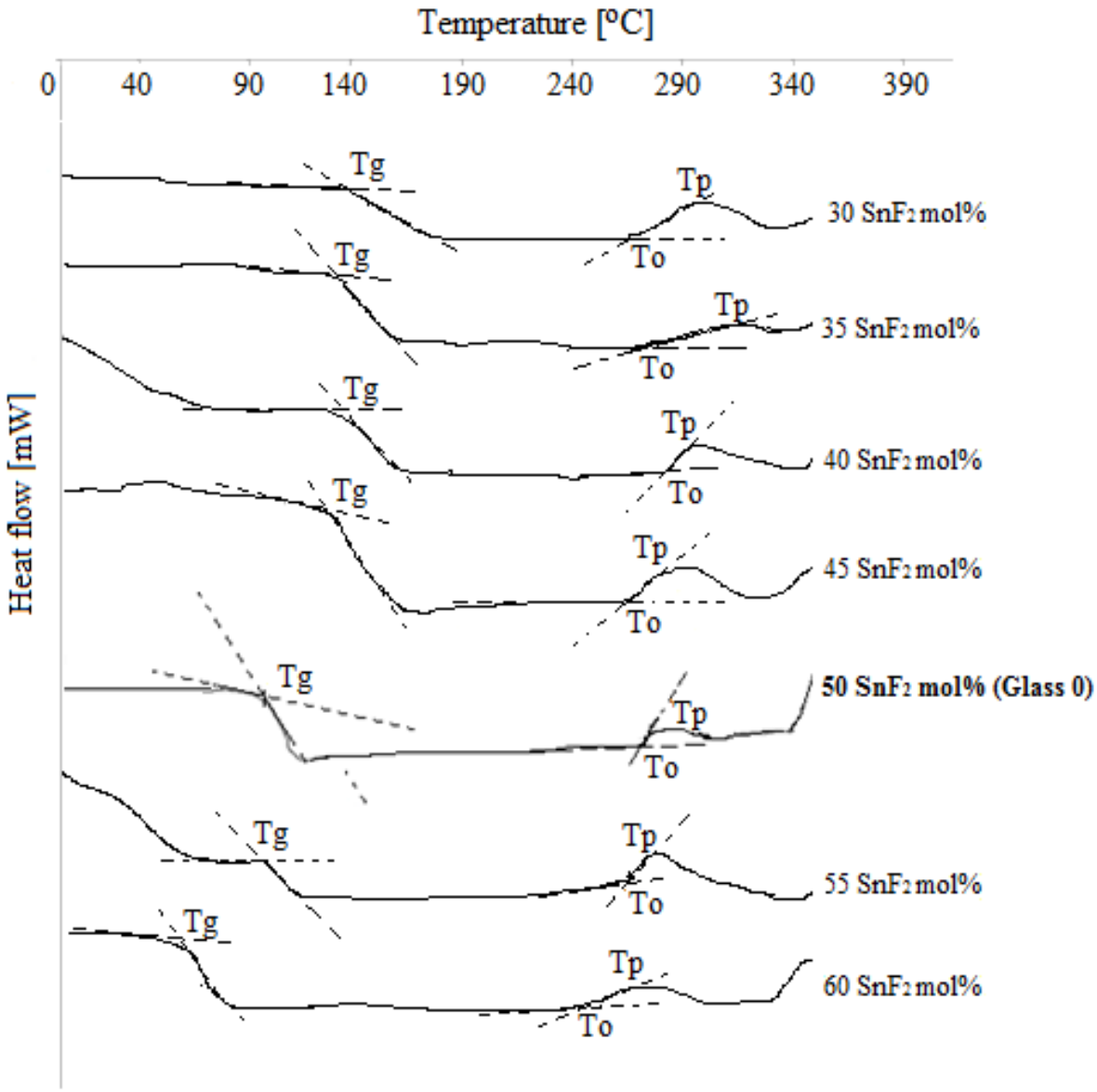

Figure 4.13: DSC traces of Class 2 glasses (P_2O_5/SnO molar ratio equal to 1.5 and SnF_2 in the range of 30-60 mol%). The glass transition temperature (Tg), crystallization onset (To) and crystallization peak temperature (Tp) are labelled in each trace.

However the introduction of Sn was reported to increase the cross links among the glass network [36-38]. This can explain why SnF_2 content did not affect the tendency of glass toward crystallization. The width of the processing window (PW) increases notably from 165˚C to 229 ˚C with SnF_2 content, which is due to the decrease of Tg with increasing SnF_2 in Class 2 compositions. Thus the Class 2 glasses are thermally stable in a temperature range which increases with SnF_2 content.

Effect of P_2O_5

DSC traces of Class 3 glasses (SnF_2/SnO molar ratio equal to 2.5 and P_2O_5 in the range of 20-40 mol%) are reported in Table 4.4 and Figure 4.14.

Each Class 3 composition revealed a single Tg. The glass transitions of Class 3 glasses are in the range between 102˚C-125˚C. The glass transition temperature requirement for hybridization stated in Section 4.1 is met. Tg decreases sharply when P_2O_5 content is less than 25 mol%. This has been related to the limited number of P-O-P bridges in the glass structure [36-38], which would decrease the linkage of the network, the viscosity and glass transition temperature. Tg decreases when P_2O_5 is great than 35 mol%, which has been attributed to the hydrophilic nature of P_2O_5. Also, The FTIR traces show that the decreased content of SnO and increased content of SnF_2 with increasing content of P_2O_5 could lead to the formation of Q_0 units (Figure 4.10).

No crystallization onset was visible for glasses with phosphate content below 25 mol% and above 30 mol%, preventing the determination of a proper processing window. The processing windows for the remaining glasses of Class 3 were similar to those ones Class 1 and Class 2 with PW values ranging between 172-210 ˚C.

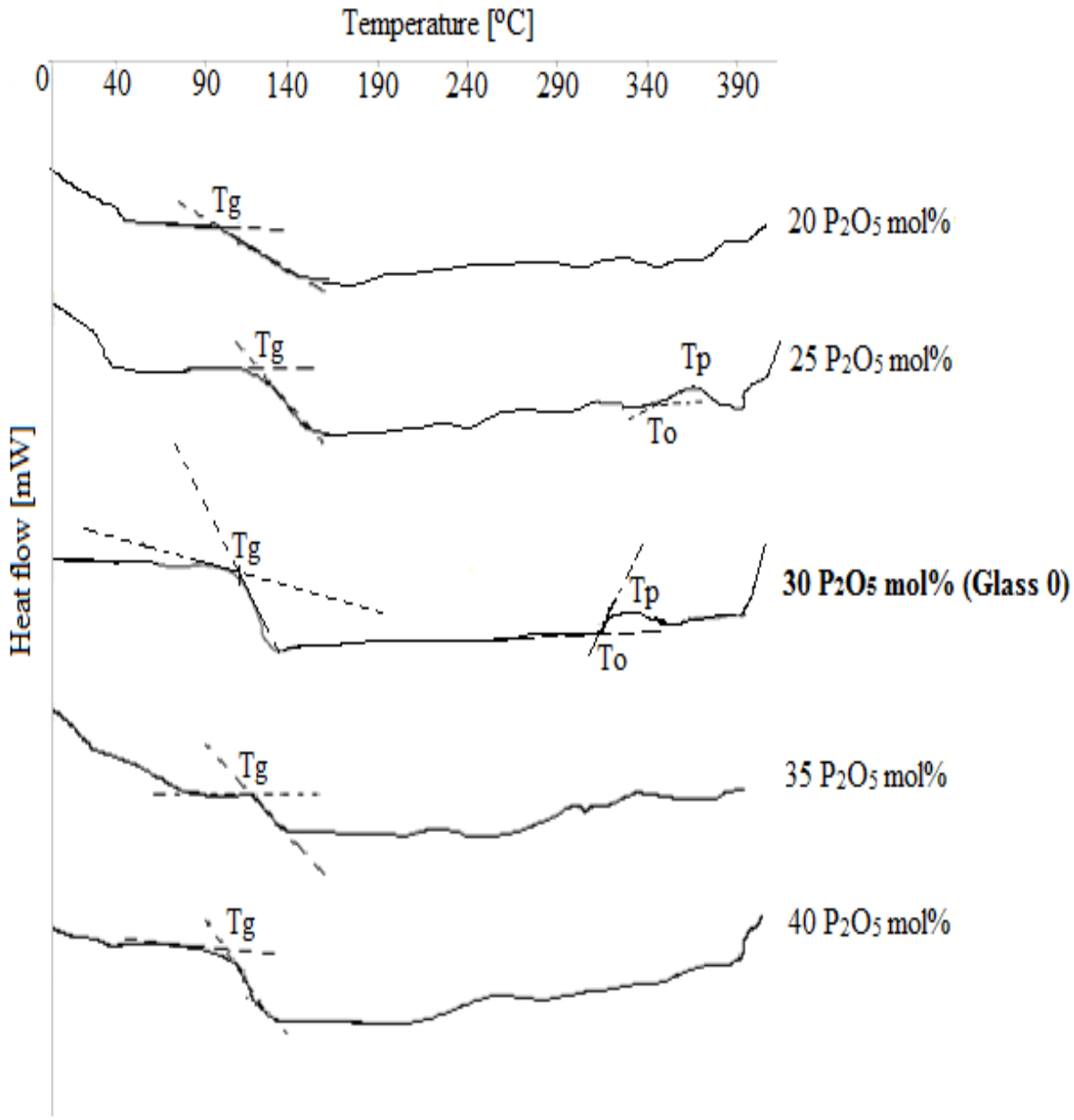

Figure 4.14: DSC traces of Class 3 glasses (SnF_2/SnO molar ratio equal to 2.5 and P_2O_5 in the range of 20-40 mol%)). The glass transition temperature (Tg), crystallization onset (To) and crystallization peak temperature (Tp) are labelled in each trace.

Table 4.4: Glass transitions, Crystallization Onset and Processing Window identified for Class 1, Class 2 and Class 3 glass compositions.

Glass	SnF_2 [mol%]	P_2O_5 [mol%]	SnO [mol%]	Tg [˚C]	To [˚C]	PW [˚C]
0	50.00	30.00	20.00	125.0 ± 4.5	332.0 ± 9.0	202.5 ± 7.0
Class 1						
1	62.1	37.9	0.0	107.5 ± 13.5	-	-
2	59.4	35.6	5.0	103.0 ± 12.5	-	-
3	56.3	33.7	10.0	109.5 ± 6.5	-	-
4	53.1	31.9	15.0	122.0 ± 4.0	300.8 ± 4.5	179.5 ± 3.5
5	46.9	28.1	25.0	147.0 ± 5.0	325.5 ± 7.5	190.0 ± 5.0
6	43.7	26.3	30.0	145.0 ± 5.0	333.5 ± 5.0	188.0 ± 3.0
Class 2						
7	30.0	42.0	28.0	162.5 ±5.5	328.0 ± 4.5	166.0 ± 3.5
8	35.0	39.0	26.0	158.5 ±7.0	332.5 ± 3.0	173.5 ± 6.5
9	40.0	36.0	24.0	157.5 ± 5.5	328.0 ± 5.5	171.0 ± 7.5
10	45.0	33.0	22.0	156.5 ± 3.5	331.0 ± 2.5	174.5 ± 3.5
11	55.0	27.0	18.0	118.0 ± 6.0	333.0 ± 5.0	214.5 ± 5.0
12	60.0	24.0	16.0	106.0 ± 4.5	335.0 ± 3.5	229.0 ± 5.0
Class 3						
13	57.1	20.00	22.9	102.5 ± 23.0	-	176.0 ± 6.5
14	56.2	25.00	18.8	125.0 ± 12.5	336.0 ± 8.0	211.0 ± 8.5
15	46.4	35.00	18.6	124.5 ± 18.0	-	-
16	42.9	40.00	17.1	105.0 ± 13.5	-	-

4.7 Effect of composition on softening point of glasses

The softening point of each glass composition was determined according the procedure reported in Section 3.6.2. The results are shown in Figure 4.15 and summarized in Table 4.5.

The softening point of the Glass 0 (20 SnO mol%) is ~ 310 ˚C.

The softening points of Class 1 glasses (SnF_2/P_2O_5 molar ratio equal to 1.67 and SnO in the range of 0-30 mol%) are in the range of 287-402 ˚C with a sharp increase for SnO > 20 mol% in the composition.

The softening points of Class 2 glasses (P_2O_5/SnO molar ratio equal to 1.5 and SnF_2 in the range of 30-60 mol%) are in the range of 289-350 ˚C and decrease with increasing SnF_2 content in the composition.

The softening points of Class 3 glasses (SnF_2/SnO molar ratio equal to 2.5 and P_2O_5 in the range of 20-40 mol%) are in the range of 275-335 ˚C, and decreases sharply for P_2O_5 < 25 mol% and P_2O_5 > 30 mol%.

The effect of glass composition on the softening points of glasses follows the same trend of glass transition temperatures (see Section 4.6). Except for Glass 6, which exhibits a Ts of ~ 402 ˚C, the highest of all compositions, the softening points of the glasses vary in the range of 200-350 °C. This implies that the softening point of those glasses met the requirement stated in Section 4.1.

It should be noted that Glass 1 to Glass 3 (Class 1 glasses with SnO < 20 mol%), Glass 11 and Glass 12 (Class 2 glasses with SnF_2 > 50 mol%) and, Glass 13 and Glass 16 (Class 3 glasses with 20 P_2O_5 mol% and 40 P_2O_5 mol%, respectively) possess a softening point value slightly higher than the processing temperature range of polyamides. This condition could facilitate the hybridization with polyamide 11.

Table 4.5: Softening points of phosphate glasses.

Glass	SnF_2 [mol%]	P_2O_5 [mol%]	SnO [mol%]	Softening point [˚C]
Base glass				
0	50.0	30.0	20.0	310.0 ± 12.0
Class 1 (SnF_2/P_2O_5 = 1.67)				
1	62.1	37.9	0.0	287.0 ± 62.0
2	59.4	35.6	5.0	291.0 ± 51.0
3	56.3	33.7	10.0	302.0 ± 45.0
4	53.1	31.9	15.0	307.0 ± 31.0
5	46.9	28.1	25.0	349.0 ± 17.0
6	43.8	26.2	30.0	402.0 ± 15.0
Class 2 (P_2O_5/SnO = 1.5)				
7	30.0	42.0	28.0	350.0 ± 12.0
8	35.0	39.0	26.0	342.0 ± 11.0
9	40.0	36.0	24.0	331.0 ± 14.0
10	45.0	33.0	22.0	328.0 ± 15.0
11	55.0	27.0	18.0	304.0 ± 19.0
12	60.0	24.0	16.0	289.0 ± 12.0
Class 3 (SnF_2/SnO = 2.5)				
13	57.1	20.0	22.9	275.0 ± 35.0
14	56.2	25.0	18.8	320.0 ± 20.0
15	46.4	35.0	18.6	335.0 ± 16.0
16	42.9	40.0	17.1	282.0 ± 52.0

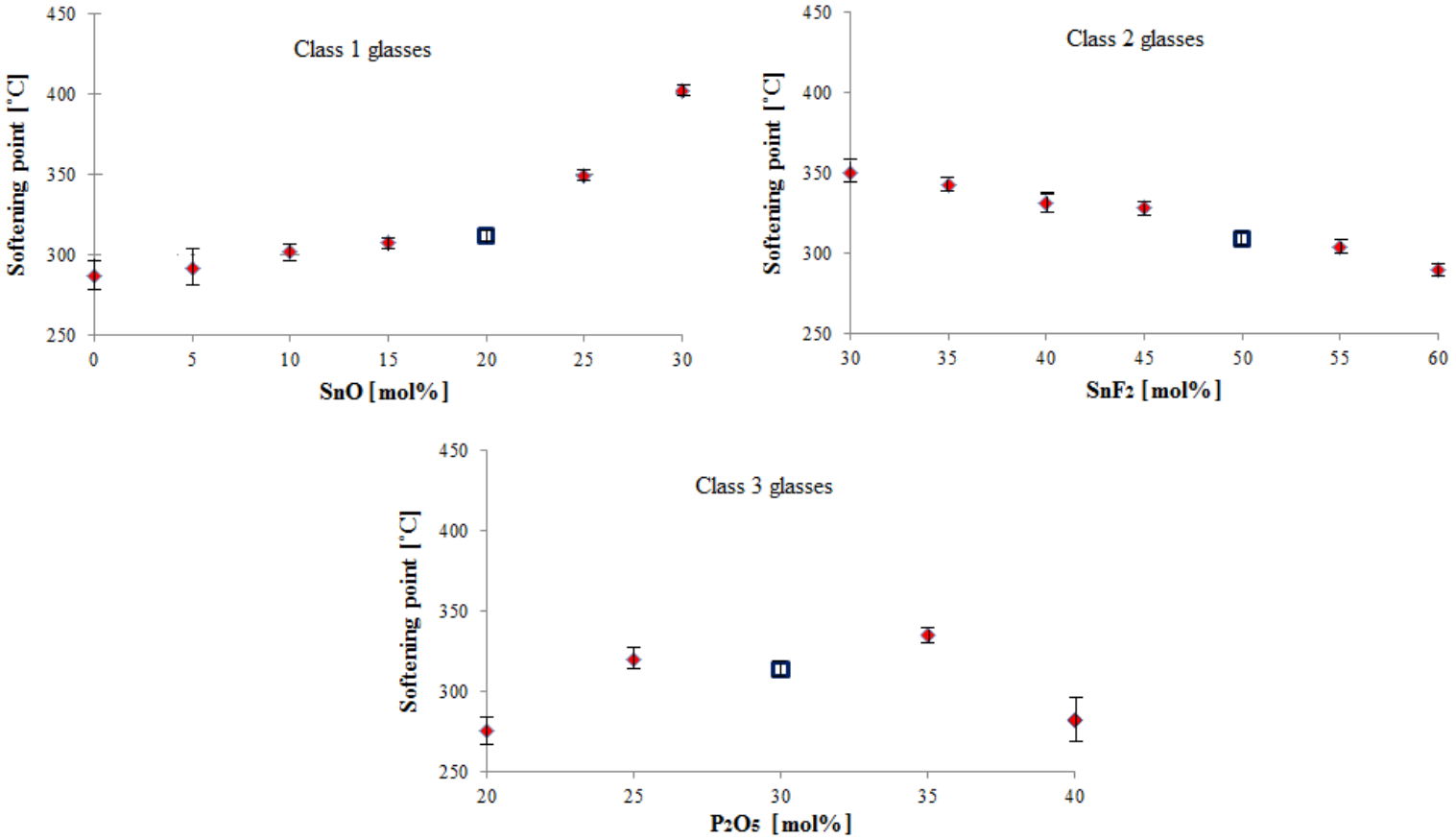

Figure 4.15: Softening point of Class 1 (SnF_2/P_2O_5 molar ratio equal to 1.67 and SnO in the range of 0-30 mol%), Class 2 (P_2O_5/SnO molar ratio equal to 1.5 and SnF_2 in the range of 30-60 mol%) and Class 3 (SnF_2/SnO molar ratio equal to 2.5 and P_2O_5 in the range of 20-40 mol%) glasses.

4.8 Effect of composition on stability in water of glasses

Stability in water is one of the main issues of phosphate glasses [26, 27] as water induces their depolymerisation via the formation of hydroxyl groups [26, 27]. The dissolution in water of phosphate glasses is described in details in Section 2.3.3. To quantify the water stability of glasses, the dissolution rate was calculated as described in Section 3.7.1.

The dissolution rate calculated for the base composition (Glass 0) was 0.0039 mg cm^{-2} hr^{-1}. The effect of glass composition on the dissolution rate was investigated.

Effect of SnO

The morphology and weight loss of Class 1 glasses (SnF_2/P_2O_5 molar ratio equal to 1.67 and SnO in the range of 0-30 mol%) were sampled over 576 hours. Class 1 glasses showed evident heterogeneity and phase-separation. Bubbles were prominent in glasses with 0-5 SnO mol% (Figure 4.16), clarifying that SnO was clearly responsible for reducing water absorption of phosphate glasses. Furthermore as the SnO decreases in the composition the hydroscopic nature of phosphate tetrahedron becomes important.

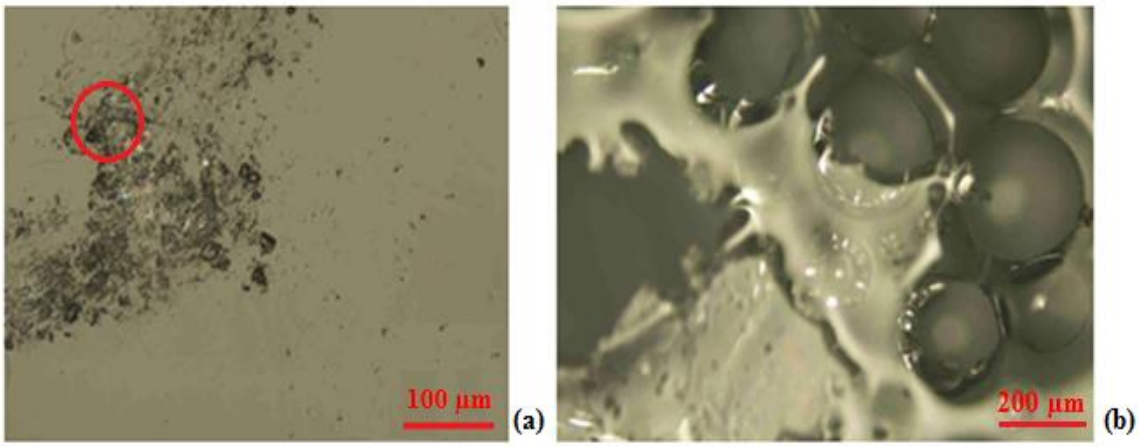

Figure 4.16: Optical micrograph of cross section of class 1 glass with composition of 59.4 SnF_2 +5 SnO + 35.6 P_2O_5 mol% prepared using Route 3.

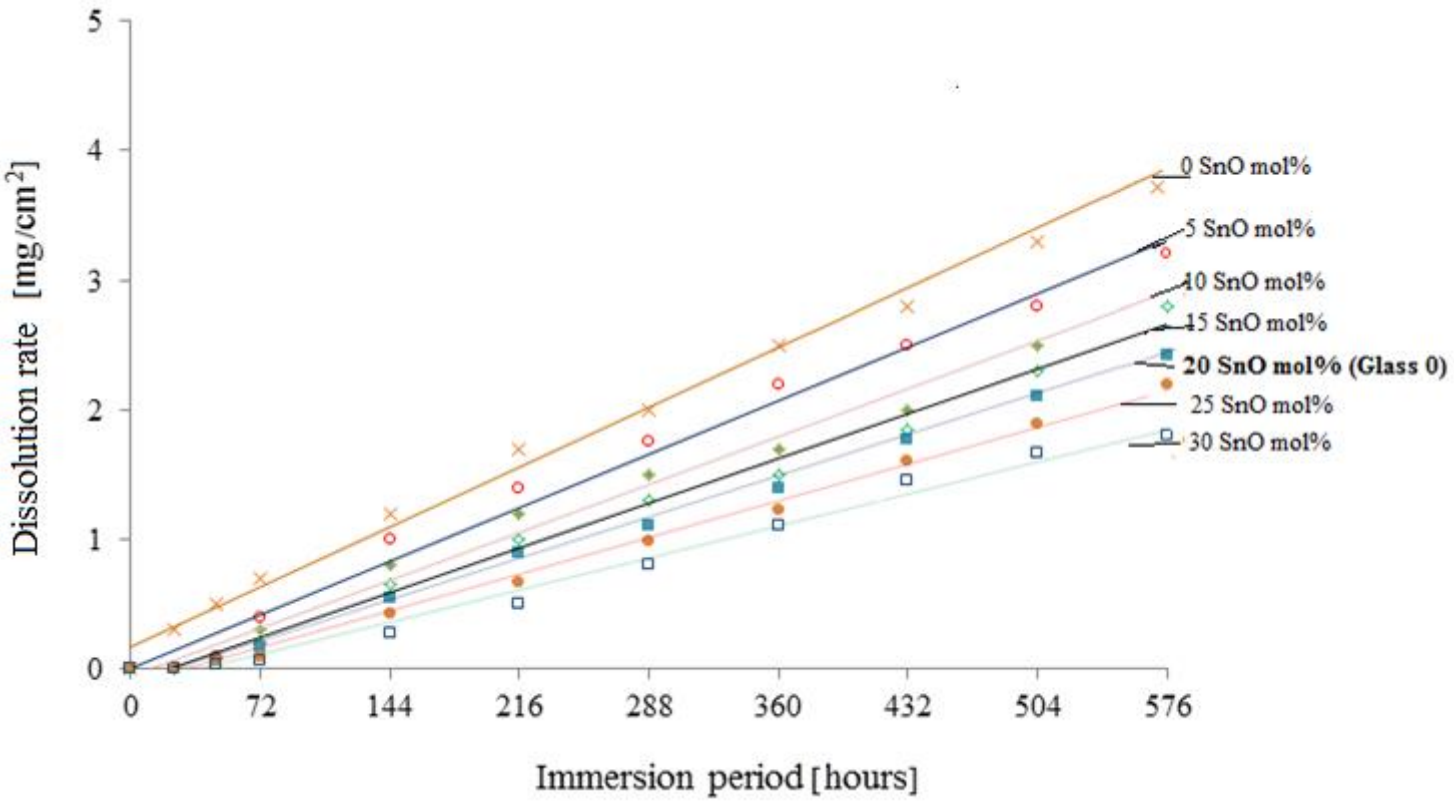

Figure 4.17: Weight loss during dissolution of Class 1 (SnF_2/P_2O_5 molar ratio equal to 1.67 and SnO in the range of 0-30 mol%) glass disks immersed in distilled water at 37°C with the overlaid trend-lines plotted through the origin indicative of the glass's dissolution rate.

The glasses dissolution rates (weight loss per unit area and per time unit) in water over 576 hours were determined from an overlaid linear trend-line passing through the origin. Figure 4.17 shows the measured weight loss of the Class 1 glasses as function of the immersion time. The values are summarized in Table 4.6. The dissolution rates are in the range of 0.0031-0.0069 mg cm^{-2} hr^{-1} and increase with decreasing content of SnO in the composition.

As the SnO in the glass decreases, the quantity of acceptor oxygen inside the network, and thus the cross links, decrease [36-38]. On the other hand, at a too low amount of SnO (0-15 mol%) the limited number of cross links and a too high content of both fluoride and phosphate oxide present could lead to the depolymerisation of the glass network [36-38].

Effect of SnF_2

After immersing the glasses in water for 576 hours, an excellent morphology with good homogeneity and no phase separation was still evident in Class 2 glasses (P_2O_5/SnO molar ratio equal to 1.5 and SnF_2 in the range of 30-60 mol%) even for high content of SnF_2 as shown in Figure 4.18.

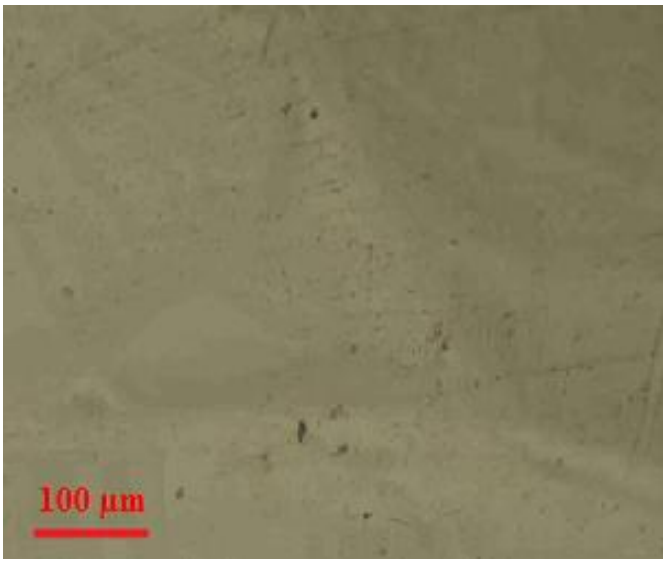

Figure 4.18: Optical micrograph of cross section of Class 2 glass with composition of 45 SnF_2 +22 SnO + 33 P_2O_5 mol% prepared according Route 3 and after 576 hours of immersion in water.

At high content of SnF_2, the phosphate content is relatively low, which limited the moisture absorption in the glass. It was hypothesized that the depolymerisation of the network was avoided thanks to the medium Sn content, present in all the compositions. The amount of SnO in the range of 18-28 mol% allowed a few P-P bonds to break and to form $P0_3F$- Q_1 units or PO_2F_2 –Q_0 units [36-38], which avoided a pronounced network depolymerisation. On the other hand the presumably limited number of cross-link maintained a relatively low Tg in the glasses.

Figure 4.19 shows the measured weight loss of the Class 2 glasses as function of the immersion time. The dissolution rates are in the range of 0.0037-0.0054 mg cm^{-2} hr^{-1} and decrease with increasing content of SnF_2 in the composition.

As the SnF2 in the glass increases, the chance of fluoride atom to form P03F-Q1 units or PO2F2–Q0 depolymerisation units increases [36-38].

On the other hand the quantity of acceptor oxygen inside the network, given by amount of Sn in SnF2 and SnO in the glass compositions, has been kept almost constant. It has been hypothesized that at higher SnF_2 content, the optimum of P/Sn ratio and the number of Sn-O-P-P bonds at a maximum has been achieved, causing an increase in water durability [36-38]; any further decreases in the SnF_2 content eventually results in the formation of Sn-F-Sn bonds, which are also easily attacked by water and which, again, lead to a decrease in chemical durability.

Furthermore, the Class 2 glasses possibly have a structure with a limited number of cross links, and a low amount of $P0_3F$-Q1 units or PO_2F_2–Q_0 [36-38] that might help to achieve a low Tg without compromising in large amount the polymerisation of the network.

P_2O_5 is considered to be the main responsible for moisture absorption in Class 2 glasses. The structural changes which occur in the melt as the Sn^{2+} content increases with increasing SnF_2 content, i.e. as more Sn-O-P-O bonds replace P-O-P bonds is reported in a few works in literature [26-27].

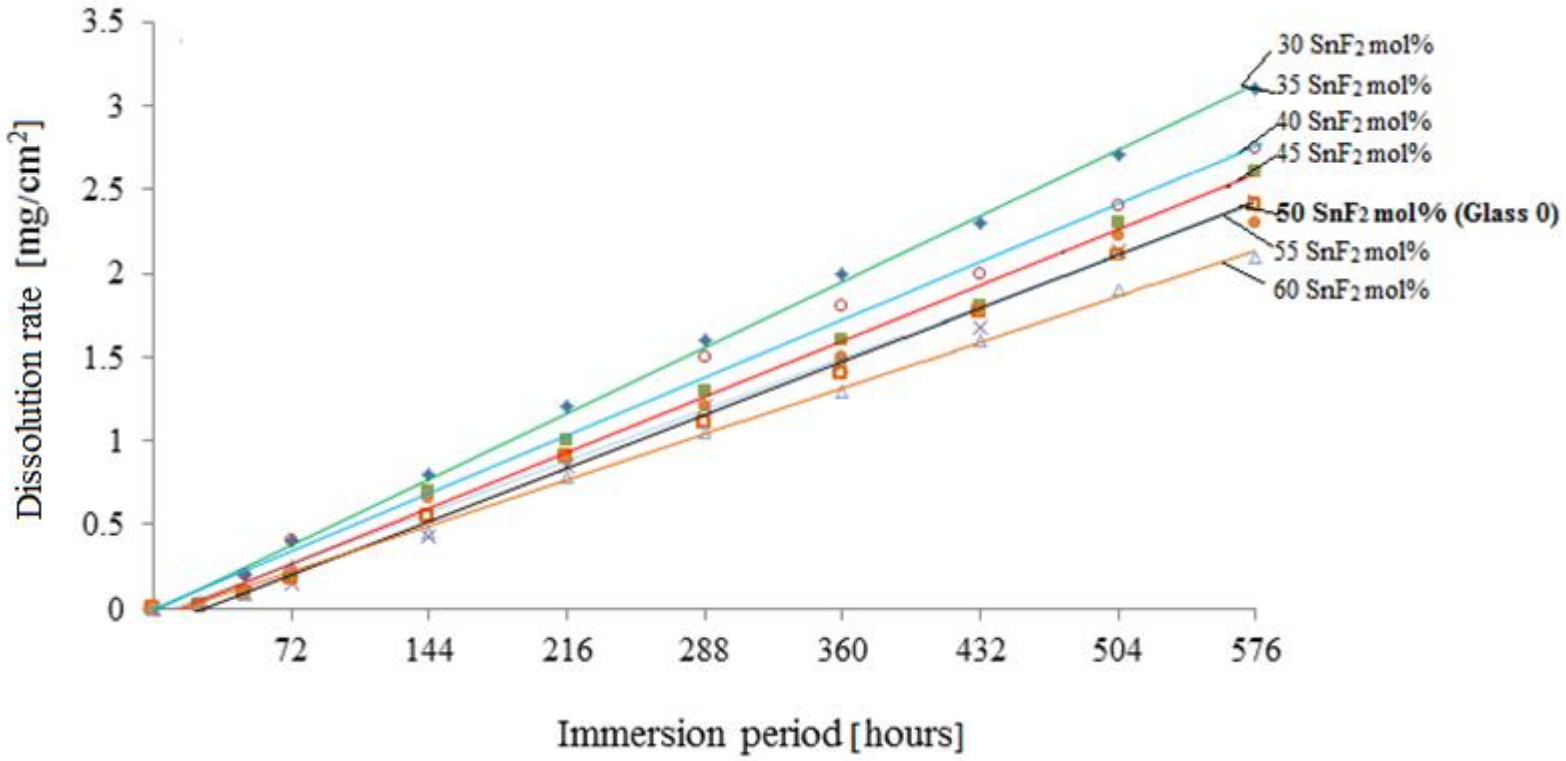

Figure 4.19: Weight loss during dissolution of Class 2 (P_2O_5/SnO molar ratio equal to 1.5 and SnF_2 in the range of 30-60 mol%) glass disks immersed in distilled water at 37°C with the overlaid trend-lines plotted through the origin indicative of the glass's dissolution rate.

Effect of P_2O_5

After immersing the glasses in water for 576 hours, many bobbles and black spots were visible in Class 3 glasses (SnF_2/SnO molar ratio equal to 2.5 and P_2O_5 in the range of 20-40 mol%) with 20 mol% P_2O_5 and 40 mol% P_2O_5. Figure 4.20 shows the micrograph of Glass 16 (40 mol% P_2O_5) after immersion in water. The black spot was analysed by EDX and confirmed to be tin phosphate fluoride agglomerates (Figure 4.21).

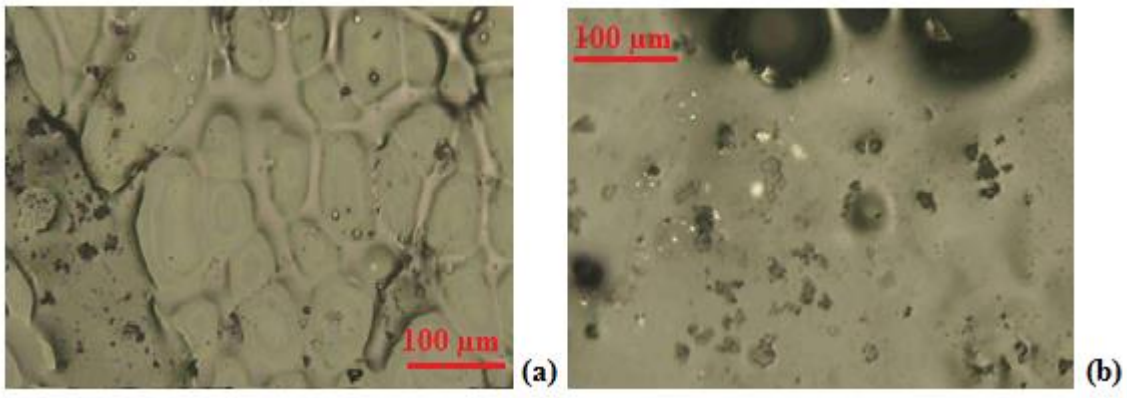

Figure 4.20: Optical micrograph of cross section of Class 3 glass with composition of 42.9 SnF_2 +17.1 SnO + 40 P_2O_5 mol% prepared according Route 3. Water absorption and structure alterations are well visible.

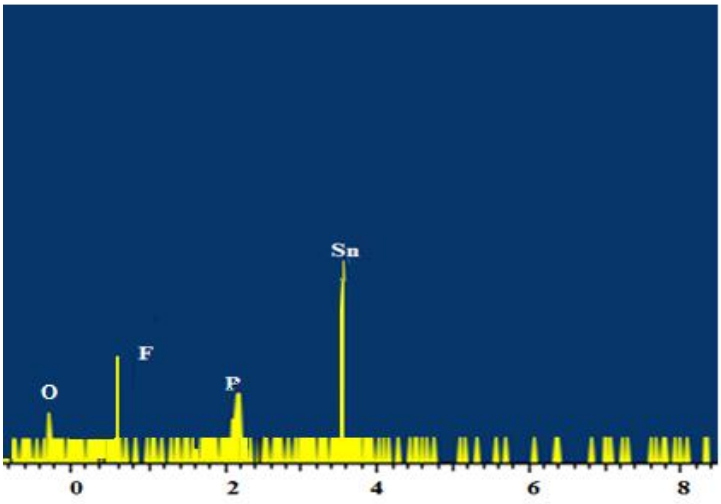

Figure 4.21: EDX of cross section of Class 3 glass with composition of 42.9 SnF_2 +17.1 SnO + 40 P_2O_5 mol% prepared according Route 3.

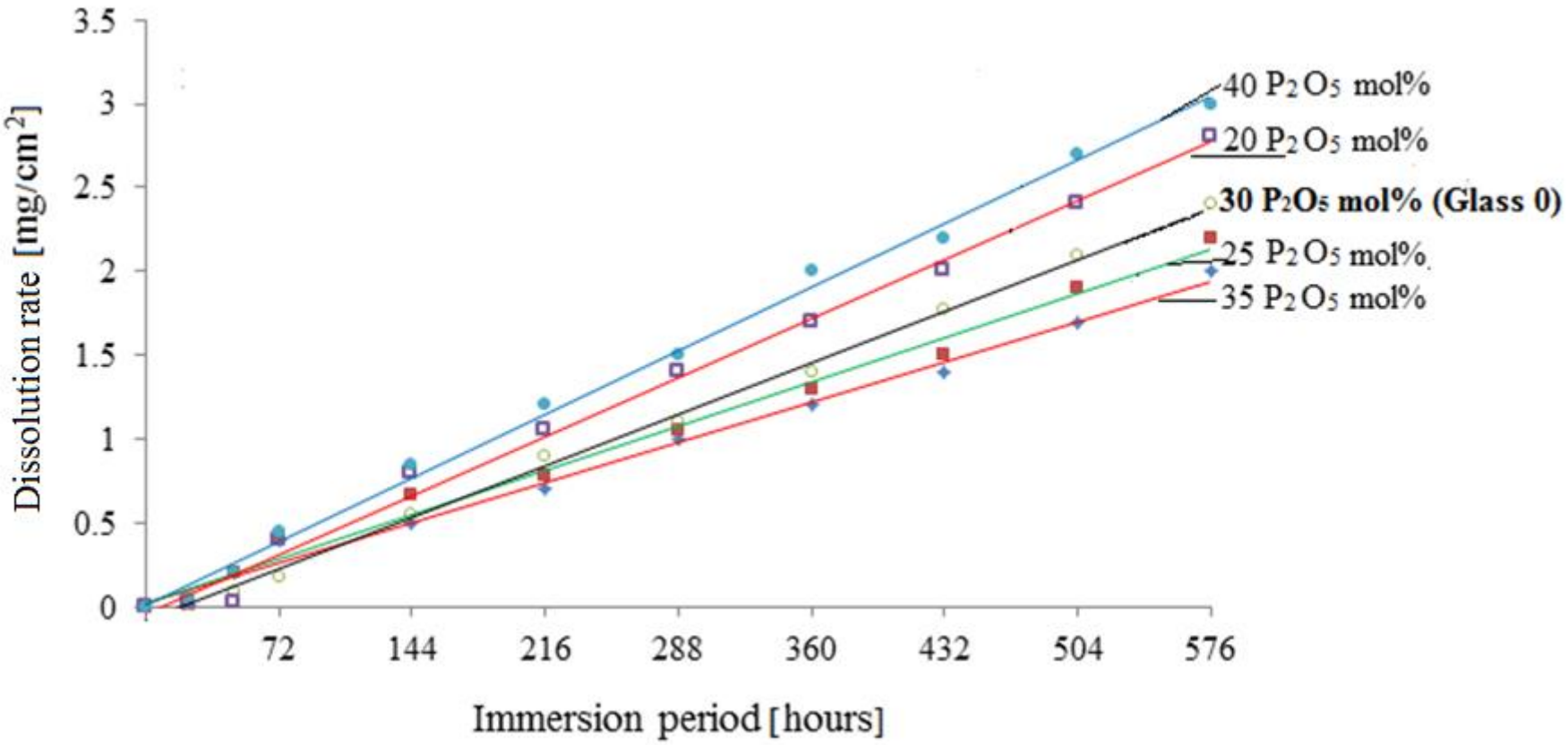

Figure 4.22: Weight loss during dissolution of Class 3 (SnF_2/SnO molar ratio equal to 2.5 and P_2O_5 in the range of 20-40 mol%) glass disks immersed in distilled water at 37°C with the overlaid trend-lines plotted through the origin indicative of the glass's dissolution rate.

Table 4.6: Dissolution rates identified of phosphate glasses. The glass disks were immersed in distilled water at 37°C with the overlaid trend-lines plotted through the origin indicative of the glass's dissolution rate.

Glass		SnF_2 [mol%]	P_2O_5 [mol%]	SnO [mol%]	Dissolution rate, [mg cm^{-2} h^{-1}]
Base glass					
	0	50.0	30.0	20.0	0.0039 ±0.002
Class 1 SnF_2/P_2O_5 =1.67					
	1	63.1	37.9	0.0	0.0069 ± 0.002
	2	59.4	35.6	5.0	0.0058 ± 0.009
	3	56.3	33.7	10.0	0.0050 ± 0.0008
	4	53.1	31.9	15.0	0.0045 ± 0.0005
	5	46.8	28.2	25.0	0.0036 ± 0.0002
	6	43.8	26.2	30.0	0.0031 ± 0.0001
Class 2 (P_2O_5/SnO molar ratio = 1.5)					
	7	30.0	42.0	28.0	0.0054 ± 0.0007
	8	35.0	39.0	26.0	0.0048 ± 0.0005
	9	40.0	36.0	24.0	0.0045 ± 0.0004
	10	45.0	33.0	22.0	0.0042 ± 0.0004
	11	55.00	27.00	18.00	0.0041 ± 0.0003
	12	60.00	24.00	16.00	0.0037 ± 0.0003
Class 3 (SnF_2/SnO molar = 2.5)					
	13	57.1	20.0	22.9	0.0048 ± 0.0006
	14	56.2	25.0	18.8	0.0037 ± 0.0002
	15	46.4	35.0	18.6	0.0034 ± 0.0003
	16	42.9	40.0	17.1	0.0053 ± 0.0008

Figure 4.22 shows the measured weight loss of the Class 3 glasses in function of the immersion time. The dissolution rates are in the range of 0.0034-0.0053 mg cm^{-2} hr^{-1} (Table 4.6). Glass 13 (20 mol% P_2O_5) and Glass 16 (40 mol% P_2O_5) show the highest dissolution rates in water, 0.0048 and 0.0053 mg cm^{-2} hr^{-1} respectively. The dissolution rates results are in agreement with the experimental evidence from micrographs.

The decrease of water stability in glass with 20 mol% P_2O_5 has been related in [36-38] to the limited number of P-O-P bridges in the glass structure, which would decrease the linkage of the network and its stability in water. The decrease in water stability of the glass with 40 P_2O_5 mol%, has been attributed to the hydrophilic nature of P_2O_5. This result disagrees with the work in [26] where the best resistance to attack by water is reported at 40 mol% P_2O_5, a composition exhibiting an optimum of P/Sn ratio and the number of Sn-O-P-P bonds at a maximum.

4.9 Effect of composition on thermal stability of glasses

In this research the phosphate glasses were subjected to medium temperature during extrusion and injection moulding processes, which could lead to degradation/depolymerisation of the glasses. As even a very small degree of degradation can massively influence the properties of the final hybrids, it was important monitoring mass changes in the phosphate glass samples with temperature up to 400 ˚C.

The percentage of mass loss of each glass composition was determined according the procedure reported in Section 3.7.2.

The base composition (Glass 0) shows a mass loss of 0.10% at 400°C.

Effect of SnO

The TGA traces for Class 1 glasses (SnF_2/P_2O_5 molar ratio equal to 1.67 and SnO in the range of 0-30 mol%) are shown in Figure 4.23.

The mass loss at 400°C decreases from 4.25% to 0.75% with increased SnO content in the glass network, with Glass 1 (0 SnO mol%) and Glass 6 (30 SnO mol%) showing the highest and lowest values respectively. This behaviour was likely related to the increased crosslinks of Q^2 and Q^3 units across the glass chains as the SnO increased, which is evident from the FTIR traces in Figure 4.8. Also, it was hypothesized that, as Sn is incorporated in the basic structural units and the number of Sn-O-P bridges increases [36], the linkage of the glass network would increase with SnO content.

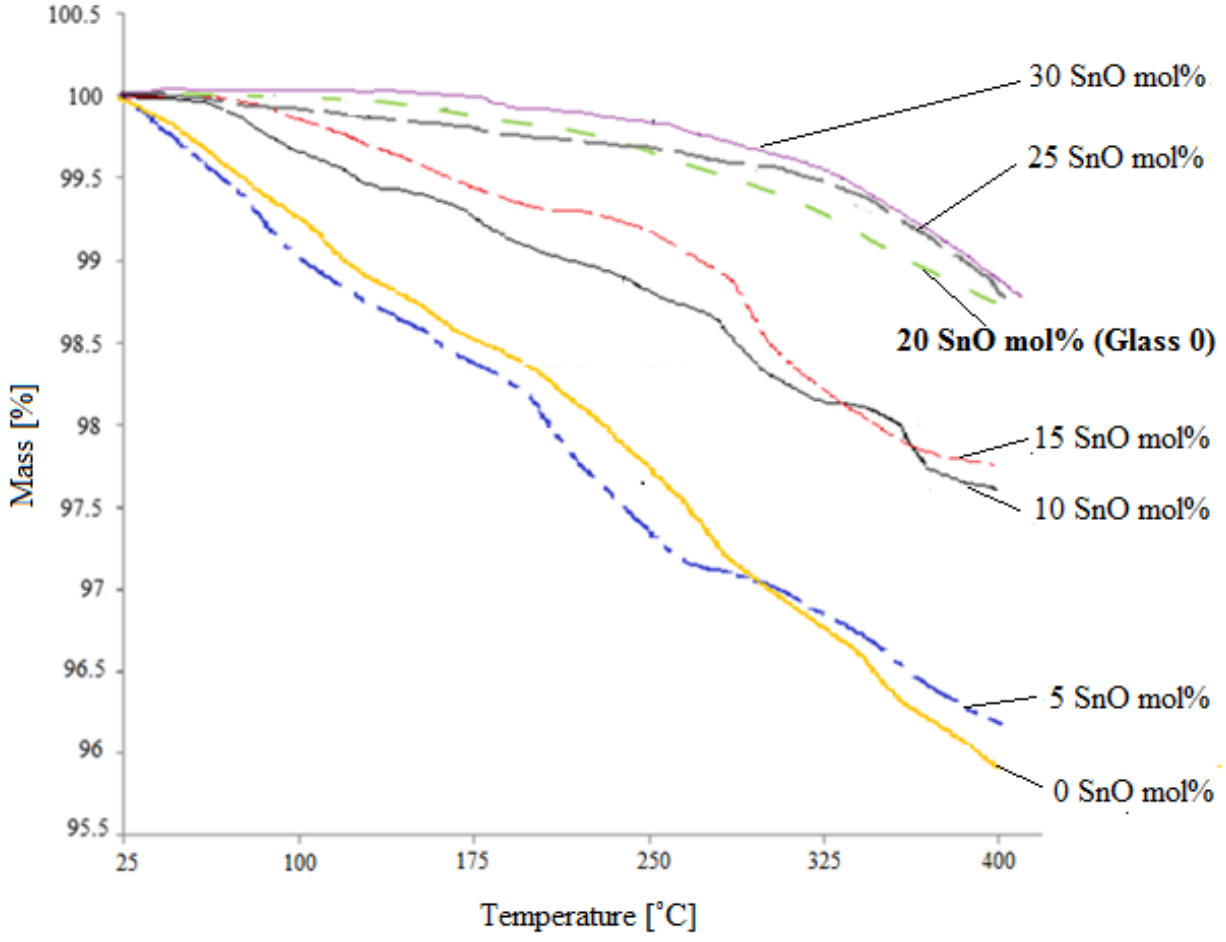

Figure 4.23: TGA trends of Class 1 glasses (SnF_2/P_2O_5 molar ratio equal to 1.67 and SnO in the range of 0-30 mol%).

Effect of SnF_2

The TGA traces for Class 2 glasses (P_2O_5/SnO molar ratio equal to 1.5 and SnF_2 in the range of 30-60 mol%) are shown in Figure 4.24.

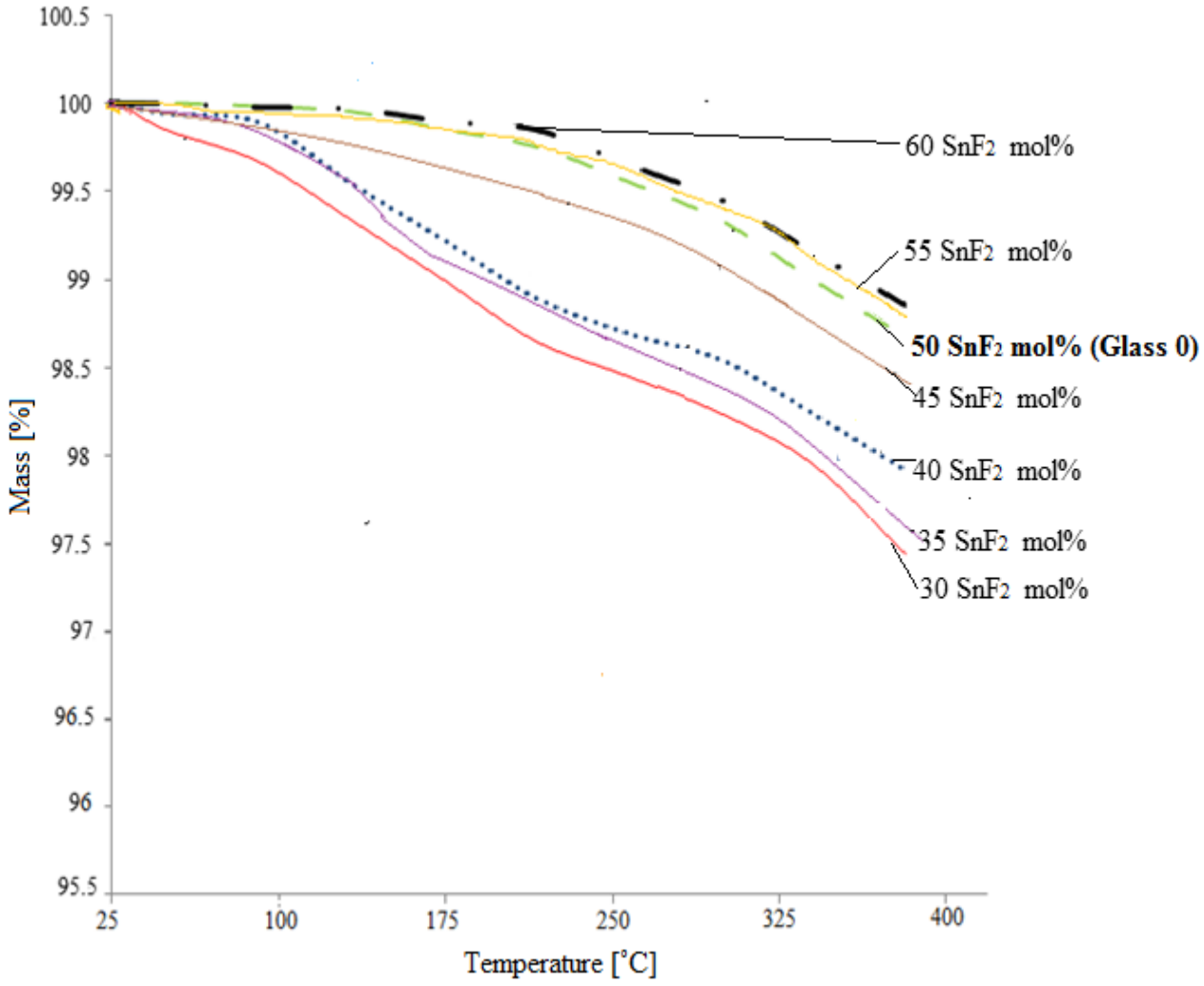

Figure 4.24: TGA trends of Class 2 glasses (P_2O_5/SnO molar ratio equal to 1.5 and SnF_2 in the range of 30-60 mol%).

The mass loss at 400°C decreases from 2.50 % to 0.75% with increasing SnF2 content in the glass network, with Glass 7 (30 SnF2 mol%) and Glass 12 (60 SnF2 mol%) showing the highest and lowest values respectively. The thermal stability of Class 2 glasses was affected by the increased fluoride, in opposition to the results reported in [2] where the increased fluoride content into a phosphate network was reported to reduce the entanglement of glass network. However the introduction of Sn was reported to increase the cross links among the

glass network [2, 36-38]. As the SnF2 is added to the glass composition, the Sn2+ 2 content increased, which was hypothesized to increase Sn-O-P-O bonds replace P-O-P bonds, as reported in many works in literature [2,36-38]. Also, it was hypothesized that, Sn could have been incorporated in the basic structural units and the number of Sn-O-P bridges have been increased. This was related to the increased linkage of the glass network and to the thermal stability increasing with SnF2 mol% in the glass composition.

Effect of P_2O_5

The TGA trace for Class 3 glasses (SnF_2/SnO molar ratio equal to 2.5 and P_2O_5 in the range of 20-40 mol%) are presented in Figure 4.25.

Glass 13 (20 P2O5 mol%) exhibited a mass loss of 4.20% at 400°C. The glasses with 25 P_2O_5 mol% and 35 P_2O_5 mol% exhibited no relevant changes in thermal stability compared to the base composition Glass 0. In particular the mass loss at 400°C of Glass 14 (25 P_2O_5 mol%) and Glass 15 (35 P_2O_5 mol%) were 1.5 and 1.2 % respectively. Glass 16 (40 P_2O_5 mol%) exhibited a mass loss of 4.80% at 400°C.

The major mass loss of Glass 13 was attributed to a too low content of P_2O_5. The amount of P_2O_5 (~ 20 mol%) was not enough to form the glassy structure. Furthermore, the high amount of F in the glass network (57 SnF_2 mol%) could lead to the disruption of the Sn-O-P-O basic structural units and the formation of PO_2F_2 –Q_0 units, as reported in Section 2.3. The major mass loss of Glass 16 was attributed to the high content of P_2O_5 and its hydrophilic nature. Also the low content of SnO (~ 17 mol%) and increased content of fluoride (SnF_2 ~ 43 mol%) led to the breakage of the P-P bonds and the formation PO_2F_2 –Q_0 units as reported in Section 2.3.

[2] The amount of Sn in the glass composition is determined by both SnF_2 and SnO molar contents. In Class 2 glasses the SnF_2 content increases from Glass 7 to Glass 12 in the range of 30-60 mol%; the SnO content decreases fron Glass 7 to Glass 12 in the range of 28-16 mol%.

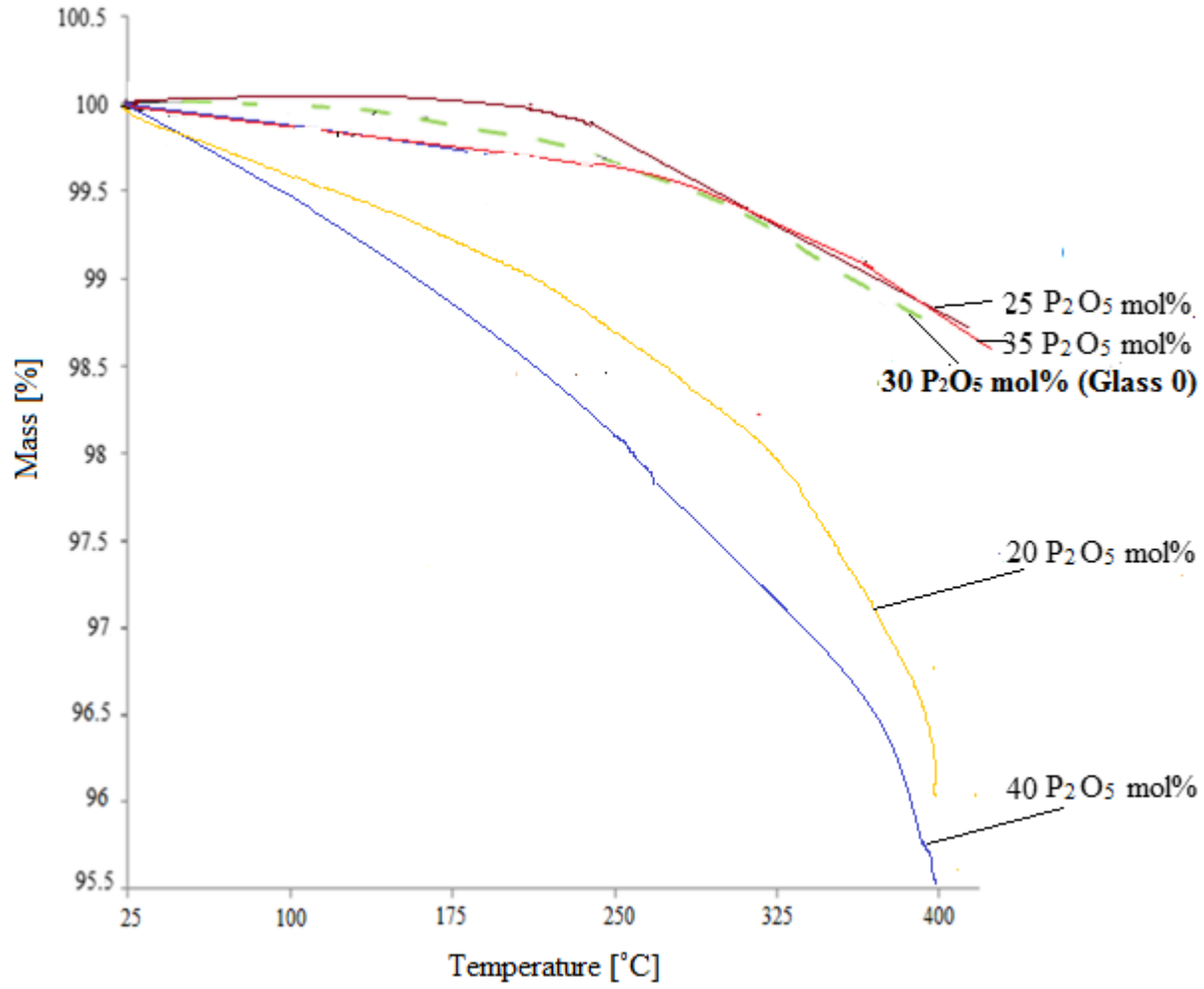

Figure 4.25: TGA trends of Class 3 glasses (SnF_2/SnO molar ratio equal to 2.5 and P_2O_5 in the range of 20-40 mol%).

4.10 Effect of composition on mechanical properties of glasses

Hardness is a measurement of the resistance of a material to localized plastic deformation [91] and is an essential property to evaluate the underlying the physio-chemical structure of glasses.

Fracture toughness is a measurement of a material's resistance to brittle fracture when a crack is present [92]. It's important to evaluate this property because phosphate glasses are brittle materials and the crack formations in the glass sample could compromise the properties of the hybrid materials.

Micro-hardness and fracture toughness of glass samples were measured by indentation technique according to the procedure in Section 3.9.1. The Vickers hardness and fracture toughness values are reported in Table 4.7.

The Vickers hardness and fracture toughness of Glass 0 are 3.57 ± 0.19 GPa and 0.78 ± 0.03 MPa $m^{1/2}$ respectively.

Effect of SnO

The Vickers hardness and fracture toughness trends of Class 1 glasses (SnF_2/P_2O_5 molar ratio equal to 1.67 and SnO in the range of 0-30 mol%) are shown in Figure 4.26. The hardness values varied in the range of 3.10-3.82 GPa. Fracture toughness varied in the range of 0.170-0.85 MPa $m^{1/2}$.

Both hardness and fracture toughness did not change linearly with SnO for low SnO content. The high standard deviation measured in both hardness and toughness for Glass 1 (0 SnO mol%) and Glass 2 (5 mol%) was related to the Sn-F-Sn weak units and depolymerisation phenomena [36-38] in the glass network because of the too high content of both fluoride and phosphate oxide. In glasses with SnO > 5 mol% the hardness and toughness values varied in the range of 3.12 - 3.82 GPa and 0.18 – 0.85 MPa $m^{1/2}$ and were directly related to the content of SnO.

It was hypothesized that, as SnO increased in the glass composition, Sn could have been incorporated in the basic structural units and Sn-O-P bridges increased [36]. This could increase the aggregation of the glass network, its density and the hardness and fracture toughness of the glass sample.

Effect of SnF_2

The Vickers hardness and fracture toughness trends of Class 2 glasses (P_2O_5/SnO molar ratio equal to 1.5 and SnF_2 in the range of 30-60 mol%) are shown in Figure 4.27.

The hardness value varied in the range of 3.20 - 3.65 GPa. The hardness is directly related to SnF_2 content. Fracture toughness varied in the range of 0.43-0.82 MPa $m^{1/2}$ and increased with increasing SnF_2 content.

The FTIR traces of Class 2 glasses show that the bridging oxygens decrease and the Q^1-Q^0 tetrahedral units within the glass increase as SnF_2 molar fraction increases (see Figure 4.8).

Samples with high SnF_2 content are composed predominantly by the Q^1 tetrahedra and short-length chains linked with Wan Der Waals forces and a few cross links, which have been considered to decrease the volume of the network and increase the density (see Table 4.3) and the hardness of the glasses.

Effect of P_2O_5

The Vickers hardness and fracture toughness trends of Class 3 glasses (SnF_2/SnO molar ratio equal to 2.5 and P_2O_5 in the range of 20-40 mol%) are shown in Figure 4.28.

The hardness values varied in the range of 3.02-3.58 GPa. Fracture toughness varied in the range of 0.25-0.78 MPa $m^{1/2}$. Both hardness and toughness values did not follow any specific trend.

Glass 13 (20 P_2O_5 mol%) and Glass 16 (40 P_2O_5 mol%) showed the lowest values of both hardness and toughness, The high standard deviation measured for Glass 13 and Glass 16 were related to the disruption of the glass networks. Glass 13 has a too low content of SnO (≈ 17 mol%) and a too high content of fluoride (SnF_2 ≈ 43 mol%), which led to the breakage of the P-P bonds and the formation PO_2F_2 –Q_0 units as reported in Section 2.3. Glass 16 has a too high content of P_2O_5 and absorbs moisture easily, which affected the structure of the glass and prevented the measurement of hardness and toughness.

The glasses with intermediate content of P_2O_5 exhibit no relevant changes in both hardness and toughness compared to the Glass 0.

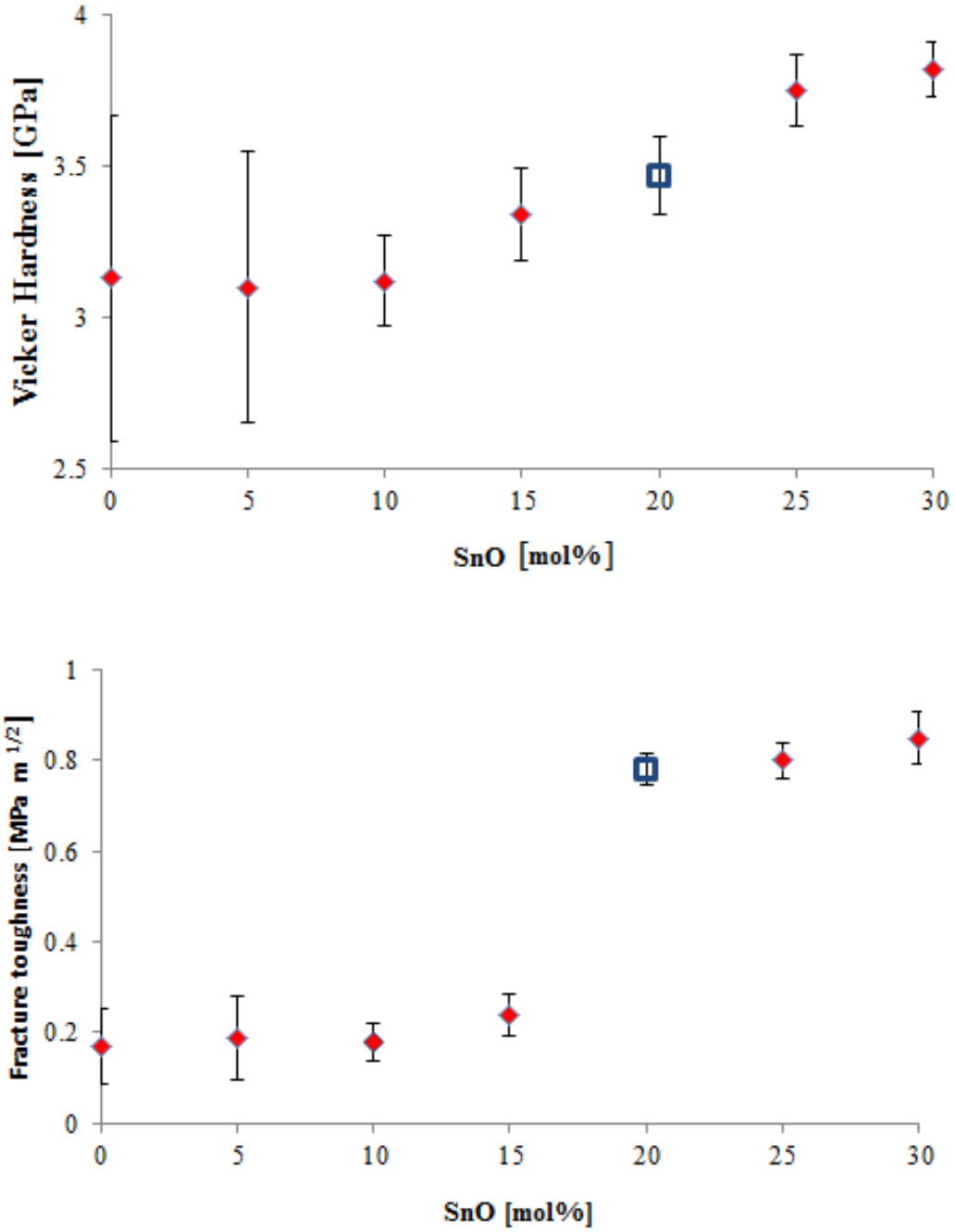

Figure 4.26: Vickers hardness and fracture toughness values for Class 1 glasses (SnF_2/P_2O_5 molar ratio equal to 1.67 and SnO in the range of 0-30 mol%).

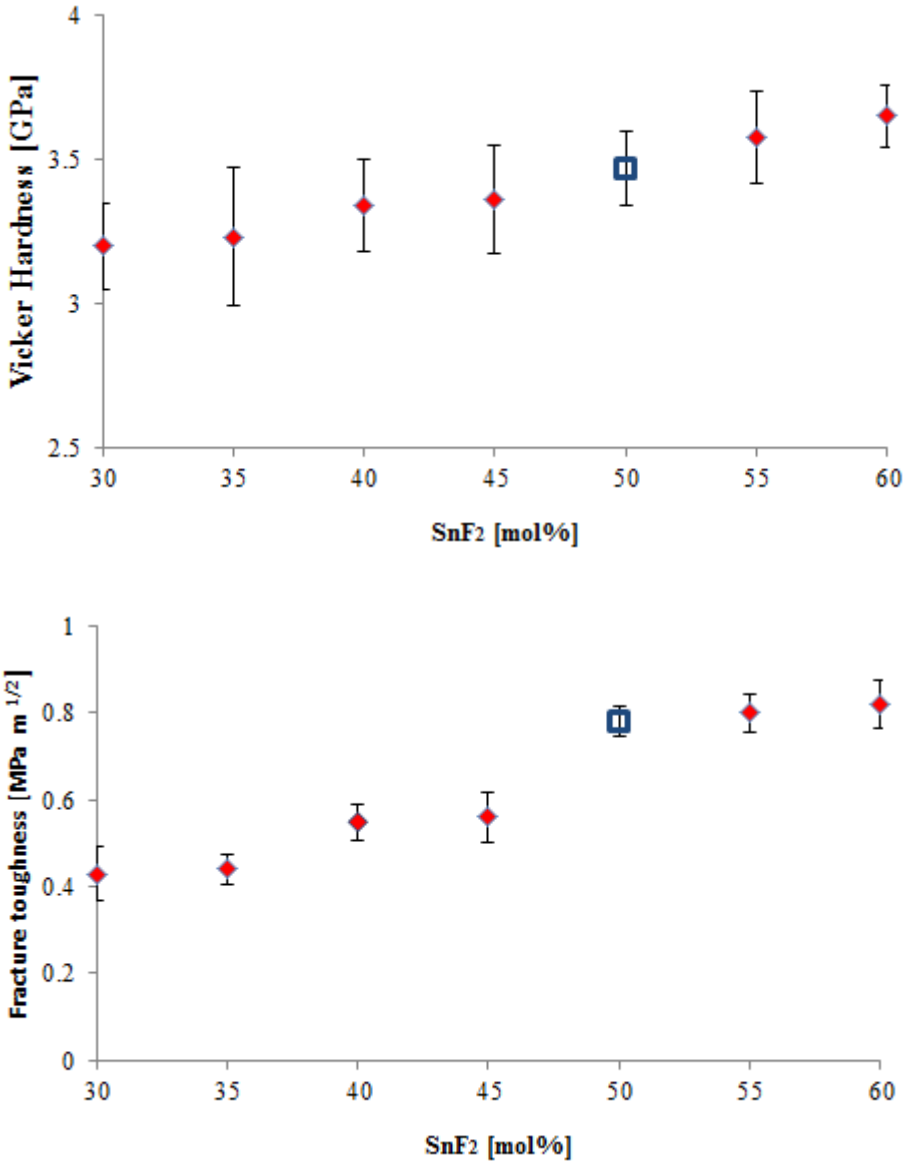

Figure 4.27: Vickers hardness and toughness values for Class 2 glasses (P_2O_5/SnO molar ratio equal to 1.5 and SnF_2 in the range of 30-60 mol%)

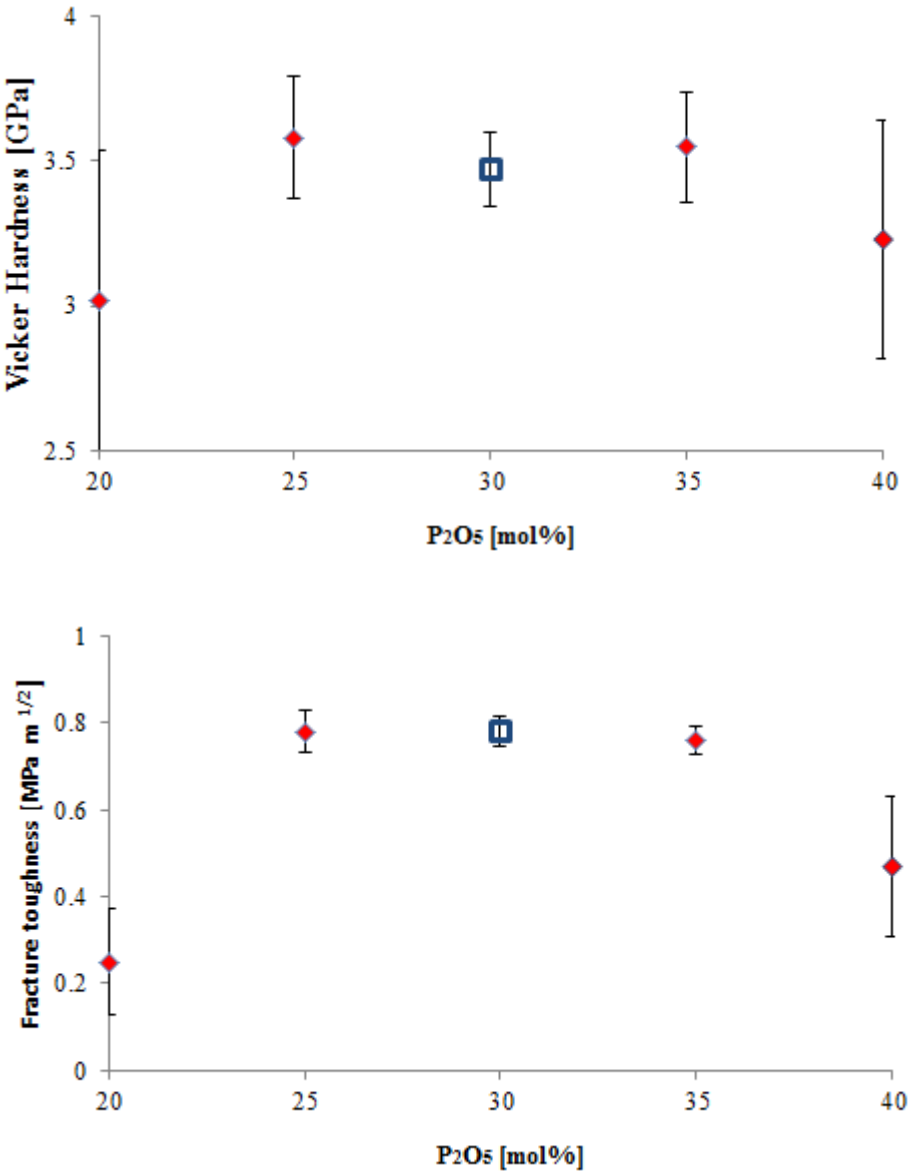

Figure 4.28: Vickers hardness and fracture toughness for Class 3 glasses (SnF_2/SnO molar ratio equal to 2.5 and P_2O_5 in the range of 20-40 mol%).

Table 4.7: Vickers Hardness and fracture toughness of phosphate glasses.

Glass	SnF_2 [mol%]	P_2O_5 [mol%]	SnO [mol%]	Vickers Hardness [GPa]	Fracture toughness [MPa $m^{½}$]
0	50.00	30.00	20.00	3.47 ± 0.13	0.780 ± 0.034
Class 1					
1	62.1	37.9	0.0	3.1 ± 0.54	0.170 ± 0.084
2	59.4	35.6	5.0	3.10 ± 0.45	0.190 ± 0.092
3	56.3	33.7	10.0	3.12 ± 0.15	0.180 ± 0.043
4	53.1	31.9	15.0	3.34 ± 0.15	0.240 ± 0.046
5	46.9	28.1	25.0	3.75 ± 0.12	0.800 ± 0.039
6	43.8	26.2	30.0	3.82 ± 0.09	0.850 ± 0.057
Class 2					
7	30.0	42.0	28.0	3.20 ± 0.15	0.430 ± 0.063
8	35.0	39.0	26.0	3.23 ± 0.24	0.440 ± 0.034
9	40.0	36.0	24.0	3.34 ± 0.16	0.550 ± 0.042
10	45.0	33.0	22.0	3.36 ± 0.19	0.560 ± 0.057
11	55.0	27.0	18.0	3.58 ± 0.16	0.800 ± 0.043
12	60.0	24.0	16.0	3.65 ± 0.11	0.820 ± 0.056
Class 3					
13	57.1	20.0	22.9	3.02 ± 0.53	0.250 ± 0.122
14	56.2	25.0	18.8	3.58 ± 0.21	0.780 ± 0.048
15	46.4	35.0	18.6	3.55 ± 0.19	0.760 ± 0.032
16	42.9	40.0	17.1	3.23 ± 0.41	0.470 ± 0.163

4.11 Glasses selected for hybridization

Compositions in Class 1 (SnF_2/P_2O_5 molar ratio equal to 1.67 and SnO in the range of 0-30 mol%) and Class 3 (SnF_2/SnO molar ratio equal to 2.5 and P_2O_5 in the range of 20-40 mol%) showed a highly non-linear behaviour, responding to small changes in component ratios with large changes in the measured values for many properties. On the other hand, glass compositions in Class 2 (P_2O_5/SnO molar ratio equal to 1.5 and SnF_2 in a range 30-60 mol%) showed a much more predictable and constrained behaviour, which is a desirable property.

Class 2 glasses showed linear response to thermal, chemical and mechanical properties responding to small changes to the quantity of SnF_2. Furthermore Class 2 glasses showed a good compromise between Tg and water/thermal stability. In particular, Glass 12 has a Tg of 106°C and a wide processing window (PW ≈ 230).

The water resistance and morphology improved in comparison with the other glass classes. The dissolution rate for these glasses was inversely related to SnF_2 content in the composition. The thermal stability and mechanical properties of Class 2 glasses increased with increasing SnF_2 content in the composition. For this reason four glasses of Class 2 were selected for hybridization with PA 11. The selected compositions are reported in Table 4.8.

Glass 8 (35 SnF_2 mol%) was not selected for further experimentation as it has similar properties to Glass 9 (40 SnF_2 mol%) but higher Tg and softening point than Glass 9. Glass 10 (45 SnF_2 mol%) and Glass 11 (55 SnF_2 mol%) were not selected for further experimentation as they have similar properties to Glass 0 (50 SnF_2 mol%).

Table 4.8: Glasses belonging to Class 2 (P_2O_5/SnO molar ratio equal to 1.5 and 30-60 mol% SnF_2) selected for hybridization.

Glass	P_2O_5 [mol%]	SnO [mol%]	SnF_2 [mol%]	Micro structure	ρ [kg/m^3]	Tg [˚C]	PW [˚C]	Ts [˚C]	Dissolution rate, [mg cm^{-2} h^{-1}]	M_L at 400˚C, [%]	Hv [GPa]	Kic [MPa m ^{½}]
0	30	20	50	pyro/poly phosphate	3560 ± 40	125.0 ± 4.5	202.43 ± 7.34	310.00 ± 12.00	0.0039± 0.002	0.10 ± 0.02	3.47 ± 0.13	0.780 ± 0.034
7	42	28	30	poly phosphate	3230 ± 220	162.5 ± 5.5	165.77 ± 3.57	350.00 ± 12.00	0.0054± 0.0007	2.50 ± 0.08	3.2 ± 0.15	0.430 ± 0.063
9	36	24	40	poly phosphate	3500 ± 90	157.5 ± 5.5	170.98 ± 7.34	331.00 ± 14.00	0.0045± 0.0004	1.65 ± 0.07	3.34 ± 0.16	0.550 ± 0.042
12	24	16	60	pyro phosphate	3920 ± 60	106.0 ± 4.5	228.78 ± 4.69	289.00 ± 12.00	0.0037± 0.0003	0.75 ± 0.02	3.65 ± 0.11	0.820 ± 0.056

Chapter 5 Development of Glass/Polyamide Hybrids

5.1 Design of hybrid compositions

The glasses selected for hybridization with PA 11 were Glass 0, Glass 7, Glass 9 and Glass 12, all belonging to Class 2 (P_2O_5/SnO molar ratio equal to 1.5 and SnF_2 in a range of 30-60 mol%). The properties of these glasses are summarized in Table 4.8.

Powdered glass samples and the PA11 polymer were used to produce a series of hybrids with nominal total glass content in the range of 0-20 vol% to verify the effect of glass content and compositions on the hybridization. Preliminary tests showed that it was impossible to introduce a content of glass higher than 20 vol% without compromising the mixing procedure: the melt resulted too liquid at higher glass content, affecting the reliability and repeatability of the procedure. The hybrid compositions are listed in Table 5.1.

5.2 Optimization of extrusion process

An important issue with regards the manufacturing of phosphate glass/polyamide hybrids is the processability of the hybrids during the blending process. The processability of a polymer blend is defined as the ease at which the blend components can be hot-melt-extruded to deliver a high quality extrudate, free of contamination or defects such as bubbles or un-melted polymer and with high smoothness [60]. The nature of the blend phases played a huge role in determining the processability and the quality of the final extrudate as changes in the glass structure and content could affect the interactions between the polyamide and the viscosity.

As part of this study, the processability of the melts and visual observation on the final extrudates were used as quality control for manufacturing hybrids.

A quick method to quantify the processability is the analysis of the force-time trends generated during the blending process by the equipment used to manufacture the hybrids, which, as described in Section 3.3.1, is a Micro-DSM intermeshing counter-rotating twin screw extruder. No lubricants were used since the goal of this test was to evaluate the natural processability of the materials.

Table 5.1: Compositions of glass/polyamide hybrids selected for hybridization.

Melt name	Glass name	Glass vol%	PA 11 vol%
PA 11	-	0.0	100.0
Hybrid 1	Glass 0	2.5	97.5
Hybrid 2	Glass 0	5.0	95.0
Hybrid 3	Glass 0	10.0	90.0
Hybrid 4	Glass 0	20.0	80.0
Hybrid 5	Glass 7	2.5	97.5
Hybrid 6	Glass 7	5.0	95.0
Hybrid 7	Glass 7	10.0	90.0
Hybrid 8	Glass 7	20.0	80.0
Hybrid 9	Glass 9	2.5	97.5
Hybrid 10	Glass 9	5.0	95.0
Hybrid 11	Glass 9	10.0	90.0
Hybrid 12	Glass 9	20	80.0
Hybrid 13	Glass 12	2.5	97.5
Hybrid 14	Glass 12	5.0	95.5
Hybrid 15	Glass 12	10.0	90.0
Hybrid 16	Glass 12	20.0	80.0

The load force-time trends are related to resistance to shear deformation and the viscosity of the blends; considering that the velocity profile in the micro-extruder is linear, the shear stress applied on the melt during extrusion can be written as:

$$\tau = \eta k \omega \tag{5.1}$$

Where: τ is the viscous shear stress; η is the fluid viscosity; k is a constant that depends only on the geometry of the extruder; ω is the angular velocity. Given the shear stress from Equation 5.1, the torque exerted by the rotating screws on the melt is:

$$T = (\tau A) r \tag{5.2}$$

Where: A is the wetted surface area of the screws; r is the radius of the screw.

The force F applied by the rotating screws on the melt is:

$$F = \tau A \tag{5.3}$$

It follows that:

$$T = Fr \tag{5.4}$$

Equation 5.3 can be combined with Equation 5.1 and be rewritten as:

$$F = \eta k \omega A \tag{5.5}$$

A typical load force/time plots of PA 11 is shown in Figure 5.1. The trend is the representative curve taken from a sample of three runs. Here, the time 0 corresponds to the time when the chamber is completely closed. A spike in the load force F was detectable for every sample at the beginning of the test (peak A). As the maximum F corresponds to the time when the plunger pushes the material and closes the chamber, this maximum F was not accurate and was not examined. The decrease in the load force after the peak A is linked to a decrease of the viscosity of the melt as the material melts during the process. A closer look at the equilibrium or stabilized forces, when present, should give a sufficient insight on the processability of the materials. The equilibrium load force Fe can also be an indicator of a complete melt or softening, or, with filled polymers, a fully mixed system. In case of PA 11 the load force F usually converged to a constant value of ~ 3000 N corresponding to Fe after 2 minutes of blending. A decrease in the loading force after reaching the equilibrium value

and before the peak B could be related to a decrease of the melt density and could be an indicator of sample degradation. The decrease of the load force F observed after peak B is caused by the decrease in the amount of material present inside the extruder when the chamber was opened at the end of the process.

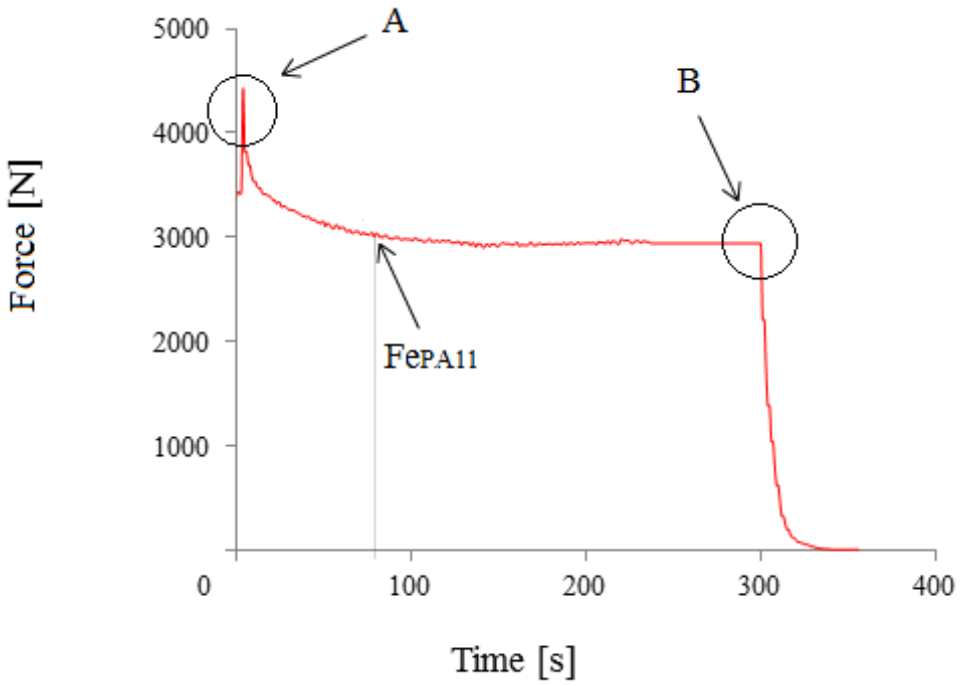

Figure 5.1: A typical load force/time plot of PA 11.

After blending, the produced hybrids were subjected to visual observation. Other than the force values, the criteria used to select the process conditions during extrusion were: homogeneous mixing, difficulty in the incorporation of glass, and degree of material degradation (yellowing of the sample). A viable blending produced a hybrid that looks uniform and smooth at the processing temperature. On the other hand, non-viable blending yielded a wet and incoherent powder lacking integrity. The smoothness of each sample was assessed by measuring the diameter and its standard deviation along the length of the extrudate.

The analysis of the load force-time trends were always accompanied by thermal stability tests of the sample up to the same temperature of the extrusion process. The viable blends were selected for further characterization.

5.3 Effect of extrusion parameters

In order to optimize the extrusion process, the selected PA 11 and hybrid blends (Table 5.1) were extruded by modifying slightly one extrusion parameter at a time (see Section 3.3.1).

The choice of these parameters was aided by a preliminary blended trails carried out using the base composition Glass 0 (50% SnF_2 +20% SnO + 30% P_2O_5). Here a mixing time of 300 s and a fill time of 95% gave the best homogeneity while the hybrids having the best quality were produced at working temperatures in the range of 210-250 ºC and speed in the range of 50-200 rpm with minimal material degradation. Further experiments were carried out using the conditions within these ranges. The blending conditions are summarized in Table 5.2.

Table 5.2: Blending conditions for PA 11 and hybrids.

	Temperature profile [˚C]	Screw speed [rpm]	Residence time [s]	Fill factor [%]
A	210/230/230	100	300	95
B	210/250/250	100	300	95
C	210/270/270	100	300	95
D	210/250/250	50	300	95
E	210/250/250	200	300	95
F	210/250/250	100	400	95

5.3.1 Profile temperature

The viscosity of a polymer melt η varies exponentially with the temperature as shown in Equation 5.6 [60].

$$\eta = \eta_{ref} exp(-b\Delta T) \tag{5.6}$$

Where: η_{ref} is the reference viscosity; b is a temperature sensitivity coefficient (K^{-1}); ΔT is the temperature range in K.

As the temperature increases, the entanglement of the polymer chains is lowered, the intermolecular forces among the polymer segments appears to decrease and so does the material viscosity.

The melting point of Rilsan PA 11 ® is ~188 ˚C, while the softening points of the glasses fall in the range of 289-350 ˚C. The PA 11 and the hybrid compositions (Table 5.1) were blended at different temperature profiles in order to select an extruder temperature profile close to the softening point range of the glasses but low enough not to degrade the PA 11. The experiments were performed at a fixed screw speed of 100 rpm and residence time of 300 s. The fill factor, defined as the percentage of fill in the mixing chamber, was 95%. The temperature profiles used were: 210/230/230 °C (Condition A), 210/250/250 °C (Condition B) and 210/270/270 °C (Condition C). See Table 5.2 for the full list of conditions.

The force/time trends for the pure PA 11 blends are shown in Figure 5.2. The blends processed at 210/230/230 °C, 210/250/250 °C and 210/270/270 °C exhibited an equilibrium force Fe of ~ 3000 N, ~ 2350 N and ~ 2075 N, respectively. The Fe decreases with decreased temperature profile. The reduction in force F was due to the reduction of the viscosity (Equation 5.5), which was caused by the disentanglement of the polymer chain and their higher degree of movement as the temperature increased. The equilibrium force Fe was constant till the opening of the chamber for blends processed at 210/230/230 °C and 210/250/250 °C. The force of blend processed at 210/270/270 °C decreased of ~ 300 N before the opening of the chamber. The maximum temperature set in the extruder was 270 °C which was ~ 80 °C higher than the melting point of PA 11. Due to the high shear stress on the material during the extrusion, the temperature of the melt could possibly be even higher. Thus, the decrease of the force F at higher processing profile temperature could be related to some degradation affecting the polymer.

The PA 11 extrudates are shown in Figure 5.3. All samples produced with conditions A, B and C were smooth with homogenous diameters along the length of the extrudate. A decrease in diameter with increasing profile temperatures was observed. This was likely caused by the decrease in blend viscosity. The samples obtained at 210/270/270 ˚C were yellowish, in contrast to samples produced at the other two temperature profiles, which were transparent. The discoloration was attributed to the PA 11 degradation.

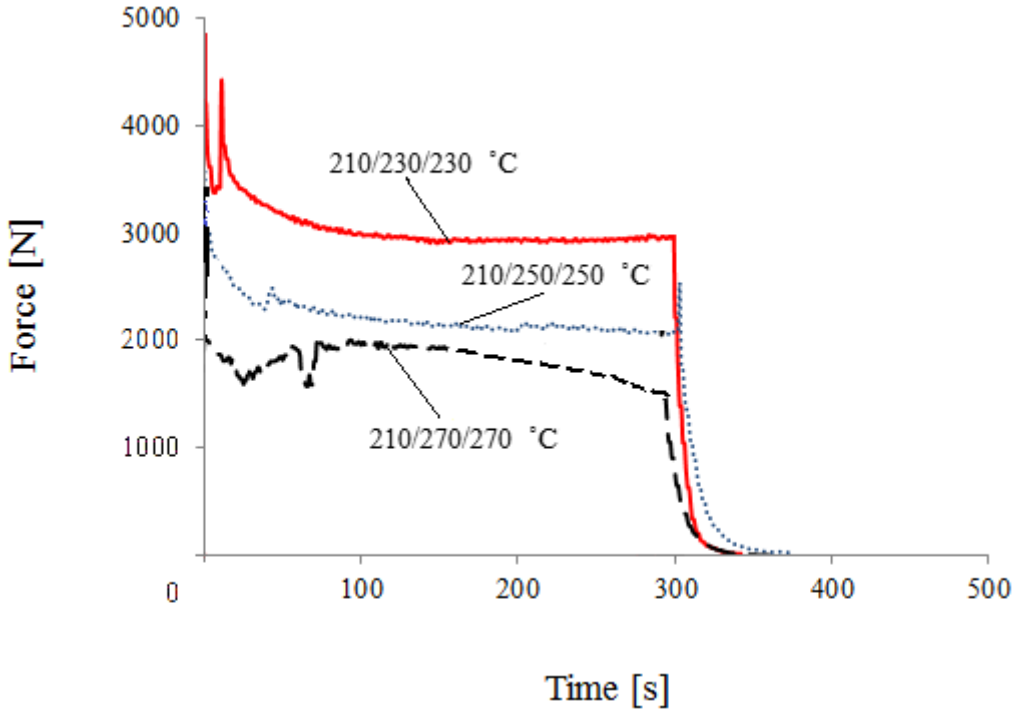

Figure 5.2: Force/time plots of PA 11 processed at three different extruder profile temperature: 210/230/230 ˚C (Conditions A), 210/250/250˚C (Conditions B), 210/270/270˚C (Conditions C).

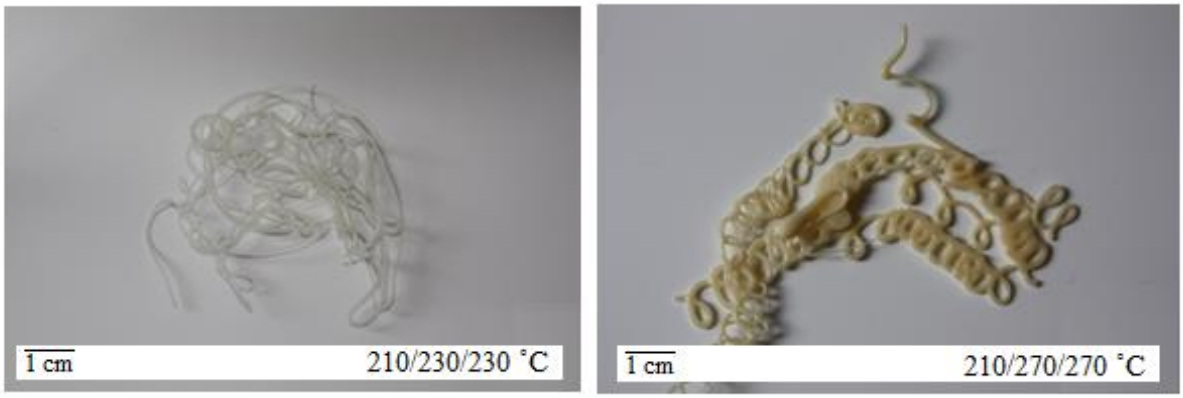

Figure 5.3: Example of PA 11 extrudates processed at 210/230/230 ˚C (Conditions A) and 210/270/270 ˚C (Conditions B).

Almost all hybrid compositions behaved similarly to PA 11: increasing processing temperatures results in exhibiting decreased equilibrium force and diameters, increased yellowing and no significant changes in smoothness. The equilibrium forces Fe and diameters for selected samples are summarized in Table 5.3.

Hybrid 7 to 12 (see Table 5.1), processed at the lowest temperature profile (Conditions A), showed a rough texture (Figure 5.4). This temperature profile, 210/230/230 ˚C, is

significantly lower than the softening points of the Glass 7 (~ 350 ˚C) and Glass 9 (~ 330 ˚C), which are part of the Hybrid 7 to 12. The rough surface was thus attributed to un-melted glass in the extrudate.

As a result of these tests, the intermediate profile temperature 210/250/250 °C (Conditions B) was selected for further experimentation.

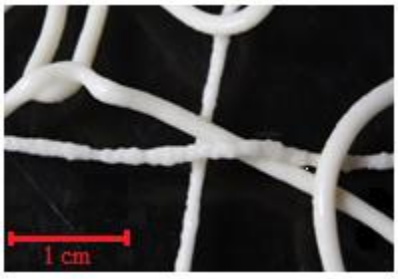

Figure 5.4: Example of Hybrid 8 extrudate. The composition was processed at 210/230/230 ˚C (Conditions A).

5.3.2 Screw speed

Most of the energy that a screw imparts to the blend during extrusion is by means of shear. In a twin screw extruder the blend is sheared between the barrel inner wall and the root of the screws while these surfaces are moving in relation to each other. The rate of energy transfer to the blend is directly correlated to the shear rate which increases as the relative speed of the two surface increases and the distance between the surfaces decreases. The shear rate at any single point along a screw can be related to the screw speed according to Equation 5.7 [60]:

$$\acute{\gamma} = \frac{DN}{19.1 h_s} \tag{5.7}$$

Where: D is the screw diameter (mm); N is the screw speed (rpm); h_s is the screw channel depth (mm).

Generally polymers exhibit a shear thinning behaviour [64], which is defined as the decrease of viscosity when the shear rate increases. In this case the shear rate $\acute{\gamma}$ of the blend is related to the viscosity of the blend according to power-law model expressed in Equation 5.8 [60]:

$$\eta = K(\dot{\gamma})^{n-1} \tag{5.8}$$

Where K in a constant; n is the power law exponent.

By combining Equation 5.7 and Equation 5.8, it can be inferred that the screw speed is related to the viscosity of the melt according to Equation 5.9:

$$\eta = K\left(\frac{DN}{19.1h}\right)^{n-1} \tag{5.9}$$

Lowering the screw speed can be an option whenever excessive shear is the cause for high melt temperatures and degradation of the material. On the other hand non-uniform mixing, low melt temperatures, and un-melted material may be due to low shear rate and may require an increase of the screw speed.

The experiments on the effect of screw speed were performed at a fixed profile temperature of 210/250/250 °C, a residence time of 300 s and fill factor of 95%. The chosen screw speeds were: 50 rpm (Conditions D), 100 rpm (Conditions B) and 200 rpm (Conditions E). See Table 5.2 for the full list of conditions.

The force/time trends for the selected Hybrid 2 blends are shown in Figure 5.5.

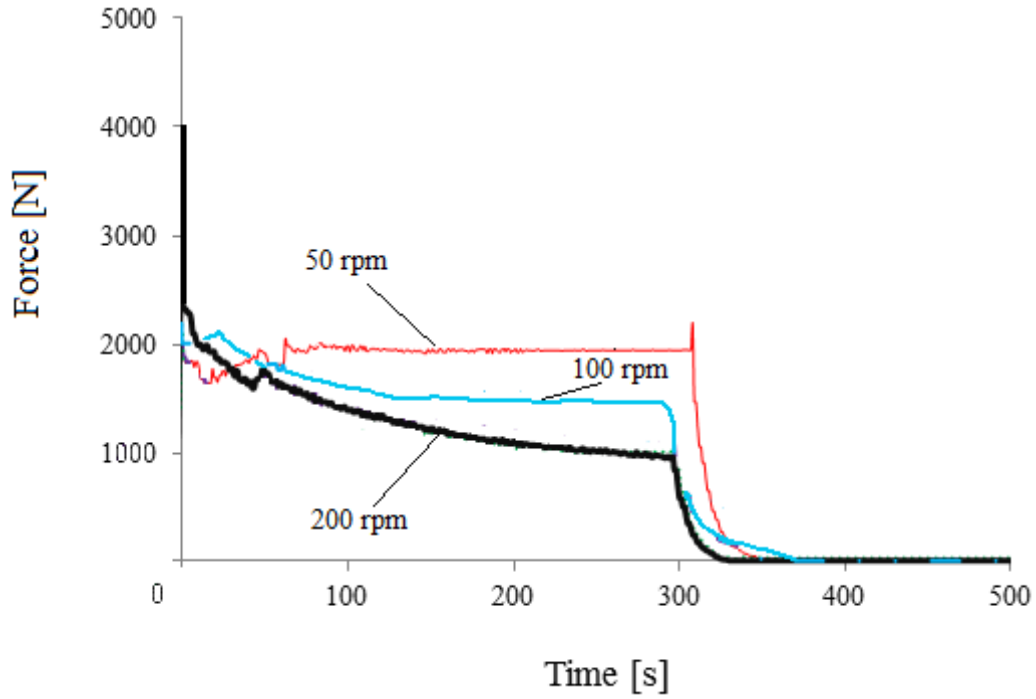

Figure 5.5: Force/time plots of Hybrid 2 composition processed at three different screw speeds: 50 rpm (Conditions D), 100 rpm (Conditions B), 200 rpm (Conditions E).

The blends processed at 50 rpm and 100 rpm exhibited an equilibrium force Fe of ~2000 N and ~ 1750 N, respectively. The decreased Fe with increasing screw speed N was related to

the reduction of the viscosity of the blend, which was linked to the higher shear rate at which the material was subjected at higher screw speeds. The Hybrid 2 composition processed at the highest screw speed (Conditions E) did not reach an equilibrium force. Instead, the force decreased till the end of the test, which was possibly due to degradation caused by an excessive shear rate.

An example of Hybrid 2 extrudate is shown in Figure 5.6.

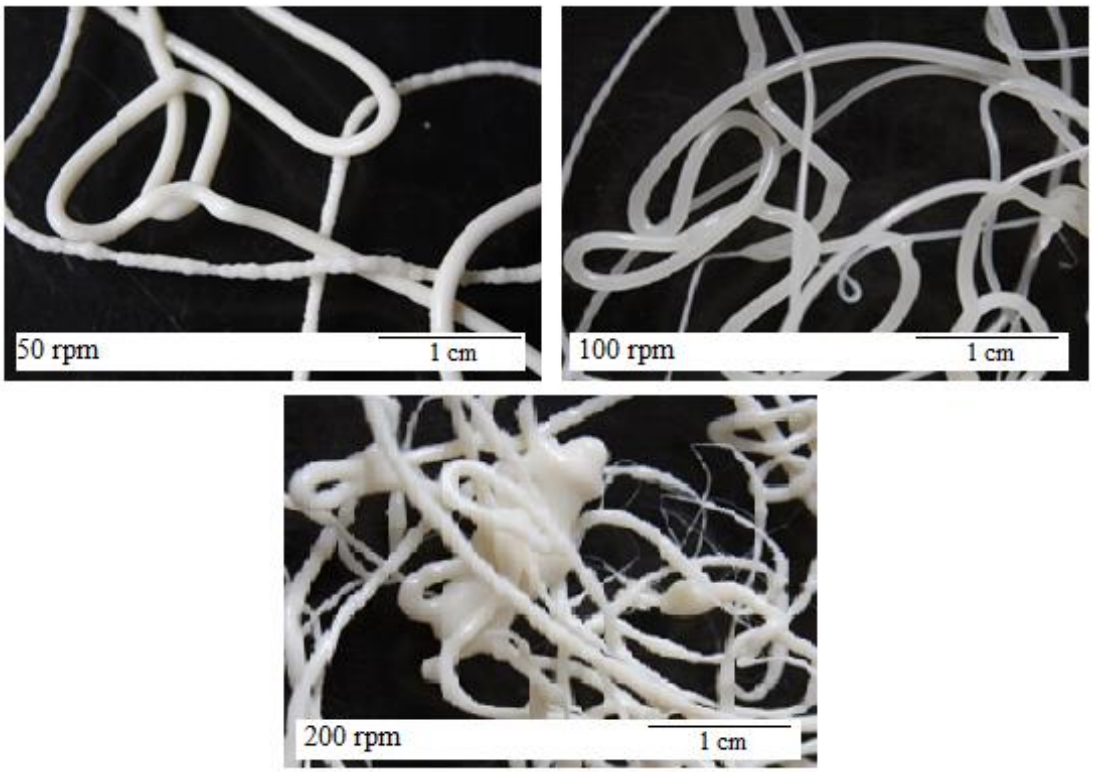

Figure 5.6: Extrudates of Hybrid 2 processed at 210/250/250 ˚C, for 300 s with a filling factor of 95% at a screw speed of (a) 50 rpm; (b)100 rpm; (c) 200 rpm.

The extrudates of the blends processed at 100 rpm (Conditions B) were white and smooth with a homogenous diameter along the length of the extrudate. The extrudates processed at 50 rpm (Conditions D) were homogenously white and showed a rough texture, indicating that the screw speed 50 rpm at which the blends were processed was not high enough to mix properly glass and polyamide. The rough surface was thus attributed to the un-melted glass in the extrudate. The extrudates of blends processed at 200 rpm (Conditions E) lacked in smoothness and were slightly yellowish in contrast to the extrudates produced at the lower screw speeds. The non-uniform diameter and discoloration were attributed to degradation.

Almost all hybrid compositions behaved similarly to Hybrid 2 to changes in screw speeds. The extrudates exhibited lack of smoothness at 50 rpm (Conditions D) and exhibited lack of smoothness, decreasing equilibrium force, increased yellowing at 200 rpm (Conditions E).Based on the above results, the intermediate screw speed 100 rpm (Conditions B) was selected for further experimentation.

5.3.3 Residence time

The residence time is the amount of time that the blend is inside the chamber and is subjected to the set temperature profile and to the shear rate generated by the screw speed. The experiments were performed at a fixed profile temperature of 210/250/250 °C, screw speed of 100 rpm and fill factor of 95%. The blends were prepared at two residence times: 300 s (Condition B) and 400 s (Condition F). See Table 5.2 for the full list of conditions. The force/time trends for the selected Hybrid 5 blends are shown in Figure 5.7.

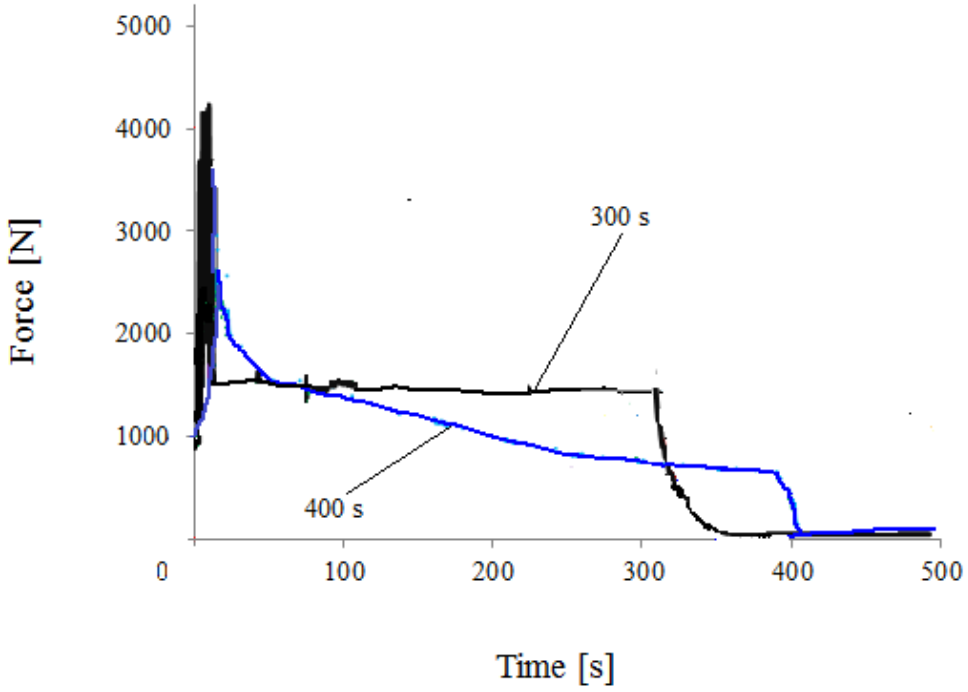

Figure 5.7: Force/time plots of Hybrid 5 composition processed at two different residence time: 300 s (Conditions B) and 400 s (Conditions F).

The blend processed at 300 s (Condition B) exhibited an equilibrium force Fe of ~ 1600 N. The Hybrid 5 composition processed at 400 s, the highest residence time (Conditions F), did

not reach an equilibrium force. Instead, the force decreased till the end of the test, which was related to possible degradation due to a too high shear rate during extrusion.

An example of Hybrid 5 extrudate is shown in Figure 5.8. The extrudates of the blends processed at 300 s rpm (Conditions B) were white and smooth with uniform diameters along the length of the extrudate. The extrudates processed at 400 s (Conditions E) were slightly yellowish in contrast to the extrudates produced at 300 s, suggesting that the sample may be subjected to a too long residence time and degraded. Also, since the batch mixing can be scaled up to twin screw extrusion, the residence time in the extruder should be kept as short as possible in order to reduce PA 11 degradation, while providing enough time to complete the blending with phosphate glass.

As a consequence of the experimental results, the residence time was kept constant to 300 s.

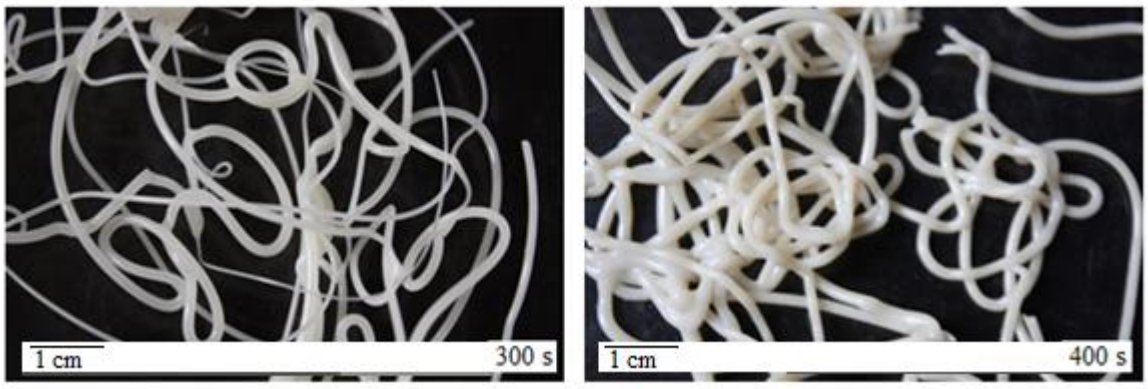

Figure 5.8: Extrudates of Hybrid 5 blends processed at 300 s (Condition B) 5 and 400 s (Condition F).

5.3.4 Effect of glass content

In order to verify the effects of glass composition on the quality of extrudates, the hybrid compositions were prepared at 0, 5, 10 and 20 vol% of glass at the optimized extrusion Condition B (see Table 5.2); Glass 0, Glass 7, Glass 9, Glass 12 were used in this study. The list of processed hybrids is shown in Table 5.1.

The force/time trends for selected PA 11 and hybrid blends which contain Glass 12 (Hybrid 13 to 16) are shown in Figure 5.9. In a few cases the curves of the hybrids show small peaks between the one and two minute marks. This is due to the fusion, i.e. the thermal reduction of the boundary surface of particles (grains) of phosphate glass [94]. During this process, the

grains are destroyed and the resulting micro-particles are compacted as the heat and the shear stress inside the extruder increases.

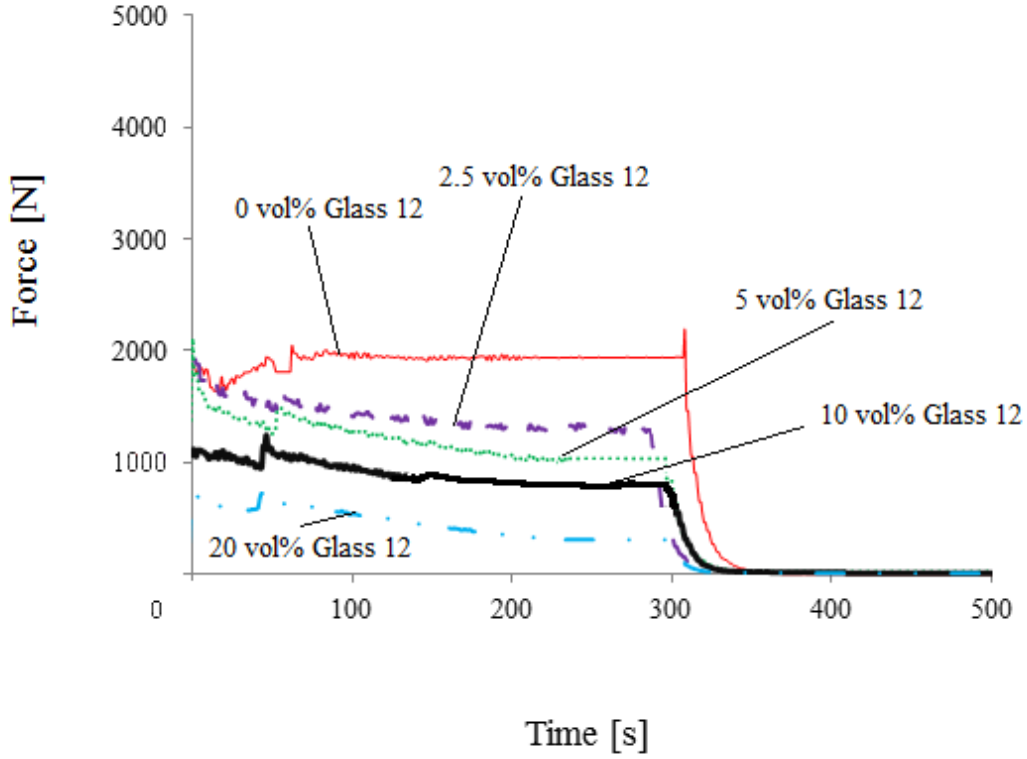

Figure 5.9: Force-time trends for glass/polyamide hybrids with Glass 12 at 0 vol% (PA 11) at 2.5 vol% (Hybrid 13), 5 vol% (Hybrid 14), 10 vol% (Hybrid 15) and 20 vol% (Hybrid 16).

All Glass 12/PA 11 blends exhibited an equilibrium force (Fe) which, with increasing glass content, decreased from the highest value of ~ 1950 N, measured for pure of PA 11, to the lowest value of ~ 350 N measured in Hybrid 16 (20 vol% Glass 12/PA 11), as shown in Figure 5.9. This phenomenon is often associated to the partial miscibility of blends [4, 5]. The equilibrium forces of blends are summarized in Table 5.3. Glass 12 (60 SnF_2 mol%) is the composition with the lowest glass transition temperature Tg (~ 106 ˚C) and softening point Ts (~ 289 ˚C) close to the range of profile temperature chosen for hybrid extrusion. It was hypothesized that the Glass 12 softens and partially melts during extrusion thanks to both high temperature and shear rate, causing the reduction of load force with increased glass content. Hybrid 1 to 4, containing Glass 0 (50 SnF_2 mol%) with a Tg and a softening point Ts of ~ 125 ˚C and ~ 375˚C respectively, showed a similar but less pronounced trend of

force/time. Hybrid 5 to 8, containing Glass 7 (30 SnF_2 mol%) and Hybrid 9 to 12, containing Glass 9 (40 SnF_2 mol%), did not show any trend. The Fe values are summarized in Table 5.3.

Examples of hybrids containing Glass 12 are shown in Figure 5.10. The extrudates of the blends processed at 0 to 20 vol% of Glass 12 (Hybrid 13 to 16) were smooth with uniform diameters along the length of the extrudate. The measured diameters decreased with increasing glass content (Table 5.3), which was related to the decreased viscosity with glass content. PA 11 extrudates were transparent and the whiteness of the hybrid extrudates increased with glass content in the composition (from Hybrid 13 to 16). The extrudates of Hybrid 1 to 4 containing Glass 0 (50 SnF_2 mol%) showed a similar but less pronounced behaviour. The Hybrid 5 to 8, containing Glass 7 (30 SnF_2 mol%) and Hybrid 9 to 12, containing Glass 9 (40 SnF_2 mol%) exhibiting whiteness but lack of smoothness, which was attributed to un-melted glass particles in the extrudates.

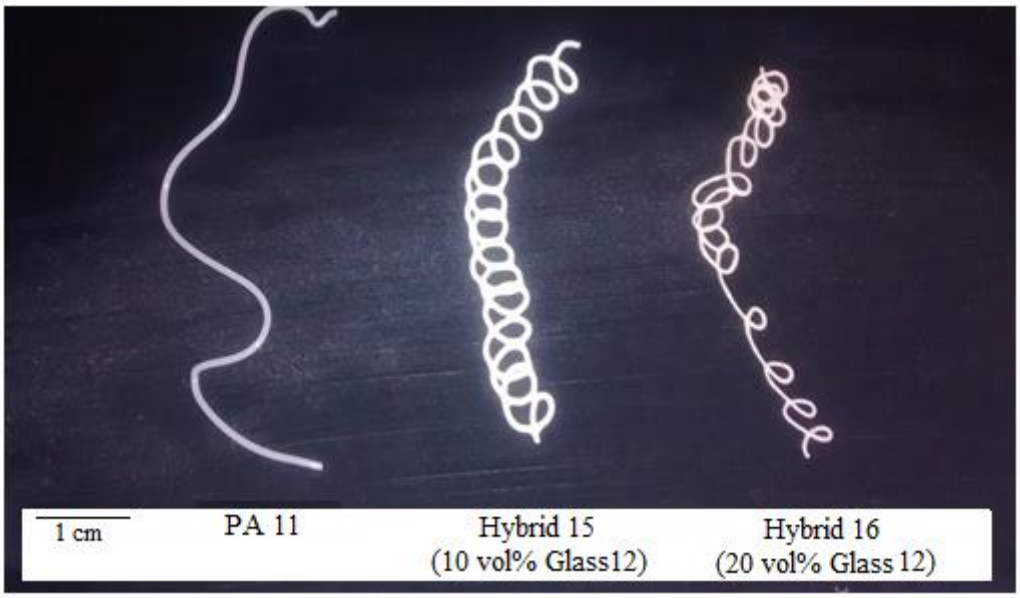

Figure 5.10: Extrudates of PA 11, Hybrid 15 (10 vol% Glass 9) and Hybrid 16 (20 vol% Glass 9) processed at 210/250/250 ˚C, for 300 s with a filling factor of 95% at a screw speed of 100 rpm (Condition B).

5.3.5 Effect of glass composition

The force/time trends for PA 11 and hybrids containing constant 20 vol% of Glass 0 (Hybrid 4), Glass 7 (Hybrid 8), Glass 9 (Hybrid 12) and Glass 12 (Hybrid 16) are shown in Figure 5.12.

As already discussed in Section 5.3.4, all blends showed an equilibrium force Fe, which are summarized in Table 5.3.The equilibrium forces of hybrid blends decreased from ~ 1900 N to ~ 350 N, with Hybrid 8 (20 vol% Glass 7/PA 11) and Hybrid 16 (20 vol% Glass 12/PA 11) exhibiting the highest and lowest Fe, respectively. Recalling that Glass 12 has the highest SnF_2 content (60 mol%) and the lowest Tg (~ 106 ˚C) and Ts (~ 289 ˚C) among all the experimental glasses, therefore the 20 vol% Glass 12/PA 11 (Hybrid 16) is the hybrid containing the largest amount of SnF_2. It has been hypothesized that the increasing content of SnF_2 in the glass compositions might enhance the mobility of the glass network. In particular, the high amount of SnF_2 in Glass 12 could lead to disentanglement of the PA 11 chain, favouring the decrease of the viscosity of the hybrids. The blends showed a similar but less pronounced behaviour with decreasing Glass 0 from 20 to 0 vol%, in the hybrids.

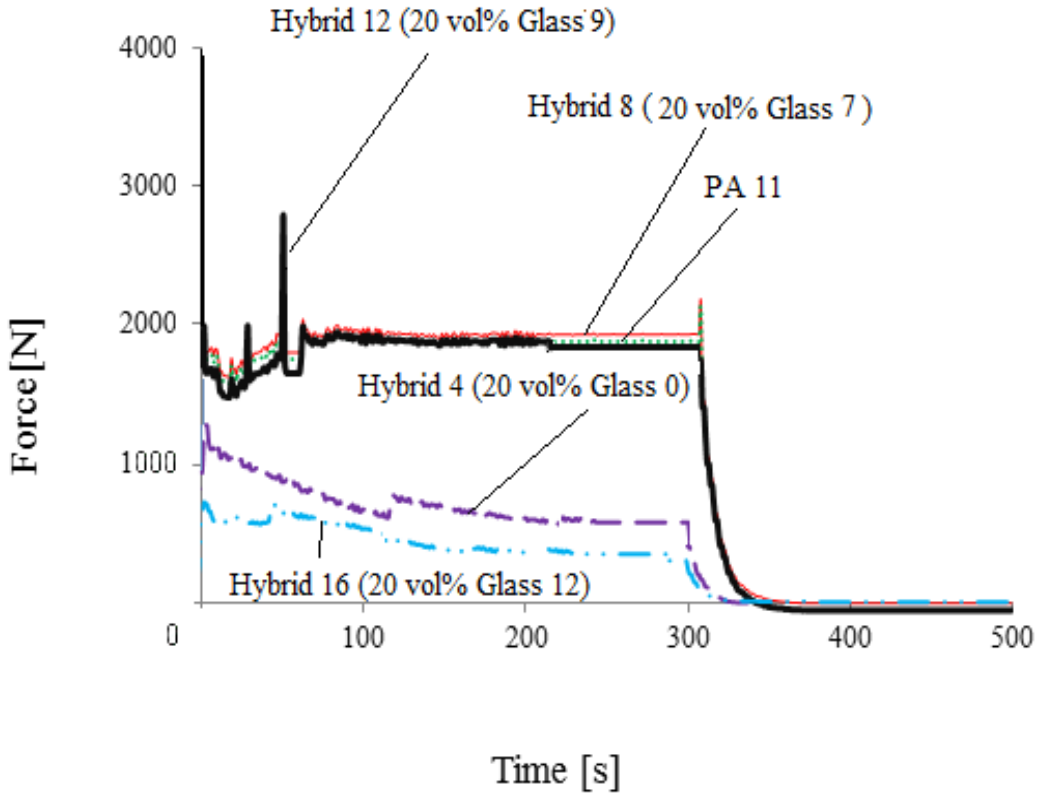

Figure 5.11: Force-time trends for PA 11 and hybrids with 20 vol% of Glass 0 (Hybrid 4), 20 vol% of Glass 7 (Hybrid 8), 20 vol% of Glass 9 (Hybrid 12) and 20 vol% of Glass 12 (Hybrid 16).

Examples of extrudates of polyamide reinforced with 20 vol% of the selected glass compositions and prepared at Condition B are shown in Figure 5.12.

The extrudates of the Hybrid 16 containing Glass 12 (60 SnF_2 mol%) were white and smooth with homogeneous diameters along the length. The extrudates of Hybrid 4, containing Glass 0 (50 SnF_2 mol%) showed a similar morphology. The extrudates of Hybrid 8, containing Glass 7 (30 SnF_2 mol%) and Hybrid 12, containing Glass 9 (40 SnF_2 mol%) exhibited whiteness but lacked smoothness which was attributed to un-melted glass particles in the extrudates.

The morphology of extrudates confirmed the results from the force/time trends. As discussed in Section 4.6, the high content of SnF_2 in Glass 12 and Glass 0 was responsible for the decreased glass transition temperature (~ 106 ˚C and ~ 125 ˚C in Glass 12 and Glass 0, respectively) and softening points (~ 289 ˚C and ~ 310 ˚C in Glass 12 and Glass 0, respectively); it is possible that the glasses could softened and partially melt during extrusion in Hybrid 12 (Glass 0/PA 11) and Hybrid 16 (Glass 12/PA 11), leading to a good mixing of glass and PA and good quality of the extrudates.

In opposition, the glass transitions Tg and softening point Ts of Glass 7 (~ 162 ˚C and ~ 350 ˚C, respectively), and Glass 9 (~ 156 ˚C and ~ 331 ˚C, respectively) were not low enough to allow the glass to flow during extrusion, causing the lack of smoothness of the extrudate of Hybrid 8 (Glass 7/PA 11) and Hybrid 12 (Glass 9/PA 11).

Almost all hybrid compositions behaved similarly to changes of glass composition. The extrudates containing Glass 7 (30 SnF2 mol%) and Glass 9 (40 SnF2 mol%) exhibited a lack of smoothness. The extrudates containing Glass 0 (50 SnF2 mol%) and Glass 12 (60 SnF2 mol%) were smooth. This behaviour was more evident with increasing glass content in the hybrids. As the only variable in the composition of the glass analysed was SnF2, (see Section 4.2), it was hypothesized the SnF2 was responsible of some interaction between the glasses and polyamide.

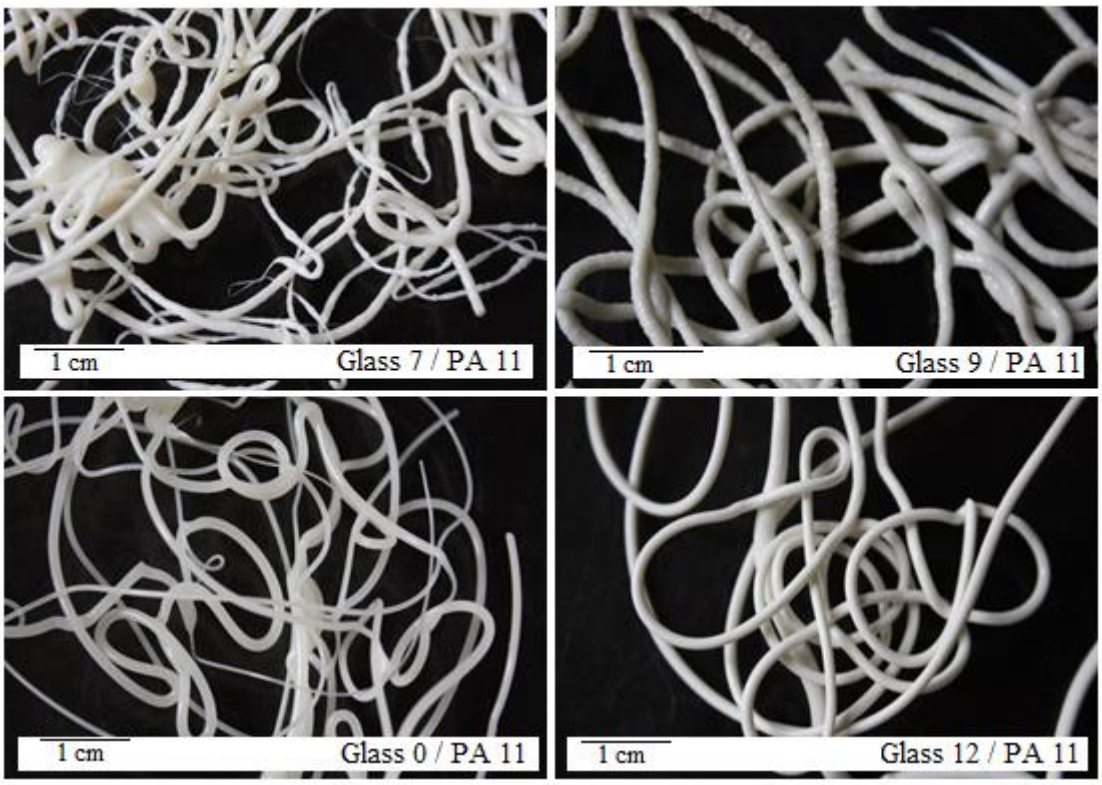

Figure 5.12: Extrudates of Glass 7/PA 11 (Hybrid 8), Glass 9/PA 11 (Hybrid 12), Glass 0/PA 11 (Hybrid 4) and Glass 12/PA 11 (Hybrid 16) containing 20 vol% of glass and prepared at 210/250/250 ˚C, for 300 s with a filling factor of 95% at a screw speed of 100 rpm (Condition B).

5.3.6 Hybrids selected for characterization

A series of glass/PA 11 hybrids were prepared using different working conditions, glass content and compositions with a micro-DSM extruder. The list of all the selected blends is shown in Table 5.3.

Hybrid 4 (20 vol% Glass 0/PA 11) and Hybrid 16 (20 vol% Glass 12/PA 11) processed at Condition B (210/250/250 ˚C, for 300 s with a filling factor of 95% at a screw speed of 100 rpm) showed no degradation during extrusion and the best morphology in the extrudates. Thus, these hybrids were selected for further experimentations. Hybrid 8 (20 vol% Glass 7/PA 11) and Hybrid 12 (20 vol% Glass 9/PA 11) processed at Condition B showed lack of smoothness. However, because of their dissimilar behaviour compared to Hybrid 4 and Hybrid 16, Hybrid 8 and Hybrid 12 were selected for further characterization for comparison. As a predictable force/time trend was evident in hybrids reinforced with Glass 12, these

hybrids (Hybrid 13 to 15) were selected for the *melting point depression analysis* (see Chapter 6). PA 11 processed at Condition B was used as reference material.

Table 5.3: Equilibrium force Fe and diameter D of the extrudates of PA 11 and hybrid blends processed at Condition B (screw speed: 100 rpm; processing profile temperature: 210/250/250 ˚C; filling factor: 95%; blending time: 300 s).

Melt name	Glass name	Glass vol%	PA 11 vol%	Fe [N]	D [mm]
PA 11	-	0.0	100.0	1932.0 ± 432.0	1.8 ± 0.2
Hybrid 1	Glass 0	2.5	97.5	1792.0 ± 156.0	1.9 ± 0.5
Hybrid 2	Glass 0	5.0	95.0	1129.0 ± 182.0	1.8 ± 0.3
Hybrid 3	Glass 0	10.0	90.0	998.0 ± 182.0	1.8 ± 0.3
Hybrid 4	Glass 0	20.0	80.0	612.0 ± 135.0	1.6 ± 0.4
Hybrid 8	Glass 7	20.0	80.0	1882.0 ± 234.0	2.2 ± 0.3
Hybrid 12	Glass 9	20	80.0	1759.0 ± 367.0	2.6 ± 0.4
Hybrid 13	Glass 12	2.5	97.5	1317.0 ± 178.0	1.7 ± 0.5
Hybrid 14	Glass 12	5.0	95.5	1075.0 ± 56.0	1.7 ± 0.3
Hybrid 15	Glass 12	10.0	90.0	698.0 ± 82.0	1.4 ± 0.3
Hybrid 16	Glass 12	20.0	80.0	348.0 ± 72.0	1.3 ± 0.2

Chapter 6 Properties of Glass/Polyamide Hybrids

Since both the glass and polyamide are expected to be fluid during processing, their miscibility at a molecular level is possible. Individual properties of phosphate glass/PA 11 hybrids components, their composition, their mixing degree and morphology could affect the behaviour of hybrid blends and the mutual interaction between their components. This chapter discusses the characterization of the hybrids reinforced with the selected glass compositions to a better understanding of the effect of glass composition on hybrid properties and the interaction between hybrid components.

6.1 Structural characterization of hybrids

6.1.1 Microstructure of hybrids

Figure 6.1 shows the SEM cross section micrographs of hybrids containing 20 vol% of each selected glass composition.

All micrographs reveal a two-phase heterogeneous hybrid of phosphate glass (light) in a polyamide matrix (dark). However the morphologies and distribution of phases vary significantly with glass composition.

Hybrid 8 (20 vol% Glass 7/PA 11) showed a wide distribution of glass particle sizes in the polyamide matrix. The average particle size was ~ 62 μm. Some defects, like circular cracks around the biggest particles and pores, were observed. Glass 7 has the highest glass transition Tg (~162˚C) and softening temperatures Ts (~ 350˚C), which prevented the glass from melting during blending with PA 11 and flow inside the PA 11 matrix. As the extrudate cooled down and the PA 11 solidified, open pores were left by the non-interacting glass on the polymer surface which adversely influence the smoothness and the quality of the

extrudate and affect the final properties of the hybrid. Approximately 90 pores/cm^2 were observed.

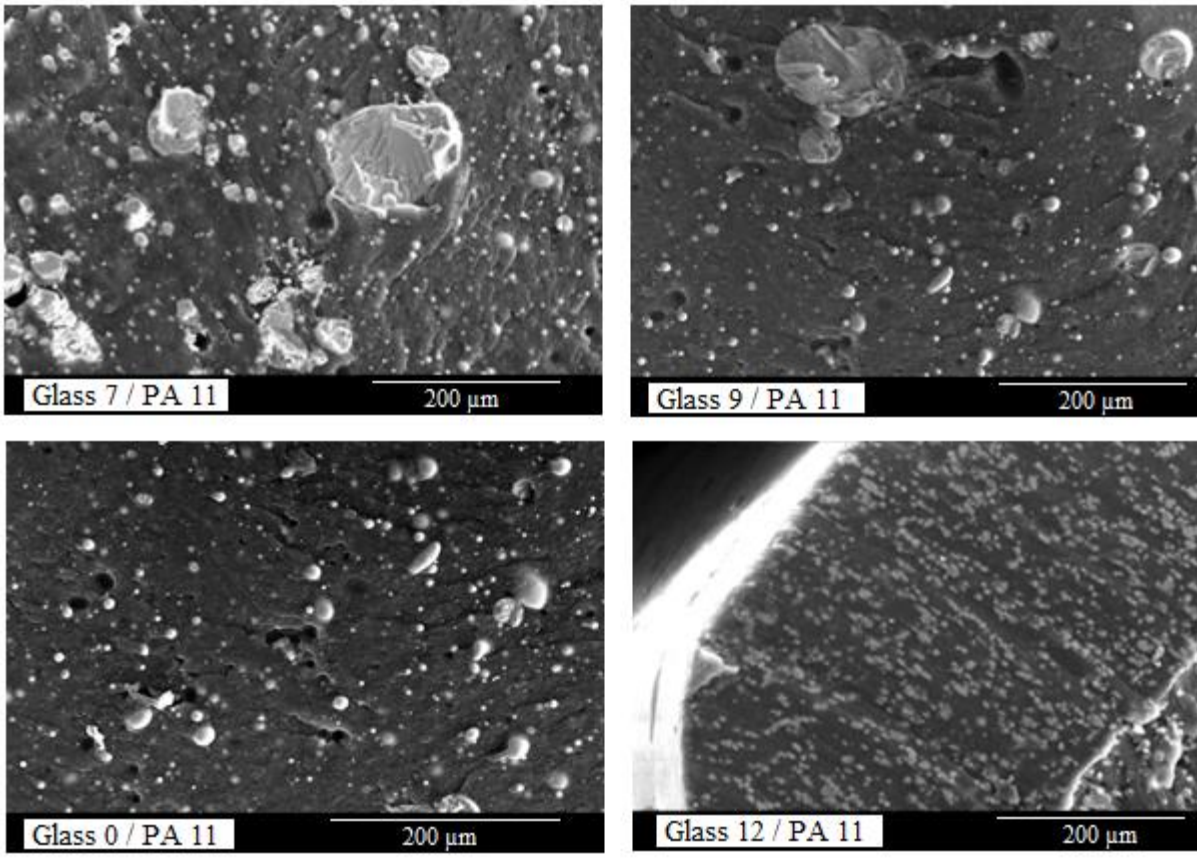

Figure 6.1: Micrographs of cross sections of Glass 7/PA 11 (Hybrid 8); Glass 9/PA 11 (Hybrid 12); Glass 0/PA 11 (Hybrid 4) and Glass 12/PA 11 (Hybrid 16) containing 20 vol% of glass and prepared at 210/250/250 ˚C, for 300 s with a filling factor of 95% at a screw speed of 100 rpm (Condition B).

Hybrid 12 (20 vol% Glass 9/PA 11) exhibited slightly better particle dispersion than Hybrid 8. Hybrid 12 showed an average particle size of ~ 59 µm. The Tg (~ 158 ˚C) and Ts (~ 331 ˚C) of Glass 9 were slightly lower than those of Glass 7, but not low enough to allow the glass particles to flow during blending. Approximately 82 pores/cm^2 were observed.

Hybrid 4 (20 vol% Glass 0/PA 11) showed a narrower particle size distribution than the two hybrids analysed above. The average particle size dimension decreased to ~ 28 µm. The pores were smaller and less common: approximately 20 pores/cm^2 were observed.

Hybrid 16 (20 vol% Glass 12/PA 11) showed the best morphology among the hybrids. Glass 12 was the composition exhibiting the lowest Tg (~ 106 ˚C) and Ts (~ 289 ˚C). The cross

section area exhibits nano-micro particles separated from each other and with a narrow size distribution: the average particle size decreased to ~ 520 nm. Pores along the cross-section were almost absent: approximately 0.4 pores/cm^2 were present in the analysed cross-section area. The glass particles were not perfectly rounded but were slightly deformed. This phenomenon was attributed to the softening point of Glass 12 (~ 289˚C) which is close to the highest working temperature of polyamide during the extrusion (~ 250˚C). Considering that the melt is subjected to high shear rate during extrusion, the glass/hybrid melt temperature could reach higher values than the profile temperature. This would have allowed Glass 12 particles to flow sufficiently during extrusion and to be aligned along the direction of extrusion, even if the softening point of the glass is lower than the highest extrusion temperature. This might increase the contact area between glass and PA 11 and might favour possible interaction between the two components of the hybrid.

The morphology of the hybrids can be explained by the flow mechanisms that the polyamide and the glasses are subjected to during the extrusion process.

In conventional glass/polymer composites, the softening point Ts of glass is higher than the working temperature of the polymer matrix and the glass has a too high viscosity to flow. Initially large drops of glass are present in the liquid polyamide because of the the shear stress induced by the mechanical action of the screws; the glass drops breaks into small droplets; when the melt temperature is below the melting point, collision between the two phases occur due to the turbulent flow during mixing. The glass drops can collide with each other's or with the polymer particles. If the interaction forces among the glass drops are larger than those between the glass and the polymer phases, the glass tends to form agglomerates and coalescence phenomena occur. When, at the end of the process, the temperature is below the melting point of the matrix the viscosity of the polymer increases and the polymer is in a semi-solid state. Here glass droplets are dispersed by turbulence and suspended in the polymer. This is expected in the case of the Hybrid 8 and Hybrid 12, containing 20 vol% of Glass 7 and Glass 9, respectively. However, no coalescence phenomena are observed in the micrograph of Hybrid 8 and Hybrid 12: the large particles observed in Glass 7/PA 11 (Hybrid 8) and Glass 9/PA 11 (Hybrid 12) do not seem to be formed by coalescence or small particle aggregation but seem to be original un-melted glass particles.

In polyamide blended with Glass 0 and Glass 12 (Hybrid 4 and Hybrid 16 respectively), the softening point of the glass is similar to the working temperature of the polyamide. Thus, the two phases can flow at the same time during the extrusion and the system act as a biphasic liquid/liquid polymeric system. Recall that phosphate glasses are composed by entanglement of segments similar to those of polymers but shorter. When the blending temperature is below the softening point of the glass, droplet break up could occur because collision phenomena. When the temperature is higher the softening of glass the droplets extend into long threads and finally break-up into small droplets as described in Section 2.6.3.

The number of pores in the cross sections of the hybrids is directly correlated to the glass transition temperature and softening point of the glasses. In Hybrid 8 and Hybrid 12, the softening point of glasses (Glass 7 and Glass 9, respectively) is higher than the processing temperature. During flow, the glass droplets do not deform and collide forming pores in the extrudate. This phenomenon is less visible in Hybrid 4 and Hybrid 16, where the glasses (Glass 0 and Glass 12, respectively) deform during flow and lead to long thread and droplet break-up. Furthermore as the temperature increases during processing, because of the hydrophilic nature of P_2O_5, evaporation of the residual water possibly present in the glass can cause the separation of glass drops from the polyamide matrix leading to formation of pores. This phenomenon is more evident in Hybrid 8 and Hybrid 12 containing Glass 7 and Glass 9, which are the compositions with the highest amount of P_2O_5 (42 mol% and 36 mo%, respectively).

6.1.2 Chemical structure of hybrids

Generally, the specific intermolecular interactions occurring between two different polymer chains miscible together are: hydrogen bond, ionic bond and dipole-dipole interaction. In this section the structure of hybrids will be elucidated. PA 11 is used as control sample. The hybrids spectra will be compared with glass spectra as well to consider the difference between the analyzed peaks.

The FTIR trace of the PA 11 is shown in Figure 6.2. All the characteristic absorptions of amide groups and methylene segments of polyamide are summarized in Table 6.1.

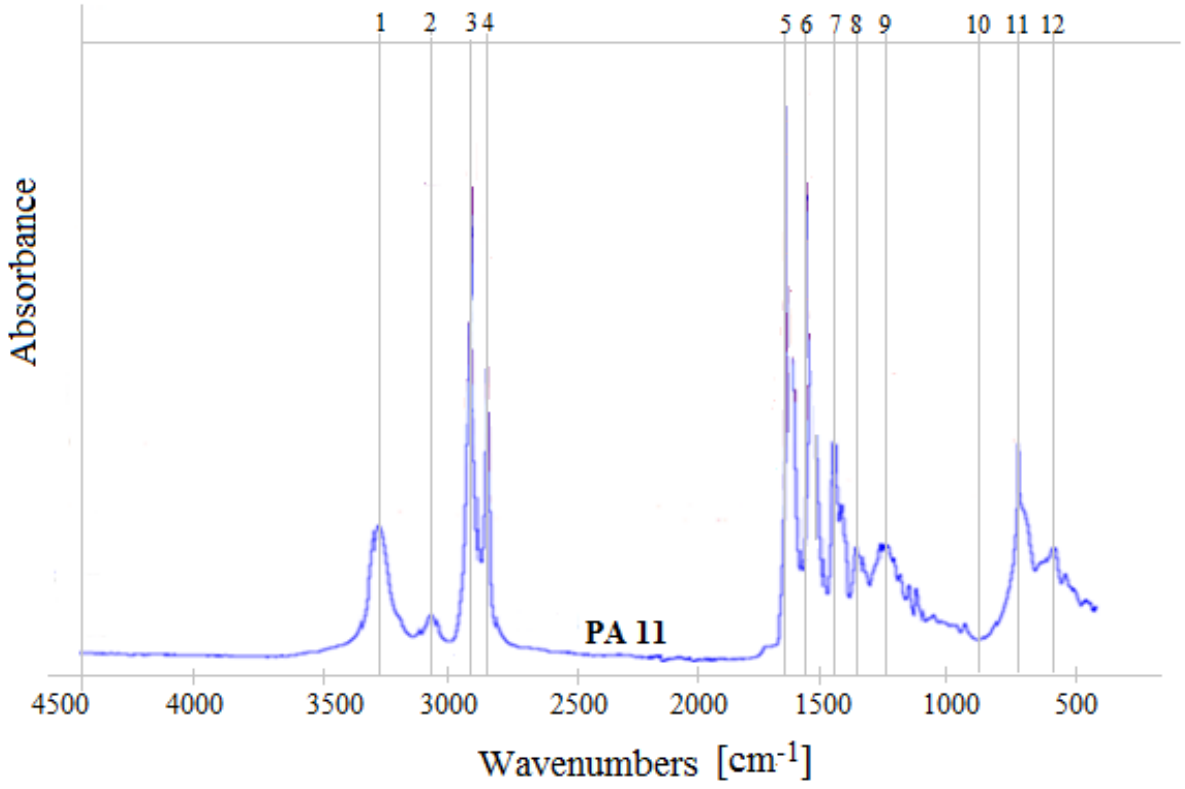

Figure 6.2: FTIR spectrum of polyamide 11.

FTIR spectra of PA 11, glasses and glass/PA 11 hybrids are shown in Figure 6.3 and Figure 6.4.

In Hybrid 4 (20 vol% Glass 0/PA 11), Hybrid 8 (20 vol% Glass 7/PA 11), Hybrid 12 (20 vol% Glass 9/PA 11) and Hybrid 16 (20 vol% Glass 12/PA 11) no absorption band frequency shifts but only intensity modifications among PA 11 and hybrids were present. All glass/PA 11 hybrids show small amount of interactions: new peaks, not visible in the PA 11 spectrum, appeared in the hybrids at a frequency of ~ 630 cm^{-1} and assigned to CF deformation or CF_3 asymmetric deformation. This resonance bands could be due to halogen presence, evidence that the halogen fluoride may be the responsible for the interaction between PA 11 and phosphate glass.

Table 6.1: Bands of PA 11 and 20 vol% phosphate glass/PA 11 hybrids detected by FTIR.

	Band [cm^{-1}]	Attributes
1	3302	hydrogen-bonded and N–H stretching vibration
2	3082	Fermi's resonance (δ)NH amide II
3	2918	Asymmetric stretching of CH_2
4	2848	Symmetric stretching of CH_2
5	1734	Ester groups and impurities
6	1634	amide I, C=O stretching vibration
7	1541	amide II, C–N stretching
8	1466	CO–N–H bending vibration
9	1161	Interaction between (δ)NH and (ν)O=C-N stretching
10	937	amide IV, (δ)CONH stretching vibration
11	721	CH_2 wagging (rocking)
12	688	amide V, N–H out-of-plane bending vibration
	630	CF deformation, CF_3 asymmetric deformation

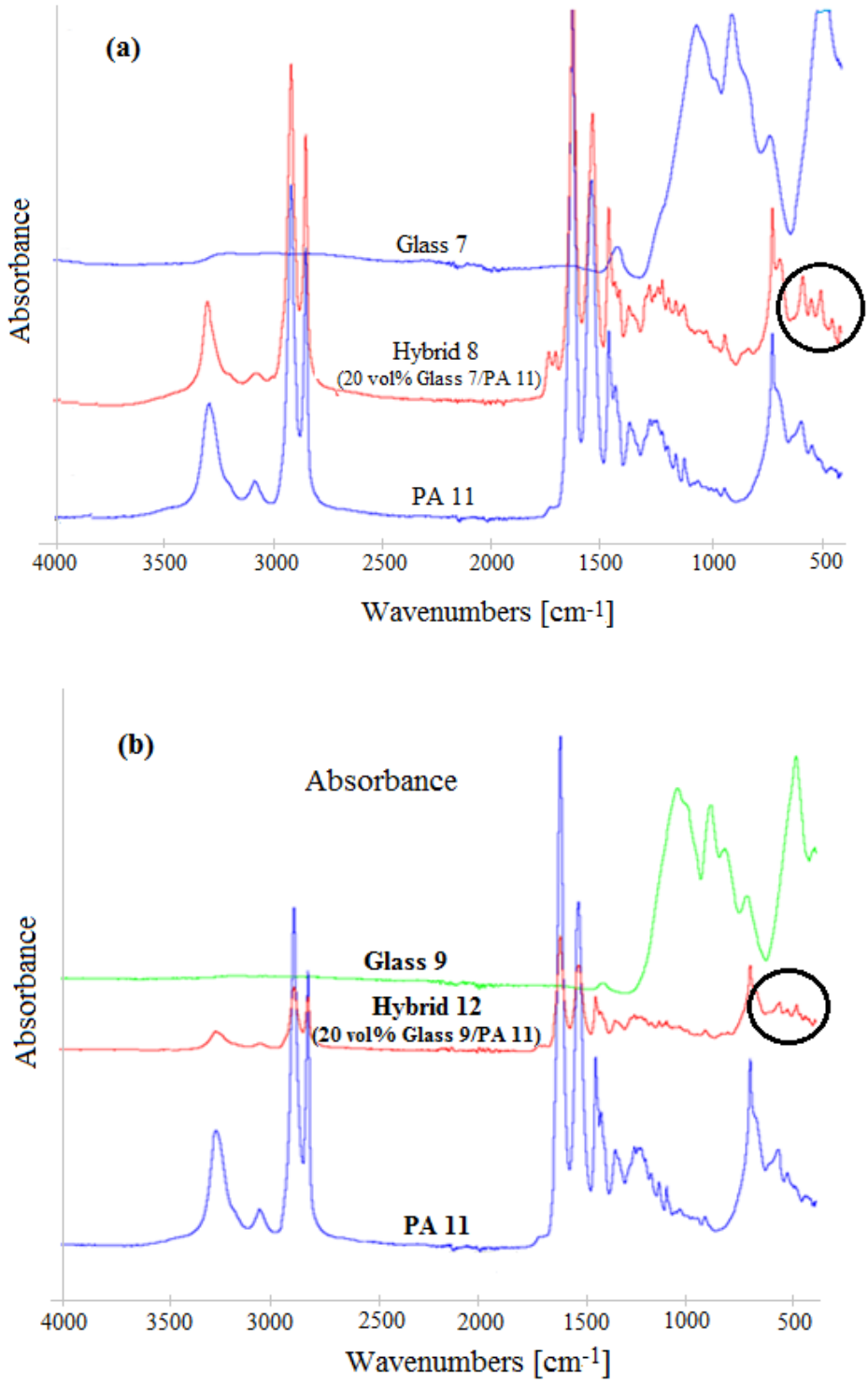

Figure 6.3: FTIR spectra of PA 11, glasses and hybrid reinforced with 20% of: (a) Glass 7 and (b) Glass 9.

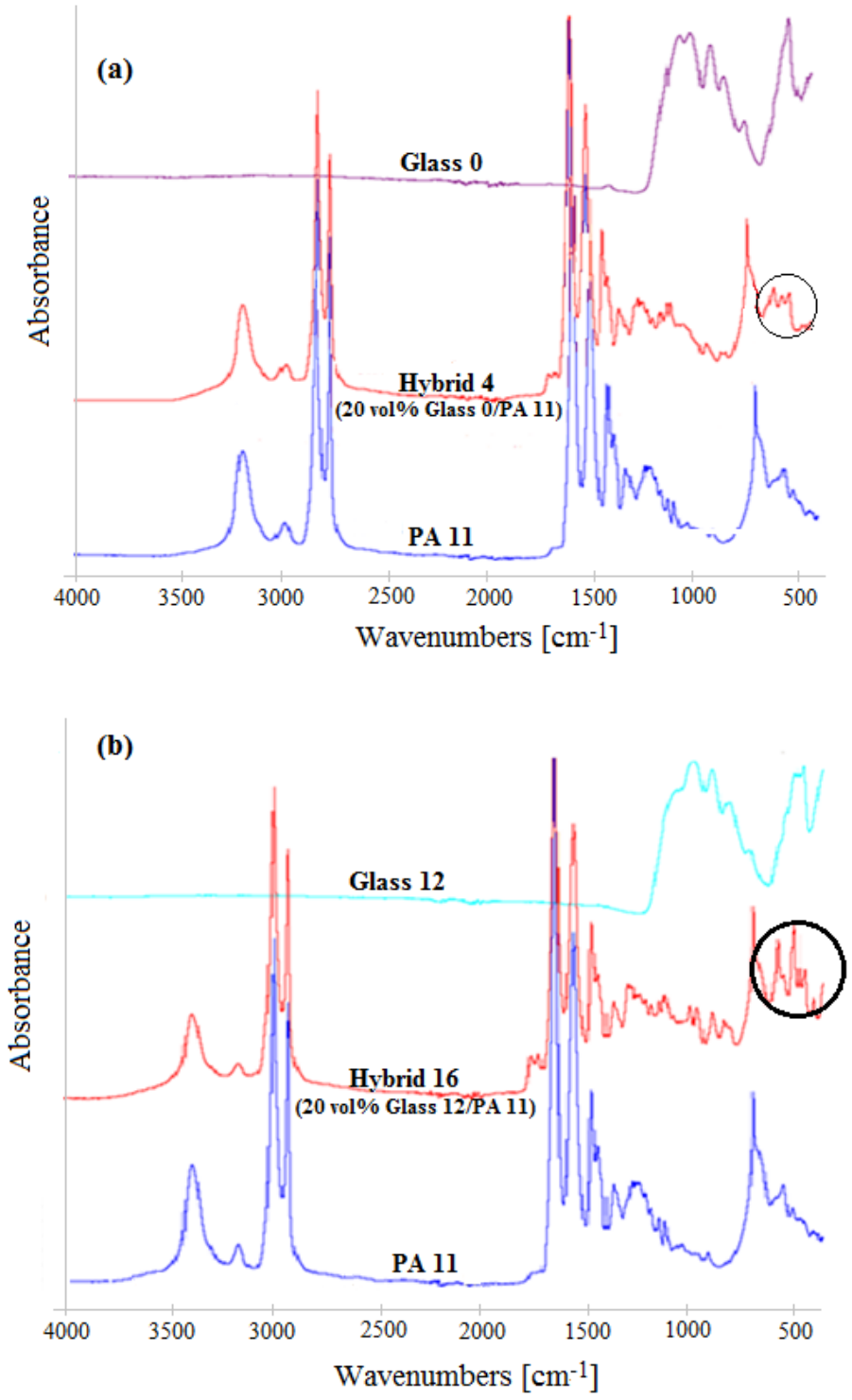

Figure 6.4: FTIR spectra of PA 11, glasses and hybrid reinforced with 20% of: (a) Glass 0 and (b) Glass 12.

6.2 Rheology of polyamide and hybrids

6.2.1 Shear rheology

Rheological characterization may provide a means to determine the degree of dispersion of glass particles in the polymer melt during extrusion as rheological properties of particulate suspensions are sensitive to structure, particle size and composition, and surface modification. Furthermore rheological properties change significantly with favourable particle matrix interactions compared to non-interacting systems or strong particle-particle attractions. The shear rheology of PA 11 and hybrids was investigated in Section 3.8.

The frequency dependence of the complex viscosity for PA 11 and hybrids containing 20 vol% of glass is shown in Figure 6.5.

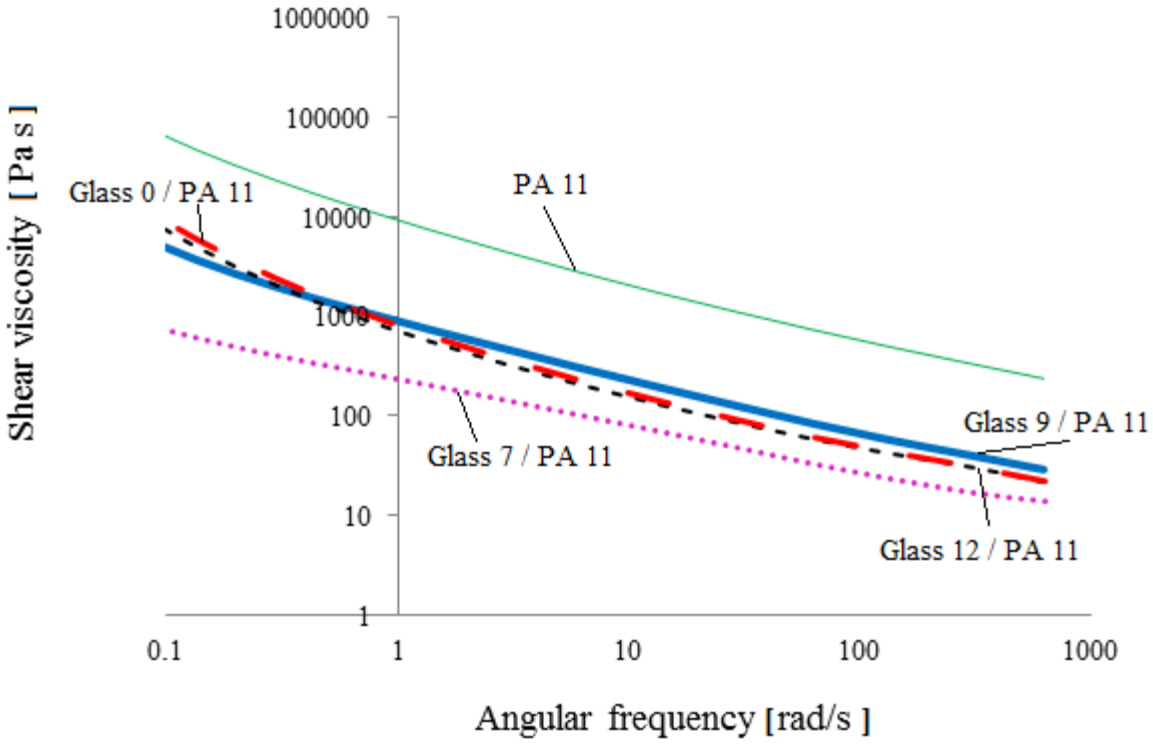

Figure 6.5: Trends of complex shear viscosity versus angular frequency of PA 11, Glass 7/PA 11 (Hybrid 8), Glass 9/PA 11 (Hybrid 12), Glass 0/PA 11 (Hybrid 4) and Glass 12/PA 11 (Hybrid 16) containing 20 vol% of glass.

The pure PA 11 and hybrids exhibited a decrease of shear viscosity with higher angular frequency and displayed a shear thinning behaviour. The values of shear viscosity for PA 11 were in the range of 104500-340 Pas. The shear viscosity of PA 11 was affected by the each

glass addition. The 20 vol% Glass 7/PA 11 showed the lowest values of shear viscosity among of the range of angular frequency analyzed. The shear viscosity values varied in the range of 1050 – 18 Pas. The shear viscosity of 20 vol% Glass 9/PA 11 varied between 7750 Pas and 40 Pas. The shear viscosity of 20 vol% Glass 0/PA 11 varied between 13950 Pas and 25 Pas. The shear viscosity of 20 vol% Glass 12/PA 11 varied between 17700 Pas and 30 Pas.

The decrease of the viscosity with increasing angular frequency can be explained by the destruction of polymer and glass networks: as the angular frequency increases, the disentanglement of polymer chains and glass segments decreases and both components are simultaneously aligned to the flow, which results in a decrease in the hybrid viscosity. Also, the addition of each glass to the PA 11 could cause enhanced mobility of chain segments, a possible disruption or constraint release of the polymer chain entanglements and dramatic changes. Mackay et al. in [95] showed that when the particles are smaller than the root-mean-squared radius of gyration, they act as a plasticizer to produce a viscosity decrease. Generally this decrease in viscosity is accompanied by a decrease in the Tg of the hybrid, which is caused by an increase of the free volume inversely correlated with the particle sizes.

The viscosities vastly decreased in all hybrids, results which are in agreement with the load force/time findings in Section 5.3.4 and Section 5.3.5. Here, the load force/time trends of hybrids indicate that the presence of glass perturbs the normal polymer flow. All hybrid blends showed lower load force and thus lower viscosity than the pure polyamide. The hybrid exhibiting the lowest force was the Hybrid 16 (20 vol% Glass 12/PA 11). Glass 12 had the highest SnF_2 content and lowest Tg (~ 116 ˚C) and Ts (~ 285˚C) among all the experimental glasses.

The lowest shear viscosity of 20 vol% Glass 7/PA 11 along the range of frequencies analyzed can be explained by the evaporation of the residual water present in Glass 7 which has the highest amount of P_2O_5 (42 mol%). The water evaporation could cause the destruction of Glass 7 segments and the consequent decrease in viscosity of the hybrid.

The hybrids exhibited non-Newtonian shear thinning at low angular frequencies. Urman et al. [4- 6, 31] have reference the absence of Newtonian behaviour as the presence of an apparent yield stress. This phenomenon could be due to interfacial effect of the hybrid components. The yield stress was absent in PA 11 and more dramatic in the hybrids as glass transition

temperature and softening point decreased with increasing SnF_2 content. The presence of an apparent yield stress could be related to a strong interaction between the hybrid components. Also, larger apparent yield stresses indicate stronger inter-particle and/or particle polymer interactions.

6.2.2 Elongational rheology

Elongational viscosity measurements of PA 11 hybrids were performed as reported in Section 3.8. The results are shown in Figure 6.6.

All the hybrids showed a dramatic decrease of elongational viscosity compared with PA 11, consistently with the shear rheology results. The values of elongational viscosity for PA 11 were in the range of 2300-196 Pas. The shear viscosity of PA 11 was affected by the addition of each glass composition. The 20 vol% Glass 7/PA 11 showed the lowest values of shear viscosity among of the range of angular frequency analyzed. The elongational viscosity values varied in the range of 90-7 Pas. The elongational viscosity of 20 vol% Glass 9/PA 11 varied between 248 Pas and 19 Pas. The elongational viscosity of 20 vol% Glass 0/PA 11 varied between 161 Pas and 27 Pas. The elongational viscosity of 20 vol% Glass 12 /PA 11 varied between 193 Pas and 31 Pas.

The increase of viscosity with shear rate is known as *strain hardening behaviour***.** Many polymers and polymer blends undergo strain hardening behaviour under elongational flow [58, 63, 69, 72, 77]. This phenomenon, common in a large number of melt blending processing methods, consists in a dramatic increase in the viscosity of the material subjected to extensional flow at high strains. The stain hardening phenomenon is related to the uncoiling of polymer chains resulting in very long, aligned particles under extensional flow [77].

Glass 7/PA 11 (Hybrid 7) and Glass 9/PA 11 (Hybrid 12) showed the same trends as PA 11.

Changes in elongation viscosity/angular frequency trends appeared in the Glass 0/ PA 11 (Hybrid 4) and Glass 12/PA 11 (Hybrid 16). This behaviour could be related to a physicochemical interaction between Glass 12 and PA 11 and a consequent disentanglement and/or scission of PA 11 chains.

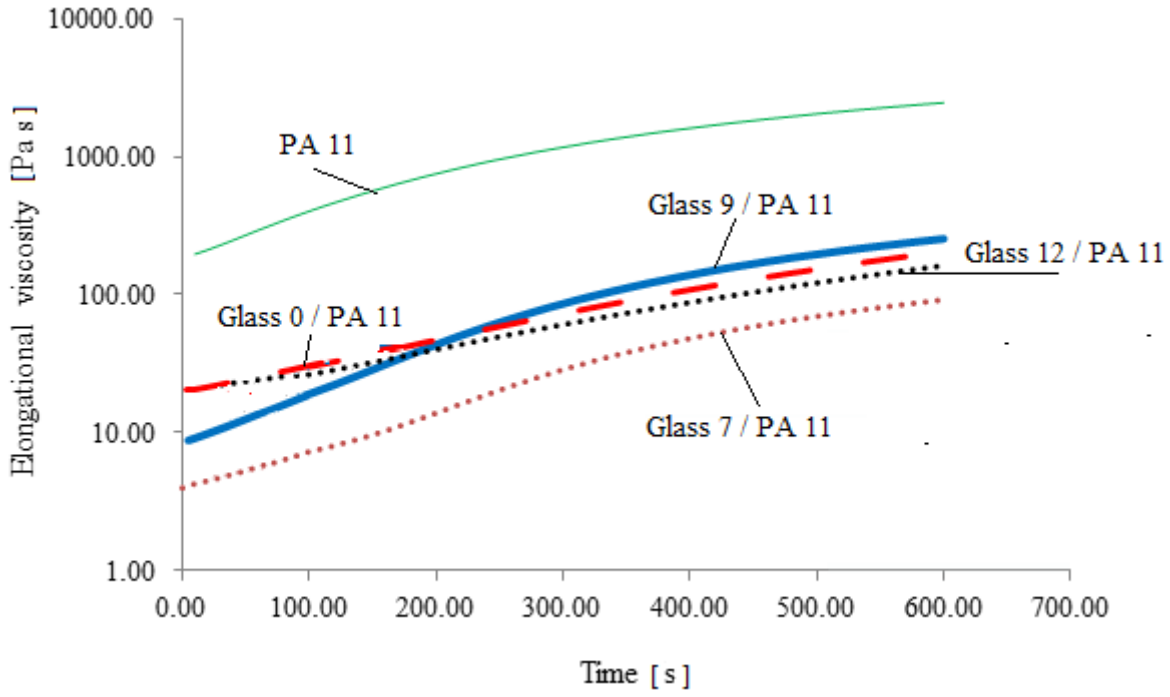

Figure 6.6: Elongational viscosity of PA 11, Glass7 /PA 11 (Hybrid 8); Glass 9/PA 11 (Hybrid 12); Glass 0/PA 11 (Hybrid 4) and Glass 12/PA 11 (Hybrid 16) containing 20 vol% of glass. The test was performed at 250 °C and at a constant strain rate of 1.0 s^{-1}.

6.3 Glass transition temperature of PA 11 and hybrids

The microstructure of hybrids (Figure 6.1) indicates that phosphate glasses and PA 11 are immiscible. However, small amount of interactions might exist between the two components in the hybrids.

A popular experimental method of classifying a miscible blend on a macroscopic scale has been the identification of a single Tg value, which lies between the Tg values of the pure individual blend components [4, 6]. Many research papers define immiscible as those polymer blends or heterogeneous polymer blends that separately show the Tg of each polymer components, while, miscible polymer blends or homogeneous polymer blends show a single Tg from a single phase structure [4, 6].

The glass-transition temperatures (Tg) of PA 11 is about 45˚C. The Tgs of the phosphate glasses are in the range of 106-155 ℃ and decrease with increasing SnF_2 mol% content (from

Glass 7 to Glass 12), behaviour associated to the breaking of phosphate chain when fluoride is added (Table 4.8).

To identify Tgs of the hybrids, DMA was performed on the samples according to the procedure in Section 3.6.1. The DMA gives information on the change in stiffness and energy dissipation of the sample. In particular, the loss factor tanδ (dissipation factor) corresponded to the dissipation of energy during solicitations, in particular during glass transitions; the storage modulus E' was the measure of the sample's elastic behaviour.

The dissipation factor/temperature trends for PA 11 and Glass 12/PA 11 (Hybrid 16) are shown in Figure 6.7. The glass transition temperatures determined from the loss factor data of all hybrids are summarized in Table 6.2.

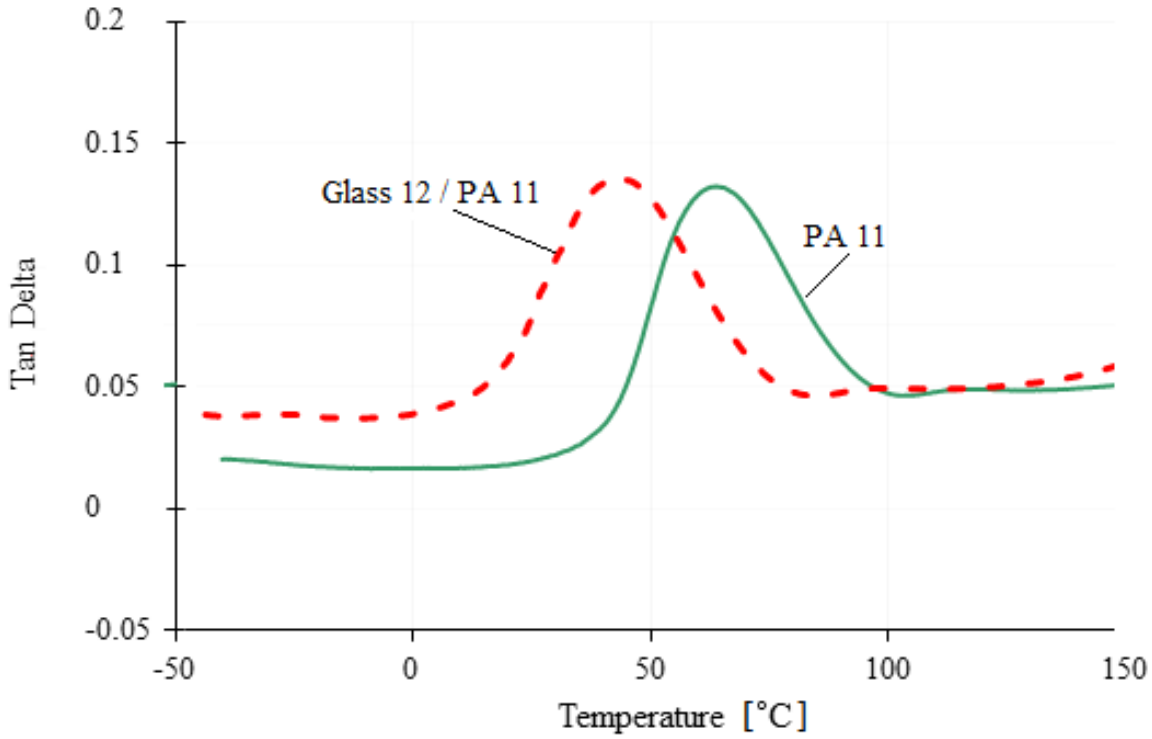

Figure 6.7: Dissipation factor tan δ versus temperature from torsional DMA for pure PA 11 and PA 11 melt blended with 20vol% of Glass 12.

Table 6.2: Glass transition temperature of Polyamide 11 and hybrids with 20 vol% of glass measured by Dynamic Mechanical Analysis at a frequency rate of 1 Hz.

Blend	SnF_2 in glass [vol%]	Glass [vol%]	Tg [°C]	St. Dev.
PA 11	-	0	63.5	± 7.5
Glass 7/PA 11	30	20	59.0	± 4.5
Glass 9/PA 11	40	20	57.5	± 9.5
Glass 0/PA 11	50	20	56.0	± 6.5
Glass 12/PA 11	60	20	38.5	± 4.5

For pure PA 11 and each hybrid composition, the polymer main relaxation corresponding to the glass transition temperature Tg was always observed as the main peak in the curve. Its position and intensity was related to the change in mobility and dissipative mechanism of the macromolecules. No glass-transition peak was visible for the glass component in the hybrids. The glass Tg peak should appear around 100-160 ˚C depending on the glass composition.

These results are in line with the study reported in [6], where a similar behaviour was observed. By introducing 20 vol% of each of the four glasses to the PA network, it was observed a decrease in Tg (shift of tan δ peak to lower temperature) of the resulting hybrid compared to PA 11. This corresponds to an increase in mobility of the macromolecules and a possible interaction between the inorganic particles and the polymer matrix.

Furthermore the Tg of hybrids decreased from 59.0 to 38.5 ˚C (from Glass 7 to Glass 12). The reduction of Tg was directly related to the increasing SnF_2 content in the glass. This behaviour was linked to the formation of terminal group PO_3F and to the consequent increase of chain mobility when fluoride was added.

Studies have often shown miscibility in terms of single Tg as methods of detection of miscibility under the conditions of the experiment [56, 58, 62, 64, 65, 69]. However, a single Tg might be observed in a state of apparent miscibility, where the components of the blend are not permanently miscible. An example of this behaviour was observed in [6] where the glass/PA 6 hybrid showed one Tg but the TEM analysis of glass/PA 6 showed a two-phase microstructure with the glass being distributed as droplets in the polymer matrix. So it is perfectly legitimate to observe clarity and Tg in order to make an experimentally based

comment about the sample at that time but not to assume that the thermodynamic conditions for miscibility have been precisely met.

6.4 Chemical stability of PA 11 and hybrids

The addition of phosphate glass to the polyamide caused a decrease in the viscosity of the polymer. This phenomenon was more prominent as the glass transition temperature of the glasses decreased (from Glass 7 to Glass 12). However the decrease in viscosity of the hybrid could be related to reactions occurring during the melt processing, As P_2O_5 is extremely unstable and reacts violently with water, and PA 11 highly absorb water, free water release could occur during the extrusion. Furthermore, the melt is subjected to high shear rate during extrusion; thus the melt temperature could reach higher values than the set profile temperature during extrusion causing degradation of PA 11. These events could lead to a decrease in molecular weight and be directly related to the observed decrease of the hybrid viscosity and morphology changes as a decreasing of glass size.

To study the possibility of thermal degradation and water release phenomena, thermogravimetric analysis and water stability tests were performed on all hybrids listed in Table 5.1.

6.4.1 Thermal stability

The mass loss with respect to temperature for PA 11 and hybrids is shown in Figure 6.8 (a). Characteristic values from TGA curves are shown in Table 6.3. The inflection point is well visible in Figure 6.8 (b), representing the greatest rate of mass loss of pure PA 11 and hybrids.

The degradation process was a single stage for PA 11 and 20% glass filled PA 11. The decomposition temperature of pure PA 11 was ~ 415 °C at 5% of mass loss, ~ 425°C at 10% of mass loss, ~ 445 °C at the inflection point and ~ 455°C at 50% of mass loss. The decomposition temperature of PA 11 filled with 20 vol% Glass 7 was ~ 410 °C at 5% of mass loss, ~ 425°C at 10% of mass loss, ~ 440 °C at the inflection point, ~ 478 °C at 50% of mass loss. The decomposition temperatures of 20 Glass 9/PA 11 and 20 Glass 0/ PA 11 were

similar, ~ 42 0°C at 5% of mass loss, ~ 440 °C at 10% of mass loss, ~ 455 °C at the inflection point, and ~ 475 °C at 50% of mass loss. The decomposition temperature of PA 11 filled with 20 vol% Glass 12 was ~ 425 °C at 5% of mass loss, ~ 440°C at 10% of mass loss, ~ 450 °C at the inflection point, ~ 475 °C at 50% of mass loss.

The overall trend is that the thermal stability increased with the addition of phosphate glass to polyamide except for Glass 7/PA 11 hybrids. This hybrid showed degradation temperatures slightly lower than PA 11. This phenomenon was linked to the presence of residual water in the hybrid due to the high amount of P_2O_5 present in Glass 7 (42 mol%) and its hydrophilic nature. Recall that Glass 7 showed the highest mass loss over temperature (~ 2.5% of mass loss at 400 °C) as shown in Figure 4.24.

The thermal stability increased from Glass 9 to Glass 12 as the Tg and Ts of glasses decreased, for the whole range of temperature analyzed. Recall that Glass 7 and Glass 9 showed the highest mass loss over temperature (2.5% and 2% respectively of mass loss at ~ 450 °C); Glass 0 and Glass 12 had the lowest mass loss (1.5% and 1% respectively of mass loss at ~ 450 °C) (Figure 4.17). In particular the decomposition temperature of the Glass 12/PA 11 hybrid relative to PA 11 was 11˚C higher at 5% mass loss, 15˚C at 10% mass loss and 23˚C at 50% mass loss. Furthermore the mass loss of hybrids started at ~ 400°C, a higher temperature than the processing temperature of the PA 11.

This result confirms that the decrease in viscosity was not related to thermal degradation phenomena. During degradation, the polyamide molecules break at the C-N bond of the peptide group creating smaller polymer molecules with the same unit of chemical structure as well as carbon dioxide, carbon monoxide, water and hydrocarbons [63, 79]. The peptide is a focal point of attack for degradation. A possible explanation of the behaviour observed in this research is that the positive interaction between the phosphate and amide groups provides a degree of increased stability of the peptide group from degradation attack and raises the decomposition temperature of polyamide.

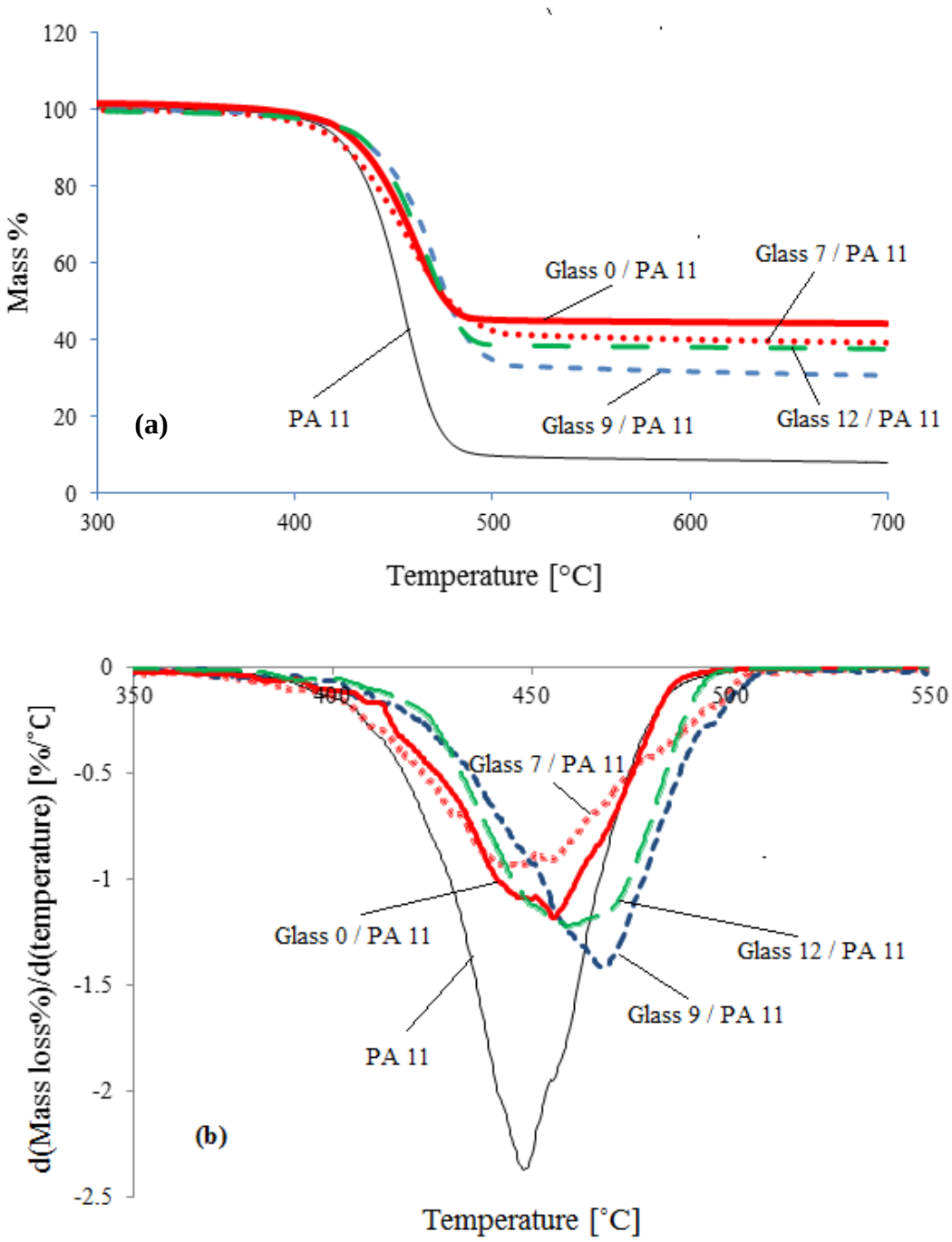

Figure 6.8: Thermogravimetric analysis data of PA 11 and hybrids with 20 vol% glass content measured at a scan rate of 10˚C/min in air: (a) mass% versus temperature; (b) mass loss rate versus temperature.

Table 6.3: Characteristic values from TGA curves for pure PA 11 and hybrids with 20 vol% glass content.

	Decomposition Temperature [°C]			
	At 5% of mass loss	At 10% of mass loss	Inflection Point	At 50% of mass loss
PA 11	415 ± 6	426 ± 5	447 ± 5	454 ± 4
Glass 7/PA 11	411 ± 3	425 ± 3	442 ± 5	478 ± 5
Glass 9/PA 11	423 ± 7	438 ± 5	452 ± 4	477 ± 4
Glass 0/PA 11	422 ± 4	439 ± 7	455 ± 6	476 ± 3
Glass 12/PA 11	426 ± 3	441 ± 6	460 ± 5	477 ± 6

6.4.2 Water stability

The weight losses of PA 11 and hybrids versus the immersion time are showed in Figure 6.9.

PA 11 showed a dissolution rate of ~ 0.0061 mg cm^{-2} h^{-1}, the highest among the samples. This was due to hydrophilic nature of the amide groups. The dissolution rates of hybrids were in the range of 0.0037-0.0058 mg cm^{-2} h^{-1}.

Phosphate glasses improved slightly the stability of PA 11 in water, with Glass 12/PA 11 showing the lowest dissolution rate among the hybrids.

The dissolution rate were directly related to the Tg and Ts of glasses and inversely related to the SnF_2 content in the glasses (Table 6.4) As the SnF_2 in the glass increases, the chance of fluoride atom to form $P0_3F$- Q^1 units or PO_2F_2 $–Q^0$ depolymerisation units increases. It was hypothesized that these units could link to the C-N bond of the peptide group creating smaller polymer molecules, increasing the water stability of the peptide group and the hybrids.

Thus, it was inferred that the decrease in the viscosity was not related to dissolution phenomena occurring inside the hybrid network, reinforcing the hypothesis of stronger interaction taking place between glass and PA 11 when the Tg and Ts of glasses decreased.

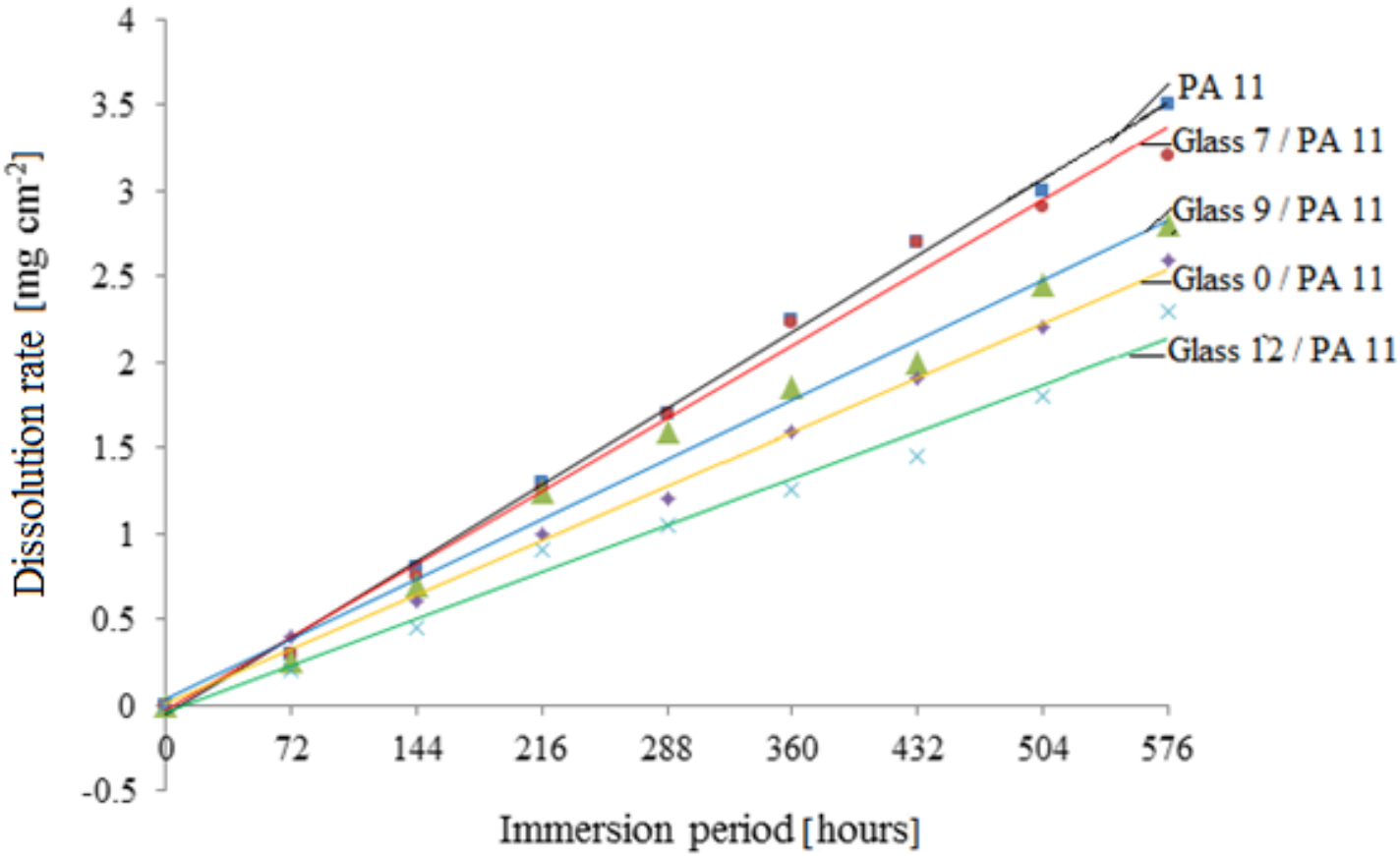

Figure 6.9: Weight loss during dissolution of PA 11 and hybrid disks immersed in distilled water at 37°. The overlaid trend-lines plotted through the origin are indicative of the glass's dissolution rate.

Table 6.4: Dissolution rates identified for PA 11 and hybrids with 20vol% glass. The samples were immersed in distilled water at 37°C with the overlaid trend-lines plotted through the origin indicative of the glass's dissolution rate.

Blend	Dissolution Rate [mg cm^{-2}]	SnF_2 in the glass [mol%]	Tg of blends [˚C]	Ts of glass [˚C]
PA 11	0.0061 ± 0.0005	0	45.0	-
Glass 7 / PA 11	0.0058 ± 0.001	30	162.0	398.0
Glass 9 / PA 11	0.0049 ± 0.0015	40	157.5	389.0
Glass 0 / PA 11	0.0044 ± 0.0008	50	122.0	375.0
Glass12 / PA 11	0.0037 ± 0.0007	60	107.0	289.0

6.5 Mechanical properties of PA 11 and hybrids

6.5.1 Static mechanical properties

A general analysis of the static tensile and flexural behaviour of PA 11 and hybrid specimens is shown in this section.

The static mechanical properties were determined as reported in Section 3.9. The tensile and flexural strengths (σ_{th},σ_{fh}) were calculated from the maximum on load-deformation and load-deflection curves, respectively. The moduli (E_{th}, E_{fh}) were calculated from the linear section of the respective curves.

The typical load-extension and load-deflection curves for the PA 11-control specimens and for the hybrids are shown in Figure 6.10. The tensile and flexural data are presented in Table 6.5.

The data of PA 11 specimens are reported as control. The curves reveal the deformation of PA 11 and its hybrids during the early stages is linearly elastic for all specimens. Non-linear deformation behaviour is present for PA 11 at high deflection.

The tensile strength of PA 11 was ~ 33 MPa. The tensile strengths of hybrids were in the range of 20-35 MPa, with no observed trend with glass composition. The lowest tensile strength and the highest tensile strength were observed in Glass 7/PA 11 (Hybrid 8) and Glass 12/ PA 11 (Hybrid 16), respectively.

The tensile modulus of PA 11 was ~ 1010 MPa. The tensile modulus of hybrids were in the range of 740-1510 MPa, with no observed trend with glass composition; the lowest tensile modulus and the highest tensile modulus were observed in Glass 9/PA 11 (Hybrids 12) and Glass 12/ PA 11 (hybrid 16), respectively.

The yield strength of PA 11 was ~ 20.5 MPa. The yield strength of hybrids were in the range of 14-26.5 MPa, with no observed trend with glass composition; the lowest tensile modulus and the highest tensile modulus were observed in Glass 9/PA 11 (Hybrids 12) and Glass 12/ PA 11 (Hybrid 16), respectively.

The elongation at yield of PA 11 was ~ 2.5 %. The elongation at yield of hybrids were in the range of 1.40-2.5 %, with no observed trend with glass composition; the lowest elongation at yield and the highest elongation at yield were observed in Glass 9/PA 11 (Hybrids 12) and Glass 12/ PA 11 (Hybrid 16), respectively.

The strength at break of PA 11 was ~ 53 MPa. The strength at break of hybrids were lower than PA 11 and varied in the range of 22-33.5 %, with no observed trend with glass composition; the lowest strength at break and the highest strength at break were observed in Glass 7/PA 11 (Hybrids 8) and Glass 12/ PA 11 (Hybrid 16), respectively.

The elongation at break of PA 11 was ~ 310 %. The elongation at break of hybrids were lower than PA 11 and varied in the range of 2-91 %, with no observed trend with glass composition; the lowest elongation at break and the elongation strength at break were observed in Glass 7/PA 11 (Hybrids 8) and Glass 9/PA 11 (Hybrid 12), respectively.

The flexural strength of PA 11 was ~ 34.5 MPa. The flexural strength of hybrids were in the range of 26-37.5 MPa and decreased with increasing SnF_2 in the glass compositions; the lowest flexural strength and the highest flexural strength were observed in Glass 7/PA 11 (Hybrids 4) and Glass 12/PA 11 (Hybrid 16), respectively.

The flexural modulus of PA 11 was ~ 830 MPa. The flexural moduli of hybrids were in the range of 945-1220 MPa and increased with increasing SnF_2 in the glass compositions; the lowest flexural modulus and the highest flexural modulus were observed in Glass 7/PA 11 (Hybrids 4) and Glass 12/PA 11 (Hybrid 16), respectively.

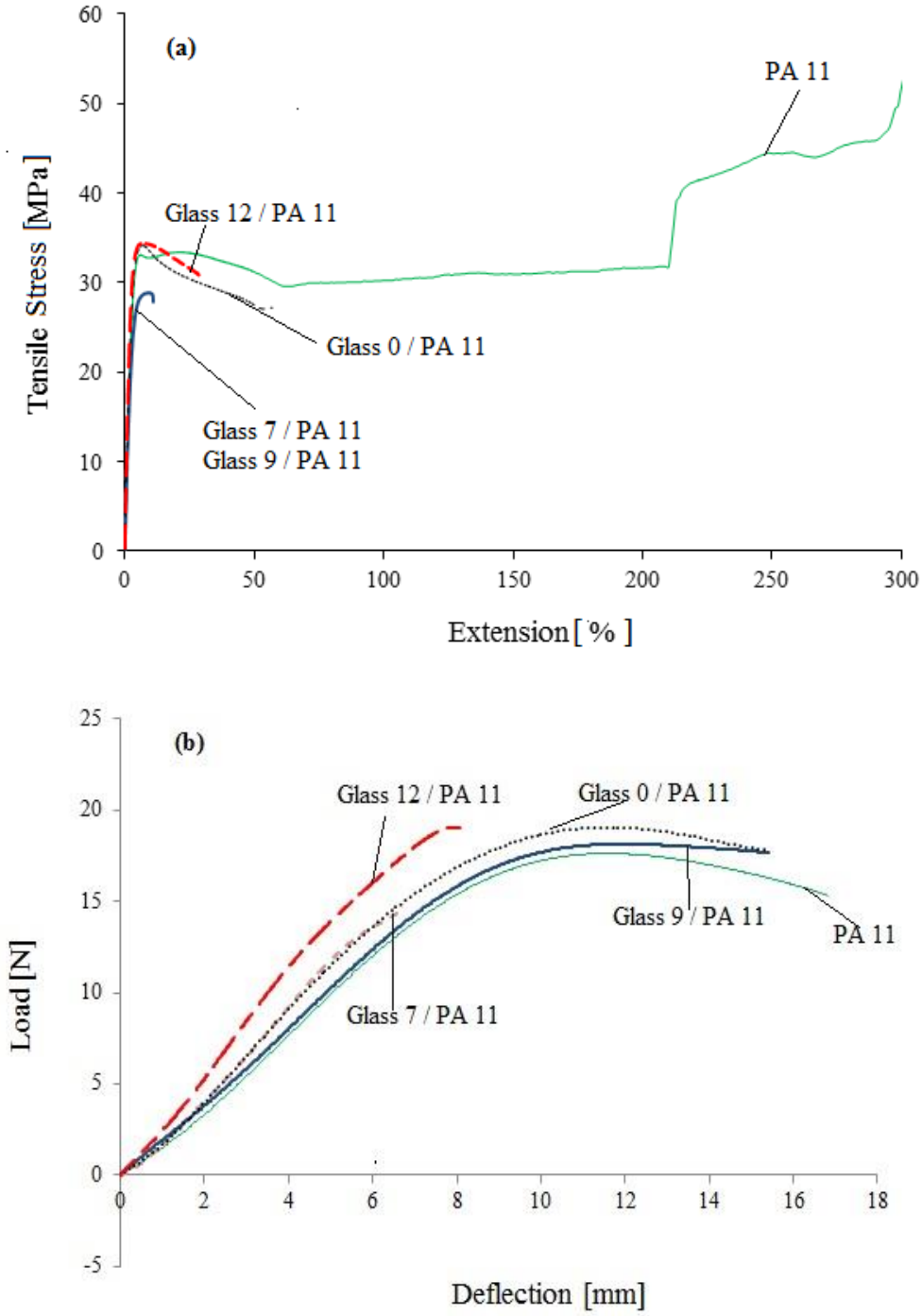

Figure 6.10: (a) Stress/extension (a) and (b) load/deflection trends of PA 11 and 20 vol% glass/PA 11 hybrids.

Table 6.5: Static tensile and flexural properties of PA 11 and hybrids.

	PA 11	Glass 7/PA 11	Glass 9/PA 11	Glass 0/PA 11	Glass 12/PA 11
SnF_2 content [mol%]	-	30	40	50	60
Tensile Strength [MPa]	32.9 ± 0.2	22.0 ± 0.6	29.5 ±0.7	33.75 ± 0.3	34.9 ± 0.4
Tensile Modulus [MPa]	1008.1 ± 53.8	1264.8 ±77.7	746.3 ± 14.4	1172.0 ± 55.9	1508.1 ±28.1
Yield Strength [MPa]	20.4 ± 0.5	20.0 ±0.4	14.9 ± 0.1	25.6 ± 0.2	26.3 ± 1.0
Elongation at Yield [%]	2.3 ± 0.3	2.2 ± 0.6	1.4 ±0.1	2.3 ± 0.1	2.4 ± 0.1
Strength at Break [MPa]	53.3 ± 1.9	22.0 ± 0.6	28.5 ± 0.6	27.0 ± 0.2	33.4 ± 1.8
Elongation at Break [%]	309.7 ± 3.7	2.2 ± 0.7	11.9 ± 2.6	90.8 ±33.1	17.9 ±7.6
Flexural Strength [MPa]	34.5 ± 5.3	26.0 ± 3.6	32.5 ± 2.2	36.1 ± 3.7	37.4 ± 3.4
Flexural Modulus [MPa]	828.0 ± 35.4	947.4 ± 57.7	954.0 ± 59.0	970.0 ± 45.4	1212.9 ± 87.6

The characteristic properties show a significant increase in flexural modulus and a substantial decrease in ductility (elongation at break) after the addition of phosphate glass. The increase in flexural modulus is related to the reinforcing effect of the much stiffer glass in the polymer matrix. The reduction in ductility is attributed to the interaction of the ultra-fine glass particles with the polymer on a molecular scale restricting rearrangement mechanisms. Also, the low static mechanical properties of the presence of coarse, angular un-melted glass particles in Glass 7/PA 11 (Hybrid 4) and Glass 9/PA 11 (Hybrid 8) might cause local stress concentrations and de-bonding from the polyamide matrix, which might affect the static mechanical properties of these hybrids.

This phenomenon is similar to that one observed in conventional solid glass filler composites in which an increase in Young's modulus and a decrease in the strain at break are observed [17, 58, 79]. However this behaviour is in discordance with the results of the study [5], where the Young's modulus and the energy at break of hybrids were observed to decreased with increasing glass in the hybrid, a behaviour that is similar to that obtained when a plasticizer is added to a pure polymer [58, 79]. In [6], the plasticizing effect on tensile mechanical properties of the hybrids was observed together with the drop of the hybrid Tg, which was related to the partial miscibility of the components in the polymer blends and a high degree of interaction. The glass/PA 11 hybrids in this study did not show clear evidence of plasticizing effect.

6.5.2 Dynamic mechanical proprieties

The dynamic storage modulus E' was calculated to measure the change in stiffness of the samples as reported in Section 3.8.

The variation of the elastic storage modulus E'(ω) versus temperature for PA 11 and selected hybrids is shown in Figure 6.11. The samples were tested at a temperature range of -50-200˚C and at a frequency rate of 1 Hz.

The storage modulus of PA 11 varied in the range of 149-1075 MPa. The storage modulus of Glass 7/PA 11 (Hybrid 8) varied in the range of 163-1511 MPa. The storage modulus of Glass 9/PA 11 (Hybrid 12) varied in the range of 165-1992 MPa. The storage modulus of Glass 0/PA 11 (Hybrid 4) varied in the range of 205-2160 MPa. The storage modulus of Glass 12/PA 11 (Hybrid 16) varied in the range of 329-2730 MPa.

The storage modulus decreased slowly at first with increased temperature for all the samples. As the temperature increased further, a sharp decrement was observed and, then, a constant modulus value independent of glass composition was reached at higher temperatures.

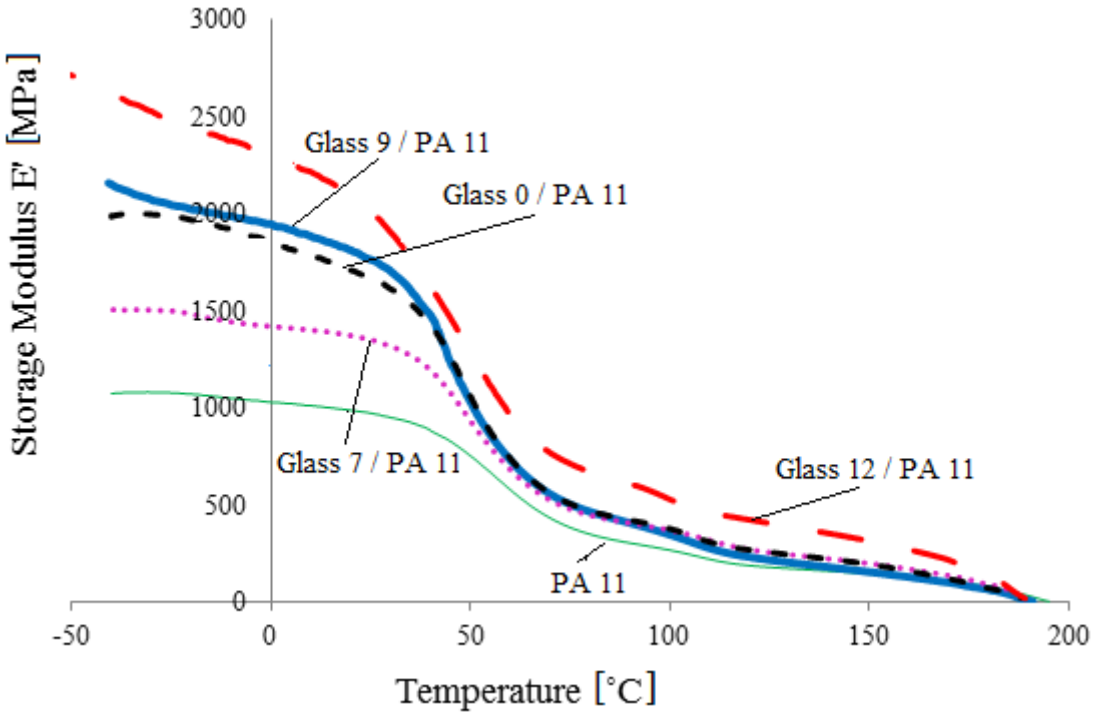

Figure 6.11: Trends of storage modulus versus temperature of PA 11, Glass 7/PA 11 (Hybrid 8), Glass 9/PA 11 (Hybrid 12), Glass 0/PA 11 (Hybrid 4) and Glass 12/PA 11 (Hybrid 16) containing 20 vol% of glass. The samples were tested at a temperature range of -50-200˚C and at a frequency rate of 1 Hz.

This behaviour is related to the degree of free molecular movement. At lower temperature the hybrid is solid and the oscillations of the molecules about mean position are small and their kinetic energies are low. In this condition the possibility of motion due to the lack of free volume is restricted; hence the molecules are unable to respond to the load applied to the sample. As the temperature increases the kinetics energy of the molecules increases as well, resulting in an increment of the motion of molecular chains and a higher strain in the sample subjected to the applied load.

The variation of the shear storage modulus G'(ω) versus temperature for PA 11 and selected hybrids is shown in Figure 6.12.

The shear storage modulus of PA 11 varied in the range of 9750-98925 MPa. The shear storage modulus of Glass 7/PA 11 (Hybrid 8) varied in the range of 47-3243 MPa. The shear

storage modulus of Glass 9/PA 11 (Hybrid 12) varied in the range of 545-4789 MPa. The shear storage modulus of Glass 0/PA 11 (Hybrid 4) varied in the range of 834- 3478 MPa. The shear storage modulus of Glass 12/PA 11 (Hybrid 16) varied in the range of 876-3542 MPa.

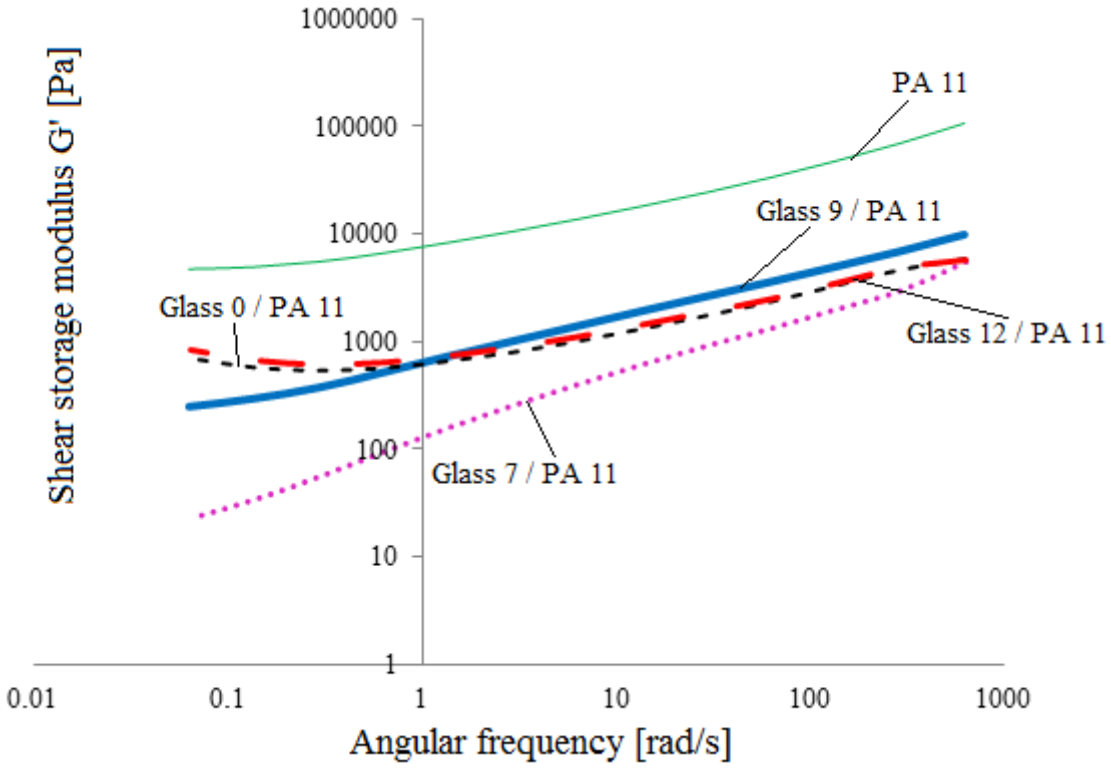

Figure 6.12: Trends of shear storage modulus versus temperature of PA 11, Glass 7/PA 11 (Hybrid 8); Glass 9/PA 11 (Hybrid 12); Glass 0/PA 11 (Hybrid 4) and Glass 12/PA 11 (Hybrid 16) containing 20 vol% of glass. The sample were tested at 250˚C and in a frequency range of 0.1-100 rad/s.

G'(ω) of the hybrids were lower than pure matrix. At lower angular frequency the shear storage modulus G'(ω) increased slightly as SnF_2 content increased in phosphate glasses. At higher angular frequency the storage modulus trend was independent from SnF_2 content. Finally based on G'(ω) data, it can be stated the rigidity of the sample at 250 ˚C decreased when phosphate glass was added to PA 11. Such results suggest that the processability of the system was not compromised by the presence of phosphate glasses.

In hybrids with higher content of SnF_2 a slight reduction of the slopes was evident in the terminal region of the storage modulus G'(ω) versus angular frequency plots . This behaviour was linked to the tendency of PA 11 and glasses to form a structure displaying a yield stress.

This phenomenon is reported in [31]: in this study polyamide 12 melted with a novel phosphate glass showed a decrease in the slope in last portion of loss modulus versus angular frequency plot when the testing temperature was increased to 250 ˚C. The same frequency dependence of storage modulus G'(ω) was observed for loss modulus G"(ω).

The presence of yield stress was related to the glass compositions, responsible in promoting new links and aggregates in the polymer melts. The glass transition temperature Tg and the softening point Ts of glasses decreased with increasing SnF_2 content in the compositions from Glass 7 to Glass 12. The mobility of glass particles increased with SnF_2 content, especially at the processing temperature 250˚C. At this temperature an increasing SnF_2 in the glass could cause interactions of Glass 12 dispersed particles among themselves and with the PA 11 matrix.

6.6 Thermodynamics of miscibility of hybrids

It is generally agreed that the thermodynamic basis for the mixing of polymer blends is an exothermic heat of mixing, since the entropic contribution is small in such systems [64-71]. The two polymers in a binary blend may contain units capable of some type of specific interaction favouring homogeneity and/or may display repulsive intramolecular interactions between groups that likewise promote exothermic mixing. In general, when the first polymer is mixed to the second polymer, a melting point depression of a polymeric system indicates a thermodynamically favourable interaction between the two polymers.

The well know Nishi-Wang expression (Equation 2.12) [67] relates the equilibrium melting point depression to the thermodynamic mixing i.e. miscibility, of crystalline and amorphous polymers.

$$\left(\frac{1}{T_{bm}^0}-\frac{1}{T_m^0}\right)=\frac{Rv_c}{\Delta H_f^0 va}\chi_{ac}{\phi_a}^2 \qquad (2.12)$$

Where: T_{bm}^0 and T_m^0 are the equilibrium melting point of the blend and the crystalline component of the blend, respectively; $\left(\frac{1}{T_{bm}^0}-\frac{1}{T_m^0}\right)$ is the melting point depression.

The equilibrium melting temperature of a polymer may be defined as the melting point of an assembly of crystals, each of which is so large that size (i.e., surface) effects are negligible,

with the provision that each such large crystal is in equilibrium with the normal polymer liquid. (Small crystals will tend to melt well below Tm) [64-71]. v_a and v_c are the molar volumes of the repeat unit of the amorphous and the crystalline polymers respectively; Φa is the volume fraction of the amorphous component; ΔH_f^0 is the heat of fusion of the crystalline component; $\chi_{ac}$is the Flory-Huggins interaction parameter; R is the universal gas constant. The interaction parameter χ_{ac} is used to quantify the degree of interaction between two components of the polymer blend.

In this section the depression of the equilibrium melting point of the selected hybrids listed in Table 6.6 was investigated by the Hoffman-Weeks approach. It is fundamental to measure the equilibrium melting temperature of a polymer instead of that the direct melting point Tm for a number of reasons. Melting point depression in the blends is a result of kinetic and thermodynamic factors. In any crystallisable blend, the crystals are formed at temperature below the equilibrium melting point of the polymer mixture. At temperatures of crystallization, lower than melting point Tm, thinner lamellae develop which, therefore, melt at below Tm. Polymers as they are ordinarily crystallized tend to melt well below Tm. Also crystals are imperfect and may melt at different melting points. The result is that a direct measurement of Tm for a polymer could be affected by crystal size effects.

In order to determine the equilibrium melting point, isothermal crystallization was performed based on the Hoffman-Weeks method following the procedure described in Section 3.6.1. The Flory-Huggins theory (Equation 2.12) was used to calculate the miscibility interaction parameter between the phosphate glasses and the PA 11 matrix. The results were related to the morphological and structure results of hybrids.

6.6.1 Effect of glass composition on equilibrium melting point

The plots representing the melting point Tm after crystallization versus the crystallization temperature Tc for each glass composition are shown in Figure 6.13. The equilibrium melting point of the material Tm^0 was determined by the intersection of the plot for a given type of hybrid with the line Tc = Tm. The equilibrium melting point values are listed in Table 6.6.

The equilibrium melting point Tm^0 of neat PA 11 was equal to 200.5 °C, which is in close agreement to the value reported in the literature [4, 5].

Table 6.6: Equilibrium melting points of PA 11 and Glass/PA 11 hybrids determined by Hoffman-Weeks approach.

Blend	Glass name	Glass [vol%]	Tm^0 [°C]	St. Dev.
PA 11	-	0	200.5	± 2.5
Hybrid 1	Glass 0	2.5	188.0	± 1.6
Hybrid 2	Glass 0	5.0	188.9	± 1.5
Hybrid 3	Glass 0	10.0	187.3	± 2.2
Hybrid 4	Glass 0	20.0	188.8	± 1.2
Hybrid 5	Glass 7	2.5	188.3	± 1.5
Hybrid 6	Glass 7	5.0	188.2	± 2.8
Hybrid 7	Glass 7	10.0	190.4	± 3.6
Hybrid 8	Glass 7	20.0	187.5	± 1.6
Hybrid 9	Glass 9	2.5	194.0	± 1.7
Hybrid 10	Glass 9	5.0	193.8	± 1.9
Hybrid 11	Glass 9	10.0	194.4	± 1.5
Hybrid 12	Glass 9	20.0	193.0	± 1.3
Hybrid 13	Glass 12	2.5	189.2	± 1.3
Hybrid 14	Glass 12	5.0	189.0	± 0.6
Hybrid 15	Glass 12	10.0	188.3	± 0.2
Hybrid 16	Glass 12	20.0	186.5	± 0.7

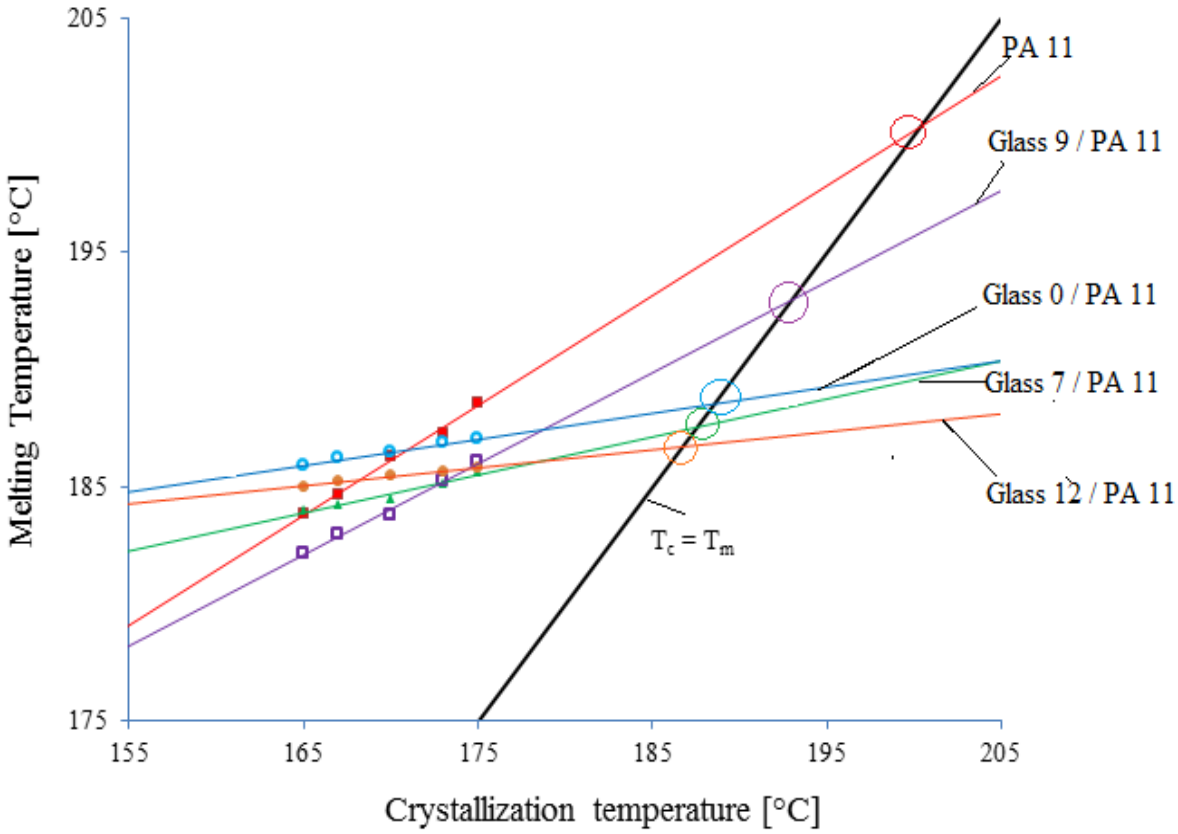

Figure 6.13: Plot of crystallization temperature Tc against melting temperature Tm for phosphate glass hybrids with 20 vol% of each glass composition.

The Tm^0s of Glass 0/PA 11 hybrids (Hybrid 1 to 4) varied in the range of 187-189 ˚C. The Tm^0s of Glass 7/PA 11 hybrids (Hybrid 5 to 8) varied in the range of 187-191 ˚C. The Tm^0s of Glass 9/PA 11 hybrids (Hybrid 9 to 12) varied in the range of 193-195 ˚C. The Tm^0s of Glass 12/PA 11 hybrids (Hybrid 13 to 16) varied in the range of 190-186 ˚C.

The results showed that the addition of each of the four glasses in the range of 2.5-20 vol% to the polyamide decreased the Tm^0 of the resulting hybrid compared to the Tm^0 of PA 11. The greatest reduction was obtained for Hybrid 16, which contains 20 vol% of Glass 12.The sharp melting point depression in Hybrid 16 was likely related to SnF_2 as Hybrid 16 contains the highest Glass 12 content and, thus, the highest quantity of SnF_2 among the hybrids.

The extrapolated equilibrium melting points of PA 11 and hybrids with 20 vol% of each glass composition are shown in Figure 6.13. The equilibrium melting point of Hybrid 8 (20 vol% Glass 7/PA 11) and Hybrid 4 (20 vol% Glass 0/PA 11) were similar (~ 187°C and ~ 189°C, respectively). The equilibrium melting point of Hybrid 12 (20 vol% Glass 9/PA 11) was

slightly higher than of Hybrid 4 and Hybrid 7, with a value of ~ 193°C. The equilibrium melting point of Hybrid 16 (20 vol% Glass 12/PA 11) was ~ 186°C, the lowest value among the hybrids.

These results are in agreement with the hybrid morphologies observed in Figure 6.1. Many studies reported a Tm^0 variation inversely correlated with the particles size [4, 64-71]. The smaller particles melt at a lower a melting point, which leads to a melting point depression of the whole material.

The hybrid reinforced with Glass 12 had the smallest glass particles size and the lowest equilibrium melting point among the hybrids decreases. The particle size distributions of hybrids reinforced with Glass 7, Glass 9 and Glass 0 were wide and defects were present, even though morphology of Hybrid 4 (20 vol% Glass 0/PA 11) was slightly improved. This morphological factor could affect the measurement of the equilibrium melting point of the system: when a particulate material has a wide particle size distribution, the average particles size of a section of the material could differ to the one of another section, causing a wide change in the melting point between the two sections.

The reduction of melting point in Hybrid 16 (20 vol% Glass 12/PA 11) with respect to the other hybrids indicates a greater improvement of the interactions between Glass 12 and PA 11 respect the interactions between other glasses and PA 11. The high melting point depression might be related to the presence of nanoparticles which generally melt at temperatures hundreds of degrees lower than the bulk material.

6.6.2 Effect of glass content on equilibrium melting point

The equilibrium melting point Tm^0 did not show any correlation with glass content in the Glass 0/PA 11 (Hybrid 1 to 4), Glass 7/PA 11 (Hybrid 5 to 8), and Glass 9/PA 11 (Hybrid 9 to 12), as shown in Table 6.6.

The plots representing the melting point Tm after crystallization versus the crystallization temperature Tc at different glass content in hybrids containing Glass 12 are shown in Figure 6.14.

The Tm^0 of Hybrid 13 (2.5 vol% Glass 12/PA 11) was reduced by ~ 11°C, respect to the Tm^0 of pure PA 11. The Tm^0 of Hybrid 14 (5 vol% Glass 12/PA 11) and Hybrid 15 (10 vol% Glass 12/PA 11) were slightly lower than the Hybrid 13, reaching values of ~189°C and ~188°C, respectively. The Tm^0 of Hybrid 16 (20 vol% Glass 12/PA 11) was ~186 ˚C. Thus, the equilibrium melting point in Glass 12/PA11 hybrids decreased with glass content (from Hybrid 13 to 16), strengthening the possibility of a thermodynamically favourable interaction between Glass 12 and PA 11. It might be inferred that the Tm^0 depression was directly related to the SnF_2 content in the hybrids.

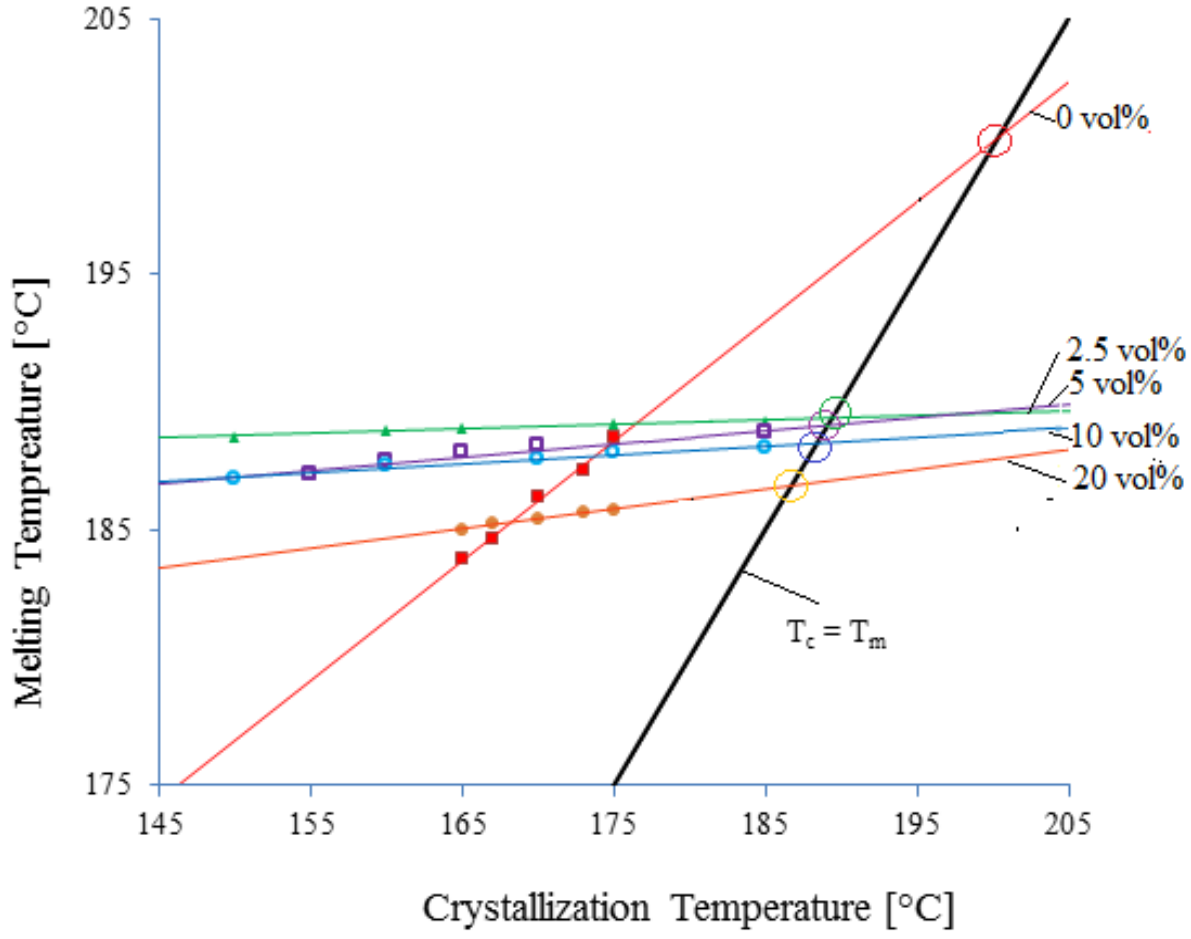

Figure 6.14: Melting point versus crystallization temperature of Glass 12 / PA 11 hybrids with glass content in the range 0–20 vol% according to the Hoffman-Weeks approach.

6.6.3 Equilibrium melting point depression

The effect of the amount of Glass 12 in the hybrids over the range of 0 to 20 vol% was investigated according to the Flory-Huggins approach.

Equation 2.12 describes the melting point depression due to mixing of a crystalline polymer and an amorphous polymer. If χ_{ac} is less than zero there is a melting point depression and the smaller is the value of $\chi_{ac}$the greater is the depression. Tm^0 is expected to decrease as ${\phi_a}^2$ increases. A plot of $\left(\frac{1}{T_{bm}^0}-\frac{1}{T_m^0}\right)$ against ${\phi_a}^2$ should give a straight line passing through the zero of the axes and from the slope the χ_{ac} value can be calculated. Here the phosphate glass is taken as the amorphous polymer. The repeat unit of the phosphate glass was that proposed by Tick [2] and used to calculate the molar volume (v_a) of the phosphate glass. The heat of fusion of the polyamide 11 is 230 kJ/mol.

The melting point depression results in Table 6.7 and Table 6.8 were applied to the Equation 2.12 in order to calculate the interaction parameter χ_{ac}. The equilibrium melting point depression $\left(\frac{1}{T_{bm}^0}-\frac{1}{T_m^0}\right)$ was plotted against the square of the glass volume fraction ϕ_a^2. The expected straight line is shown in Figure 6.15.

Measurement of the latter's slope yields an interaction parameter χ of -0.012. This indicates that there is a degree of miscibility between Glass 12 and polyamide 11 in the melt. This finding is in agreement with the decrease of the viscosities (see Section 6.2) and the decrease of glass transition temperature Tgs (see Section 6.3) in Glass 12/PA 11 hybrids. The Glass 12/PA 11 hybrids (Hybrid 13 to Hybrid 16) were classified as partially miscible as the micrographs in Figure 6.1 showed a two phase microstructure in the hybrids.

Urman and Otaigbe [5] carried out a similar analysis on polyamide 6 and a phosphate glass (Glass 0), and obtained an interaction parameter χ of -0.067. This confirms the current results that there is a positive interaction or attraction between polyamide and phosphate glass. The larger value of χ is attributed to the higher density (almost double) of nitrogen atoms in the polymer chain of polyamide 6 compared with polyamide 11 and an possible higher number of CF linkages between phosphate glasses and polyamide 11 due to the higher amount of fluoride in Glass 12.

As the melt temperature increases during blending, the disentanglement and motion of the polymer and glass segments can happen at the same time and some interaction can occur between the two phases. Intermolecular interactions, such as Lewis acid–base interactions involving hydrogen bonds are examples of favourable interactions between the polymer chains and the glass chains (Figure 6.16 c). Brow et al. (1990) have shown that ammonia will adsorb to the surface of phosphate glasses [7], potentially improving the miscibility in the liquid state and the adhesion in the solid state of the hybrid components.

Also, at high temperature and under high shear rate the polyamide molecules break at the C-N bond of the peptide group creating smaller polymer molecules. This can create a positive interaction between the phosphate groups of glasses and the amide groups of polyamide (Figure 6.16 d). Consequently, the viscosity of the hybrid decreases, confirming the force/time trends recorded during the blending of the hybrids (Figure 5.9).

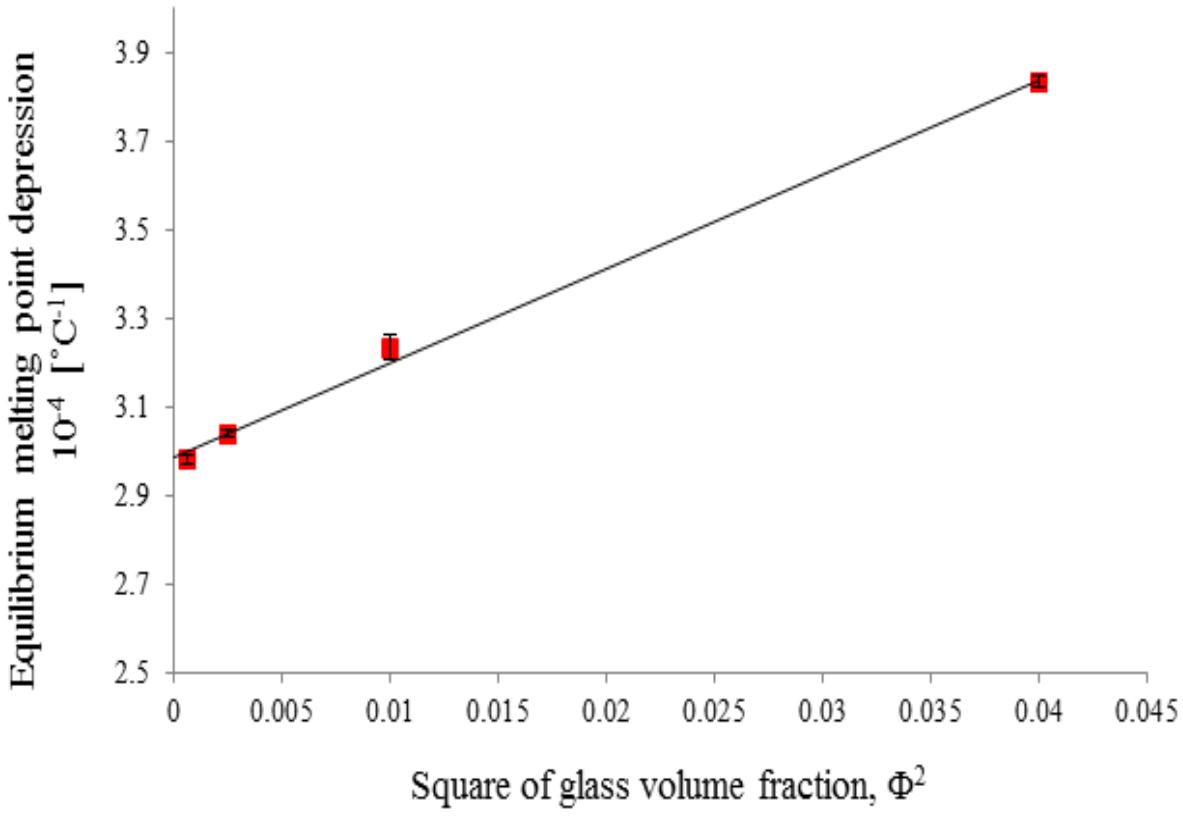

Figure 6.15: Melting-point depression of hybrids as a function of the square of Glass 12 volume fraction.

Table 6.7: ϕ_a and ϕ_a^2 and parameters of Glass 12/PA 11 hybrids.

Blend	Glass 12 in the blend [vol%]	ϕ_a	ϕ_a^2
PA 11	0.0	0.000	0.000000
Hybrid 13	2.5	0.025	0.000625
Hybrid 14	5.0	0.050	0.002500
Hybrid 15	10.0	0.100	0.010000
Hybrid 16	20.0	0.200	0.040000

Table 6.8: Example of parameters used to calculate the melting point depression in Glass 12/PA 11 hybrids.

Blend	Tmb^0 [°C]	$1/Tmb^0$ [$°C^{-1}$]	$1/Tm^0$ [$°C^{-1}$]	$1/Tmb^0-1/Tm^0$ [$°C^{-1}$]
PA 11	200.52	0	0.004987	
Hybrid 13	189.21	00.05285		0.000298
Hybrid 14	189.00	0.005291		0.000304
Hybrid 15	188.33	0.005310		0.000323
Hybrid 16	186.21	0.005370		0.000383

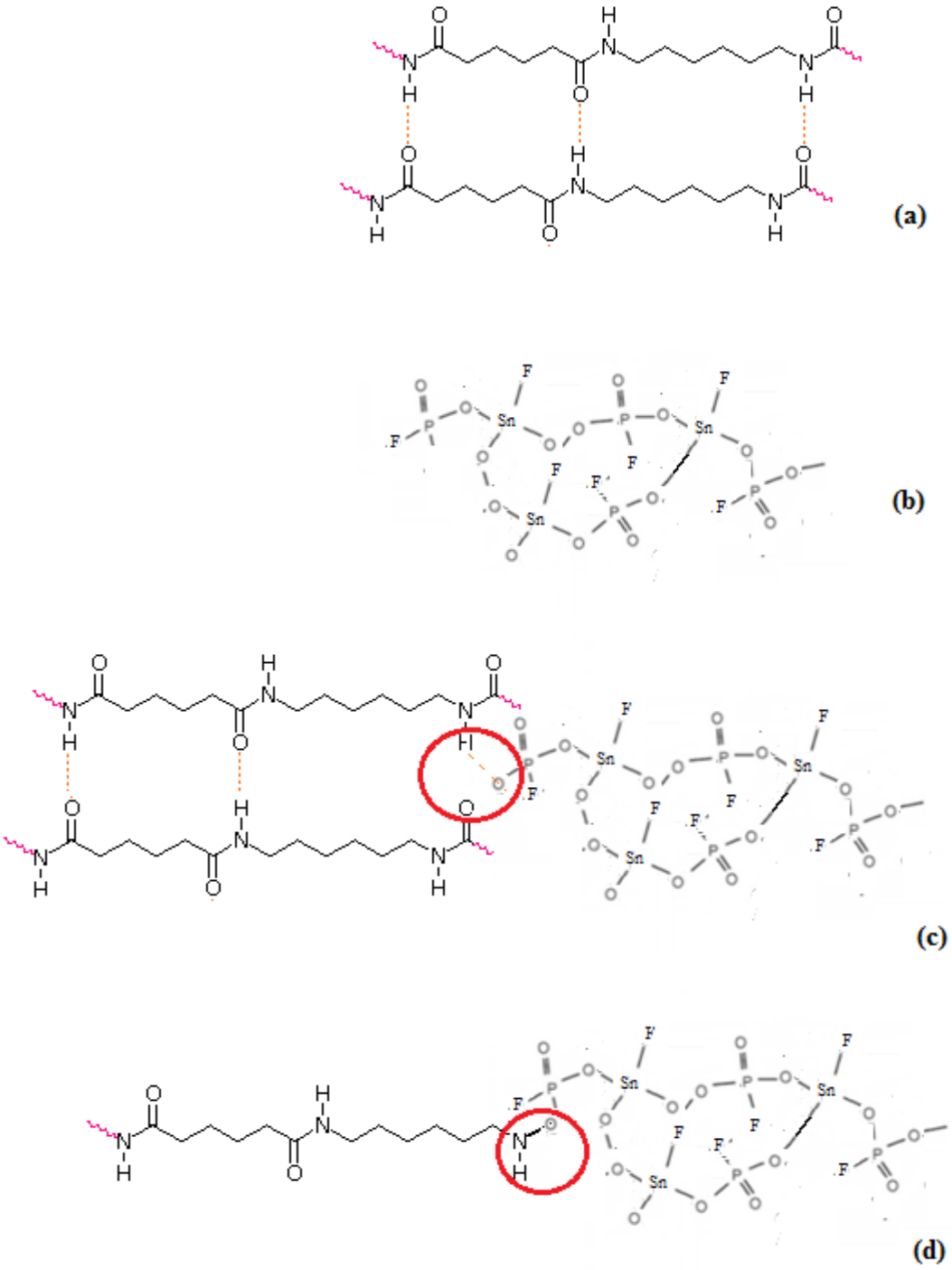

Figure 6.16 (a) Hydrogen bonding between polyamide chains; (b) repeat unit of Sn-O-F-P glass; (c) breakage of hydrogen bonding between two polyamide chains and formation of an hydrogen bonding between an oxygen in a phosphate glass tetrahedron and a hydrogen of a peptide group in polyamide; (d) breakage of a polyamide chain at the C-N bond of the peptide group and interaction between the phosphate tetrahedron of glass and the amide groups of polyamide.

6.7 Final remarks

The phosphate glasses improved the properties of pure PA 11. The glass composition was the parameter mostly affecting the final properties of the hybrids and the interaction between the hybrid components. The main difference was particle size distribution: clearly narrower for hybrids filled with 20 vol% of Glass 12, the glass showing the lowest glass transition temperature Tg and softening point Ts. Another important difference was the depression of the equilibrium melting point in hybrids compared to the one of PA 11, phenomenon related to a possible interaction between glass and polyamide. The elastic dynamic mechanical properties were sensitive to the chemistry of phosphate glass composition in the hybrids. A decrease in Tg was observed in all hybrid, phenomenon related with the increase in the mobility of the PA 11 macromolecule when SnF_2 is added in the glass. The observed elastic storage modulus E'(ω) observed was found to be a function of the SnF_2 content in the phosphate glasses at lower temperatures and independent of glass composition at higher temperatures. No glass-transition peak was visible for the pure phosphate glass in the hybrids, which indicates compatibility between two components of novel materials. The shear viscosity decreased and shear moduli G'(ω) and G"(ω) increased as angular frequency increased for PA 11 and hybrids. The shear viscosity and modulus were found to decrease by adding phosphate glass to PA 11. This behaviour indicates that the phosphate glasses enhances the deformation of PA 11 and improves the workability of PA 11 during melt blending. The yield stress was slightly evident in all samples and increasing in hybrids with higher SnF_2 content in the phosphate glass. The glass composition affected the stiffness (especially flexural modulus) of the hybrid, with Glass 12/PA 11 clearly showing the highest stiffness among hybrids. No relevant effects were observed on the tensile and flexural strengths.

An important finding was the depression of the equilibrium melting point in hybrids compared to the one of PA 11, phenomenon related to possible interaction between glass and polyamide. Also the equilibrium melting point decreased from Glass 7 to Glass 12, which was related to the reduction of glass particle size and their narrower distribution. The equilibrium melting point was found to decrease with Glass 12 content from Hybrid 13 to 16. The -0.012 negative value of the interaction parameter indicates that there might be a degree of miscibility between Glass 12 and polyamide 11 in the melt. The Glass 12/PA 11 hybrids were classified as partially miscible.

Chapter 7 Contribution to Original Knowledge

7.1 Major contribution

This work comprises different findings that contribute original knowledge to the field of developing low Tg phosphate glass /polymer hybrids.

The design of phosphate glass/PA hybrids with glass composition different from the base composition $30P_2O_5$-$50SnF_2$-20SnO (Glass 0) was not attempted before. By doing this, it was possible to establish the effect of glass composition and glass content on properties of hybrids and on the interactions between the glasses and polyamide. Sixteen low Tg glasses were developed by slightly changing the composition of Glass 0. It was established that SnF_2 was the component that most reduced the glass transition temperature of the phosphate glasses without compromising the overall properties of the glass. In particular it was possible to developed a glass (Glass 12) having lower Tg and Ts of the base composition Glass 0,

The polyamide PA 11 was a polyamide used for the first time in manufacturing of phosphate glass/polymer hybrids. An important contribution was the finding that the SnF_2 content in the glass composition played an important and decisive role on the definition of the microstructure and properties of phosphate glass/PA 11 hybrids. By increasing SnF_2 content in the glass composition and hybrids, the viscosity of the hybrids decreased, which allowed to improve the processability during extrusion and to manufacture high quality extrudates with enhanced thermo-mechanical properties. The hybrids obtained with higher amount of SnF_2 had better properties, in terms of microstructure, thermal and water stability, tensile and flexural properties. This happens because, at higher content of SnF_2, the softening point of glass was in the same range of the working temperature of PA 11, which allowed both components to flow during extrusion.

7.2 Methodology for manufacturing phosphate glass/polyamide 11 hybrids with enhanced thermal-mechanical properties

In this research project a methodology to successfully manufacture phosphate glass/polyamide 11 hybrids by extrusion processing was developed. In the traditional phosphate glass/polyamide hybrids, the base composition $30P_2O_5$-$50SnF_2$-20SnO was always kept constant. The glass transition temperature of this glass is ~ 125˚C. In the research by Urman et al. [5] interacting glass/polyamide hybrids were developed. However no study on the investigation of glass composition on the interaction between the hybrid components and the hybrid properties is available in literature.

In the case of the phosphate glass/polyamide hybrids developed in this study, a new approach is used. Generally, as glass has a Tg higher than polymer, the glass will never be fluid during extrusion with polymer, which is the factor increasing the viscosity of the melt and affecting the quality of the final material. By modifying the glass composition, it is possible to affect the glass transition temperature of the glass. Decreasing the glass transition temperature allows the glass and polymer to be fluid during processing. This will allow lowering the hybrid viscosity during processing and, therefore, improving the interaction between the glass and polymer and the properties of the final hybrids.

Another key factor influencing the quality of hybrids is the processing condition during extrusion. By modifying the processing conditions, it is possible to affect the torque and, thus, the viscosity during the extrusion, which allows modifying the interaction between the glass component and the polymer. For example, by increasing the temperature during extrusion the polyamide might be processed in a temperature range where the glass is fluid. In this way, higher processability and lower viscosity during processing is obtained, which lead to the production of higher quality extrudate with lower porosity and smooth surface finish.

Chapter 8 Conclusions and Future Work

8.1 Conclusions

The conclusions of this research work are summarized as follows:

1 The processing route affected the morphology and the properties of the phosphate glass. The glass having composition of $30P_2O_5$-$50SnF_2$-20SnO (Glass 0) was prepared using three processing routes. The process route showing the best glass morphology and the lowest moisture absorption was Route 3: $NH_4H_2PO_4$, SnO and SnF_2 were melted for 1-2 hrs at temperature ranging from 500-600 ºC depending on composition and poured. The glass transition temperature of the Glass 0 produced by Route 3 was ~125˚C. The Route 3 was used for small-scale preparation of seventeen compositions.

2 Three classes of glass were prepared using optimal route 3: Class 1 glasses with SnF_2/P_2O_5 molar ratio equal to 1.67; Class 2 glasses having P_2O_5/SnO molar ratio equal to 1.5; Class 3 glasses with SnF_2/SnO molar ratio equal to 2.5. Class 1 glasses showed a clearly evident phase separation and moisture absorption. At a constant SnF_2/P_2O_5 molar ratio the glass transition temperature (Tg) and the softening point (Ts) increased as the SnO content increased. Class 2 glasses showed little phase separation and moisture absorption. At a constant P_2O_5/SnO molar ratio Tg and Ts decreased as the SnF_2 content increased. Class 3 glasses showed evident heterogeneity and moisture absorption related to high the amount of P_2O_5.

3 A good compromise between low Tg and high thermal and water stability was given by Class 2 glasses, which were selected for hybridization with PA 11. The SnF_2 led to a favourable decrease in the Tg and Ts of glasses down to ~106˚C and ~289˚C respectively in Glass 12. Note that the melting point of PA 11 is ~180℃ and its extrusion temperature can reach 250˚C without causing degradation. The low Tg and Ts

of Glass 12 allowed the glass and PA 11 to be fluid during extrusion, which facilitated the miscibility between the glass and the PA 11 during extrusion. At a constant P_2O_5/SnO molar ratio the dissolution rate of glasses decreased as the SnF_2 content increased whereas the thermal stability and the mechanical properties of these glasses improved as the SnF_2 content increased.

4 The processing conditions during blending affected the processability of the phosphate glass/PA 11 hybrids. A series of PA 11 blends and phosphate/PA 11 hybrids were prepared using different processing conditions, with a micro-DSM extruder. The conditions showing the best processability and high quality extrudates were the following: temperature: 210-250-250 °C; rotor speed: 100 rpm; residence time: 300 s; fill factor: 95%. Given the minimal quantity of material found inside the extruder after the melting and the repeatability of Force /time data, the results for Glass 12/PA 11 were considered to be the most reliable. Increasing the SnF_2 content facilitated the processability of the melt without compromising the stability of the material. A decrease in the load force during extrusion was found in the hybrids containing Glass 0 and Glass 12, which was related to a decrease in the viscosity during extrusion. Given the smoothness of the extrudates and the repeatability of F/time results, the following compositions were selected for further experimentations: Glass 12/PA 11 with Glass 12 vol% in the range 2.5-20 vol% (Hybrid 13 to 16); all hybrid compositions containing 20% vol% (Hybrid 4, Hybrid 7, Hybrid 9).

5 The glass composition affected the rheology of the hybrids. Melt blending the selected Class 2 glasses with polyamide 11 had a major effect on the rheology of the hybrids. At a constant P_2O_5/SnO molar ratio the hybrid viscosities were lowered as SnF_2 content in the glass increased. In particular the shear viscosity and the elongational viscosity were decreased by adding phosphate glass to PA 11. This behaviour indicated the phosphate glasses enhanced the deformation of PA 11 and improved the processability of PA 11 during melt blending.

6 The glass composition affected the morphology of the hybrids. An ultra-fine dispersion was generated in the Hybrid 16 containing 20 vol% of Glass 12, which was the glass showing the lowest glass transition temperature and softening point.

7 The phosphate glass presence affected the Tg of the hybrids. By adding each phosphate glass to the polyamide network, a shift of the dissipation factor peak, thus a decrease in Tg, was observed, in all hybrids. The SnF_2 content in the glass compositions was responsible for increasing the mobility of the PA 11 macromolecule as Tg of hybrids decreased from 59˚C to 38˚C with increasing SnF_2 vol% in the glasses. No glass-transition peak was visible for the pure phosphate glass in the hybrids, which indicates compatibility between two components of novel materials.

8 The phosphate glass presence affected the thermal stability of the hybrids. Except for Glass 7/PA 11 hybrid, the thermal stability was improved by the addition of phosphate glass to polyamide. The dissolution rate in water were directly related to the Tg and Ts of glasses and inversely related to the SnF_2 content in the glasses. The lowest dissolution rate was 0.0037 mg cm^{-2} h^{-1} in Hybrid 16 (20 vol% Glass 12/PA 11). These findings suggested that the decrease of viscosity was not related to loss of water or degradation phenomena in the hybrids.

9 The glass composition affected the static mechanical properties of the hybrids. The increase of SnF_2 content leads to an increase of the stiffness (especially flexural modulus) of the hybrid, with Hybrid 16 (20 vol% Glass 12/PA 11) showing the highest stiffness among hybrids. No significant effect was seen on the tensile and flexural strength.

10 The glass composition affected the elastic dynamic mechanical properties of the hybrids. The elastic storage modulus E'(ω) observed was found to be a function of the SnF_2 content in the phosphate glasses at lower temperature and independent of glass composition at higher temperature. The shear moduli G'(ω) and G"(ω) increased as angular frequency increased for PA 11 and hybrids. The yield stress was barely evident in all samples and increasing in hybrids with higher SnF_2 content in the phosphate glass.

11 The glass composition affected the melting point depression of hybrids. In Glass 12/PA 11 hybrids (Hybrid 13 to 16) melting point depression measurements provided a thermodynamic interaction parameter between the phosphate glass and polyamide 11 of

– 0.011, which indicates a tendency for miscibility between these two components of the hybrid. The Hybrids 13 to 16 were classified as partially miscible.

8.2 Future work

A fundamental area of interest is the understanding of the origin of the interaction and, thus, the miscibility behaviour between phosphate glasses and polymer matrixes.

One parameter that might affect the miscibility of the phosphate glass and polyamide matrix in the hybrid system is the degree of crystallinity of the single constituents of the system. Also, the degree of miscibility of the two constituents might affect the crystallinity of the hybrid material.

The crystalline properties of the constituent homo-polymers in classical polymer blends have been extensively studied and reported in literature [4, 5, 65-71, 81-85]. In particular it has been experimentally shown that the presence of nanoparticles might affect the morphology of semi-crystalline polymers. Also, the crystallization of these materials might affect the spatial distribution of nanoparticles. Many studies have shown that the addition of phosphate glass to a semi-crystalline polymer leads to a reduction of the percentage of crystallinity of the polymer [4, 5, 84, 85], a phenomenon that is not yet clearly understood.

In polyamides, the concentration of the amide groups (CONH–) in the polymer chain is an important variable that affects the polymer properties. The ratio between the CH_2 and CONH groups, which controls the amount of crystallinity, has a large effect on most properties of polyamides and is the most important differentiator between polyamide polymers. Polyamides like polyamide 66 (PA 66), which are made of diamines and dibasic acids, tend to crystallize more thanks to their lower CH_2/CONH ratio (higher CONH groups concentration). On the other hand, polyamide 11 (PA 11), polyamide 12 (PA 12) and other polyamides prepared of amino-acids or lactams tend to have lower crystallization (higher CH_2/CONH ratio). The research in [5] showed that the degree of crystallinity of $30P_2O_5$-$50SnF_2$-20SnO phosphate glass was responsible in decreasing the degree of crystallinity of the semi-crystalline polyamide 6 (PA 6). This behaviour was not completely understood. The

reduced percent crystallinity was observed at very high phosphate glass concentrations in the $30P_2O_5$-$50SnF_2$-20SnO glass/PA 6 hybrids. This phenomenon was related to the presence of glass particles of nanometer size scale.

The phosphate glasses developed in this research did not show any change in the percent crystallinity of the PA 11, phenomenon possibly related to the lower CONH groups concentration compared to that one of PA 6. As some other mechanisms may be contributing to the crystallinity behaviour in phosphate glass/polymer material, further experimentation need to be carried out to understand the behaviour of phosphate glasses on the crystallinity of polymers in general. The effect of the phosphate glass composition on the amount of crystallinity of the phosphate glasses/polyamide hybrids should be further investigated. This might help understand the effect of glass composition on the CH_2/CONH ratio in the polyamide matrix and the structure of polyamide.

The percent crystallinity X_c of the hybrids might be estimated using Equation 8.1 [4]:

$$X_c = \frac{(\Delta H_m)}{\Delta H_f^0} \tag{8.1}$$

Where: ΔH_m is the heat of fusion observed in the experiment; ΔH_f^0 is the standard heat of fusion of a 100% crystalline polymer.

The experimentation might be carried out by using DSC and small angle X-ray scattering SAXS using different glass compositions and polymer matrices.

Another method to study the degree of interaction between the two phases of a phosphate glass/polymer hybrid is measuring the interfacial tension between the glass droplet and the polymer matrix in the hybrid. In fact a high interfacial tension between the phosphate glass droplet and polymer might be linked to a high degree of interaction between the two phases in the hybrid.

One of the most common methods used to measure the interfacial tension is the *stalagmometric method*, a method developed by Tate in 1864 [70]. In order to determinate the interfacial tension the melt glass should be let drip out of a glass capillary. After counting the

glass drops and weighting each glass drop, the interfacial tension can be determined using the *Tate's law* (Equation 8.2):

$$W_d = 2\pi r_c \gamma \tag{8.2}$$

Where: W_d is the drop weight; r_c is the capillary radius; γ is the surface tension of the liquid.

No relevant studies on interfacial tension of phosphate glass/polyamide hybrids using the stalagmometric method are available in literature. However a study is being carried out at the company Arkema (France) on interfacial tension of $30P_2O_5$-$50SnF_2$-20SnO and polyamide 11 using this method.

Another common method used to estimate either the size of the dispersed phase or the interfacial tension between phases of a system is the *Palierne emulsion model* [4]. The interfacial tension might be expressed by the Palierne model equation (Equation 8.3), which expresses the complex modulus of an emulsion where the dispersed phase is spherical in terms of the phases, interfacial tension, volume fraction, and radius of the dispersed phase:

$$G^* = G_c^* \left(\frac{1+3\Phi H}{1-2\Phi H}\right) \tag{8.3}$$

Where: G^* is the complex modulus of the system; G_c^* is the complex modulus of the continuous phase; Φ is the volume fraction of the dispersed phase; H is defined as follows:

$$H = \frac{(G_d^*-G_c^*)(19G_d^*+16G_c^*)+(G_d^*-G_c^*)+(4\gamma/r_d)(2G_d^*+5G_c^*)}{(2G_d^*+3G_c^*)(19G_d^*+16G_c^*)+(40\gamma/r_d)(G_d^*+G_c^*)} \tag{8.4}$$

Where: G_d^* is the complex modulus of the dispersed phase; r_d is the radius of the dispersed droplets; and γ is the interfacial tension between the phases. The complex modula are determined from a small amplitude oscillatory shear test.

In the study [31] the Palierne model was used to fit the storage modulus with the interfacial tension. The model did provide a good fit of the interfacial tension for 10 vol% phosphate glass/polyamide 12 hybrids at 250 ˚C. The extremely small interfacial tension estimated, 1.69 nN m, demonstrated a very favourable interaction between polyamide 12 and phosphate glass at high temperatures, supporting the partial miscibility of these hybrids at high temperature.

However, the model did not provide a good fit to the data for the phosphate glass/polyamide 12 hybrids containing 10 vol% phosphate glass at 190˚C. Since the shear complex viscosity displayed by the hybrids was significantly lower than that of each of the pure components, the viscoelastic behaviour of the hybrids was not successfully predicted.

The effect of the phosphate glass composition on the interfacial tension between the phosphate glasses and polyamide or other thermoplastics should be further investigated. This might help understand the effect of glass composition and matrix structure on the interaction and miscibility of the phosphate glass composition and the polymer matrix selected.

A theoretical approach to determinate the degree of interaction between the phosphate glass and the polymer matrix in a hybrid is estimating the interaction parameter.

In the study [5] glass composition $30P_2O_5$-$50SnF_2$-20SnO showed a partially miscibility in the PA 6 melt with an interaction parameter χ of -0.067. In this research, the interaction parameter for $30P_2O_5$-$50SnF_2$-20SnO (Glass 0) and PA 11 was impossible to measure while the interaction parameter measured for $24P_2O_5$-$60SnF_2$-16SnO (Glass 12) and PA 11 was -0.012. As discussed in Section 6.7 the less negative value of the interaction parameter might be related to the lower density of nitrogen atoms in the polymer chain and, thus, of the amide groups in the PA 11 compared with that one of PA 6. However, as both polymer matrixes and glass compositions have been changed in these two hybrid systems, further investigation need to be done to have more information on the interaction parameter values and their trends. The Hoffman-Weeks and Flory-Huggins approaches might be carried out on phosphate glass/polyamide 11 hybrids using all the glass compositions developed in this research. This might help to understand the link between glass composition and polyamide 11. The influence of different polymer matrixes on the interaction parameter of phosphate glass/polyamide hybrid should be carried out by keeping constant the glass composition to understand the effect of amide groups on the miscibility of these systems. If changes in the interaction parameter value are observed for the new phosphate glass/polymer combination, then it can be deduced that the amide functionality is responsible for the high degree of interaction observed in the system.

The viscosity behaviour of hybrid is often linked to the interaction and miscibility of two phases in a system. In this study the viscosity of selected phosphate glass/PA 11 hybrids at high amount of phosphate glass (20 vol%) was analysed. However the viscosity behaviour of phosphate glasses/polymer hybrids has shown an anomalous behaviour, especially at low concentration of phosphate glass. In the study [45], even if the phosphate glass ($30P_2O_5$-$50SnF_2$-20SnO) was in the liquid state during the experiment, no deformation of the glass particle was evident in glass/LDPE hybrid compositions having low amount of glass (1-2% by volume). The hybrids in question showed the highest value of elongational viscosity among the compositions. The glass particle started to deform only when the phosphate glass phosphate glass concentration was higher than 5 vol%. Further research need to be done to explain this behaviour presently unclear. In particular the viscosity of phosphate glass/PA 11 hybrids need to be tested for amounts of phosphate glass in the range of 0.1-10 vol% in order to compare the experimental values to the data presented in literature [45]. Further experimentation need to be carried out by changing the glass composition and the polymer matrix to better understand the interactional behaviour between the glass and the matrix phases.

As the dramatic effect of shear on the miscibility of polymer blends has been studied in depth in [4, 5, 58-61, 72-76, 78, 95], investigations on the shear rheology of phosphate glass/polymer hybrids might be carried out to better understand the miscibility of these novel materials.

The rheo-small angle X-ray and rheo-wide angle X-ray techniques and rheo-small-angle neutron scattering (Rheo-SAXS, rheo-WAXD and RheoSANS respectively) might be used to determine the effect of shear on crystallization mechanism and crystal structure of phosphate glass/polymer hybrid. Researchers have used these techniques to determine the effect of shear on orientation of polymer clay solutions and on the morphology of micellar networks [5]. Using these techniques the dissolution of each composition of phosphate glasses developed in this study inside the polyamide 11 matrix might be analysed. The experimentation might be expanded to other polymer matrixes. Furthermore, the interaction parameter of the phosphate glass/polymer system might be determined using these scattering techniques via the equation below [5]:

$$S^{-1}(q) = \frac{1}{N_1\phi_1 S_1(q)} + \frac{1}{N_2\phi_2 S_2(q)} - 2\chi \quad (8.5)$$

Where: $S^{-1}(q)$ is the structure factor of a binary blend; $N_{1,2}$ is the number of segments in the chains of component 1 or 2; $\phi_{1,2}$ is the volume fraction of component 1 or 2; $S_{1,2}(q)$ are the form factors of either component; χ is the interaction parameter between the components.

The interactions taking place in a phosphate glass/polyamide hybrid might be understood in depth by analysing the phase diagram of the hybrid system. However, a phase diagram of a phosphate glass/polymer hybrid has not been developed yet.

The most common technique used to determinate a phase diagram of a system is the so-called *cloud-point technique*. This experiment allows measuring the temperature of the phase separation, which is the temperature of the initial cloudiness of a solution at set experimental parameters. However this technique cannot be applied to the phosphate glass/polyamide system. In fact, both phosphate glass/PA 6 and phosphate glass/PA 11, have shown to be opaque at elevate temperatures even if the polyamide and the glass of these systems could be partial miscible and a single phase could be formed in the melt. Temperature resolved X-ray diffraction peaks might be effectively used to monitor the phase change in the phosphate glass/PA 11 hybrids as phosphate glasses should scatter X-rays differently from polymers. The presence of an ordered phase over a range of temperatures might be effectively monitored using the diffraction peaks.

The static mechanical properties of phosphate glass/polymer hybrids might provide a good estimation of interaction behaviour between the pure components of the hybrid material. Only a few studies on static mechanical properties of $30P_2O_5$-$50SnF_2$-20SnO glass/PA 6 are available in literature [4, 5]. In [5] the material behaved like a pseudo-ductile material at high phosphate glass vol%, with a clear evidence of a yield stress, a monotonic increase in stress with increasing strain, followed by the failure of the material. The study suggested that the phosphate glass affects the failure mechanism of the polymer matrix. The hybrids were found to be less stiff than the pure polyamide and with a Young's Modulus significantly lower than the pure PA 6, indicating that the phosphate glass might act as a plasticizer for the pure PA 6. The mechanical properties described in the study mentioned above are opposite to those found in the research in this PhD thesis, where each phosphate glass leads to a slightly

increase of the stiffness of the phosphate glass/PA 11 hybrids. More work need to be carried out for a better understanding of the effect of glass composition and matrix structure on the static mechanical properties of hybrids.

Novel systems could be developed by introducing more than one polyamide to the hybrid system and developing a ternary phosphate glass/polyamide/polyamide system. This might increase the interaction among polyamides and glasses and help improving the interaction between amide groups of polyamide and phosphate tetrahedron of glasses.

One approach to increase the miscibility in a hybrid system might be to choose two phases having the melting point of the polymer matrix similar to the softening point of the phosphate glass. Investigation of polymer matrixes different from polyamides might be carried out. One potential polymer that could be used as polymer matrix in phosphate glass/polymer hybrids is the Polyether ether ketone (PEEK), a colourless organic semi-crystalline thermoplastic with excellent high temperature-mechanical-chemical properties. This material melts around 343 °C, a temperature very close to softening point of phosphate glasses developed in this research.

The use of PEEK as polymer matrix might expand the application field of phosphate glass/polymer hybrids. In fact, because of its excellent proprieties, PEEK is extensively used in the chemical process, automotive and aerospace industries.[101]. Also PEEK is compatible with ultra-high vacuum applications. Furthermore this polymer is used in the development of biomedical implants, especially in spinal fusion devices and reinforcing rods. Recently shape memory behaviour in PEEK with mechanical activation has been developed, technology that might be expanded to orthopaedic surgery applications.[101]. The phosphate glass/PEEK hybrids, for example might be used as coatings for biomedical implants, allowing for an increase of their durability and decreasing the release of metallic ions into the human body.

The higher melting point of PEEK compared to those of polyamides might allow choosing a phosphate glass having a higher glass transition temperature and softening point. This might permit the reduction of SnF_2 in the glass composition and, therefore in the hybrid system, reducing the toxicity and increasing the biocompability of the hybrid system.

Finally, a wholly miscible system has not been developed yet. This could be another important area of future research interest. Were a miscible phosphate glass/polymer hybrid to be found, many pure polymer and pure glass replacement applications for the hybrids would become available or new ones with enhanced benefits might be invented. For example, a wholly miscible hybrid could potentially generate an advanced optical and gas/liquid barrier, sector needing further investigation. A starting point to determinate if a polymer might be completely miscible with phosphate glass is to test if the polymer is soluble in hydrochloric acid (HCl). In fact, as the phosphate glass can dissolve in pure phosphate glasses, there might be a good compatibility between phosphate glass and a polymer that capable of dissolving in HCl. If this is not possible, the hybrids might be prepared using solvent casting techniques. No studies about phosphate glass/hybrid developed using solvent casting techniques are available in literature.

References

1) Young RT, Baird DG. The influence of processing variables on injection moulded in situ composites based on polyphenylene sulfide and a melt processable glass. Composites Part B 2000; 31: 209-221.

2) Tick PA. Water Durable Glasses with Ultra Low Melting Temperature. Physics and Chemistry of Glasses 1984; 25: 149-154.

3) Niida H, Takahashi M, Uchino T, Yoko T. Preparation and structure of organic–inorganic hybrid precursors for new type low-melting glasses. J. Non-Crystalline Solids 2002; 306: 292-299.

4) Urman K, Otaigbe JU. New phosphate glass/polymer hybrids—Current status and future prospects. Progress in Polymer Science 2007; 32: 1462–1498.

5) Urman K, Otaigbe JU. Novel phosphate glass/polyamide 6 hybrids: miscibility, crystallization kinetics, and mechanical properties. J. Polymer Science Part B 2006; 44: 441–50.

6) Urman K, Madbouly S, Otaigbe JU. Unusual accelerated molecular relaxations of a tin fluorophosphate glass/polyamide 6 hybrid studied by broadband dielectric spectroscopy. Polymer 2006; 48: 1659–66.

7) Brow RK, Zhu Y,.Day DSE, Arnold GW. Surface nitridation of phosphate glass. J. Non-Crystalline Solids 1990; 120: 172-177.

8) Loy DA. Hybrid organic–inorganic materials. J. Materials Research Bulletin 2001; 26(5): 364–365.

9) Arkles B. Commercial applications of sol–gel-derived hybrid materials. J. Materials Research Bulletin 2001; 26(5): 402–8.

10) Mackenzie JD. Sol–gel research-achievements since 1981 and prospects for the future. J. Sol-Gel Science and Technology 2003; 26: 23–7.

11) Ogoshi T, Chujo Y. Organic–inorganic polymer hybrids prepared by the sol–gel method. J. Composite Interfaces 2005; 11: 539–66.

12) Niida H, Takahashi M, Uchino T, Yoko T. Preparation and structure of organic–inorganic hybrid precursors for new type low-melting glasses. J. Non-Crystalline Solids 2002; 306: 292–9.

13) Chujo Y, Tamaki R. New preparation methods for organic–inorganic polymer hybrids. J. Materials Research Bulletin 2001; 26(5): 389–92.

14) Vaia RA, Giannelis EP. Polymer nanocomposites: status and opportunities. J. Materials Research Bulletin 2001; 26(5): 394–401.

15) Krishnamoorti R, Vaia RA, editors. Polymer nanocomposites: synthesis, characterization and modelling. American Chemical Symposium Series 804. Washington, DC: American Chemical Society; 2002.

16) Ray SS, Okamoto M. Polymer/layered silicate nanocomposites: a review from preparation to processing. J. Progress in Polymer Science 2003; 28: 1539–641.

17) Shelby JE. Introduction to Glass Science and Technology. Royal Society of Chemistry, 2005.

18) Jones J and Clare A, Bio-Glasses: An Introduction. Wiley, 2012.

19) Varshneya, AK. Fundamental of inorganic glasses. Boston: Academic Press, 1993.

20) Otaigbe JU, Beall GH. Inorganic phosphate glasses as polymers. Trends in Polymer Science 1997; 5: 369–79.

21) Brow RK. Review: the structure of simple phosphate glasses. J. Non-Crystalline Solids 2000; 263–264: 1–28.

22) Ray NH; The structure and properties of inorganic polymeric phosphates. British Polymer Journal 1979; 11: 163–77.

23) Zachariasen WH. The atomic arrangement in glass. J. American Chemical Society 1932; 54 (10): 3841–3851.

24) Hagg G. The vitreous state, J. Chemical Physics 1935; 3: 42-45.

25) Van Wazer J R. Structure and properties of the condensed phosphates. II. A theory of the molecular structure of sodium phosphate glasses. J. American Chemical Society 1950; 72: 644-646.

26) Bunker BC, Arnold GW, and Wilder JA. Phosphate glass dissolution in aqueous solutions. J. Non-Crystalline Solids, 1984; 64(3): 291-316.

27) Gao H., Tan T, and Wang D. Dissolution mechanism and release kinetics of phosphate controlled release glasses in aqueous medium. J. Controlled Release 2004: 96(1): 29-36.

28) Sales BC, Otaigbe JU, Beall GH, Boatner LA, Ramey JO. Structure of zinc polyphosphate glasses. J. Non-Crystalline Solids 1998; 226: 287–93.

29) Appen AA, Chemistry of Glass, Khimiya, Leningrad, 1974.

30) Pavlushkina TK and Morozova IV. Synthesis of polyphosphate glasses. Steklo i Keramika 2010; 10: 18 – 21.

31) Urman K and Otaigbe JU. Rheology of tin fluorophosphate glass/polyamide 12 hybrids in the low concentration regime. Rheology 2007; 51, 1171; doi:10.1122/1.2789954.

32) Fletcher JP, Risbud, SH, Kirkpatrick RJ. MAS-NMR structural analysis of barium aluminofluoriphosphate glasses with and without nitridation. J. Materials Research 1990; 5-04: 835-840.

33) Sanford LM, Tick PA. Tin-phosphorous oxyfluoride glasses. 1982, US Patent: 4,314,031.

34) Popova E, Yanko D. Tin-based amorphous and composite materials. J. Material Science 2007; 42: 3358-3366.

35) Tischendorf BC, Harris DJ, Otaigbe JU, Alam TM. Investigations of structure and morphology dynamics in tin fluorophosphate glass-polyethylene hybrids using solidstate 1 H, 13C, and 31P MAS NMR. Chemical Materials 2002; 14: 341–7.

36) Tick PA. Tin-phosphorous oxychloride glass containing aromatic organic compounds. 1983, US Patent: 4,379,070.

37) Xu XJ, Day DE. Properties and structure of Sn–P–O–F glasses. Physics and Chemistry of Glasses 1990; 31: 183–7.

38) Xu XJ, Day DE, Brow RK, Callahan PM. Structure of tin fluorophosphate glasses containing PbO or B_2O_3. Physics and Chemistry of Glasses 1995; 36: 264–71.

39) Sammler RL, Otaigbe JU, Lapham ML, Bradley NL, Monahan BC, Quinn CJ. Melt rheology of zinc alkali phosphate glasses. J. Rheology 1996; 40: 285–302.

40) Wiench JW Pruski M, Tischendorf BC, Otaigbe JU, Sales BC. Structural studies of zinc polyphosphate glasses by nuclear magnetic resonance. J. Non-Crystalline Solids 2000; 263-264: 101–10.

41) Hoppe U, Walter G, Kranold R, Stachel D. Structural specifics of phosphate glasses probed by diffraction methods: a review. J Non-Crystalline Solids 2000; 263-264: 29–47.

42) Adalja SB, Otaigbe JU. Melt rheology of tin phosphate glasses. Applied Rheology 2001; 11: 10–8.

43) Van Wazer JR. Phosphorous and its compounds, vols. I and II. New York: Wiley; 1958.

44) Urman K, Iverson D, Otaigbe JU. A study of the effects of processing conditions on the structure and properties of phosphate glass/polyamide 12 hybrid materials. J. Applied Polymer Science 2006; 105: 1297–308.

45) Urman K, Schweizer T, Otaigbe JU. Uniaxial elongation flow effects and morphology development in LDPE/ phosphate glass hybrids. Rheologica Acta 2007; 46: 989–1001.

46) Stuart, B.H., Infrared Spectroscopy: Fundamentals and Applications. Wiley, 2004.

47) Schwarz J, Ticha H, Tichy L and Mertens R., Physical properties of PbO-ZnOP_2O_5 glasses - I. Infrared and Raman spectra. J. Optoelectronics and Advanced Materials 2004; 6(3): 737-746.

48) Elisa MBA, Sava R, Iordanescu I, Feraru, C, Vasiliu, M, Calin C, Diaconu A, Ursu LD, Boroica L, Plaiasu Z, Nastase F, Nastase C, and Dumitru A. Obtaining and characterization of calcium/magnesium/iron lithium phosphate glasses. Optoelectronics and Advanced Materials-Rapid Communications 2010; 4(9): 1301-1303.

49) Moustafa YM and El-Egili K. Infrared spectra of sodium phosphate glasses. J. Non-Crystalline Solids 1998; 240(1-3): 144-153.

50) Ducel, JF, Videau JJ, Suh KJ, Senegas J., Physics and Chemistry of Glasses 1994; 35, 10.

51) Ermov AM. J. Non-Crystalline. Solids 1997; 209; and references theirein.

52) Smith F. Industrial Applications of X-Ray Diffraction. 1999: Taylor & Francis.

53) Suryanarayana, C and Norton G. X-Ray Diffraction: A Practical Approach. 1998: Springer.

54) Jones JR. Review of bioactive glass: From Hench to hybrids. Acta Biomaterialia, 2013; 9(1): 4457-4486.

55) Larry L Hench, Jon K West. The sol-gel process. Chemical Reviews 1990; 90 (1), 33–72.

56) IUPAC, Compendium of Chemical Terminology, 2nd ed. (the *Gold Book*). Compiled by McNaught AD and Wilkinson A. Blackwell Scientific Publications, Oxford (1997), XML on-line corrected version: http://goldbook.iupac.org (2006) created by Nic M, Jirat J, Kosata B; updates compiled by Jenkins A.

57) Crowley MM, Zhang F, Repka MA, Thumma SB, Kumar Battu S, McGinity JW and Martin C. Pharmaceutical Applications of Hot-Melt Extrusion: Part I. Drug Development and Industrial Pharmacy 2007; 33: 909-926.

58) Polymer mixing, technology and engineering, by J. White, A. Coran and A. Moet 2001.

59) Injection moulding machine. [ONLINE] Available at: http://www.capetronics.com/info/injmachine.htm [Accessed 17 April 2015].

60) Tang H, Wrobel LC and Fan Z, Fluid flow aspects of twin-screw extruder process: numerical simulations of TSE rheo-mixing, Modelling and Simulation in. Material Science and Engineering 2003; 11: 771–790.

61) Puyvelde PV, Moldenaers P. Rheology and morphology development in immiscible polymer blends. Rheology Reviews 2005; 101-145.

62) Utracki LA, Walsh DJ, Weiss RA. Multiphase Polymers: Blends and Ionomers, ACS 1989; 1–35.

63) Lee MH, Fleicher CA, Morales AR, Koberstein JT, Koningsveld R. The effect of end groups on thermodynamics of immiscible polymer blends. 2. Cloud point curves. Polymer 2001; 42: 9163–9172.

64) Flory PJ. Thermodynamics of Heterogeneous Polymers and Their Solutions. J. Chemistry and Physics 1944; 12, 425.

65) Prigogine I. The Molecular Theory of Solutions. North-Holland, Amsterdam 1957.

66) Ratzsch M, Haudel G, Pompe G, Meyer E. Interaction between polymers J. Macromolecular Science and Applied Chemistry Part A 1990; 27: 1631–1655.

67) Nishi T, Wang T. Melting Point Depression and Kinetic Effects of Cooling on Crystallization in Poly(vinylidene fluoride)-Poly(methyl methacrylate) Mixtures. Macromolecules 1975; 8 (6): 909–915.

68) Scott RL. The Thermodynamics of High Polymer Solutions. V. Phase Equilibria in the Ternary System: Polymer 1—Polymer 2—Solvent. J. Chemistry and. Physics 1949: 17, 279.

69) Flory PJ, Principles of Polymer Chemistry, Cornell University Press, Ithaca, New York, 1953.

70) Tate, T. On the magnitude of a drop of liquid formed under different circumstances. Philosophical Magazine Series 4, 1864. 27(181): 176-180.

71) Hoffmann J and Weeks J. J. Research of the National Bureau of Standards 1962; 66A, 17.

72) Introduction to Polymer Viscoelasticity, Shaw M and, MacKnight WJ. Wiley, New York, 2005.

73) Adalja SB, Otaigbe JU, Thalacker J. Glass-polymer melt hybrids. I: viscoelastic properties of novel affordable organic–inorganic polymer hybrids. J. Polymer Engineering and Science 2001; 41: 1055–67.

74) Otaigbe JU, Quinn CJ, Beall GH. Processability and properties of novel glass-polymer melt blends. Polymer Composites 1998; 19: 18–22.

75) Quinn CJ, Frayer P, Beall G. Glass-polymer melt blends. In: J.C. Salamone, editor. Polymeric materials encyclopedia. New York: CRC Press; 1996; 2766–2777.

76) Frayer PD, Monahan RJ, Pierson MD. Glass/polymer melt blends. Corning, Inc., 2001, US Patent: 6268425.

77) Young RT, McLeod MA, Baird DG. Extensional processing behaviour of thermoplastics reinforced with a melt processable glass. Polymer Composites 2000; 21: 900.

78) Adalja SB, Otaigbe JU. Creep and recovery behaviour of novel organic–inorganic polymer hybrids. Polymer Composites 2002; 23: 171–81.

79) Rubin II, editor. Handbook of plastic materials and technology. New York: Wiley; 1990.

80) Guschl P, Otaigbe JU. Experimental observation and prediction of interfacial tension and viscoelastic emulsion model behaviour in novel phosphate glass-polymer hybrids. J. Colloid Interface Science 2003; 266: 82–91.

81) Guschl P, Otaigbe JU, Loong C-K. Investigation of phase behaviour during melt processing of novel inorganic–organic polymer hybrid material. Polymer Engineering and Science 2004; 44: 1692–701.

82) Palierne JF. Linear rheology of viscoelastic emulsions with interfacial tension. Rheologica Acta 1990; 29: 204–14.

83) Guschl PC, Otaigbe JU. An experimental study of morphology and rheology of ternary pglass-PS-LDPE hybrids. Polymer Engineering and Science 2003; 43: 1180–96.

84) Guschl PC, Otaigbe JU. The crystallization kinetics of low density polyethylene and polypropylene melt-blended with a low-Tg tin-based phosphate glass. J Applied Polymer Science 2003; 90: 3445–56.

85) Guschl PC, Otaigbe JU, Taylor EP. Engineered hybrid organic–inorganic thermoplastic materials: crystallization kinetics and tensile properties. SPE Antec Technical Papers 2003; 61(2): 2137–41.

86) Carre A. Surface tension of molten glass from drop profile: application to the characterization of the interface in glass/ polymer blends. J Adhesion 1995; 54: 167–74

87) Young RT, McLeod MA, Baird DG. Deformation behaviour of thermoplastics reinforced with melt processable glasses. SPE Antec Technical Papers 1999; 57(2): 2698–702.

88) Jafari SH, Potshke P, Stephan M, Warth H, Alberts H. Multicomponent blends based on polyamide 6 and styrenic polymers: morphology and melt rheology. Polymer Bulletin 2002; 43: 6985–92.

89) Khonakdar HA, Jafari SH, Yavari A, Asadinezhad A, Wagenknecht U. Rheology, morphology, and estimation of interfacial tension of LDPE/EVA and HDPE/EVA blends. Polymer Bulletin 2005; 54: 75–84.

90) Zarraga A, Pena JJ, Munoz ME, Santamaria A. Thermo-rheological analysis of PVC blends. J. Polymer Science B 2000; 38: 469–77.

91) C.B. Ponton, R.D. Rawlings, Vickers indentation fracture toughness test Part 1 Review of literature and formulation of standardised indentation toughness equations, Materials Science and Technology 1989; 5: 865-872.

92) A.G. Evans, T.R. Wilshaw, Quasi-static solid particle damage in brittle solids—I. Observations analysis and implications, Acta Metallurgica 1976; 24: 939-956.

93) Vogel, A.I., Tatchell, A.R., Furnis, B.S., Hannaford, A.J. and P.W.G. Smith. *Vogel's* Textbook of Practical Organic Chemistry, 5th Edition. Prentice Hall, 1996. ISBN 0582462363.

94) Matuana, LM and Kim JW. Fusion characterization of rigid PVC/wood-flour composites by torque rheometry. J. Vinyl and Additive Technology 2007; 13 (1): 7-13. DOI: 10.1002/vnl.20092.

95) Mackay ME, Dao TT, Tuteja A, Ho, DL, Van Horn, B, Kim, HC and Hawker, CJ, Nanoscale effects leading to non-Einstien-like decrease in viscosity, Nature Materials 2003; 2: 762-766.

96) Rilsan PA 11. [ONLINE] Available at: http://www.arkema.com/en [Accessed 28 March 2015].

97) General overview of melt-extrusion. [ONLINE] Available at http://www.xplore-together.com/products/pharma-melt-extruder [Accessed 22 May 2014].

98) Bazilevs Y, Akkerman I. Large eddy simulation of turbulent Taylor–Couette flow using isogeometric analysis and the residual-based variational multiscale method- J Computational Physics 2010 – Elsevier.

99) Introduction to DMA. [ONLINE] Available at http://www.perkinelmer.co.uk/CMSResources/Images/4474546GDE_IntroductionToDMA.pdf [Accessed 10 June 2015].

100) Brabender. [ONLINE] Available at http://www.brabender.com [Accessed 05 May 2015].

101) *Thryft, Ann. "3D Printing High-Strength Carbon Composites Using PEEK, PAEK". Design News. Retrieved 27 January 2016.*,Press release Indmatec PEEK MedTec.

Appendix A: Polyamides

A.1 General overview

Polyamides represent one of the most commonly synthetic polymers family used throughout the world. These materials are linear polymer and thus members of the so-called *engineering thermoplastics*.

Polyamides, developed by *Wallace Carothers at the Dupont* chemical company in the 1930s, have the common feature that the amide (–CONH–) linkage in their backbone (see Figure A.1)

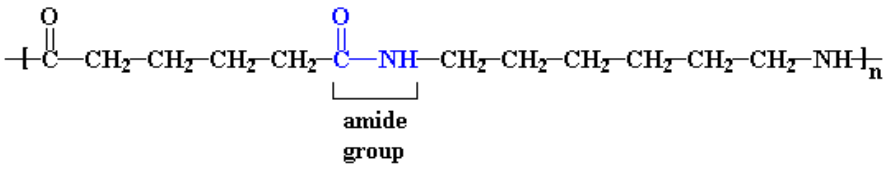

Figure A.1: Amide group of polyamide.

Polyamides are identified by a numerical suffix that specifies the numbers of carbon atoms in the monomer chains. Amino acid polymers are designed by a single number, as Polyamide 6 (see Table A.1). Polyamides from diamines and dibasic acids are designed by two number, the first representing the carbon atoms in the diamine, the second representing the carbon atoms in the acid. An example is polyamide 66 (see Table A.1).

The polar amine groups lead to the very regular and symmetrical polyamide backbone, characterized by a high degree of crystallinity. As a matter of fact the polar amide groups, spaced out at regular intervals, lead to a high intermolecular attraction among the polyamide chains. These groups are responsible for the high resistance to swelling and dissolution in

hydrocarbons, high stiffness and heat deformation resistance, increasing in water absorption, reducing electrical insulation resistance, particularly at high frequencies.

The hydrogen bonding between chains improves the inter-chain interaction, greatly influences the overall crystallinity. Crystallinity can also be controlled by processing condition. Slow cooling will lead to greater crystallinity, around 50-60%, versus 10% crystallinity after rapid cooling. Cooling speed also affects the size of crystallites, which will be larger for slowly cooled polyamides.

Additionally the polymer chains have aliphatic segments, which confer flexibility to the amorphous region, giving polyamides low melt viscosity for easy processing. The combination of high inter-chain attraction in the crystalline zone and flexibility in the amorphous zone, leads to polyamides polymers, which are tough above their apparent glass transition temperatures. Thus, an important variable that affects polyamides properties is the concentration of the amide groups (CONH–) in the polymer chain. As a rule, the higher the concentration of the amide groups (lower the CH_2/CONH ratio), the higher intermolecular attraction, the shorter the distance the amide groups, the higher the:

- Density
- Forced required to mechanically separate the polymer molecules and hence the higher:
    - Tensile strength
    - Rigidity
    - Hardness
    - Resistance to creep
- Melting Temperature
- Heat deflection Temperature
- Water absorption

The ratio between the CH_2 and CONH groups, which controls the amount of crystallinity, has a large effect on most properties of polyamides and is the most important differentiator between polyamide polymers. Polyamides like polyamide 66, which are made of diamines and dibasic acids, tend to crystallize more thanks to their lower CH_2/CONH ratio (higher CONH groups concentration). On the other hand polyamide 11, polyamide 12 and other polyamides prepared of aminoacids or lactams tend to have lower crystallization (higher CH_2/CONH ratio). The CH_2/CONH ratios of the considered polyamides are summarized in the following table:

Table A.1: CH_2/CONH ratios of polyamides [11].

Polyamide	Formula	CH_2/CONH Ratio
66	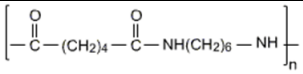	5
6	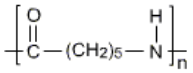	5
11	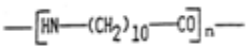	10
12	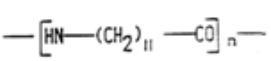	11

Polyamides have a good combination of the following properties over a relative wide temperature and humidity range: good tensile strength, good flexible properties, light weight, toughness, wear and abrasion resistance, low coefficient of friction, high chemical resistance (to oils, greases, aliphatic and aromatic hydrocarbons), good electrical insulation properties.

Polyamides are very sensitive to heat and should be washed and dried on cool settings. Polyamide can also be hung dry.

A. 2 Rilsan ® polyamide 11 [96]

Rilsan PA 11 is a reference in the world of performance polyamides. Continuously developed by Arkema for more than fifty years, this polymer is produced from a renewable source

(castor oil), and is used in a large number of applications thanks to its outstanding properties: excellent resistance to chemicals (particularly hydro-carbons), ease of processing, a wide range of working temperatures (-40 °C/+130 °C), high dimensional stability and low density to name a few. Rilsan PA 11 is easy to process, using most processing technologies (extrusion, extrusion-blow moulding, injection moulding and roto-moulding). For this reason many industries around the world (automotive, transport, textile, oil and gas, wire & cables, electronics) have used Rilsan PA 11 for decades.

A. 2.1 Physical properties

Compared to other high performance polymers, the Rilsan family and more specifically Rilsan PA 11 offers very low density some 3 to 6 times lighter than metal (see Figure A.2). This is a significant economic advantage when studying the cost versus performance aspect of using Rilsan PA 11.

Among all performance polyamides, the Rilsan family and more specifically Rilsan PA 11 has very low moisture pick-up. Other polyamides feature a more hydrophilic behaviour resulting from the polarity of the amide functions (Figure A.3). Thanks to its low concentration of amide groups, Rilsan PA 11 can be used in a wide range of humidity environments. This low moisture pick-up results in outstanding dimensional stability of final parts made out of Rilsan PA 11. The absorption characteristics of Rilsan PA 11 are similar when it is exposed to other polar liquids such as alcohols, acids and esters.

A low concentration of methylene (CH_2) groups lead do shorter distance between CONH groups causing an increase of the overall density. Thus PA 11, together with PA 12, has the lowest specific gravity.

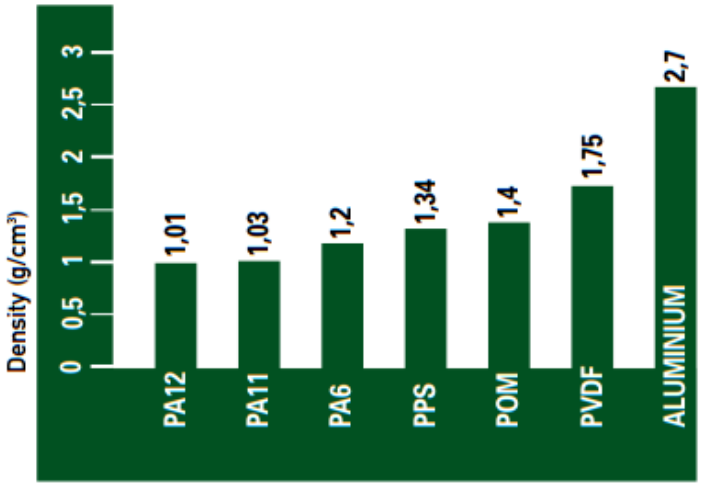

Figure A.2: Comparative density of Rilsan® PA 11 and PA 12 vs various engineering polymers and aluminium, per ISO 1183 standard.

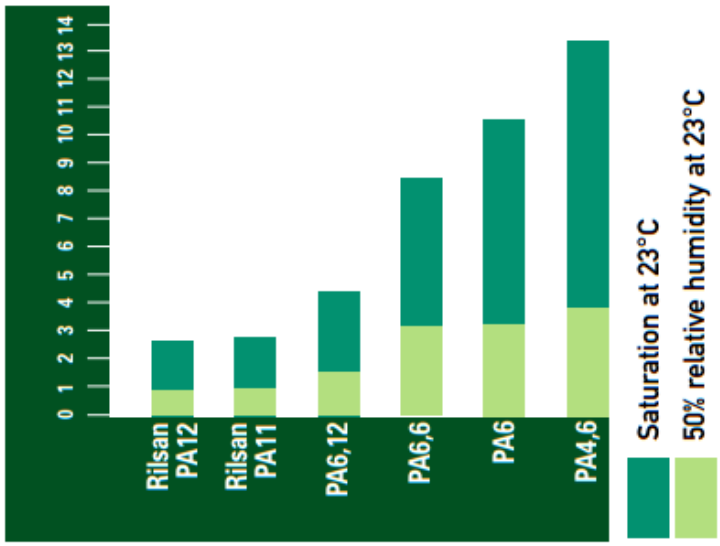

Figure A.3: Water absorption based on relative moisture rate of Rilsan® PA 11 and PA 12 vs various polyamides (ISO 62 standard).

Table A.2: Specific gravity and CH_2/CONH ratios of polyamides.

Polyamide	CH_2/CONH ratio	Specific gravity
66	5	1.14
6	5	1.13
11	10	1.04
12	11	1.01

A. 2.2 Thermo-mechanical properties

Rilsan PA 11 is a semi-crystalline thermoplastic polymer featuring 2 phase transitions:

- Melting range between 180 °C and 189 °C (depending on the grade), which corresponds to fusion of the crystalline phase (see for comparison with other polyamides).
- A glass transition temperature (Tg) of around 45° C (measured via DSC), corresponding to transition of the amorphous phase.

Rilsan PA 11 offers good thermal stability and can be used continuously at 125 °C under certain conditions. Additionally, it can withstand intermittent peaks of up to 150 °C. It can also withstand cold temperatures, and maintains its impact resistance at -40 °C. For extreme climatic conditions, a special grade is available which can withstand temperatures down to -60 °C. Rilsan PA 11 is the only polyamide in the world capable of performing in such harsh environments.

Table A.3: Specific gravity and CH_2/CONH ratios of polyamides.

Polyamide	CH_2/CONH Ratio	Melting point [˚C]
66	5	262
6	5	220
11	10	188
12	11	178

The melting point of polyamide influences properties such as heat distortion temperature and softening point. The lower the melting point, the lower is the deflection temperature. A low melting point favours the processing conditions because the resulting melt is less sensitive to oxidation and degradation. Above the melting point, the melt viscosity is low because of increasing of atomic oscillation at such high temperatures, which are usually more than 200 ℃ above the Tg.

The glass transition temperature of aliphatic polyamides is of secondary importance to melting point. Dried polyamides have Tg values around 50°C; when moisture has been absorbed Tg can go as low as 0°C. Tg can have an effect on the crystallization of polyamides; for example, polyamide 66 at room temperature may be above its Tg; as crystallization will occur slowly it may lead to post mould shrinkage. This is less significant for polyamide 6.

The effect of relative humidity on dimensional thermal stability is shown in Figure A.4**.** The dimensional change are low in PA 11, like in and PA 12, and increase in PA 6 and PA 66.

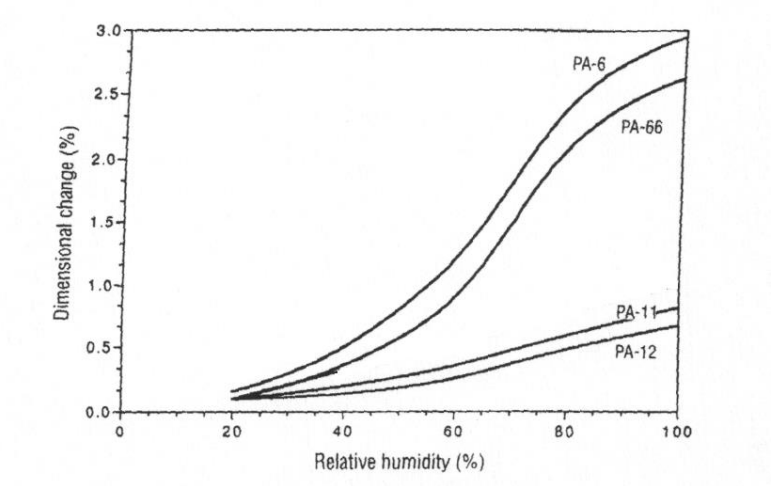

Figure A.4: Dimensional stability versus relative humidity at 20 ˚C [11].

A. 2.3 Mechanical properties

Rilsan PA 11 exhibits excellent mechanical properties over a wide temperature range. It has high elongation at break and high tensile strength at break and at yield. It is one of the toughest high-performance polymers and is therefore used extensively in engineering applications. At ambient temperature, the tensile strength of rigid (unmodified) Rilsan PA 12 leads to noticeable necking at around 20% elongation. In the same conditions, rigid Rilsan PA 11 first produces *diffuse necking*, up to 40% elongation, beyond which necking occurs (see Figure A.5). Thus, Rilsan PA 11 provides a significant safety factor in mechanical stress over PA 12.

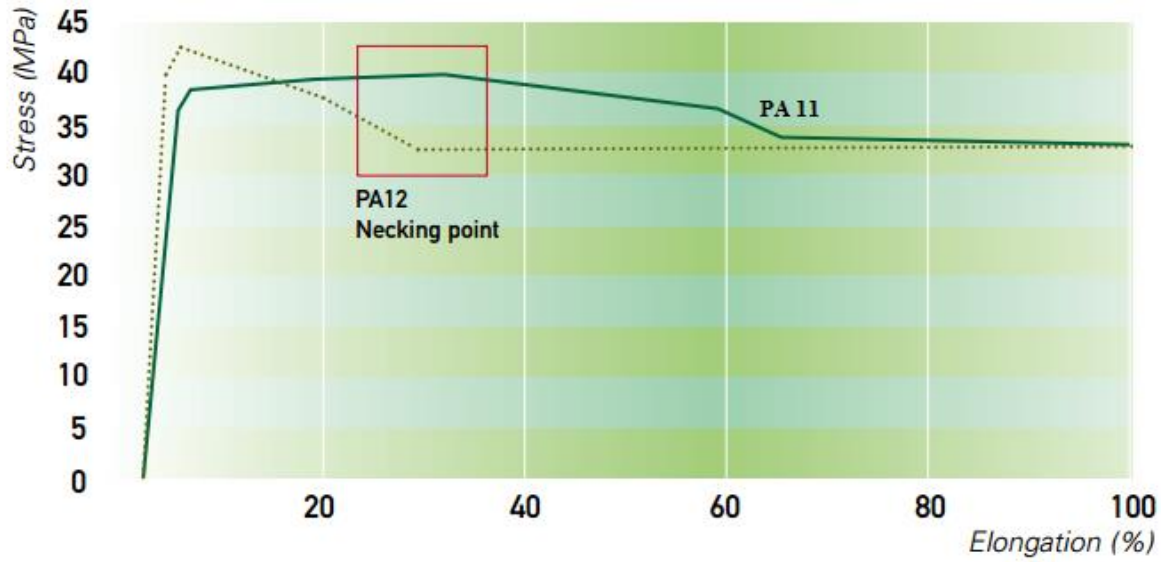

Figure A.5: Comparative tensile strength curves for Rilsan® PA 11 and PA 12 at 23°C (ISO 527 standard).

This very different performance can be attributed to the greater strength of the Rilsan PA 11 crystallites (triclinic/hexagonal) compared to the Rilsan PA 12 crystallites (monoclinic).This better stability of Rilsan PA 11 compared to Rilsan PA 12, observed above with rigid grades also applies to plasticised grades across the entire temperature range from 23 °C to the melting point. The difference increases with temperature. A very significant consequence of this difference in behaviour in actual use is that, at equivalent modulus, a Rilsan PA 11 plasticised tube exhibits a higher burst pressure than its Rilsan PA 12 counterpart.

Rilsan PA 11 is available in a wide range of flexibility. The modulus varies from 1200 MPa for non-plasticised grades to around 150 MPa for plasticised grades. Adding specific fillers (glass fiber, carbon fiber, etc.) enable an increase in modulus up to 8000 MPa. In dry conditions, PA 6 and PA 66 have significantly higher rigidity than Rilsan PA 11. After moisture pick-up however, the flexural properties of Rilsan PA 11 remain relatively stable (see Figure A.6).

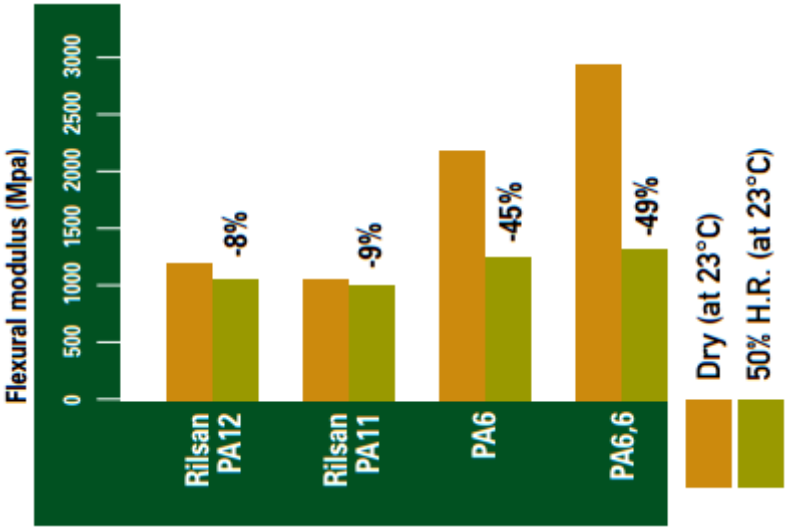

Figure A. 6: Effect of ambient conditions on the flexural modulus of Rilsan ® PA 11 and PA 12 vs PA 6 and PA 6.6. Tests conducted per ISO 178 standard.

Rilsan PA 11 demonstrates very good impact resistance at room temperature as well as at very low temperatures. It offers a significantly higher safety factor than Rilsan PA 12. In Charpy notched impact test at -30 °C, Rilsan PA 11 is twice as resilient as Rilsan PA 12. Its fragile/ductile transition is around 35 °C versus around 50 °C for Rilsan PA 12. This benefit of Rilsan PA 11 is equally seen in plasticised products. Glass transition temperatures are similar for Rilsan PA 11 and PA 12 (a slight advantage of some 5 °C for Rilsan PA 11) and do not explain differences in performance between the products. This is due to the finer crystalline grid and spherolitical structure in Rilsan PA 11.Its impact resistance is also influenced by molecular weight and polydispersity. The impact resistance of Rilsan PA 11 at low temperature is twice that of Rilsan PA 12 (Figure A.7).

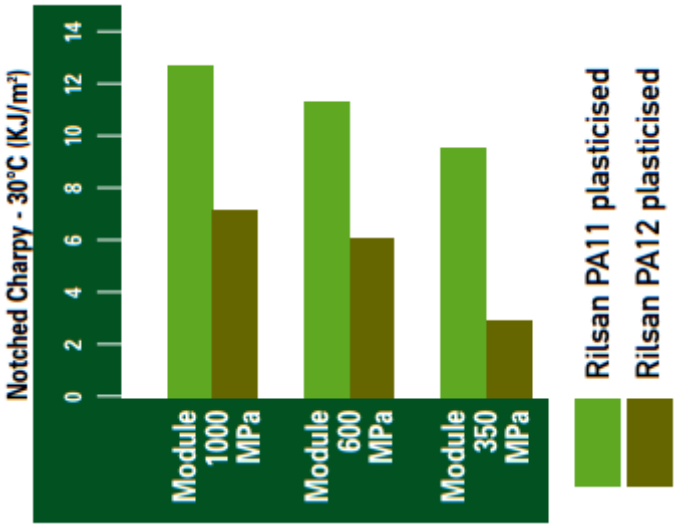

Figure A.7: Comparative impact resistance of Charpy notched plasticised Rilsan® PA 11 and PA 12 (-30°C), per ISO 179/1eA standard.

Compared to other engineering polymers, Rilsan PA 11 features good abrasion resistance and crack propagation resistance. This is largely due to its perfectly smooth surface finish, which induces an extremely low friction coefficient. Rilsan PA 11 features greater abrasion resistance than Rilsan PA 12.

A. 2.4 Long-term performance

The notion of a material's lifetime is an important factor when designing components requiring long-term performance in specific operating conditions. As a general rule, Rilsan PA 11 features visco-elactic behaviour at ambient temperature. However, under permanent stress, above a certain limit, Rilsan PA 11 undergoes plastic deformation.

Parts made from Rilsan PA 11 perform very well in a wide variety of climates around the world. Rilsan PA 11 is particularly resistant to degradation from the combined effect of the sun's rays and rainwater (see Figure A.8). The use of stabiliser packages also helps to further increase the weathering resistance of natural and coloured grades.

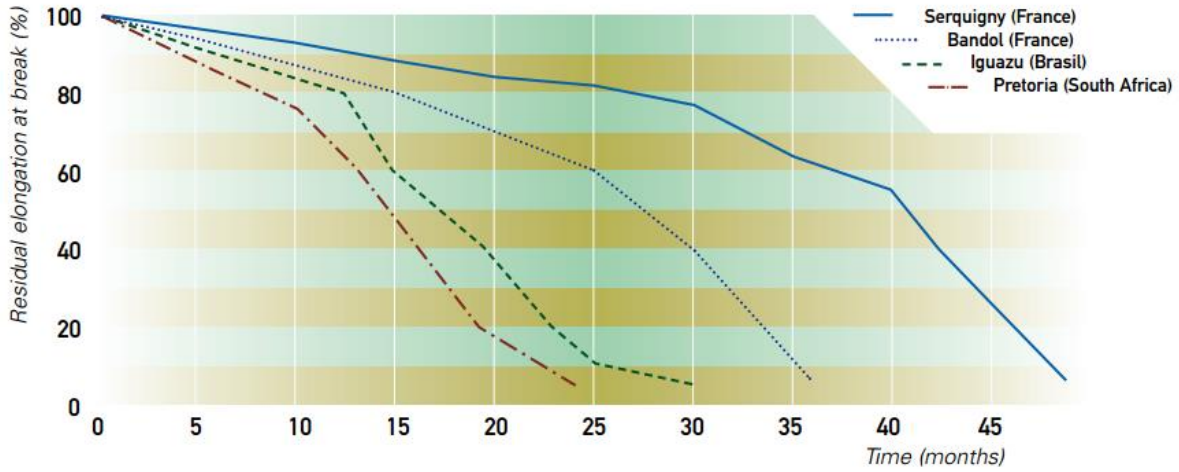

Figure A.8: Weathering of Rilsan ® PA 11 based on exposure site.

A. 2.5 Chemical resistance

Rilsan PA 11 offers an ideal balance between the resistance of polyamides to grease and hydrocarbons and the resistance to acids, bases and salts of polyolefines. The excellent chemical resistance of Rilsan PA 11 is reflected both in high dimensional stability under harsh conditions and in the non-degradation of the polymer matrix. Additionally Rilsan PA 11 features greater resistance to hydrocarbons than Rilsan PA 12, making it the ideal material for highly demanding applications in the oil and gas industry, such as offshore flow-lines.

Rilsan PA 11 features outstanding resistance to oils, hydraulic fluids, and fuels. As a general rule, Rilsan PA 11 offers better barrier properties to gases and liquids than other flexible thermoplastics or rubbers. In particular, it is twice as impermeable to fuels and hydrocarbons versus PA 12. Because of the high cohesive energy density and their crystalline state, the polymers are soluble only in few liquids of similar high solubility parameter at which are capable of specific interaction with the polymers. Polyamides are only weakly affected by non-polar solvents. However, because of the presence of the polar groups, Polyamides are sensitive to polar solvents, particularly water. Polyamides have very high resistance to aliphatic and aromatic solvents, engine fuels, lubrificants, animal and vegetable oils, and aqueous solutions of many inorganic chemicals. Polyamides are not very resistance to acids, phenols, certain oxidizing agents, and chlorinated hydrocarbon (see Figure A.9).

G = Good

L = Limited (swelling of Rilsan® PA11 – suitability depends on specific use and duration)

P = Poor

* slight browning; ** swelling action

CHEMICAL AGENT	CONCENTRATION (100%)	PERFORMANCE 20°C	40°C	60°C	90°C
Mineral acids					
Hydrochloric acid	1%	G	L	P	P
	10%	G	L	P	P
Sulphuric acid	1%	G	L	L	P
	10%	G	L	P	P
Phosphoric acid	50%	G	L	P	P
Nitric acid	any concentration	P	P	P	P
Chromic acid	10%	P	P	P	P
Sulphur dioxide		L	P	P	P
Mineral salts					
Calcium arsenate	concentrated or boiled solutions	G	G	G	
Soda carbonate	"	G	G	L	P
Baryum chloride	"	G	G	G	G
Potassium nitrate	"	G*	L*	P	P
Di-ammonium phosphate	"		G	G	L
Trisodic phosphate	"	G	G	G	G
Alumina sulphate	"	G	G	G	G
Ammonium sulphate	"	G	G	L	
Copper sulphate	"	G	G	G	G
Potassium sulphate	"	G	G	G	G
Sodium sulphide	"	G	L	L	
Calcium chloride	"	G	G	G	G
Magnesium chloride	50 %	G	G	G	G
Sodium chloride	satured	G	G	G	G
Zinc chloride	satured	G	G	L	P

Figure A.9: Chemical resistance of Rilsan ® polyamide 11

A. 2.6 Processing of Rilsan ® polyamide 11 [96]

With a relatively low melting temperature, good melt fluidity and a high speed of recrystallization, Rilsan PA 11 is well-suited to a wide range of processing technologies: extrusion, extrusion-blow moulding, injection moulding, injection-blow moulding and roto-moulding.

Rilsan PA 11 grades are supplied in the form of granules in moisture proof sealed bags or octabins. Rilsan PA 11 granules do not require pre-drying before use. However, if the packaging has been left open and exposed to air for more than two hours, the product will need to be re-dried under specific conditions.

Due to its chemical structure, Rilsan PA 11 has lower moisture pick-up than other polyamides (PA 6, PA 66, etc.). This low water absorption provides excellent dimensional stability and causes only minimum variations in its mechanical and electrical properties. Rilsan PA 11 is produced by the poly-condensation of amino acid. As a result, it undergoes an equilibrium reaction with water as shown by the following simplified formula:

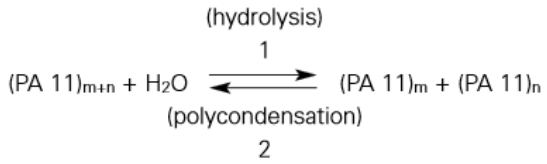

Figure A.10: Rilsan PA 11 produced by the poly-condensation of amino acid/

The presence of excess water promotes hydrolysis by reducing the length of the molecular chains. This change will result in a significant drop in mechanical properties but may not always be evident in the form of surface blemishes such as frosting or bubbles. Since excess moisture can pose problems during the processing of Rilsan PA11, it is important for the

granules to be kept dry at all times. Necessary precautions should be taken to prevent any moisture pick-up during processing.

To prevent moisture pick-up, Rilsan PA11 should first be brought up to the temperature of the plant to prevent any condensation of the ambient moisture as the bags are opened. Additionally, it is essential for the product to be processed within two hours of opening the bag. If either of these conditions is not fulfilled, Rilsan PA 11 granules should be vacuum-dried for at least 4 hours at a temperature between 80 °C and 90 °C. The migration speed of the moisture to the surface of the granules determines drying time. Raising the temperature does not significantly reduce drying time and presents a risk of oxidation.

Appendix B: Twin Screw 15 cm^3 Xplore ® Micro-DSM Compounder

B. 1 Technical specifications [97]

- Abrasion resistant barrel (hardness 60 HRc), coating hardness 2000 Vickers;
- Barrel and screws chemically resistant between pH 0 – 14;
- Batch volume: 15 ml (Vari-BatchTM: 3, 7 and 15 ml);
- Vertical barrel, fluid-tight - Heated by 8 thermo cartridges and controlled by 7 thermo couples (temperature gradient possible);
- Temperature control: in the melt and 2x3 barrel heating zones;
- Detachable conical screws, fully intermeshing (hardness 54 HRc), coating hardness 1000 Vickers;
- Maximum operating temperature 400 °C (optionally 450 °C);
- Easy to clean with dedicated cleaning cycle;
- Heating time (from 80 to 240 °C) in less than 10 min;
- Cooling time (from 240 to 80 °C) with cooling water in less than 10 min, with air in less than 35 min;

- Maximum vertical force: 8 kN (optionally 9 kN);
- Screw speed: continuously variable 1 - 250 RPM;
- Hopper volume: 15 ml;
- Supply voltage: 208 - 240 V AC, others on request;
- Main drive: DC controlled, 900 Watt;
- Computer control via: USB port;
- Maximum torque: 10 Nm per screw;
- Overall dimensions (h x b x d): 103 x 73 x 42 cm^3 - Weight 150 kg;

Figure B. 1: Overall dimensions of the twin screw 15 cm^3 Xplore ® Micro-DSM compounder [97].

B. 2 Screw design

The two screws are specially designed according the *Taylor Couette geometry* to simulate the dynamic of the melt inside the industrial scale extruder and to generate reproducible and stable data.

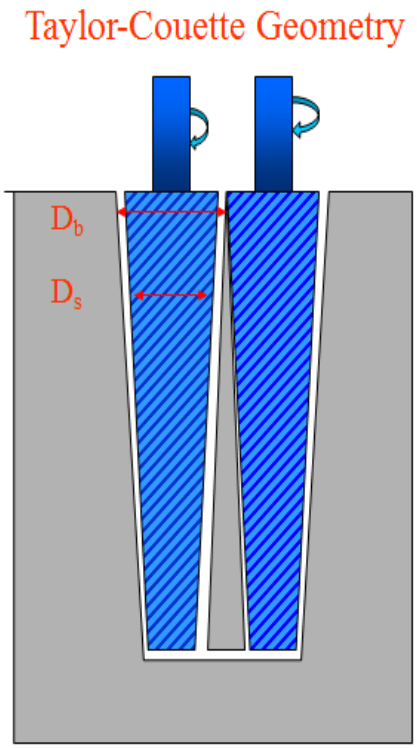

Figure B.2: Screws of the MC 15 Xplore Micro DSM compounder designed according the Taylor-Couette geometry.

According to the Tayolor-Couette geometry [98]:

$$D_b - D_s = 0.1mm \tag{B.1}$$

Where: D_b is the diameter of the barrel; D_s is the diameter of the screw.

Appendix C: Spectroscopy Techniques

C. 1 Fourier transform infrared spectroscopy (FTIR)

Fourier transform infrared spectroscopy (FTIR) is a method of vibrational spectroscopy used to analyse a material's molecular structure by the vibrational modes that occur from the absorption of an incident infrared (IR) radiation source. For a molecule to absorb IR light, a periodic change in the dipole moment (P) of the molecule must occur (in IR active molecules) with greater levels of polarity producing a more intense IR absorption [30]. However this absorption can only occur at specific resonant frequencies that are determined by the molecular structure, atomic masses and structural bonding within the material sample. For a simple covalently bonded diatomic molecule this natural vibrational mode can be represented by a spring model system (Figure C.1) with its natural vibrational frequency (v_m) described by *Hooke's law* (Equation C.1) [31].

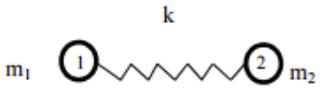

Figure C. 1: Representation of a covalent bond between two atoms of mass m1/m2 as a spring model system with spring stiffness k [31].

$$v_m = \frac{1}{2\pi}\sqrt{\frac{k}{\mu}} \quad \text{(C.1)}$$

$$\mu = \frac{m_1 * m_2}{(m_1 + m_2)} \quad \text{(C.2)}$$

Where: v_m is the frequency of vibration; k is the force constant of bond strength and μ is the reduced mass of a diatomic molecule; m_1 and m_2 are atomic masses of atoms 1 and 2 respectively.

However when analysing polyatomic molecules of different atomic masses, bond strengths and structures, a multitude of natural frequencies can exist in a material sample. These frequencies become even more complex when the molecules available degrees of freedom are considered which, for a molecule of n atoms, follows the 3n-6 and 3n-5 rule of thumb for non-linear and linear molecules respectively. For example, a simple linear diatomic carbon dioxide (CO_2) molecule (n = 3) containing 4 rotational degrees of freedom (Figure C.2) is characterised by the vibrational frequencies outlined in Table C.1 [30, 32, 33].

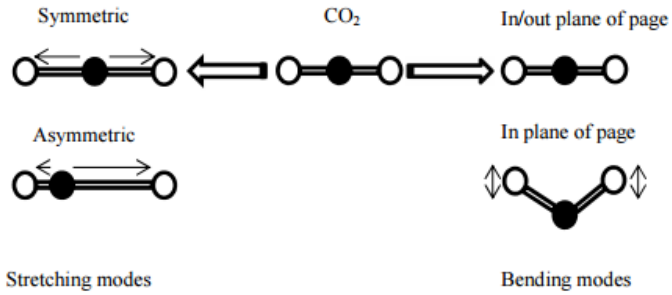

Figure C. 2: Molecular vibrations from the available degrees of freedom found in a CO_2 molecule when exposed across a range of mid-infrared radiation frequencies during FTIR [30].

Table C. 1: Vibrational modes and frequencies of a CO_2 molecule found from FTIR analysis [34].

Vibration Mode	Frequency (Hz)	Comment
Symmetric stretching	N/A	IR inactive vibration
Asymmetric stretching	7.5×10^{13}	
Bending in/out plane of page	1.99×10^{13}	

It is upon this basis that FTIR is capable of identifying a material sample through the absorption of mid-IR radiation corresponding to the sample's natural molecular vibrations due to its specific molecular structure. These results are typically expressed as plots of IR absorbance against wavenumber where the incident radiations wavenumber is defined as the inverse of the signal wavelength. This relationship is described by Equation C.3 with a complete FTIR scan commonly expressed over the 4000-400cm^{-1} wavenumber range [30, 34].

$$W = \frac{1}{\lambda} = \frac{v}{c} \tag{C.3}$$

Where: W is the wavenumber; λ is the wavelength; c is the velocity of light; v is the frequency.

From these plots, the characterisation of a material is typically conducted through the analysis of the identified functional group (4000-1000 cm^{-1}) and fingerprint regions (≈1000-400 cm^{-1}) of the spectrum in conjunction with the use of a reference spectrum database [30].

C. 2 X-ray diffraction (XRD)

X-ray diffraction (XRD) is an analytical tool used to investigate a crystalline material's atomic or molecular structure and is based on the scattering, interference and diffraction of a monochromatic incident X-ray radiation source by the samples internal atomic arrangement.

From this concept, the structural characterisation of a material is achieved by the detection of diffraction peaks (i.e. constructive interference) at specific incident angles following *Bragg's Law* (Equation C.4) as illustrated in Figure C.3 [38-40].

$$n\lambda = 2\,\mathrm{dsin}\,\theta \tag{C.4}$$

Where: n is an integer; λ is the wavelength of incident X-ray; θ is the angle of incident X-ray; d is the spacing between planes in the atomic lattice.

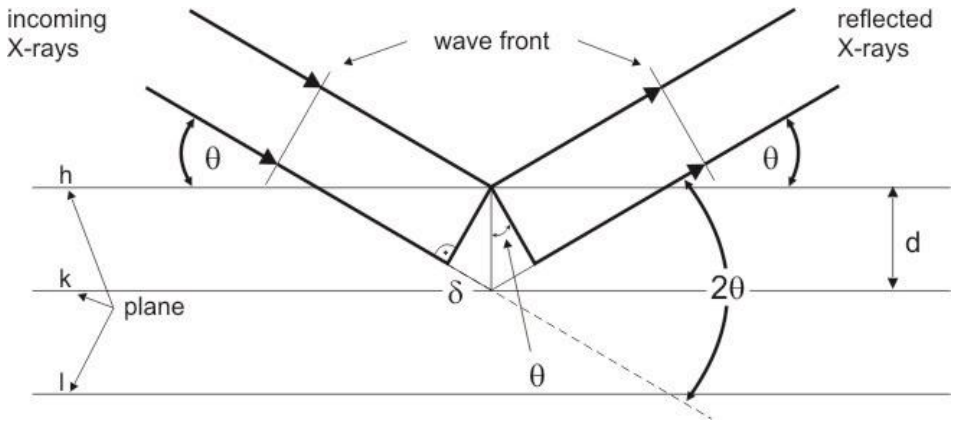

Figure C. 3 :Illustration of coherent X-ray beams striking a series of hkl lattice planes a distance dhkl apart in a crystalline material at an incident angle θ and the resultant optical path difference (2s) [38].

From Equation B.1 it is apparent that for diffraction peaks to occur, the optical path difference between two scattered X-ray beams must be equal to a positive integer of the source wavelength. Hence by scanning across a range of 2θ angles, identification of all possible diffraction directions in a material lattice can be obtained with the results typically expressed as plots of 2θ against intensity. From this the fundamental properties of the crystalline state can be obtained through the use of a materials reference database (e.g. ICDD, International Centre for Diffraction Data) in conjunction with the detected diffraction peaks, measured intensities and calculated basal spacings [38-40].

Appendix D: Dynamic Mechanical Analysis

Dynamic mechanical properties refer to the response of a material as it is subjected to a periodic force. These properties may be expressed in terms of a dynamic modulus, a dynamic loss modulus, and a mechanical damping term.

For an applied stress varying sinusoidally with time, a viscoelastic material will also respond with a sinusoidal strain for low amplitudes of stress. The sinusoidal variation in time is usually described as a rate specified by the frequency (f = Hz; ω = rad/sec). The strain of a viscoelastic body is out of phase with the stress applied, by the phase angle δ (see Figure D.1).

This phase lag is due to the excess time necessary for molecular motions and relaxations to occur. Dynamic stress, σ, and strain, ε, given as:

$$\sigma = \sigma_0 \sin(\omega t + \delta) \quad \text{(D.1)}$$

$$\varepsilon = \varepsilon_0 \sin(\omega t) \quad \text{(D.2)}$$

Where: ω is the angular frequency.

Using this notation, stress can be divided into an “in-phase” component ($\sigma_0 \cos\delta$) and an “out-of-phase” component ($\sigma_0 \sin\delta$) and rewritten as:

$$\sigma = \sigma_0 \sin(\omega t)\cos\delta + \sigma_0 \cos(\omega t)\sin\delta \quad \text{(D.3)}$$

Dividing stress by strain to yield a modulus and using the symbols E′ and E′′ for the in-phase (real) and out-of-phase (imaginary) moduli yields:

$$\sigma = \varepsilon_0 E' \sin(\omega t) + \varepsilon_0 E'' \cos(\omega t) \tag{D.4}$$

$$E' = \left(\frac{\sigma_0}{\varepsilon_0}\right)\cos\delta \qquad E'' = \left(\frac{\sigma_0}{\varepsilon_0}\right)\sin\delta \tag{D.5}$$

$$\varepsilon = \varepsilon_0 \exp(i\omega t) \qquad \sigma = \sigma_0 \exp(\omega t + \delta)\, i \tag{D.6}$$

$$E^* = \frac{\sigma}{\varepsilon} = \left(\frac{\sigma_0}{\varepsilon_0}\right) e^{i\delta} = \frac{\sigma_0}{\varepsilon_0}(\cos\delta + i\sin\delta) = E' + iE'' \tag{D.7}$$

Equation D.7 shows that the complex modulus obtained from a dynamic mechanical test consists of “real” and “imaginary” parts. The real (storage) part describes the ability of the material to store potential energy and release it upon deformation. The imaginary (loss) portion is associated with energy dissipation in the form of heat upon deformation. The above equation is rewritten for shear modulus as,

$$G^* = G' + iG'' \tag{D.8}$$

where G′ is the storage modulus and G″ is the loss modulus. The phase angle δ is given by

$$\tan\delta = (G''/G') \tag{D.9}$$

The storage modulus is often times associated with the stiffness of a material and is related to the Young’s modulus, E. The dynamic loss modulus is often associated with “internal friction” and is sensitive to different kinds of molecular motions, relaxation processes, transitions, morphology and other structural heterogeneities. Thus, the dynamic properties provide information at the molecular level to understanding the polymer mechanical behaviour. Modulus values change with temperature and transitions in materials can be seen as changes in the E’ or tan delta curves. This includes not only the glass transition and the

melt, but also other transitions that occur in the glassy or rubbery plateau, shown in Figure D.2. These transitions indicate subtler changes in the material.

The glass transition (Tg) is seen as a large drop (a decade or more) in the storage modulus when viewed on a log scale against a linear temperature scale, shown in Figure D.3 concurrent peak in the tan delta is also seen. The value reported as the Tg varies with industry with the onset of the E' drop, the peak of the tan delta, and the peak of the E' curve being the most commonly used.

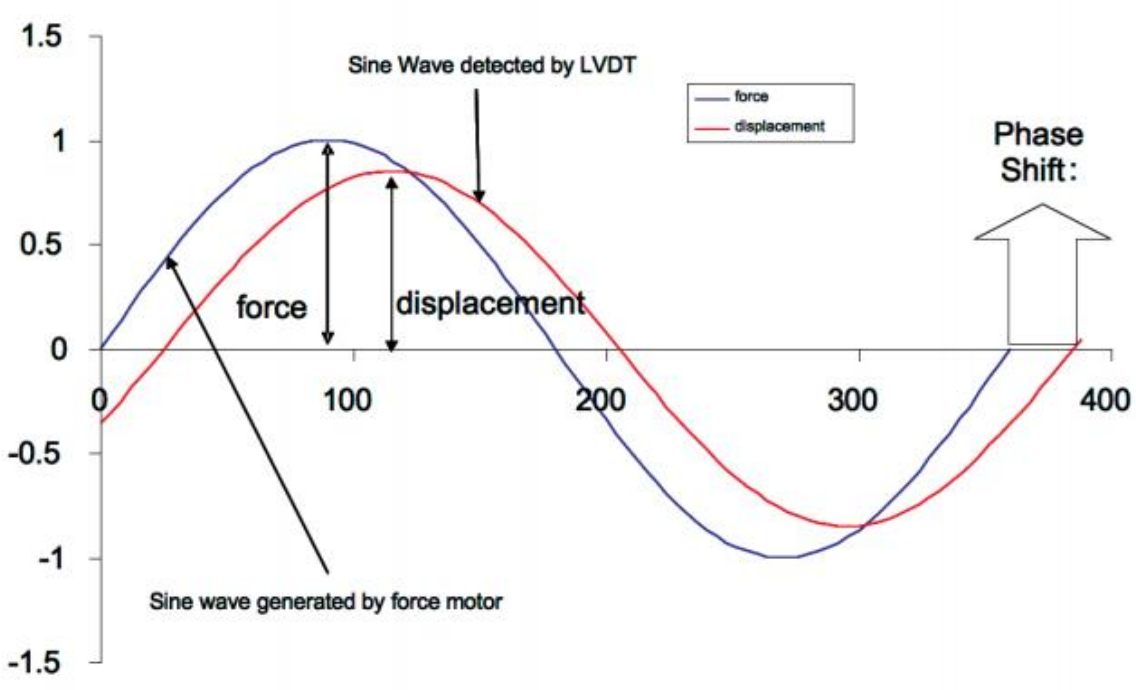

Figure D.1: The relationship of the applied sinusoidal stress to strain is shown, with the resultant phase lag and deformation [99].

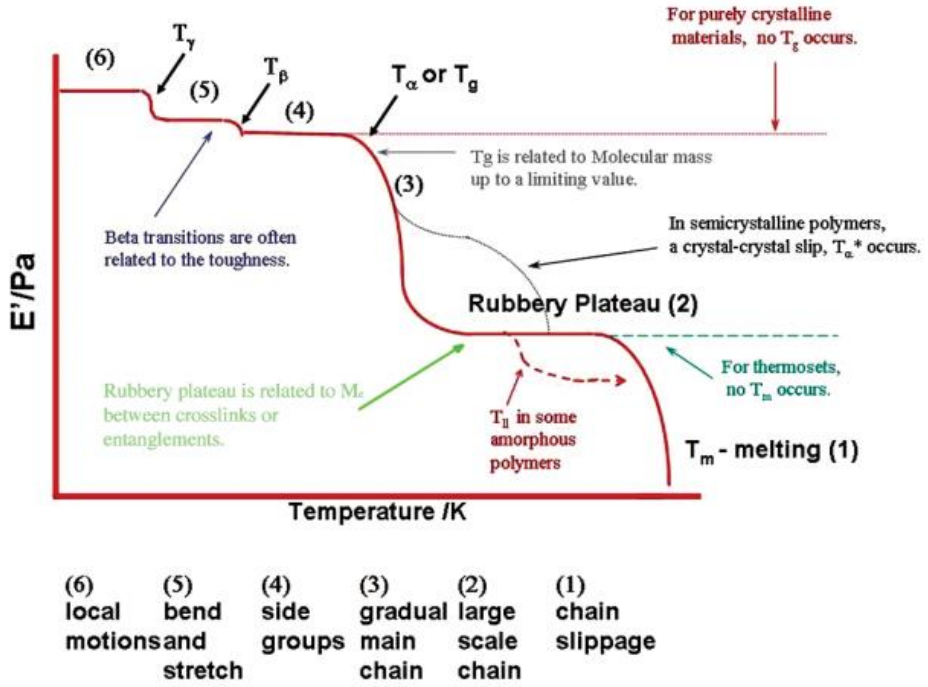

Figure D.2: Modulus values change with temperature and transitions in materials can be seen as changes in the E' or tan delta curves.

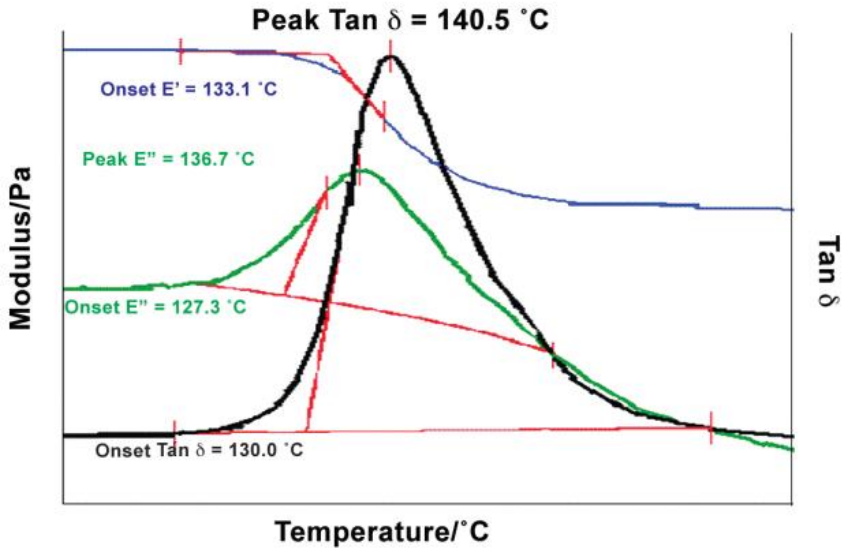

Figure D.3: The glass transition (Tg) in storage modulus and tan delta.

Appendix E: Characterization of Glasses

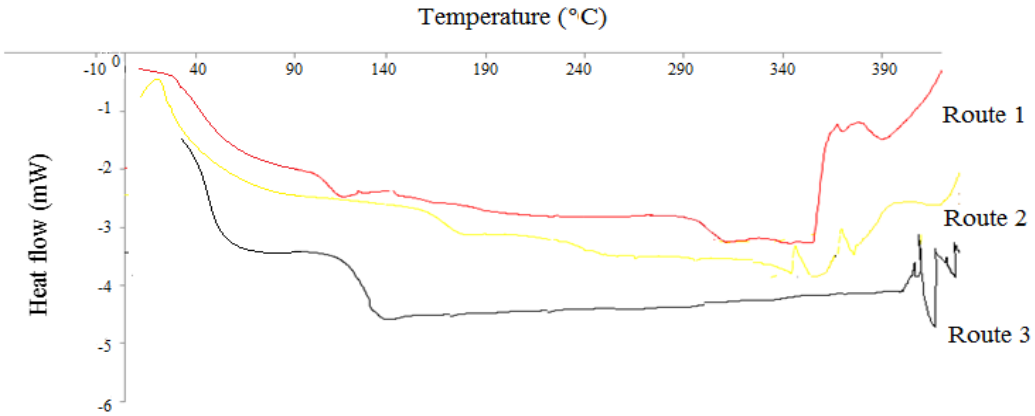

Figure E.1: DSC trace of the phosphate glass (Glass 0) prepared by Route 1, Route 2 and Route 3 over the pre-programmed heating cycle indicative of endo and exothermic events.

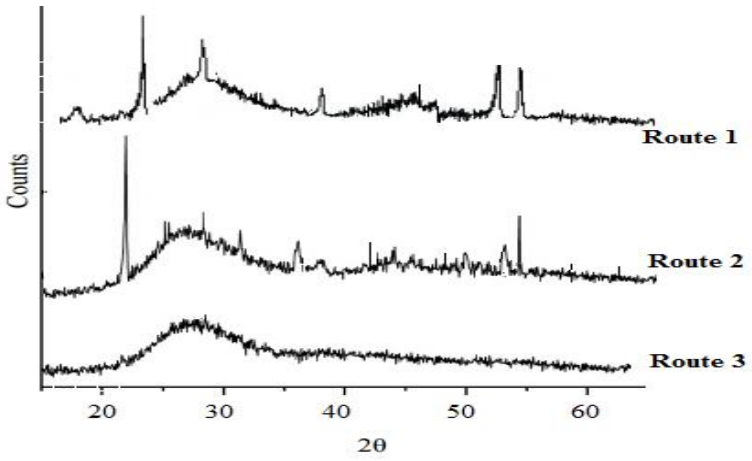

Figure E.2: XRD traces of Glass 0 prepared by Route 1, Route 2, Route 3 over 5-85° 2θ.

Table E. 1: Density of phosphate glasses measured at 21 ˚C using the Archimedes' method and using the Rule of mixture.

	SnF_2 [mol%]	P_2O_5 [mol%]	SnO [mol%]	Density ρ [g/cm^3]	Density (Rule of mixture) ρ_{RoM} [g/cm^3]
Base glass					
0	50.00	30.00	20.00	3.56 ± 0.04	4.60
Class 1 (SnF_2/P_2O_5 = 1.67)					
1	62.10	37.90	0.00	3.19 ± 0.45	4.19
2	59.37	35.63	5.00	3.23 ± 0.20	4.29
3	56.25	33.75	10.00	3. 30 ± 0.25	4.39
4	53.12	31.88	15.00	3.45 ± 0.08	4.49
5	46.87	28.13	25.00	3.75 ± 0.05	4.71
6	43.75	26.25	30.00	3.82 ± 0.04	4.82
Class 2 (P_2O_5/SnO = 1.5)					
7	30.00	42.00	28.00	3.23 ± 0.22	4.62
8	35.00	39.00	26.00	3.45 ± 0.14	4.62
9	40.00	36.00	24.00	3.50 ± 0.09	4.62
10	45.00	33.00	22.00	3.52 ± 0.07	4.61
11	55.00	27.00	18.00	3.74 ± 0.05	4.60
12	60.00	24.00	16.00	3.92 ± 0.06	4.60
Class 3 (SnF_2/SnO = 2.5)					
13	57.14	20.00	22.86	3.35 ± 0.29	4.76
14	56.25	25.00	18.75	3.44 ± 0.12	4.63
15	46.43	35.00	18.57	3.65 ± 0.09	4.53
16	42.86	40.00	17.14	3.76 ± 0.23	4.45

Appendix F: Characterization of Hybrids

F. 1 Effect of glass content on processability of hybrids

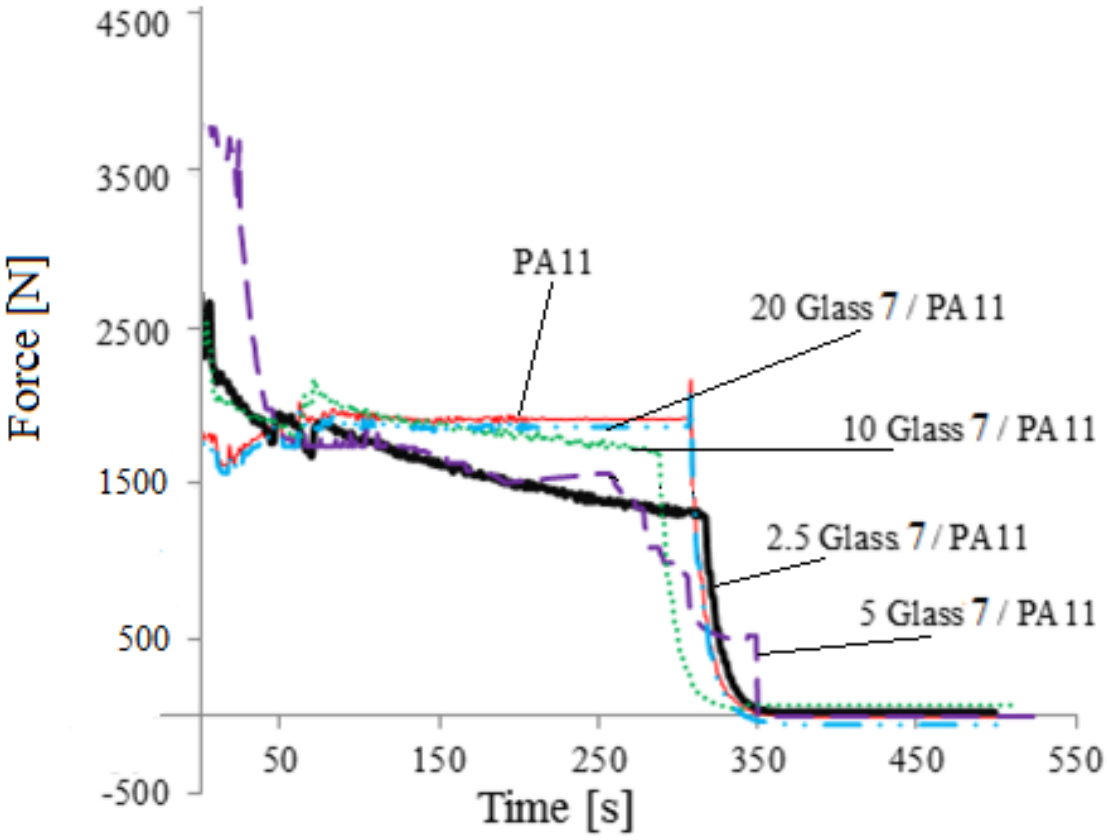

Figure F.1: Force-Time trends for glass/polyamide hybrids with Glass 7 at 0 vol% (PA 11) at 2.5 vol% (Hybrid 5), 5 vol% (Hybrid 6), 10 vol% (Hybrid 7) and 20 vol% (Hybrid 8).

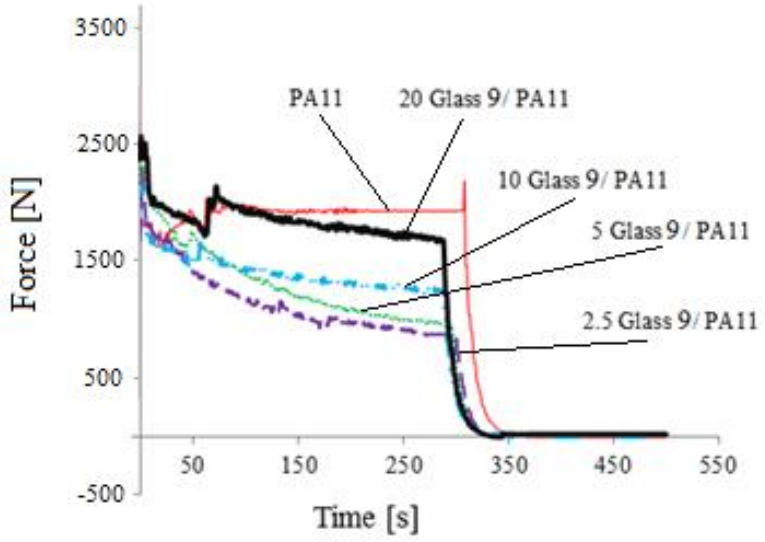

Figure F.2: Force-Time trends for glass/polyamide hybrids with Glass 9 at 0 vol% (PA 11) at 2.5 vol% (Hybrid 9), 5 vol% (Hybrid 10), 10 vol% (Hybrid 11) and 20 vol% (Hybrid 12).

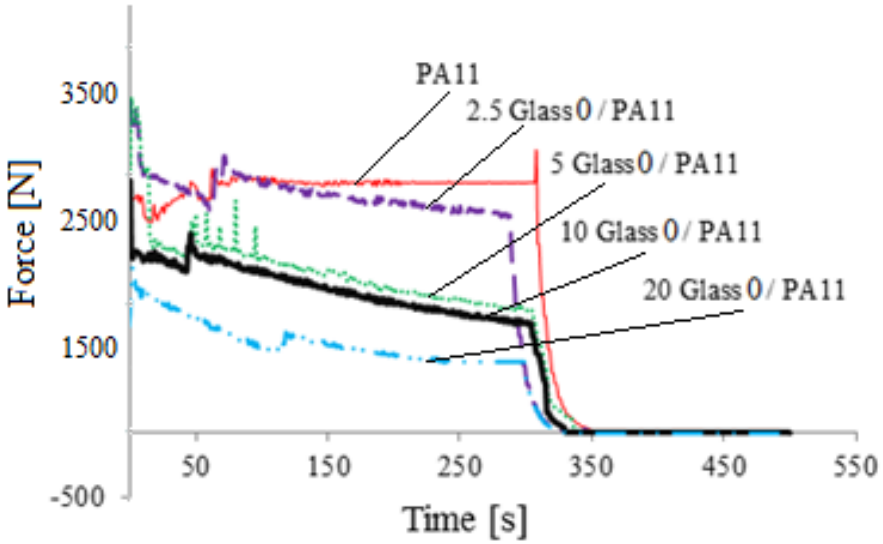

Figure F.3: Force-Time trends for glass/polyamide hybrids with Glass 0 at 0 vol% (PA 11) at 2.5 vol% (Hybrid 1), 5 vol% (Hybrid 2), 10 vol% (Hybrid 3) and 20 vol% (Hybrid 4).

F. 2 Effect of glass composition on processability of hybrids

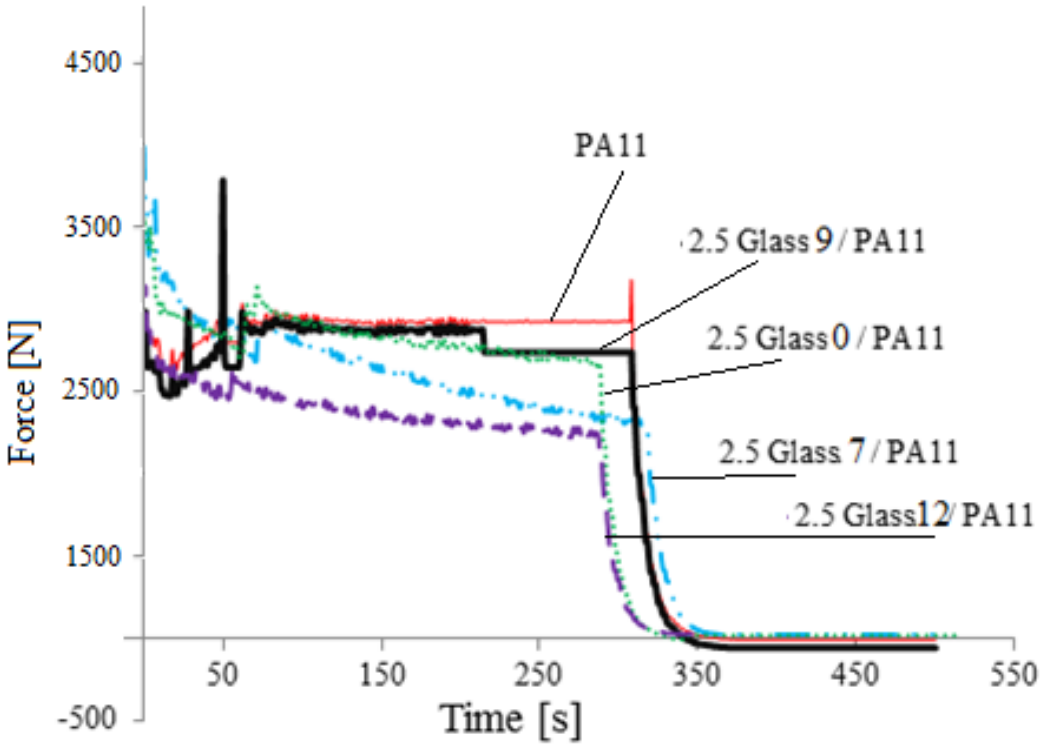

Figure F.4: Force-Time trends for polyamide and glass/polyamide hybrids with 2.5 vol% of Glass 7 (Hybrid 5), Glass 9 (Hybrid 9), Glass 0 (Hybrid 1), Glass 12 (Hybrid 13).

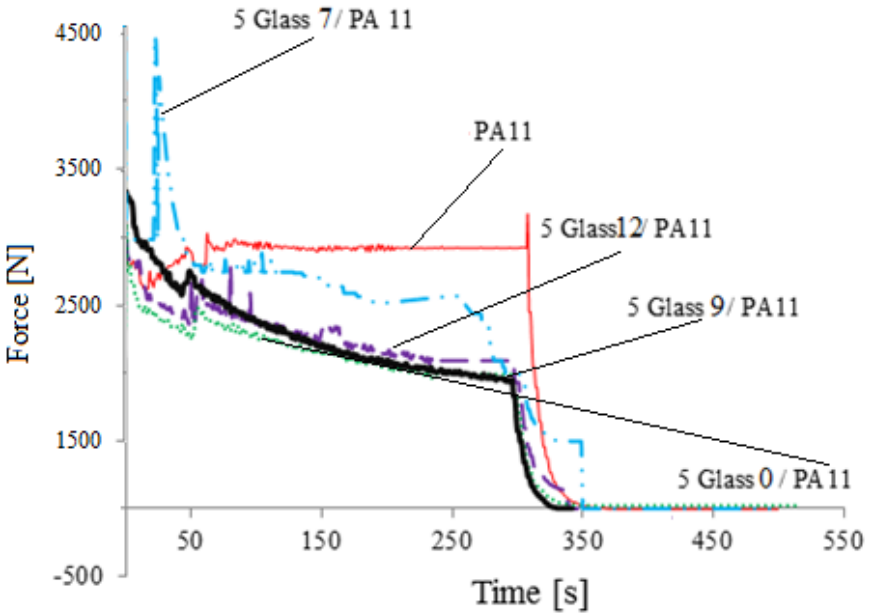

Figure F.5: Force-Time trends for polyamide and glass/polyamide hybrids with 5 vol% of Glass 7 (Hybrid 6), Glass 9 (Hybrid 10), Glass 0 (Hybrid 2), Glass 12 (Hybrid 14).

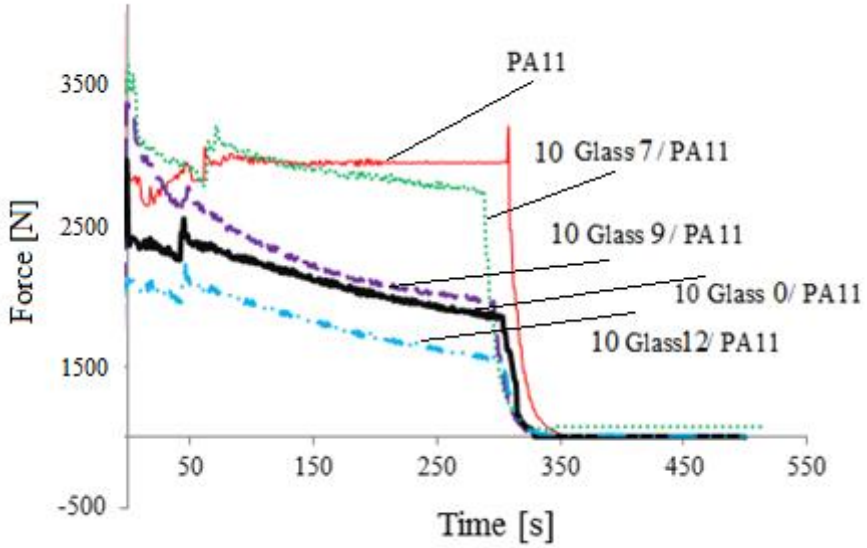

Figure F.6: Force-Time trends for polyamide and glass/polyamide hybrids with 10 vol% of Glass 7 (Hybrid 7), Glass 9 (Hybrid 11), Glass 0 (Hybrid 3), Glass 12 (Hybrid 15).

F. 3 Equilibrium force and feasibility of polyamide and hybrid blends

Table F.1: Working conditions and factors influencing the viability of the pure PA11 and hybrids during melt blending. The blending time was kept constant at 300 s. the feeding volume was 95%.

Glass	*Glass/PA 11 ratio*	*Temperature [˚C]*	*Mixing speed [rpm]*	*Blending viability*	*Force [N]*	*Extrudate diameter [mm]*
None	0	210	100	Yes	2032.0 ± 283.0	2.2±0.4
	0	210	200	Yes	1997.0 ± 328.0	1.9±0.2
	0	230	100	Yes	1996.0 ± 647.0	1.9±0.3
	0	230	200	Yes	1946.0 ± 632.0	1.8±0.3
	0	250	100	Yes	1932.0 ± 432.0	1.8±0.2
	0	250	200	Yes	1867.0 ± 396.0	1.4±0.1
7	2.5	210	100	No	1956.0 ± 569.0	2.0±0.8
	2.5	210	200	No	1852.0 ± 406.0	1.8±0.7
	2.5	230	100	No	1884.0 ± 349.0	1.9±0.3
	2.5	230	200	No	1784.0 ± 486.0	1.8±0.8
	2.5	250	100	No	1792.0 ± 156.0	1.9±0.5
	2.5	250	200	No	1687.0 ± 386.0	1.7±0.6
7	5	210	100	No	1979.0 ± 448.0	2.3±1.0
	5	210	200	No	1859.0 ± 591.0	2.1±0.8
	5	230	100	No	1887.0 ± 809.0	2.3±1.2
	5	230	200	No	1800.0 ± 492.0	2.3±1.0
	5	250	100	No	1796.0 ± 537.0	2.2±0.9

Appendix F: Characterization of Hybrids

Glass	*Glass/PA 11 ratio*	*Temperature [˚C]*	*Mixing speed [rpm]*	*Blending viability*	*Force [N]*	*Extrudate diameter [mm]*
7	5	250	200	No	1742.0 ± 609.0	2.0±0.9
7	10	210	100	No	1963.0 ± 558.0	2.2±0.9
	10	210	200	No	1962.0 ± 649.0	2.1±0.9
	10	230	100	No	1962.0 ± 589.0	2.3±0.9
	10	230	200	No	1929.0 ± 425.0	2.0±0.9
	10	250	100	No	1802.0 ± 629.0	2.1±0.9
	10	250	200	No	1797.0 ± 576.0	1.9±0.8
7	20	210	100	No	1992.0 ± 774.0	2.3±1.2
	20	210	200	No	1972.0 ± 555.0	2.1±0.8
	20	230	100	No	1989.0 ± 674.0	2.3±0.9
	20	230	200	No	1982.0 ± 544.0	1.9±0.8
	20	250	100	Yes	1882.0 ± 234.0	2.2±0.3
	20	250	200	No	1677.0 ± 454.0	1.8±0.8
9	5	210	100	No	1904.0 ± 669.0	2.9±1.2
	5	210	200	No	1861.0 ± 632.0	2.8±0.9
	5	230	100	No	1827.0 ± 622.0	2.8±0.9
	5	230	200	No	1777.0 ± 742.0	2.7±1.0
	5	250	100	No	1787.0 ± 569.0	2.7±0.9
	5	250	200	No	1650.0 ± 703.0	2.6±0.9
9	10	210	100	No	1852.0 ± 962.0	2.9 ±1.0
	10	210	200	No	1787.0 ± 681.0	2.8±0.9
	10	230	100	No	1792.0 ± 789.0	2.8±1.0

Appendix F: Characterization of Hybrids

Glass	*Glass/PA 11 ratio*	*Temperature [˚C]*	*Mixing speed [rpm]*	*Blending viability*	*Force [N]*	*Extrudate diameter [mm]*
9	10	230	200	No	1630.0 ± 902.0	2.6±0.9
	10	250	100	No	1707.0 ± 762.0	2.6±0.9
	10	250	200	No	1670.0 ± 634.0	2.5±0.8
9	20	210	100	No	1982.0 ± 667.0	2.8±0.9
	20	210	200	No	1979.0 ± 471.0	2.7±0.9
	20	230	100	No	1898.0 ± 461.0	2.7±0.8
	20	230	200	No	1809.0 ± 447.0	2.6±0.9
	20	250	100	Yes	1759.0 ± 367.0	2.6±0.4
	20	250	200	No	1709.0 ± 478.0	2.6±0.9
0	5	210	100	No	1692.0 ± 386.0	1.9±0.7
	5	210	200	No	1489.0 ± 169.0	1.8±0.3
	5	230	100	No	1467.0 ± 329.0	2.0±0.4
	5	230	200	No	1100.0 ± 268.0	1.8±0.4
	5	250	100	No	1129.0 ± 182.0	1.8±0.3
	5	250	200	No	983.0 ± 173.0	1.7±0.5
0	10	210	100	No	1215.0 ± 482.0	1.9±0.5
	10	210	200	No	1182.0 ± 398.0	1.8±0.5
	10	230	100	No	1124.0 ± 335.0	1.9±0.7
	10	230	200	No	1004.0 ± 446.0	1.7±0.6
	10	250	100	No	998.0 ± 182.0	1.8±0.3
	10	250	200	No	776.0 ± 238.0	1.6±0.5

Appendix F: Characterization of Hybrids

Glass	*Glass/PA 11 ratio*	*Temperature [˚C]*	*Mixing speed [rpm]*	*Blending viability*	*Force [N]*	*Extrudate diameter [mm]*
0	20	210	100	No	1342.0 ± 592.0	1.9±0.4
	20	210	200	No	1140.0 ± 24.0	1.7±0.7
	20	230	100	No	1200.0 ± 435.0	1.8±0.5
	20	230	200	No	934.0 ± 287.0	1.7±0.8
	20	250	100	Yes	612.0 ± 135.0	1.6±0.4
	20	250	200	No	534.0 ± 239.0	1.5±0.7
12	2.5	210	100	No	1507.0± 708.0	1.9±0.8
	2.5	210	200	No	1467.0± 532.0	1.7±0.6
	2.5	230	100	No	1499.0± 352.0	1.8±0.7
	2.5	230	200	No	1399.0± 348.0	1.7±0.5
	2.5	250	100	Yes	1317.0± 178.0	1.7±0.5
	2.5	250	200	No	1182.0± 239.0	1.6±0.6
12	5	210	100	No	1405.0 ± 134.0	1.9±0.5
	5	210	200	No	1379.0 ± 276.0	1.8±0.4
	5	230	100	No	1259.0 ± 592.0	1.8±0.5
	5	230	200	No	1379.0 ± 532.0	1.7±0.5
	5	250	100	Yes	1075.0 ± 56.0	1.7±0.3
	5	250	200	No	979.0 ± 156.0	1.6±0.6
12	10	210	100	No	1010.0 ± 467.0	1.6±0.5
	10	210	200	No	982.0 ± 342.0	1.6±0.5
	10	230	100	No	890.0 ± 245.0	1.5±0.6
	10	230	200	No	738.0 ± 199.0	1.4±0.5
	10	250	100	Yes	698 ± 82.0	1.4±0.3

Glass	Glass/PA 11 ratio	Temperature [˚C]	Mixing speed [rpm]	Blending viability	*Force [N]*	Extrudate diameter [mm]
12	10	250	200	No	427.0 ± 122.0	1.3±0.5
12	20	210	100	No	859.0 ± 352.0	1.6±0.5
	20	210	200	No	648.0 ± 242.0	1.5±0.4
	20	230	100	No	657.0 ± 230.0	1.5±0.5
	20	230	200	No	579.0 ± 132.0	1.3±0.5
	20	250	100	Yes	348.0 ± 72.0	1.3±0.2
	20	250	200	No	318.0 ± 174.0	1.2±0.6

F. 4 Microstructure and quantitative analysis of Glass 0/PA 11 hybrids

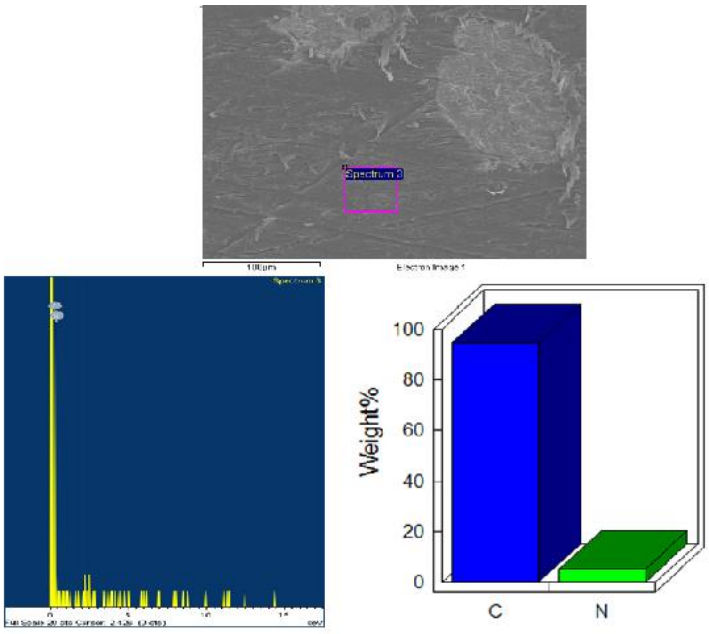

Figure F.7: Micrograph and EDX quantitative analysis of the black phase in Hybrid 7 (10 vol%Glass 0/PA 11).

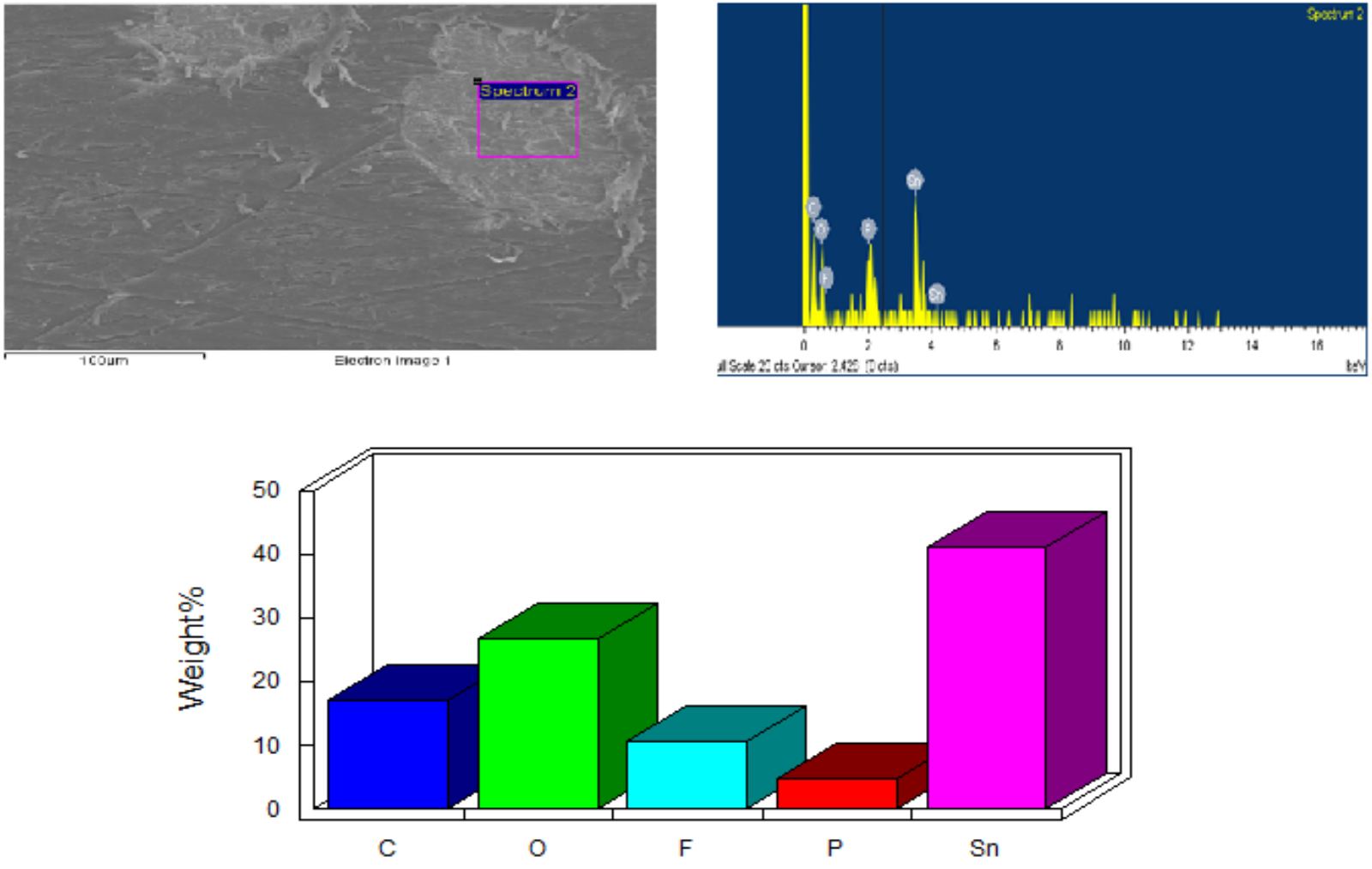

Figure F.8: Micrograph and EDX quantitative analysis of the black phase in Hybrid 7 (10 vol% Glass 0/PA 11).

F. 5 Plots of crystallization temperature against melting temperature

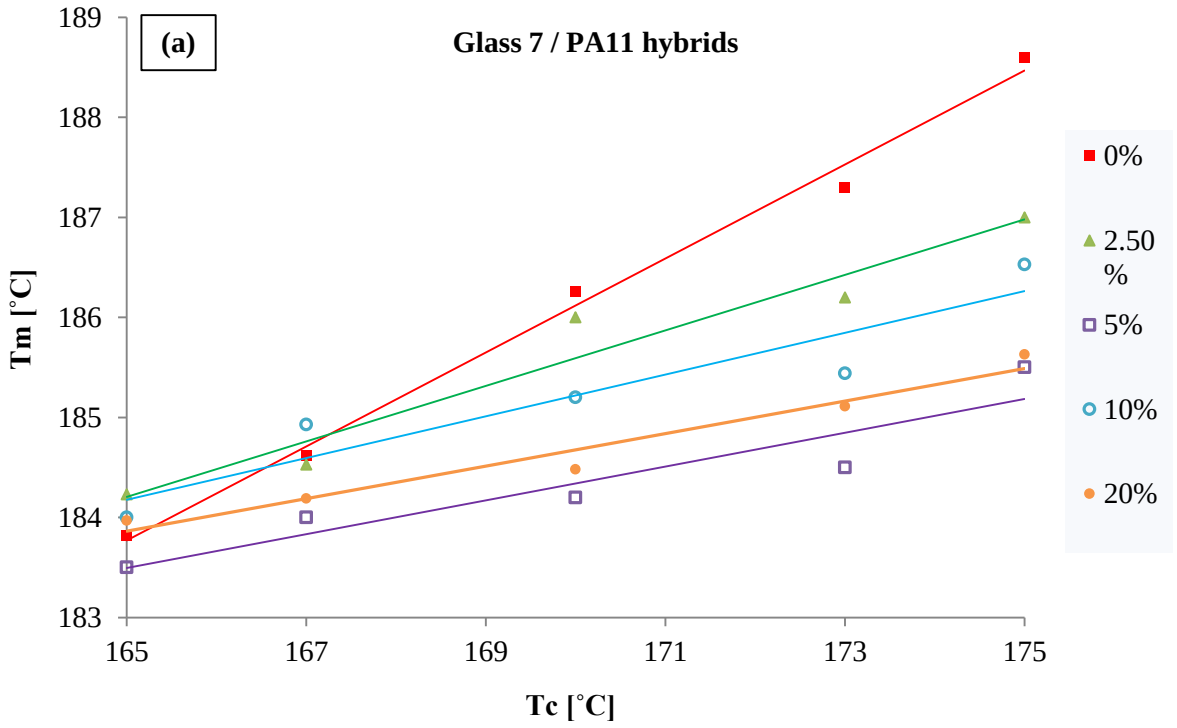

Figure F.9: Plot of crystallization temperature Tc against melting temperature Tm for Glass 7/PA 11 hybrids.

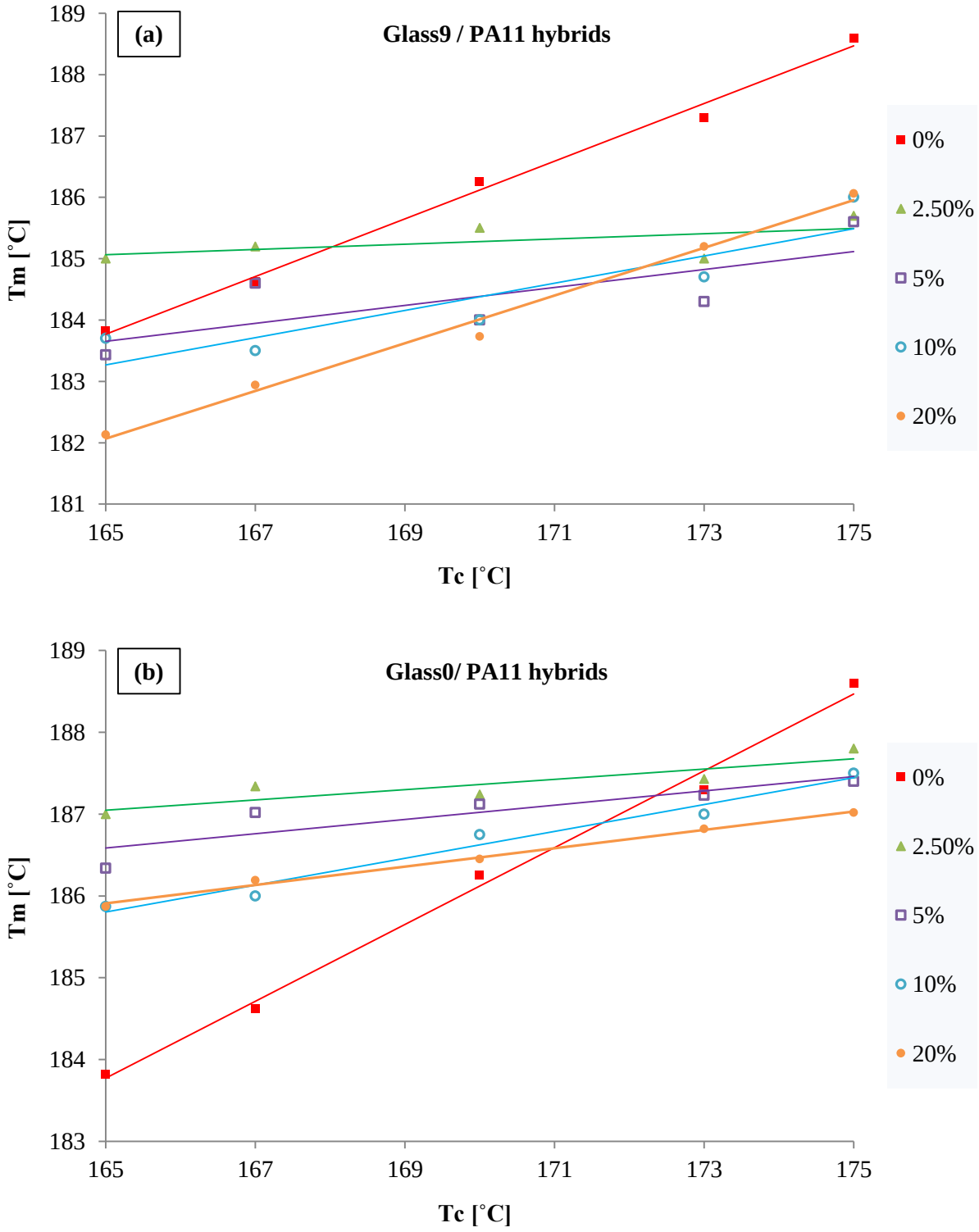

Figure F.10: Plot of crystallization temperature Tc against melting temperature Tm for Glass 9/PA 11 hybrids (a) and Glass 0/PA 11 hybrids (b).

F. 6 Dynamic mechanical properties

Table F. 2: Effect of SnF_2 content on Storage Modulus of Polyamide 11 measured by Dynamic Mechanical Analysis at different temperature.

Blend	*SnF_2 in glass (vol%)*	*Glass (vol%)*	*-40˚C*	*0 ˚C*	*50˚C*	*100˚C*	*150˚C*
PA11	-	0	1074.04 ± 63.87	1029.70 ± 134.31	770.72 ± 45.50	270.00 ± 27.35	149.54 ± 7.59
Glass7/PA11	30	20	1510.68 ± 99.55	1432.85 ± 77.98	895.26 ± 97.57	333.23 ± 97.89	163.32 ± 16.36
Glass9/PA11	40	20	1991.62 ± 26.83	1842.45 ± 90.00	1045.38 ± 103.93	335.48 ± 50.54	165.41 ± 26.29
Glass0/PA11	50	20	2159.39 ± 77.53	1865.22 ± 107.53	1236.94 ± 134.12	391.43 ± 77.53	205.44 ± 57.88
Glass12/PA11	60	20	2729.47 ± 100.83	2305.59 ± 57.30	1262.67 ± 107.53	540.57 ± 47.22	329.14 ± 19.83

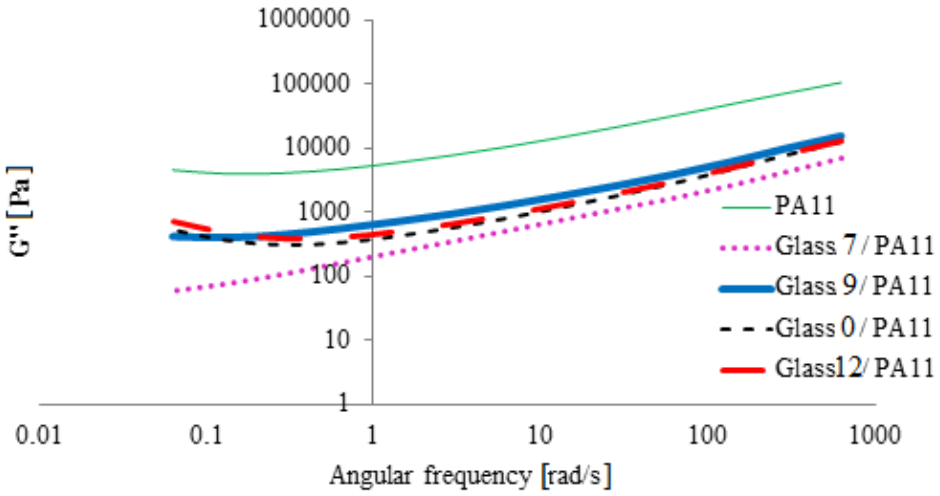

Figure F.11: Shear loss modulus G” versus angular frequency of Polyamide 11 and hybrids at 250 ˚C.